PLANETARY WAVES AND DYNAMICAL PROCESSES ASSOCIATED WITH SEASONAL PERTURBATIONS AND TRANSITIONS

A Thesis Submitted to the College of
Graduate Studies and Research
in Partial Fulfillment of the Requirements
for the Degree of Doctor of Philosophy
in the
Department of Physics and Engineering Physics
University of Saskatchewan
Saskatoon

by
TATYANA CHSHYOLKOVA

Keywords: middle atmosphere dynamics, planetary waves, stratospheric warming
© Tatyana Chshyolkova, April, 2007. All rights reserved.

PERMISSION TO USE

In presenting this thesis in partial fulfilment of the requirements for a Postgraduate degree from the University of Saskatchewan, I agree that the Libraries of this University may make it freely available for inspection. I further agree that permission for copying of this thesis in any manner, in whole or in part, for scholarly purposes may be granted by the professor or professors who supervised my thesis work or, in their absence, by the Head of the Department or the Dean of the College in which my thesis work was done. It is understood that any copying or publication or use of this thesis or parts thereof for financial gain shall not be allowed without my written permission. It is also understood that due recognition shall be given to me and to the University of Saskatchewan in any scholarly use which may be made of any material in my thesis.

Requests for permission to copy or to make other use of material in this thesis in whole or part should be addressed to:

Head of the Department of Physics and Engineering Physics
University of Saskatchewan
Saskatoon, Saskatchewan, S7N 5E2

ABSTRACT

This thesis provides highlights of the atmospheric research conducted during the program of studies 2003-07. The theme is variability of the winds at mesospheric heights (60-100 km) due to Planetary Waves (PW, 2-30 days) over middle and high latitudes. Considerable energy and momentum are transported by atmospheric waves, and their global characteristics are required to understand many phenomena and explain coupling processes within the atmosphere. The vertical propagation of PW from the upper troposphere to the mesosphere is investigated by applying the Morlet wavelet and wave number analysis to the MetO (United Kingdom Meteorological Office) stratospheric assimilated fields, TOMS total (column) ozone, and Medium Frequency (MFR) and Meteor Wind (MWR) radar measurements. The results show that large-scale eastward propagating PW dominate at tropopause and low stratospheric heights, while westward PW become comparable or even stronger in the upper stratosphere and above during months other than summer. There are also strong seasonal dependences of the PW activity in each of the stratospheric and mesospheric regions, which are attributed, at least partially, to the influence of the background wind on PW propagation. Longitudinal variations in PW activity are explained by longitudinal variations in these winds.

During summer (westward zonal winds) PW activity is reduced in the stratosphere and only relatively fast westward propagating PW, such as quasi 2-day wave (Q2DW), are able to reach mesospheric heights from below. The results obtained using 14 years of MFR data at Saskatoon provide a unique climatology (70-100 km) of this wave: in addition to summer activity the Q2DW is also present at low mesospheric heights in winter, especially when the eastward winds are weak; there are significant interannual variations in Q2DW activity in both seasons. Strong latitudinal and longitudinal differences in Q2DW occurrence and amplitude are shown from the comparisons of wind data at several stations.

During winter, when zonal winds are eastward, the PW coupling between stratosphere and mesosphere is stronger than during other seasons. Detailed data analysis has been performed for the Arctic winter of 2004/05, for which the stratospheric state is

described using conventional zonal mean parameters as well as the newer Q-diagnostic. Spectral analyses for this winter show relatively weak PW activity at stratospheric and mesospheric heights and strong latitudinal and longitudinal differences of mean winds and PW characteristics consistent with the form and location of the polar vortex.

In addition to the vertical coupling it has also been shown that weaker horizontal “inter-hemispheric” coupling occurs during equinoctial months, when eastward winds dominate globally. It is demonstrated that with favorable conditions, planetary waves with 10, 16 and 25 day periods penetrate to the opposite hemisphere.

ACKNOWLEDGMENTS

I am extremely grateful to my supervisor Professor Alan Manson for his patience, advice and financial support. Without his continuous guidance I would still be wandering among enormous research possibilities in the area of atmospheric physics.

Special thanks go to Dr. Chris Meek, whose deep knowledge in the MF radar operation, data archiving and analyses is invaluable. His critical reviews and careful editing are greatly appreciated.

There are many researchers who kindly helped me better understand different aspects of the topic of my research. I wish to recognize Drs. Lynn Harvey and Duncan Fairlie for the insights into the details of the Q-diagnostic calculations. My fellow graduate students, now Drs. Leonid Benkevich and Ivan Khalzov were invaluable for advice and discussions of different numerical techniques and their computer-realizations.

Also, thanks are provided to my co-authors Drs. C. Hall, W. Hocking, C. Jacobi, N.A. Makarov, E. Merzlyakov, N. Mitchell, S. Avery, T. Aso, M. Tsutsumi, K. Igarashi, Y. Murayama, W. Singer, D. Thorsen, and J.W. MacDougall for their data and reviews.

I would like to express my gratitude to former and current members of my Advisory Committee for devoting their time, asking challenging questions, and giving a valuable feedback on my research progress.

Significant amounts of data used in this study have been obtained from different instruments throughout the world. I would like to acknowledge the tremendous efforts that data acquisition requires, and to thank the United Kingdom Meteorological Office, British Atmospheric Data Center; National Center for Atmospheric Research/National Centers for Environmental Prediction, Aura MLS and TOMS teams for making their data sets available to the atmospheric community, and for this study in particular.

This research would not take place without financial support provided by the Department of Physics and Engineering Physics and University of Saskatchewan. I would also like to acknowledge the President/Student Fund and the College of Graduate Studies and Research whose financial assistance for travel made it possible to present

the results of this research at prestigious scientific meetings and to share new ideas with the international atmospheric community.

An enjoyable and supportive working environment was created by professors, students, and staff of the Institute of Space and Atmospheric Studies. I am sincerely thankful for the friendship provided by Brigette Hesman, Bill Marshall, Svetlana Petelina, Yuriy Tyshetskiy, and Sergei Ivanov.

To Dr. Alex Pogoreltsev, thank you for believing in me.

To Matrena, Nina, Zoya, Galina and Natalia

TABLE OF CONTENTS

LIST OF TABLES

LIST OF FIGURES

LIST OF ABBREVIATIONS

ATRAD	Atmospheric Radar Systems Pty Ltd
BADC	British Atmospheric Data Center
BGW	background wind
CANDAC	Canadian Network for the Detection of Atmospheric Change
CIRA86	COSPAR International Reference Atmosphere 1986
CIRES	Cooperative Institute for Research in Environmental Sciences
CMAM	Canadian Middle Atmosphere Model
CUJO	Canada-US-Japan-Opportunity
ECMWF	the European Centre for Medium-Range Weather Forecasts
EISCAT	European Incoherent SCATter
EP	Earth Probe
EW	East-West
FCA	Full Correlation Analysis
FIR	Finite Impulse Response
FT	Fourier Transform
GCM	Global Circulation Model
GSFC	Goddard Space Flight Center
GW	Gravity Waves
GWS	global wavelet spectrum
HF	High Frequency
HRDI	High Resolution Doppler Imager
LS	Least Square analysis
MA	Middle Atmosphere
MARDOC	Modular Antenna Radar Designs Of Canada
MetO	United Kingdom Meteorological Office
MFR	Medium Frequency Radar
MLS	Microwave Limb Sounder
MLT	Mesosphere/Lower Thermosphere
MSIS-E-90	Mass-Spectrometer-Incoherent-Scatter (Extension 1990)

MWR	Meteor Wind Radar
NASA	National Aeronautic and Space Administration
NCAR	National Center for Atmospheric Research
NCEP	National Centers for Environmental Prediction
NOAA	National Oceanic and Atmospheric Administration
NS	North-South
PEARL	Polar Environment Atmospheric Research Laboratory
PI	Principal Investigator
PMR	Pressure Modulator Radiometer
PV	potential vorticity
PW	planetary waves
Q2DW	quasi 2-day wave
QBO	Quasi-Biannual Oscillation
SABER	Sounding of the Atmosphere using Broadband Emission Radiometry
SCR	Selective Chopper Radiometer
SSW	sudden stratospheric warming
STT	spring time transition
TIMED	Thermosphere-Ionosphere-Mesosphere Energetics and Dynamics
TOMS	Total Ozone Mapping Spectrometer
UARS	Upper Atmosphere Research Satellite
UKMO	United Kingdom Meteorological Office
VHF	Very High Frequency

Chapter 1

INTRODUCTION

The objective of the thesis is to investigate coupling processes due to Planetary Waves (PW, periods of 2-30 days) in the middle atmosphere (MA). The Planetary Waves play an important role in the study of atmospheric dynamics. A goal of atmospheric science, which includes solar-terrestrial radiative processes and dynamics, is to explain the observed circulation and temperatures on the basis of fundamental physical principles. The knowledge of the atmospheric dynamics is therefore essential for improvement of weather predictions and for prognosis of climate change as a result of natural causes (e.g. variability of the Sun) as well as due to human activity.

The basic properties of the atmosphere and its dynamics are relatively well known and described in many textbooks. A very brief summary that is based on *Holton* [1972], *Andrews et al.* [1987], and *Salby* [1996] is given in Section 1.1, with the purpose to introduce basic terminology used throughout the thesis. More detailed introductions relevant to the different aspects of the study discussed are given in corresponding chapters. Climatology and the long-period variability of the mesospheric winds measured by a Medium Frequency radar (MFR) are discussed in Section 1.2. Possible sources of these long-period variabilities are listed in Section 1.3. Section 1.4 presents some theoretical consideration of Planetary Wave (PW) characteristics. The overview of the material presented in the thesis is given at the end of the chapter (Section 1.5).

1.1 The Middle Atmosphere

According to the variation of the temperature with height, the atmosphere has been divided into four layers: the troposphere (0-15 km), the stratosphere (~15-50 km), the mesosphere (~50-90 km), and the thermosphere (above ~90 km). The boundaries between each pair of layers are called the tropopause, stratopause, and mesopause, respectively (see, for example, Figure 1.1). In the troposphere the temperature decreases

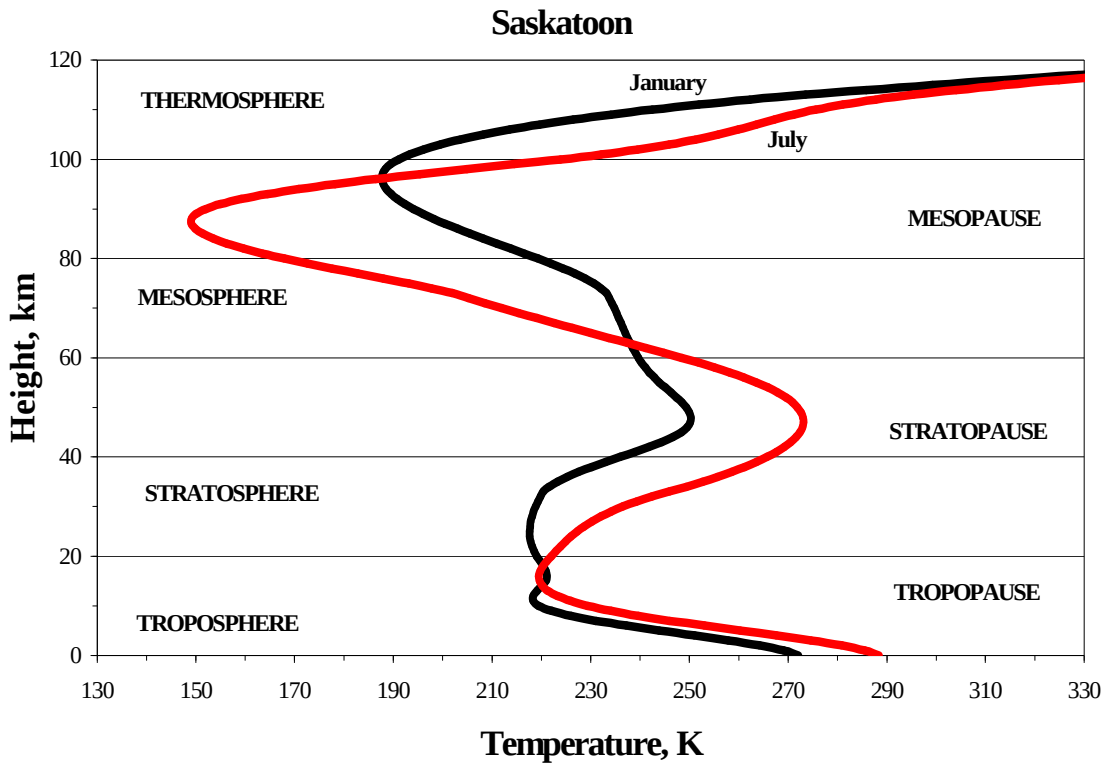

Figure 1.1 The temperature profiles calculated using MSIS-E-90 model for Saskatoon location for January 15 and July 15, 2002.

almost linearly with altitude. This region, where most meteorological phenomena occur, is dominated by convective motions, and is also called the lower atmosphere. In the stratosphere, primarily due to absorption of solar ultra-violet by ozone, the temperature rises with altitude peaking at the stratopause heights. Radiative processes are dominant here. Above the stratopause the temperature falls with height reaching its minimum in the mesopause region. Both radiative and dynamical processes are important in the mesosphere. The stratosphere and mesosphere form the Middle Atmosphere (MA). In the thermosphere the temperature increases again. In the upper atmosphere (thermosphere and above) the ionized component of the atmosphere is substantial, and the effects of the Earth's electric and magnetic fields become important. As an example, the temperature profiles calculated using the Mass-Spectrometer-Incoherent-Scatter (MSIS-E-90) model (http://nssdc.gsfc.nasa.gov/space/model/models/msis.html), for the Saskatoon location for summer and winter conditions, are shown in Figure 1.1. As is seen from the figure, the heights of the temperature minima and maxima as well as their

values change with season. There are also significant latitudinal variations, e.g. the heights and magnitudes of the temperature extrema differ for tropics, mid-latitudes, and/or polar regions.

The pressure and the density of the atmospheric gas decrease exponentially with height, so that approximately 90% of the atmospheric mass is in the troposphere (0-15 km), a little less than 10% in the stratosphere (15-50 km) and only ~0.1% in the mesosphere and above.

In the middle atmosphere the concepts and equations of fluid dynamics are applied. Wind is considered as advection of material or the horizontal component of convective flow. Combinations of the pressure-gradient force, gravity, Coriolis force and friction control the winds. The pressure-gradient force is a result of unequal temperature distribution in the atmosphere. The greater the temperature differences, the stronger the horizontal pressure gradient and resulting wind. Gravity produces density stratification in the atmosphere. The Coriolis force deflects all freely moving objects, including the wind, to the right of their original path of motion in the Northern Hemisphere and to the left in the Southern Hemisphere. It strengthens poleward and weakens equatorward, becoming nonexistent at the equator. Friction modifies the balance between Coriolis force and pressure-gradient force. Although friction significantly influences airflow near the Earth's surface, its effect is negligible above a height of a few kilometers. It becomes significant again in the stratosphere and the mesosphere due to the drag associated with waves. The last two do not create airflow, but greatly modify it. If there were no rotation of the Earth and no friction then air would flow directly from areas of higher pressure to areas of lower pressure.

In the non-inertial reference frame associated with any point on the Earth the equation of motion is

$$\frac{d\vec{V}}{dt} = -\frac{\nabla p}{\rho} - 2\vec{\Omega}\times\vec{V} - \vec{\Omega}\times(\vec{\Omega}\times\vec{r}) + \vec{g^*} + \vec{F}\,, \qquad (1.1a)$$

where $\vec{V}$ is the velocity of an air parcel, p and ρ are atmospheric pressure and density, $\vec{\Omega}$ is the angular velocity of the rotation of the Earth, $\vec{r}$ is the position vector for the

parcel relative to the center of the Earth, $\overrightarrow{g^*}$ is the acceleration due to gravity, and $\vec{F}$ represents all other forces, such as friction. The effects of the gravitational force and centrifugal force are usually combined to define an effective gravity such that

$$\vec{g} = -\vec{\Omega} \times (\vec{\Omega} \times \vec{r}) + \overrightarrow{g^*} .$$

The equation (1.1a) is often written in component form using spherical coordinates. These coordinates are defined so that the surface of the Earth corresponds to a coordinate surface (*x, y, z*) with the unit vectors *i, j, k* directed eastward, northward, and upward, respectively. Then the directions of the unit vectors are functions of position on the spherical Earth and, therefore, the (*x, y, z*) coordinate system defined in this way is not a Cartesian coordinate system. The three equations are as follows:

$$\frac{du}{dt} - \frac{uv \tan\phi}{a} + \frac{uw}{a} = -\frac{1}{\rho}\frac{\partial p}{\partial x} + 2\Omega v \sin\phi - 2\Omega w \cos\phi + F_x , \qquad (1.1b)$$

$$\frac{dv}{dt} + \frac{u^2 \tan\phi}{a} + \frac{vw}{a} = -\frac{1}{\rho}\frac{\partial p}{\partial y} - 2\Omega u \sin\phi + F_y , \qquad (1.1c)$$

$$\frac{dw}{dt} - \frac{u^2 + v^2}{a} = -\frac{1}{\rho}\frac{\partial p}{\partial z} - g + 2\Omega u \cos\phi + F_z , \qquad (1.1d)$$

where *u*, *v*, and *w* are the *x*, *y*, and *z* components of the wind $\vec{V}$ (respectively these are zonal, East-West; meridional, North-South; and vertical), a is the mean radius of the Earth and ϕ is the latitude. The terms proportional to 1/*a* arise due to the curvature of the Earth [*Holton*, 1972].

These complete equations of motion describe all types and scales of atmospheric motions. However, the presence of non-linear terms makes them difficult to solve, and in the words of Dr. James Holton: "…makes dynamic meteorology an interesting and challenging subject". Usually these equations are simplified by eliminating terms based on scaling considerations. For example, for the synoptic scale motions at middle latitudes with horizontal and vertical scales of the order of 1000 and 10 km, respectively, the total derivatives of the horizontal velocities, and the curvature terms may be ignored. The so-called geostrophic and hydrostatic approximations are then valid. When the Coriolis force is exactly equal and opposite to the pressure-gradient

force, the airflow is said to be in geostrophic balance. The geostrophic balance gives the approximate relationship between the pressure field and horizontal velocity (from equations 1.1 b, c):

$$fv = \frac{1}{\rho}\frac{\partial p}{\partial x}, \tag{1.2a}$$

$$fu = -\frac{1}{\rho}\frac{\partial p}{\partial y}. \tag{1.2b}$$

where $f=2\Omega sin\varphi$ is the Coriolis parameter. The horizontal velocity field that satisfies these equations is called the geostrophic wind. Geostrophic winds flow in a straight path, parallel to the isobars, with velocities proportional to the pressure-gradient force, and should approximate the actual horizontal wind to within about 10%.

To be able to predict the evolution of the velocity field it is necessary to have some reference to time. Approximate prognostic equations are horizontal momentum equations that keep the acceleration terms:

$$\frac{du}{dt} - fv = -\frac{1}{\rho}\frac{\partial p}{\partial x}, \tag{1.3a}$$

$$\frac{dv}{dt} + fu = -\frac{1}{\rho}\frac{\partial p}{\partial y}. \tag{1.3b}$$

For synoptic scale motions there is usually balance between the upward pressure gradient force and the downward force of gravity in the atmosphere, the so-called hydrostatic equilibrium. The equation of the hydrostatic balance can be obtained by simplifying the equation for the vertical component (1.1d), again using scale analysis:

$$\frac{\partial p}{\partial z} + \rho g = 0 \tag{1.4}$$

Another useful relationship involves horizontal temperature gradients and vertical gradients of the horizontal wind, and is known as the thermal wind equation:

$$f\frac{\partial v}{\partial z} \approx \frac{g}{T}\frac{\partial T}{\partial x}, \tag{1.5a}$$

$$f\frac{\partial u}{\partial z} \approx -\frac{g}{T}\frac{\partial T}{\partial y}. \tag{1.5b}$$

It is valid when both the geostrophic and hydrostatic balances apply and is obtained by cross-differentiation of the equations (1.2 a, b), (1.4), rearrangement and further scaling considerations. The full set of equations required for wave solutions also includes the continuity equation and suitable forms of the thermodynamic equations.

1.2 **Mesospheric Winds Measured by Medium Frequency Radar**

The climatology of the mesospheric winds from ~60 to 106 km, and for a middle latitude location, is shown in Figure 1.2. The contour plots for the meridional (NS, the left panel) and zonal (EW, the right panel) components of the wind have been constructed by averaging data obtained by Saskatoon Medium Frequency radar (MFR) over 12 years (1988-1999). It is clear from the figure that in summer the smoothly

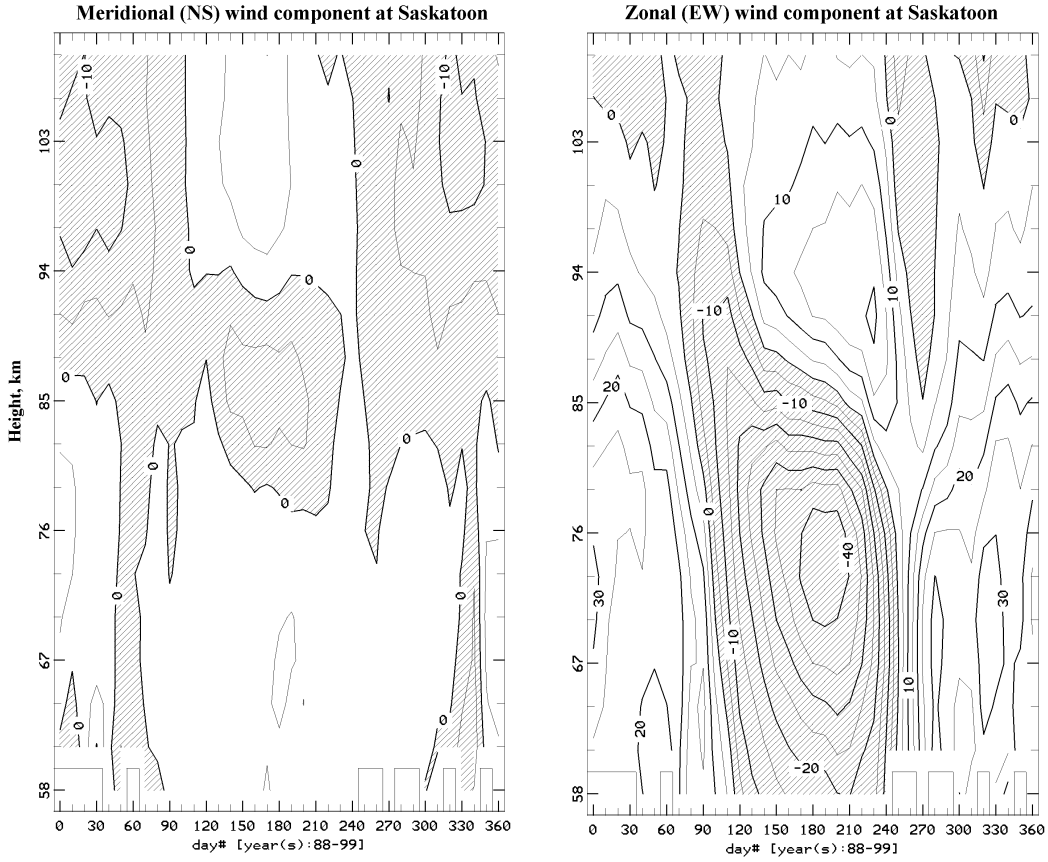

Figure 1.2 Mean meridional (NS, the left panel) and zonal (EW, the right panel) wind components produced by averaging MFR data over 1988-1999 at Saskatoon (52^{o}N, 105^{o}W).

varying westward cell dominates the heights up to ~90 km (the right panel), and its closing is consistent with equatorward flow at these heights (the left panel). During the winter the winds are directed eastward and usually show more variability, which is caused by planetary waves (PW) and sudden stratospheric warmings (SSW). The spring and autumn "tongues", westward wind cells elongated with height, are very intriguing features as they are repeatedly seen in all radar data [*Manson et al.*, 1991], while global empirical models have failed to reproduce them (e.g. CIRA-86).

The Mesosphere Lower Thermosphere (MLT, 50-100 km) region is known for its great variability. At any moment the mesospheric observations contain a mixture of wave-like disturbances with different periods and variable amplitudes. Figure 1.3 shows changes of the meridional (the left panel) and zonal (the right panel) variances with height and

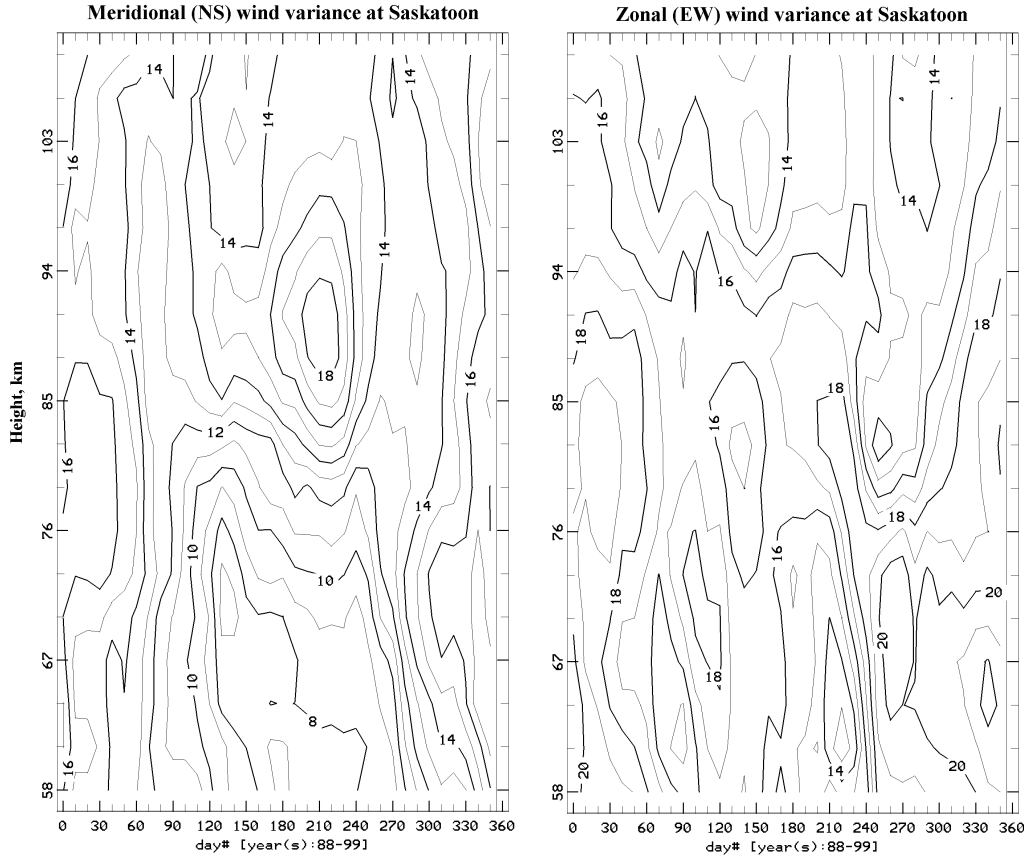

Figure 1.3 Meridional (the right panel) and zonal wind components of the spectral power (2-30 days) averaged over 12 years (1988-1999) of data obtained at Saskatoon (52^{o}N, 105^{o}W), 58-109 km virtual height.

season at Saskatoon. To calculate the variances, first a windowed Fourier Transform (FT) has been performed with a window of 30 days (720 hr) and step of 10 days. The data were considered only if more than 50% of hours existed. Then variances were integrated for periods from 2 to 30 days and those values for the windowed time intervals were averaged over 12 years (1988-1999). The contours of the meridional components of the power spectra from 2 to 30 days (the left panel) demonstrate striking resemblance to the contours of the zonal mean winds (the right panel of Figure 1.2). This will be due to two factors: the small background winds and shears (Figure 1.2); and the fact that at this latitude wind perturbations in EW and NS components are of comparable magnitude. The variances are largest during the winter season throughout the MLT and right above the westward jet (~85-95 km) in summer. They steadily decrease from winter to summer with their minimum coinciding with the core of the westward jet at the low mesospheric heights.

The PW variances of the zonal component (the right panel of Figure 1.3) are larger in magnitude than those of the meridional component. Similar to the meridional component, the maximum variability of the zonal component also tends to be during the winter season, but the contours are noisier. This could be attributed to the combination of variances due to the background wind shears (height and time) and wave-like oscillations. The former are significant during equinoxes, the times of transition from the winter (eastward zonal winds) to summer-like (westward zonal winds) circulation, as well as during summer in the upper mesosphere region, where westward winds decrease and become eastward.

The wavelet amplitudes of the MFR wind components for Saskatoon were calculated for the period range from 2 to 30 days and the time interval from December 2000 to December 2002. (This analysis provides a time sequence of wind perturbations, and is discussed in Chapter 2). The contours of the amplitudes obtained are shown in Figure 1.4 for five altitudes from 70 (on the bottom) to 94 km (on the top). The results for meridional (NS) and zonal (EW) winds are presented in the left and right column, respectively. The black thick solid lines indicate features that exceed the 90%

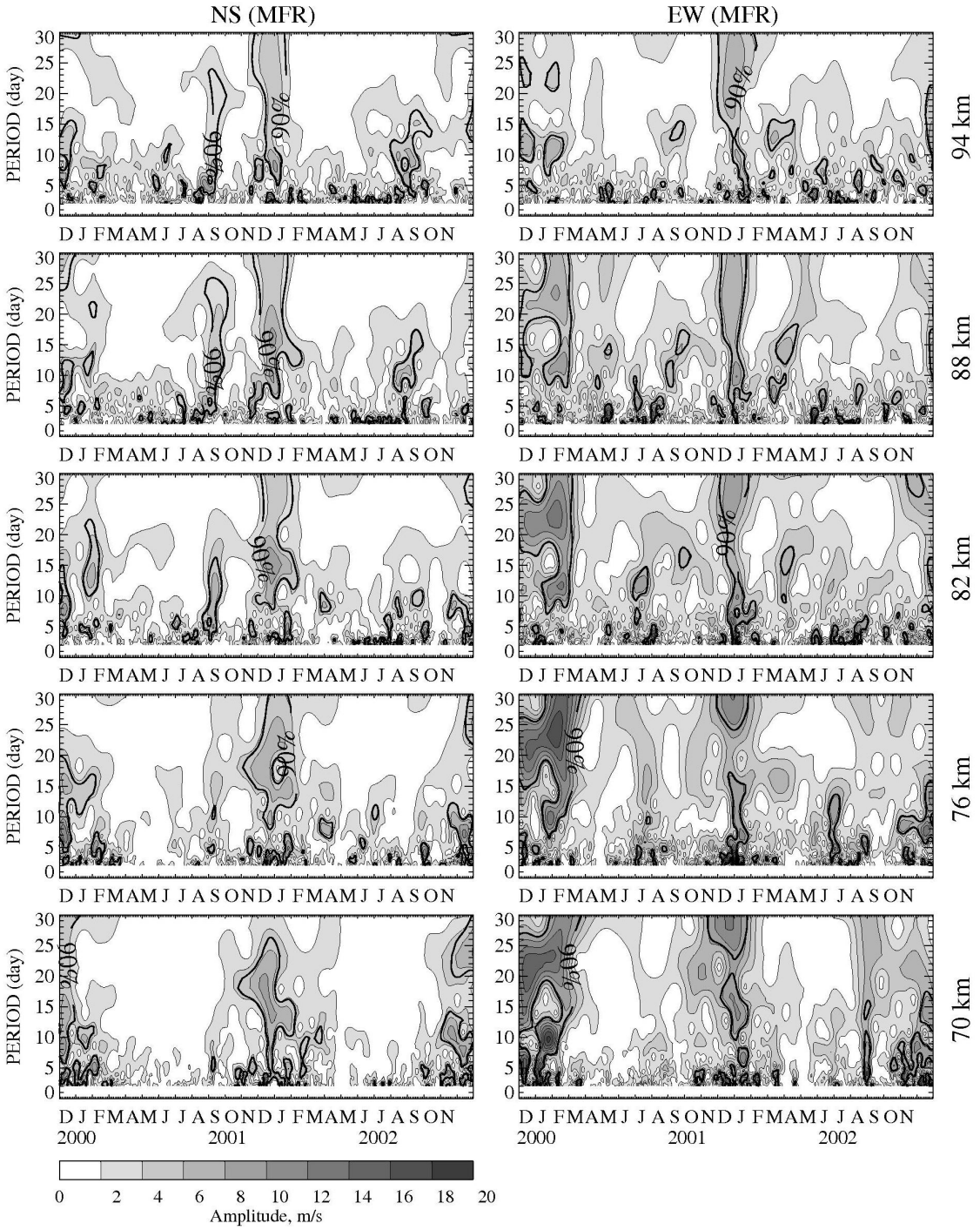

Figure 1.4 Wavelet amplitudes versus time (December 2000-December 2002) and period (2-30 days) calculated for the meridional (left column) and zonal (right column) components of the MFR winds at Saskatoon for five heights from 70 to 94 km. The black thick solid lines indicate features that exceed the 90% confidence level.

confidence level. It is clearly seen from the figure that the meridional winds exhibit weaker PW activity than the zonal winds, especially at longer periods. In addition, amplitude peaks in meridional winds do not usually coincide in period and/or time with those in zonal winds. This is likely due to the differing Hough mode (the eigenfunctions of Laplace's tidal equations which govern fluid motion on a rotating sphere) structures, and hence latitudinal variabilities of the two wind components of a planetary wave [*Luo et al.*, 2002b].

The wavelet analysis covers a time interval of just over two years to demonstrate how the character of the PW activity changes with season. Winter months at mesospheric heights are known for their strong PW activity over a wide frequency range. In summer months long period (>10d) oscillations, which are the prominent winter features, disappear and oscillations with shorter periods (<10d) become dominant. During summer time there is an indication of quasi-two–day wave activity in both components. These oscillations seem to have larger amplitudes in the NS wind component above 82 km. Occasionally some quasi 16-day peaks are found in summer. For example, there is a peak near 12-14 days in EW wind wavelets in the beginning of July 2001 with the largest amplitudes at 82 km. This is believed to be ducted from the Southern Hemisphere (see Sections 3.3. and 3.4). Spring and autumn are transition times with strong trends in mean winds and some wave activity with periods around 10-12 and 5-8 days. Combining information obtained from Figure 1.3 and Figure 1.4 it can be concluded that the variability in the mesospheric winds is caused primarily by long-period (>10 days) PW during winter time, while the quasi-two–day wave is the dominant feature of the summer mesosphere.

Comparison of the wavelets at different heights suggests that the amplitudes of the long-period oscillations in winter tend to decrease with height in the upper mesosphere, in contrast to the stratospheric heights, where they steadily increase above ~100 hPa (see for example, Figure 2.6). During the summer season the wavelets look noisier in the mesosphere and the short-period oscillations became stronger with height, e.g. above 100 hPa (~16 km) there is very weak or no activity at periods longer than 2 days until the mesospheric heights.

1.3 **Possible Sources of the Mesospheric Variability**

Different coupling processes that could be responsible for the mesospheric long-period variabilities have been named and illustrated in the literature. These are the possible sources:

- PW that have been forced in the troposphere and propagated upward [*Charney and Drazin*, 1961].

- PW that propagate from another hemisphere through a "wave guide" during summer (16-day wave) and equinoctial transitions [*Dickinson*, 1968].

- Oscillations generated in situ by GW, whose upward fluxes have been modulated by PW at low heights. *Smith* [1996, 2003] have demonstrated the importance of coupling by GW using High Resolution Doppler Imager (HRDI) measurements (Upper Atmosphere Research Satellite, UARS, satellite) and model calculations. Significant portions of the GW spectrum generated in the troposphere can propagate vertically. On their way up they are filtered due to interaction with stratospheric winds associated with PW. Those GW that reach mesospheric heights generally dissipate and deposit momentum, and as a result can generate planetary-scale disturbances in situ.

- Perturbations result due to non-linear interactions between all of above [*Carter and Balsley*, 1982; *Manson et al.*, 1982]. *Pancheva et al.* [2003] investigated variations (3-100 days) of the semidiurnal (12h) tide observed in the MLT region by the meteor radar located in Sheffield (53^{o}N). Among other results, they have shown that during winter the amplitude modulations of the semidiurnal tides have periods ~10, ~16 and ~25-28 days, and that similar temporal variations have been simultaneously present in the total ozone (vertically integrated column content). This was one of the first studies involving satellite data from the stratosphere and MLT radar data. The phase relationships between variations in total ozone (in the lower stratosphere) and those in 12h tide (in the MLT) suggested that, in most of the cases, the amplitude modulations of the semidiurnal tides observed in the MLT region were mainly

produced by non-local coupling between the semidiurnal tide and PW in the stratosphere.

- Oscillations with PW periods have also been observed in the thermosphere-ionosphere system [*Parish et al.*, 1994; *Lastovicka*, 1997; *Gurubaran et al.*, 2001]. The geomagnetic activity variability is a likely candidate for the majority of the wave-like perturbations observed. Although some of the oscillations are believed to originate at lower heights, study of the physical processes underlying the penetration of various PW into this region is sparse [*Meyer and Forbes*, 1997; *Meyer*, 1999] and still poorly understood. There are also oscillations that do not have obvious connections either to the geomagnetic activity or to the mesospheric wind variabilities [*Altadill and Apostolov*, 2003], but might be linked to other forcing mechanisms that exist in the MLT region, e.g. gravity wave dissipation, solar radiation absorption, Joule heating, etc. The downward coupling is considered less significant.

It is impossible to include investigation of all sources of mesospheric variability in one thesis. Therefore this work was limited to the study of the mesospheric variability due to PW with periods from 2 to 30 days that had propagated from tropospheric heights (the first two coupling processes above).

1.4 **Planetary Waves**

Planetary or Rossby Waves (PW) are perturbations of a global (thousands of km) scale with periods of 2 to 30 days. They exist due to the variation of the Coriolis force with latitude and are generated by large-scale weather disturbances, land-sea temperature contrasts and topography. PW play a significant role in the dynamics of the middle atmosphere by transmitting energy and momentum across large distances, and by redistributing gas constituents of the atmosphere [*Holton*, 1972; *Andrews et al.*, 1987; *Salby*, 1996]. These waves are associated with many observed large-scale disturbances such as sudden stratospheric warmings, and are a main cause of differences between the dynamics of the Northern and Southern Hemispheres.

To examine PW, first the vorticity equation is formed from prognostic equations (1.3) in the isobaric coordinates [*Holton,* 1972]. The x and y component equations are differentiated with respect to y and x, respectively. By subtracting the resultant equations and assuming the divergence term is zero (the motion can be represented in terms of a streamfunction Ψ, which is defined so that the velocity components are given as $u = -\frac{\partial \Psi}{\partial y}$, $v = \frac{\partial \Psi}{\partial x}$) we will obtain:

$$\left(\frac{\partial}{\partial t} + u\frac{\partial}{\partial x} + v\frac{\partial}{\partial y}\right)\varsigma + v\frac{df}{dy} = 0, \tag{1.6}$$

where $\varsigma = \hat{k} \cdot \nabla \times \vec{V} = \frac{\partial v}{\partial x} - \frac{\partial u}{\partial y}$ is the vertical component of vorticity, the microscopic measure of rotation in a fluid, which is defined as the curl of velocity.

Then using perturbation theory the motion is decomposed into a basic state zonal velocity and a deviation of the field from the basic state. Assuming that $\beta = df/dy$ is a constant and neglecting the products of perturbations, the linearized perturbation form of (1.6) is obtained:

$$\left(\frac{\partial}{\partial t} + \bar{u}\frac{\partial}{\partial x}\right)\nabla^2\Psi + \beta\frac{\partial \Psi}{\partial x} = 0, \tag{1.7}$$

where $\bar{u}$ is the mean zonal wind.

Substituting an assumed solution $\Psi = Ae^{ik(x-ct)}\cos ly$ into (1.7) gives the dispersion relation for Rossby waves:

$$c - \bar{u} = -\frac{\beta}{k^2 + l^2}, \tag{1.8}$$

where $k = 2\pi/\lambda_x$ is the zonal wave number, c is the zonal phase speed (related to the ground observations), and $l = 2\pi/\lambda_y$ is the meridional wave number. The equation shows that the PW propagate westward relative to the mean flow ($c - \bar{u} < 0$) and that their speed depends on the zonal and meridional wave numbers, e.g. the waves are dispersive. The propagation of these waves also depends crucially on the zonal mean flow. It was shown by *Charney and Drazin* [1961] that, when the background winds are eastward, as in winter, only the longest wavelength PW can propagate vertically; and that in summer PW frequently encounter "critical levels" ($c = \bar{u}$) due to the westward winds:

$$0 < \bar{u} - c < u_c \equiv \frac{\beta}{k^2 + l^2}. \qquad (1.9)$$

Here u_c is the so-called critical speed. Conditions for westward propagating PW are illustrated in Figure 1.5 for winter (left) and summer (right). The arrows represent waves with different phase velocities, and those that do not meet the propagation conditions (eq. 1.9) are marked by crosses. The height profile of the background wind is shown by thick lines, the dashed vertical line indicate critical speed (which is different for different waves).

For stationary waves (wave phase is fixed with respect to the Earth), which were the main interest of *Charney and Drazin* [1961], c=0; so they can exist only in relatively weak eastward winds. Stationary planetary waves, since they are dispersive, may still propagate information, because the group velocity may be non-zero even if the phase velocity is zero.

Many of the planetary waves (PW) of the middle atmosphere can be identified with the well-known "normal" atmospheric modes, which correspond to free oscillations of the terrestrial atmosphere [*Dikii,* 1965; *Longuet-Higgins,* 1968] modified by the background wind and temperature. Although these waves are not maintained by specific forcing effects, some mechanisms such as random disturbances in the atmosphere and/or fluctuations of the mean winds must excite them. The baroclinic or barotropic

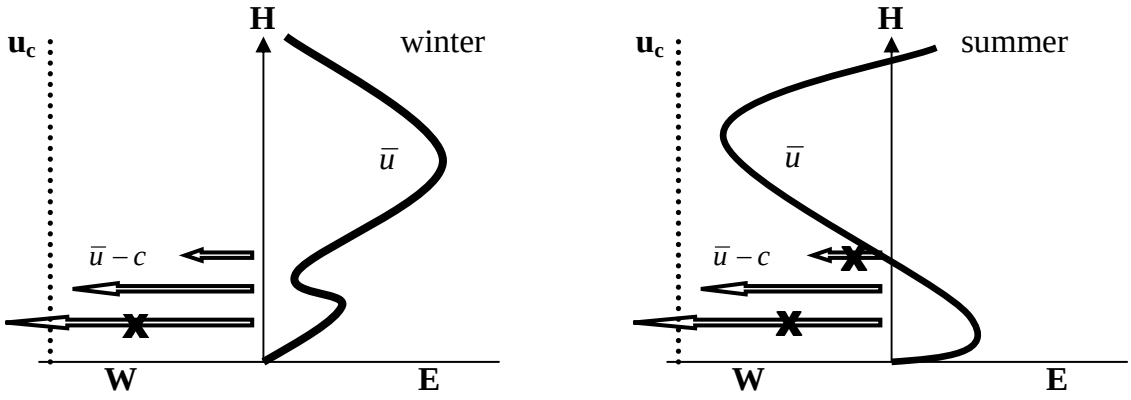

Figure 1.5 Sketch of the upward propagation of westward PW with different phase speeds (c) in the presence of the winter- (left) and summer-like (right) zonal winds ($\bar{u}$).

instabilities (which are associated with vertical and horizontal wind shears, respectively) of the background state can also generate normal modes that grow in time. For instance, recent interpretation of a quasi 2-day wave (Chapter 5) includes both the normal mode and baroclinically unstable waves.

1.5 Overview of the Presentation

In Chapter 2 the datasets and methods used throughout this study for analyses are introduced. The main body of the thesis is divided into four separate topics and presented in 4 chapters. Each of these chapters includes a review of the literature relevant to the topic, results, their discussion, and short summary. In Chapter 3 the results of the analyses of the eastward and westward propagating perturbations in different parameters at stratospheric and mesospheric heights during different seasons are reported. A case study of the vertical and inter-hemispheric coupling due to PW is presented in Chapter 4. The characteristics of the quasi-two day wave, the dominant feature of the summer mesosphere, are given in Chapter 5. In Chapter 6 the response of the mesospheric circulation to stratospheric disturbances is investigated. The conventional method using potential vorticity (PV) and more recent Q-diagnostic have been used to characterize the evolution of the polar vortex during winter of 2004/2005. This chapter also includes some discussion on the effects of the winter stratospheric circulation, the polar vortex in particular, on the distribution of chemical constituents such as ozone. Chapter 7 provides a summary and conclusions.

Chapter 2

DATA AND ANALYSES

This chapter describes datasets and methods used to analyze them. Radar mesospheric winds (Sections 2.1) and MetO fields (Section 2.2) are the main datasets employed throughout the thesis to characterize the mesospheric and stratospheric regions, respectively. For comparison and validation purposes supplementary datasets such as TOMS total (column) ozone (Section 2.4), Aura MLS (Section 2.5), and NCEP/NCAR data (Section 2.6) have also been employed. The wavelet transform, cross-wavelet, and wave number analysis were applied to the data. The methods are discussed in Section 2.7 and Section 2.8, respectively. A note on the effects of mean zonal variability on the wavelet amplitudes (Section 2.9) concludes this chapter.

2.1 Mesospheric Winds

To study dynamics at mesospheric heights (60-100 km), the meridional (NS) and zonal (EW) components of the winds obtained by MFR and MWR (Meteor Wind Radar) were used. The daily mean wind data from selected heights were provided by 12 mid- and high-latitude stations. The coordinates of the stations, main parameters and references that contain more detailed description of these radars are given in Table 2.1.

MFR employ the spaced antenna technique [*Fraser,* 1965] to detect motions of weakly ionized irregularities in the ionospheric D (~50-90 km) and lower E (~90-110 km) regions. The radar transmits energy vertically and receives the signals reflected from the weakly ionized part of the atmosphere (50-110 km). At these heights the collision frequency is high (10^{7}-$10^{4}s^{-1}$, [*Tohmatsu,* 1990.]) and number density of the neutral air

Table 2.1 Characteristics of the radars

Station	**Longitude, deg. East**	**Latitude, deg. North**	**Radar type**	**Frequency, MHz**	**Heights, km**	**References**
Collm	13	51.3	SKiYMET	32.6	82-97 (3)	*Jacobi et al.* [2005]
Andenes	16	69.3	MFR(ATRAD)	1.98	82-96 (2)	*Singer et al.* [1997]
Svalbard	16	78	VHF (ATRAD)	31	82-97 (3)	*Hall et al.* [2003]
Tromso	19.7	69.3	MFR	2.78	55-97 (3)	*Hall* [2001]
Esrange	20.4	67.9	SKiYMET	32.5	82-97 (3)	*Mitchell et al.* [2002]
Obninsk	36	52	MWR beam	33.3	~94	*Portnyagin et al.* [2006]
Wakkanai	142	45	MFR(ATRAD)	1.9585	60-96 (2)	*Murayama et al.* [2000]
Poker Flat	212.5	65.1	MFR(ATRAD)	2.43	60-96 (2)	
Yellowknife	245.5	62.5	SKiYMET	35.65	82-97 (3)	*Hocking* [2004]
Saskatoon	252	52	MFR	2.219	55-97 (3)	*Manson et al.* [1973]
Platteville	255	40	MFR	2.219	55-97 (3)	*Manson et al.* [2003]
Resolute Bay	265	74.5	SKiYMET	51.5	82-97 (3)	*Hocking* [2004]

is larger than that of the ionized part of the atmosphere. Therefore it can be assumed that the motion of the neutral gas drags the ionized patches along with it, e.g. the movement of the ionized patches (patterns) is due to the neutral wind. Radio waves reflect from these moving patches at a certain height, and the resulting horizontal diffraction pattern is sampled at three or more non-collinear separated receiving antennas on the ground. Knowing the geometry of the receiving antenna arrays and the time differences between the data sequences obtained at each of them, the horizontal wind speeds can be inferred from the radar measurements by estimating the spatial and temporal scales of the diffraction pattern using "Full Correlation Analysis" (FCA) [*Briggs,* 1984]. The variation of this method developed by *Meek* [1980] is used to obtain wind velocities from the Saskatoon MFR. *Thayaparan et al.* [1995] compared winds calculated using these two methods and found no significant difference between them. Partial reflections typically occur from heights throughout the D-region, and this makes it possible to construct vertical profiles of horizontal wind speeds. Several comparisons of the MFR winds with those from rockets [*Meek and Manson,* 1985; *Manson et al.,* 1992] at similar heights, co-located Fabry-Perot interferometer [*Manson et al.,* 1996] and additionally satellite data [*Meek et al.,* 1997] at mesopause heights (80-100 km) have shown that while there is very good agreement in the direction of the winds, the speeds measured by MFR are systematically low by factors of typically 1.5 (33% low) at the upper heights. However the most recent comparisons between co-located MWR and MFR (discussed later on p.20-21) demonstrated smaller differences (up to 1.2 factor) in winds measured by these systems.

All MFR are of similar configuration. As an example the MFR installed near Saskatoon is described in more detail. This radar operates at a frequency of 2.219 MHz, with a pulse width Δt of 20 μs, and a repetition rate of 60 Hz (17ms between pulses). The height resolution is 3 km, which is determined by $c\Delta t/2$, where c is the speed of light in a vacuum. The transmitting array consists of 16 dipoles with the full beam width of ~45 deg., which corresponds to a region with an approximately 70 km diameter at mesospheric heights. The peak power is 20 kW. Three receiving antennas (4 dipoles each) form an equilateral triangle with a side of two wavelengths (270 m) and one antenna (2 dipoles) is located in the center of this triangle. The distance between the

central and outer antennas is 156 m. Each antenna has its own receiver with simultaneous sampling every 5 minutes for 32 heights from 40 up to 133 km. The resulting 5-min wind data are averaged to get hourly mean winds. Figure 2.1 gives an example of the hourly meridional (V_N, the top panel) and zonal (V_E, the middle panel) wind components for six heights measured during January of 2002. Although the 12-hour oscillation (semi-diurnal tide) dominates wind variability, long-period oscillations (circa 8 days) are also evident as the modulation of the tide, especially in the zonal component.

As can be seen from the bottom panel of Figure 2.1, the number of measurements varies during the day. At low heights there are more echoes around local noon as the ionization and hence the reflected signal is higher during the day than at night. Above 80 km, ionization levels for 24 hrs are large enough to provide continuous data. Normally, at least 16 values are required to produce tidal fit and mean daily parameters, which are used to study tides [*Manson et al.,* 2002b] and long-period perturbations [*Luo et al.,* 2002b]. The authors of the later paper showed that 6 values per day is sufficient for PW studies. In the study of the quasi-two-day wave (Chapter 5) the hourly data have been involved. The minimum number of values required to form useful hourly mean values is typically 2 values per hour [*Luo et al.,* 2002b]. Saskatoon MFR has operated in continuous mode since 1979, which makes it possible to study variabilities of the winds in the wide range of periods from hours to the 11-year solar cycle.

The radar at Saskatoon (52^{o}N, 107^{o}W) along with four MFR installed in London (43^{o}N, 81^{o}W), Platteville (40^{o}N, 105^{o}W), Wakkanai (45^{o}N, 142^{o}E) and Yamagawa (31^{o}N, 131^{o}E) form a CUJO (Canada U.S. Japan Opportunity) network. The two pairs of stations, Saskatoon-Platteville and Yamagawa-Wakkanai, have similar longitudes, while London, Platteville and Wakkanai are located in the narrow latitudinal zone 40-45^{o}N. Such a distribution of stations allows a study of latitudinal as well as longitudinal variabilities [*Manson et al.,* 2004a]. The data obtained at these radars have been used to study the vertical and inter-hemispheric coupling due to PW (Chapters 3 and 4).

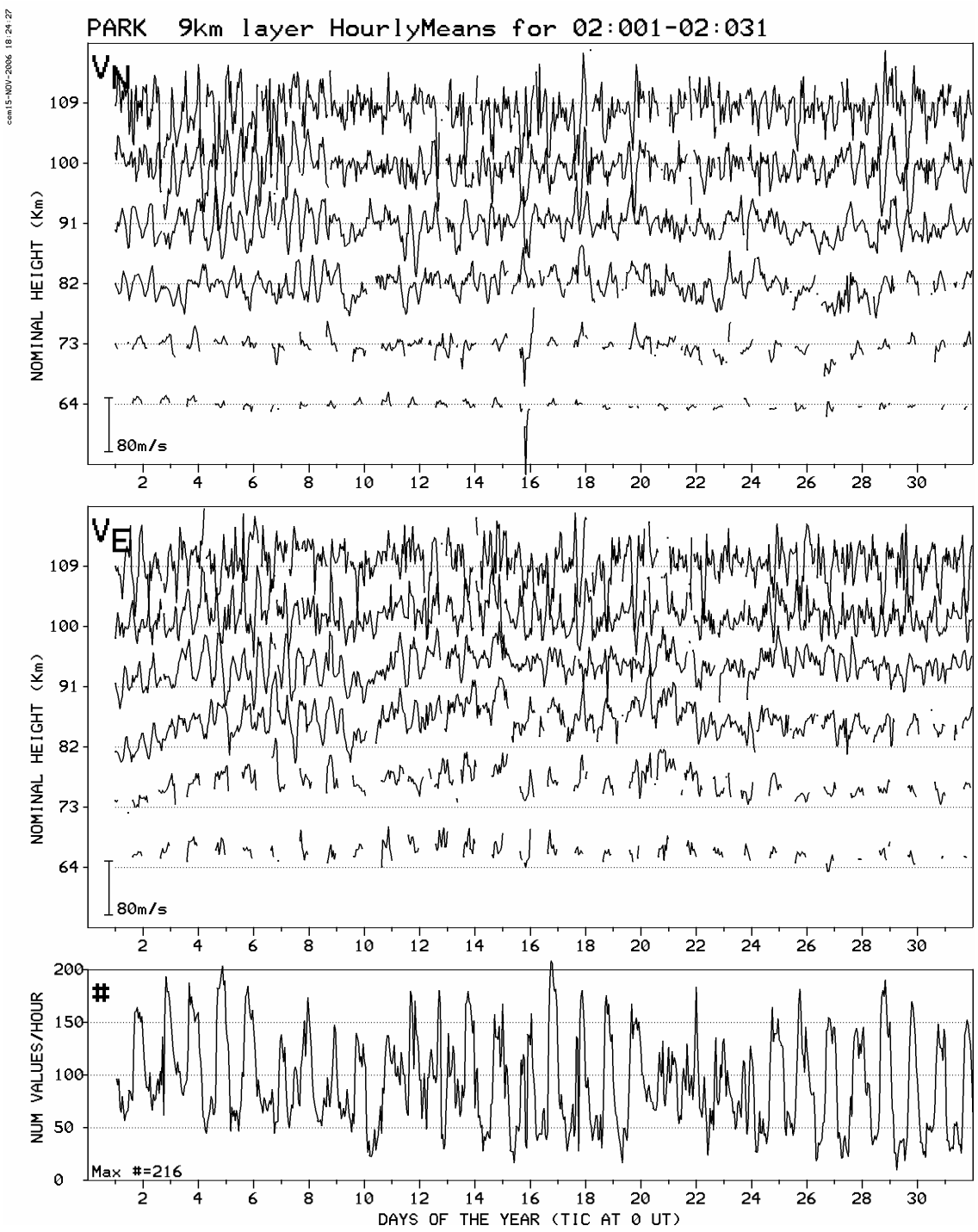

Figure 2.1 Example of the hourly mean meridional (V_N, top panel) and zonal (V_E, middle panel) winds measured with the MFR at Saskatoon (52^oN, 105^oW) for six heights during January of 2002. The bottom panel demonstrates changes in the number of measured values per hour. (This format is used as a "first look" at the data: http://www.usask.ca/physics/isas.)

To investigate the evolution of the winter polar vortex (Chapter 6) additional data have been supplied by Professors/Principal Investigators (PIs) at mid- and high-latitudinal MFR and MWR stations. Most of the MWR (except Obninsk) are commercially produced HF/VHF All-Sky Interferometric Meteor Radars by ATRAD (Atmospheric Radar Systems Pty Ltd, Australia) or by MARDOC Inc. (Modular Antenna Radar Designs Of Canada) together with Genesis Software Pty. Ltd (SKiYMET radars). Detailed description of the hardware, detection algorithms and data handling can be found in the paper by *Hocking et al.* [2001]. Briefly, meteor radars (MWR) operate at a fixed frequency in the range from 20 to 50 MHz. There is one transmitter antenna and a peak power is generally 6 kW. The radar detects the part of transmitted energy that is reflected back from the meteor's trail of ionized gas using 4 or 5 receiving antennas, which are spaced by typically 1.5-3 wavelengths. Then the atmospheric wind velocities are deduced by observing how the meteor trail drifts with time (Doppler velocity). The VHF all-sky system employs interferometric techniques to determine the angular location (azimuth and elevation) of a meteor and operates at very high pulse repetition frequencies (~2 kHz), which makes it possible to obtain additional meteor parameters such as entrance speeds. The pulse width is usually chosen so that the vertical resolution is 2 km. Over Obninsk the height determination is not available and measurements are assumed to be from ~90-95 km [*Lysenko et al.,* 1994].

Both MWR and MFR provide horizontal winds in the MLT region. However, they employ different measurement techniques, use different assumptions for the wind estimation, and have their own limitations. For example, the fields of view are approximately 45 and 140 degrees for MFR and MWR, respectively. There are also other parameters, such as signal-to-noise ratio and instrumental characteristics that can contribute to the discrepancies between observations. Several results on wind comparisons obtained by co-located MF and VHF systems have been published [*Cervera and Reid,* 1995; *Thayaparan and Hocking,* 2002; *Hall et al.,* 2005]. Although these studies employed different comparison methods and radar systems installed at various locations (Australia, Canada, and Norway), the conclusions are similar. The mesospheric wind velocities as determined by meteor and MF radars demonstrate excellent agreement below 90 km. Above ~90 km, probably due to the group delay

(radio waves propagate with speeds less than the speed of light near the heights of total reflection), the MF radar data are of lower quality; and while wind directions agree well with those from MWR, speeds are smaller: real heights are not easily estimated [*Nozawa et al.,* 2002]. Based upon more recent and detailed comparisons, in general the MFR meridional wind speeds are systematically lower by 20% at the upper heights, while the zonal component shows "modestly altitude-dependent" differences [*Hall et al.,* 2005].

2.2 **MetO Data**

To complement radar observations at mesospheric heights, the MetO (from the United Kingdom Meteorological Office, also well-known as UKMO) temperatures and horizontal wind components are used. The MetO data are results of assimilation of operational meteorological measurements from satellite, radiosondes, and aircraft into a numerical forecasting model of the stratosphere and troposphere. The UK Met. Office numerical forecasting model, the so-called Unified Model, is based on a set of primitive equations (such as eq. 1.1 in Section 1.1) and incorporates several physical parameterizations (see *Swinbank et al.* [1998] or http://metoffice.com/ for more details). The model, also described as a Global Circulation Model (GCM), produces realistic stratospheric circulations [*Swinbank et al.,* 1998] and, after a gravity wave parameterization [*Warner and McIntyre,* 1999] was introduced in year 2000, such features as the Quasi-Biennial Oscillation and improved Semi-Annual Oscillation [*Scaife et al.,* 2000] also emerged. Operators or PIs of such models consider the output of such GCM to be "data", and that word is used here.

An analysis technique that fits the model to observed data is described by *Swinbank and O'Neill* [1994]. This analysis is developed on a basis of the "Analysis Correction" scheme used for operational weather forecasting [*Lorenc et al.,* 1991]. Since November 2000 the MetO fields have been produced using a new 3D variational (3DVAR) data assimilation system [*Lorenc et al.,* 2000]. Generally, the new analysis fits observations more closely than previous analyses and its forecasts are improved in the low latitudes and the Southern Hemisphere [*Swinbank et al.,* 2002]. There are no big differences in

forecasts from the two different analyses for the Northern Hemisphere. Also, the new scheme tends to have comparatively fewer worse forecasts in the stratosphere.

The outputs of the assimilation are global fields of daily temperatures, geopotential heights and wind components interpolated to 22 standard UARS pressure levels from the surface up to 0.316 hPa (0-55 km):

$$p(i)=1000*10^{-i/6},\ i=0,\ 1,\ldots,\ 21.$$

In October 2003 the New Dynamics version of the Unified Model was introduced and three more levels (up to 0.1 hPa≈64 km) were added. The generated data fields have global coverage with 2.5^{o} and 3.75^{o} steps in latitude and longitude, respectively.

Estimates of the errors in the analyzed fields are 1 K and 6 m/s at low heights (<100hPa). These estimations are from the documentation provided by the team of the Met Office through the British Atmospheric Data Centre (BADC, http://badc.nerc.ac.uk/). In general, the errors are predicted to be larger at high latitudes and at the uppermost levels. Intercomparisons of different climatological data sets for the middle atmosphere (MetO/UKMO, ECMWF, NCEP, CIRA86, etc.) revealed uncertainties and problem areas [*Randel et al.*, 2004]. The MetO data, for instance, showed cold temperature biases (~5K) near the stratopause (upper levels of the model) and warm tropical tropopause temperatures (~1-2 K). Note however that the data used for these comparisons are from earlier years (1992-1997), before later improvements in the model and assimilation technique.

The MetO data have been used by several researchers to study different dynamical phenomena including planetary waves [*Fedulina et al.*, 2004], inertial circulation [*Orsolini et al.*, 1997], and sudden stratospheric warmings [*Manney et al.*, 1994; *Cho et al.*, 2004]. They are proving to be very useful in understanding troposphere/stratosphere dynamic processes.

The British Atmosphere Data Centre (BADC) provides access to the UK Meteorological Office stratospheric assimilated data. The data are free, but restricted to academic use only and require application to access the dataset. Data are regularly downloaded from the BADC website and stored on CDs.

2.3 Comparison of the MetO and Radar Winds

We now compare MetO and MFR winds, as this will speak to the value of the data assimilation product at the top of the MetO dataset. Such comparison is new. Zonal components (east-west) of the MetO (low panel) and MFR (middle panel) horizontal winds are shown in Figure 2.2. We have retained the pressure coordinates for MetO data throughout the thesis, but also cited an approximate height in km, where MetO are used along with radar data. The table with the conversion for 22 pressure levels can also be found in Appendix A. As can be seen from the figure there is very good general agreement for the transition heights between the two data sets: the winds are westward in summer and eastward in winter with clear equinox transitions. Strong dynamical events, such as those associated with stratospheric warmings, are also evident in both data sets. For example, during the "stratwarm" that occurred from the end of January to the beginning of February 2000 ("stratalert" information at ftp://strat50.met.fu-berlin.de/pub/stratalert/1999_2000) both MetO and MFR data sets show a reversal in the zonal (Figure 2.2) and meridional winds (Figure 2.3). On the other hand, the speeds near 55 km from MetO and MFR did not initially agree well. As was discussed in Section 2.1 the speeds measured by MF radars are systematically low by factors of up to 1.5. To account for possible bias, the MFR winds for Figure 2.2 and Figure 2.3 have been multiplied by a 1.5 factor before plotting. With this adjustment, the speeds recorded by the two systems are quite similar.

In the upper panel the contours of the cross-correlation coefficients between the winds at the highest MetO pressure level (0.32 hPa) and MFR winds at 58 km are shown. The correlation coefficients have been calculated using a 30-day window shifted by 10 days. Each 30-day time interval has been linearly detrended. Maximum values tend to occur near zero lags in all seasons. Without detrending the cross-correlation coefficient would be highest during equinox transitions. These would be due to strong wind trends existing during these months, while we are interested in wind features of smaller scale (several days). The slight shift of the maximum cross-correlation coefficients from lag=0 toward lag=1 day could be due to the 7-hour shift between MetO (12:00 UT) winds and Saskatoon daily winds defined as 24 hrs of local time. The relatively low

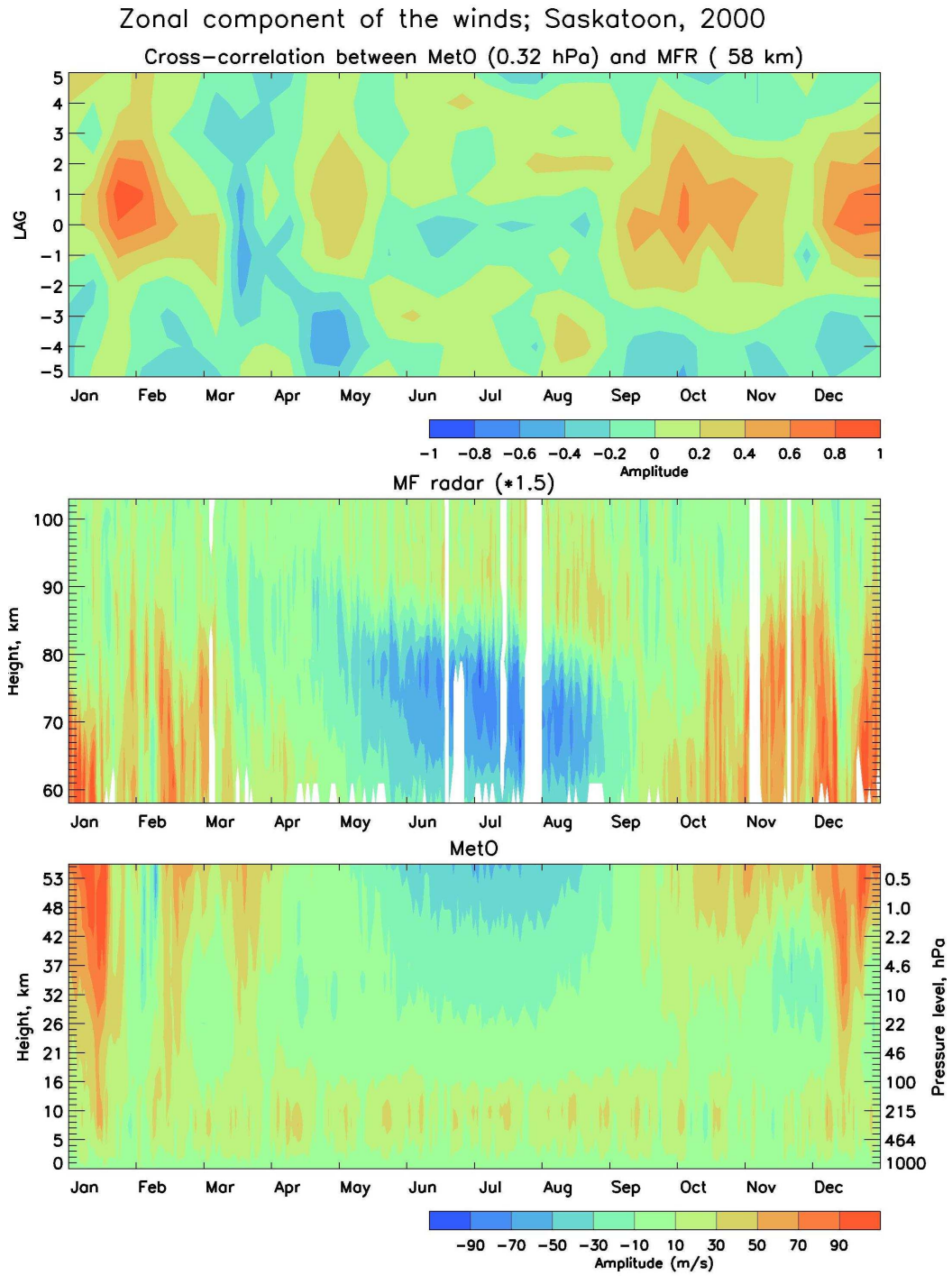

Figure 2.2 The contour plots of zonal winds from MetO (the bottom panel) and MF radar (the middle panel) for Saskatoon during 2000. The cross-correlations calculated between the MetO winds at 0.32 mbar (~ 55 km) and MFR winds measured at 58 km are shown on the upper panel.

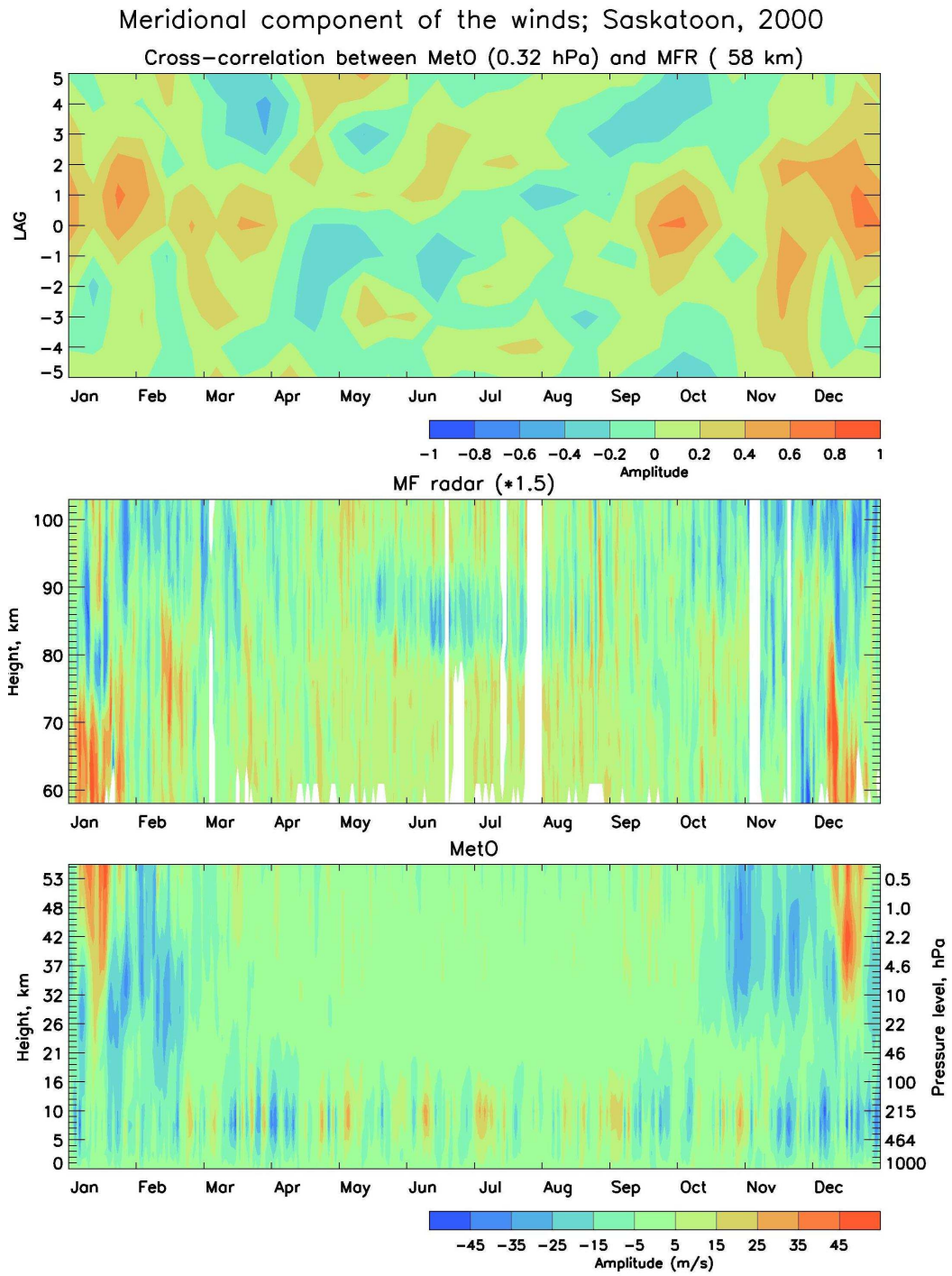

Figure 2.3 The same as Figure 2.2, but for meridional (NS) wind component

correlation coefficients, and their time shift, could also be explained by the potentially poorer reliability of the daily data parameter at the highest MetO and lowest MFR levels.

2.4 **TOMS Data**

The Total Ozone Mapping Spectrometer (TOMS) on board the Earth Probe (EP) satellite measures the total number of ozone molecules between the surface of Earth and the top of the atmosphere. The amount of ozone in this column is numerically expressed in Dobson Units. The daily product is available with a fixed global grid, which is 1 degree in latitude by 1.25 degrees in longitude. The total ozone (hereafter this phrase or "ozone" is used) daily samples for any particular location are measured near local noon. The TOMS algorithm development, evaluation of instrument performance, ground-truth validation, and data production were carried out by the Ozone Processing Team at National Aeronautic and Space Administration/Goddard Space Flight Center (NASA/GSFC). The official TOMS website, http://jwocky.gsfc.nasa.gov/, offers free access to their data as well as more detailed information about spacecraft, instrument technical specifications and data processing.

2.5 **Aura MLS Data**

As a supplement we have also employed temperatures measured by the Microwave Limb Sounder (MLS, [*Waters et al.*, 2006]) onboard the NASA Aura satellite. The Aura spacecraft was launched on July 15, 2004 on a 705-km sun-synchronous near-polar orbit with a 98.2^{o} inclination. It has a 16-day “repeat cycle” and 233 revolutions per cycle. The temperature used here are MLS data produced by the “version 1.5” data processing algorithms (along the measurement track). The daily data are available for the 316-0.001 hPa (~8-100 km) altitude region and have coverage from 82^{o}S to 82^{o}N latitudes on each orbit with horizontal and vertical resolutions of 500 km and ~4 km, respectively. The first validation results [*Froidevaux et al.,* 2006] show that MLS measurements of temperature and mixing ratios of O_3, H_2O, N_2O, HCl, HNO_3 and CO agree well with other satellite and meteorological datasets, as well as balloon-measurements in the stratospheric and mesospheric regions. The precision of a single

temperature profile was estimated to be 0.5-1 K in the middle stratosphere and noisier (estimated precision up to 2 K) at the lowest (316 hPa) and highest (0.001 hPa) pressure levels. The special issue on Aura (IEEE Transactions on Geoscience and Remote Sensing 44 (5), May 2006) offers more detailed information on the technical characteristics of the instrument and retrieval algorithms.

2.6 **NCEP/NCAR Data**

NCEP/NCAR (the National Centers for Environmental Prediction and the National Center for Atmospheric Research) is another assimilation product often used for atmospheric research. These data are provided by the NOAA-CIRES Climate Diagnostics Center, Boulder, Colorado, USA, from their web site at http://www.cdc.noaa.gov/. The NCEP/NCAR Reanalysis 1 project uses a state-of-the-art analysis/ forecast system to perform data assimilation using past data from 1948 to the present. For a detailed summary of observational data used by Reanalysis, one may visit the following web site: http://wwwt.emc.ncep.noaa.gov/gmb/bkistler/oberr/reanl-obs.html. The spatial coverage of the data, in 2.5-degrees of latitude by 2.5-degrees of longitude increments, is global (90^{o}N-90^{o}S, 0^{o}E-357.5^{o}E). Data are available since the first day of 1948 until present with output every 6 hours at 17 pressure levels (from the surface up to 10 hPa, ~36km). Although NCEP/NCAR data have better spatial and temporal resolution than the MetO data for 2004/05, MetO data have been employed for the study described here as they are available up to higher levels (55-60 km), and their lower spatial resolution is not important for studying planetary scales. Since March 2006, MetO data have a global grid of 480 points in latitude and 640 points in longitude, instead of 72 by 96, providing cells of size 0.37 degrees and 0.56 degrees in latitude and longitude.

2.7 **Wavelet Analysis**

For spectral analysis of the data the wavelet transform has been employed. This analysis was introduced in the early 1980s and has become very popular in studies of different geophysical datasets, data compression, and de-noising. The wavelet transform of a

function *f*(t) is defined as follows ([*Kumar and Foufoula-Georgiou,* 1997], in which different symbols were used):

$$Wf(s,\tau) = \int_{-\infty}^{\infty} f(t)\frac{1}{\sqrt{s}}\Psi^{*}(\frac{t-\tau}{s})dt \qquad (2.1)$$

The functions $\Psi_{s,\tau}(t)$ are called wavelets; s is a scale parameter, whereby changing its value has the effect of dilating the function Ψ (the wavelet becomes more spread out) or contracting it; τ is a location parameter, which determines around what point (τ) the function *f*(t) will be analyzed. The wavelet transform provides a flexible time-scale window that narrows when focusing on small-scale (high frequency) features and widens on large-scale (long frequency) features. This sort of scale analysis is less sensitive to noise because it measures the average fluctuations of the signal at different scales.

Compared to the more conventional Fourier Transform (FT) wavelets have more advantages in analyzing nonstationary processes that contain multiscale features and short-lived transient components. While FT are localized in frequency, wavelets are local in both frequency scale (via dilations) and in time (via translations). A modification of the classical FT, the so-called Windowed Fourier Transform, allows some time localization by shifting a Gaussian window through the signal. However, the window has a constant width, so it can include different number of oscillation for waves with different periods. Wavelets allow optimization of time and frequency resolution, i.e. a narrow wavelet will have a broadband spectrum and vice versa, which means that for a given interval the time resolution will be better for the higher frequencies (a compromise between local and spectral localization). The mean wavelet spectrum is similar to the Fourier spectrum, but it is not as sharp as in the Fourier case. Also the wavelet transform has an infinite set of possible basis functions, while FT has a single set of basis functions: sine and cosine.

There are several families of wavelets with different subclasses. One of the popular wavelets, the so-called Morlet wavelet [*Kumar and Foufoula-Georgiou,* 1997], has

been chosen as a “mother” wavelet because it is simple, looks like a wave, and is widely used in geophysical applications. The Morlet wavelet is given by

$$\Psi(t) = \pi^{-\frac{1}{4}} \exp(-i\omega_0\eta - \exp(-\omega_0^2/2)) \exp(-\frac{\eta^2}{2}), \qquad (2.2)$$

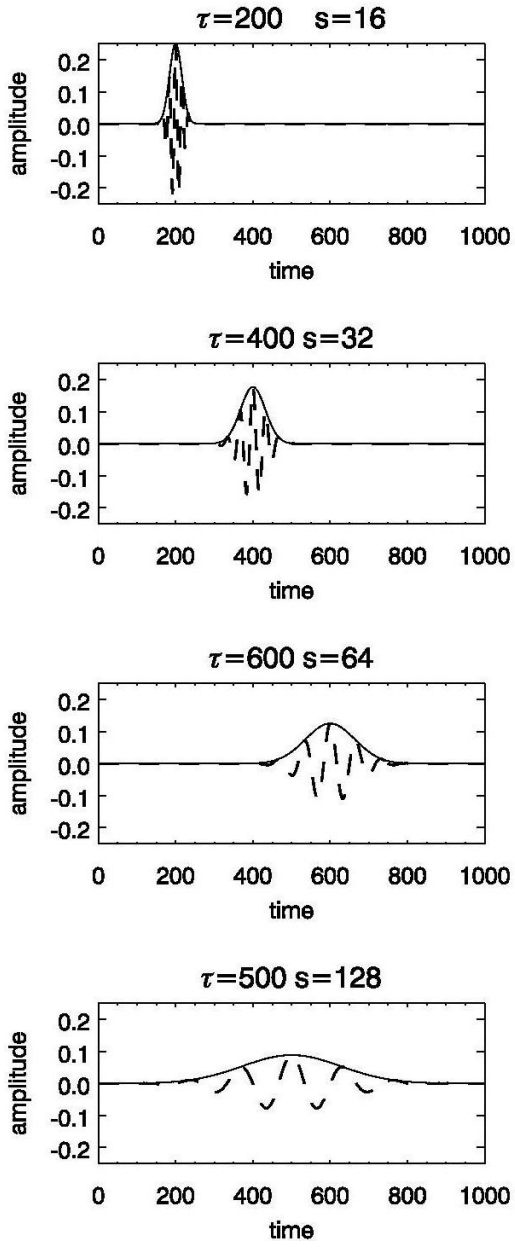

Figure 2.4 Examples of the Morlet wavelet for different τ and s.

where $\eta = \frac{t-\tau}{s}$.

The nondimensional frequency, the so-called "wave number" (ω_0) has been chosen equal to 6: this effectively is the number of oscillations windowed for each frequency in the wavelet. For ω_0=6 this expression can be approximated as

$$\Psi(t) = \pi^{-\frac{1}{4}} \exp(-i\omega_0\eta) \exp(-\frac{\eta^2}{2}) \qquad (2.3)$$

and the width of the Gaussian is tailored (through s) to match the chosen ω_0 for each frequency. Also for ω_0=6 the errors due to a non-zero mean are smaller than the typical computer round-off errors. Example of the Morlet wavelet (dashed line) for different sets of τ and s parameters is demonstrated in Figure 2.4. The solid line illustrates the Gaussian window.

The continuous wavelet transform of a discrete time series *x(t)* [with equal time spacing δt and τ=0…N-1] is defined as the product of normalized Ψ and x:

$$W_\tau(s) = \sum_{t=0}^{N-1} x_t \Psi^* \left[\frac{(t-\tau)\delta t}{s} \right]. \qquad (2.4)$$

The superscript (*) denotes a complex conjugate. A more efficient algorithm of wavelet transform calculations has been adopted from *Torrence and Compo* [1998]. They used the fact that the wavelet transform is the convolution between the two functions and carried out the wavelet transform in Fourier space using a fast FT. So, in the frequency domain the wavelet transform is a band-pass filtered FT:

$$W_\tau(s) = \sum_{k=0}^{N-1} \hat{x}_k \hat{\Psi}^*(s\omega_k) e^{i\omega_k t\delta t}, \tag{2.5}$$

where k is the frequency index, and. a "hat" indicates the Fourier Transform

$$\hat{x}_k = \frac{1}{N}\sum_{t=0}^{N-1} x_t e^{\frac{-2\pi i k t}{N}}.$$

To be able to compare directly the wavelet transforms at each scale s, the wavelets must be normalized:

$$\hat{\Psi}(s\omega_k) = \left(\frac{2\pi s}{\delta t}\right)^{1/2} \hat{\Psi}_0(s\omega_k) = \left(\frac{2\pi s}{\delta t}\right)^{1/2} \pi^{-1/4} H(\omega) e^{-(s\omega - s\omega_0)^2/2},$$

where H(ω) is the Heaviside step function, which is equal to 1 if ω>0, and is zero otherwise. The angular frequency is defined as

$$\omega_k = \begin{cases} +\dfrac{2\pi k}{N\delta t}, k \le \dfrac{N}{2} \\ -\dfrac{2\pi k}{N\delta t}, k > \dfrac{N}{2} \end{cases}$$

The set of scales is convenient to choose as fractional powers of 2:

$$s_j = s_0 2^{j\delta j}, \qquad j = 0,1,\ldots,J$$

$$J = \delta j^{-1} \log_2\left(\frac{N\delta t}{s_0}\right)$$

s_0 is the smallest resolution scale equal to ~$2\delta t$. The wavelet scale is not usually equal to the period of the oscillations, but each wavelet has a specific relationship for these two parameters. The ratio between the "true" Fourier period and the scale of the Morlet wavelet (s) with ω_0=6 is 1.03 [*Torrence and Compo*, 1998].

It is necessary to remember that large values of the function (wavelet coefficients) reflect the combined effects of a large fluctuation of the signal at this time and of a good

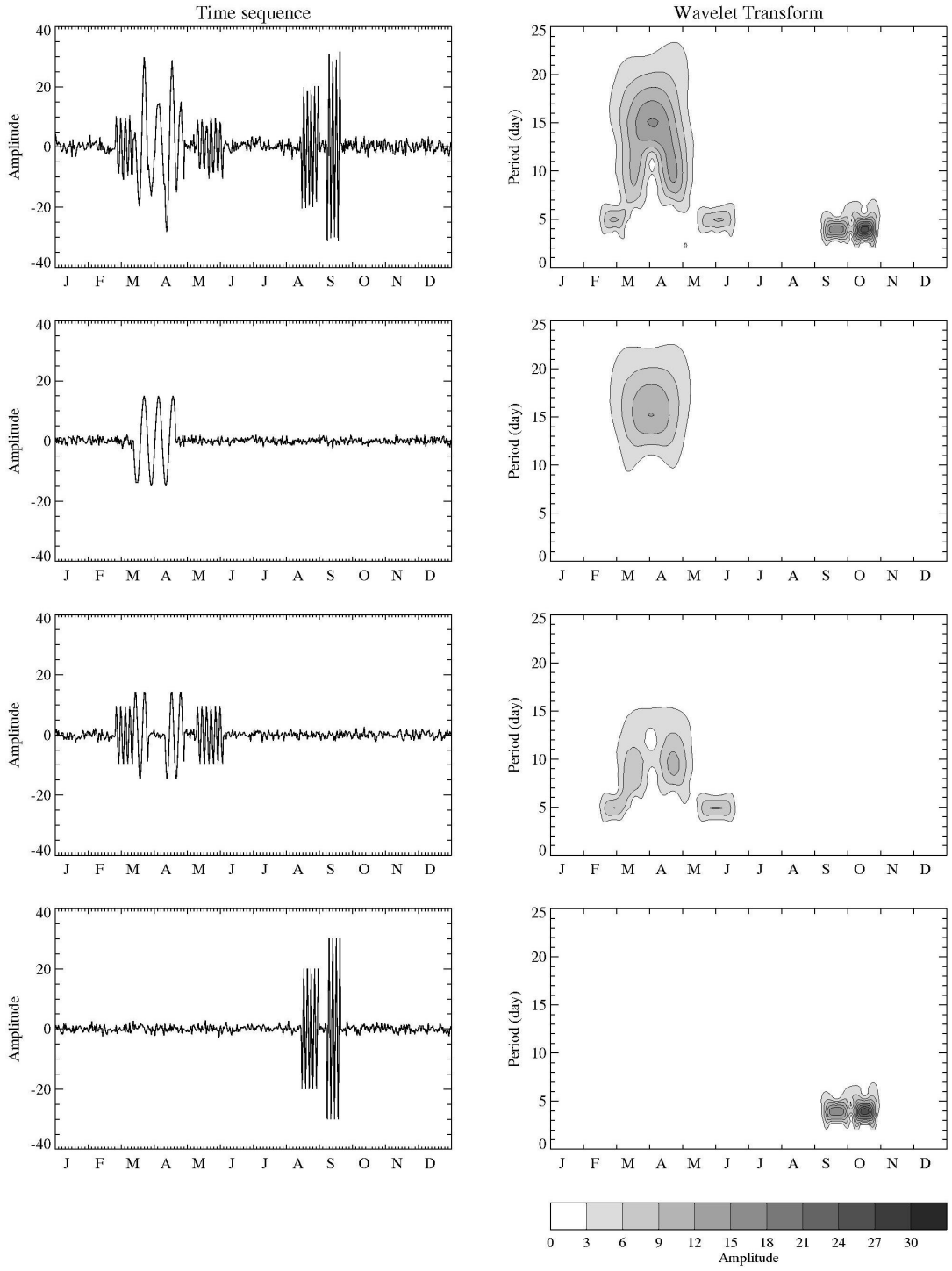

Figure 2.5 The time sequences (left column), constructed as a sum of finite oscillations with different periods and amplitudes and white noise; and their wavelet transform (right column).

matching of shape between the signal and the wavelet. Some examples of the wavelet transform of the modeled time sequences, which were constructed as a sum of white noise and finite oscillations with different periods (4, 5, 10 and 15 days) and amplitudes (from 10 to 30 arbitrary units) are illustrated in Figure 2.5. The time sequence shown on the top panel represents the sum of time sequences from the three lower plots. The wavelet transforms of these time sequences demonstrate very good time and period location of the oscillations. Note, however, that sometimes the amplitudes of the peaks are a little smaller than in the original time sequences, especially if the duration of the oscillation is very short. This could be attributed to the effects of the Gaussian window.

The cross wavelet spectra are calculated as $W_{XY} = \tilde{X}\tilde{Y}^*$, where $\tilde{X}$ and $\tilde{Y}$ are wavelet transforms ($W_\tau(s)$ in equation 2.5) for the time series data x(t) and y(t), respectively [*Liu*, 1994]. An asterisk superscript indicates the complex conjugate. The algorithm of the wavelet and cross-wavelet calculations was adopted from *Torrence and Compo* [1998].

In general, to assess significance of spectral features, the power spectrum of a time series is tested against a mean (background) power spectrum. Here the "global wavelet spectrum" (GWS) was chosen as a background spectrum. It was calculated by averaging all local (in time) wavelet spectra over the whole time interval ([*Torrence and Compo*, 1998], their eq. 22). Confidence levels were calculated for the GWS and peaks in the local wavelets were compared against them. For example, on the wavelet plots (such as Figure 1.4) black thick solid lines encircle areas where the spectral features were higher than the 90% confidence level.

2.8 **Wave Number Analysis**

The Least Square (LS) fit or FT (depending on whether data are regularly spaced or not) is used to calculate amplitudes, at fixed latitude and height, of the oscillations for pre-selected frequency, ω, and wave number, m, by fitting the data, V_{ij}, to the assumed model: $V_{ij} = V \cos(\omega t_j + mL_i - \varphi_o) + \langle V \rangle$, where V is the planetary wave amplitude, L_i is the longitude (in radians eastward of 0^o) of site i, m is the zonal wave number, ω is the wave frequency, and φ_o is the "time" of maximum at zero longitude or longitude of

maximum at zero time. <V> stands for the mean wind. A positive m indicates a westward propagating wave**;** m=0 represents disturbances spread over the whole latitudinal circle (i.e. changes in zonal mean values). The model has no latitudinal dependence, which means that only east-west planetary wave propagation is considered. Firstly a Fourier transform of the time sequence, e.g. 90 days of MetO temperatures or winds, is performed for each latitude/longitude bin, resulting in a complex amplitude at each frequency, latitude, and longitude. Then for each frequency and latitude a Fourier transform over longitude of these complex amplitudes is done, i.e. spatial Fourier transform, where the spatial frequency now represents wave number (number of waves around the earth's circumference), and the sign of the frequency represents propagation direction, eastward or westward. These spectra are coherently integrated over the selected latitude band, e.g. 4 degrees.

2.9 Note on the Possible Effects of the Zonal Mean Variability on the Calculated Wavelet Amplitudes

The oscillations of the zonal mean (average around a latitude circle) fields (U or zonal (EW) wind, in particular) can have large amplitudes in the stratosphere at mid- and high latitudes. To account for the effects of these oscillations the calculations have been carried out for MetO data with and without subtraction of the zonal mean values. As an example of such calculations the wavelet amplitudes of the zonal (EW) winds at Saskatoon are shown in Figure 2.6 for the time interval from July 2001 until June 2002. The resulting wavelets with subtracted zonal mean values (the right column) show the dominant peaks more clearly. In general the zonal mean fields fluctuate with large periods, >(20-30) days, which are the upper limit of the spectra used in this study. The cross-products of any two wavelets had no significant differences. Considering the impossibility of a separation of the zonal mean and residual mesospheric winds (from the few radars available), the zonal mean values were not removed from the daily local MetO data.

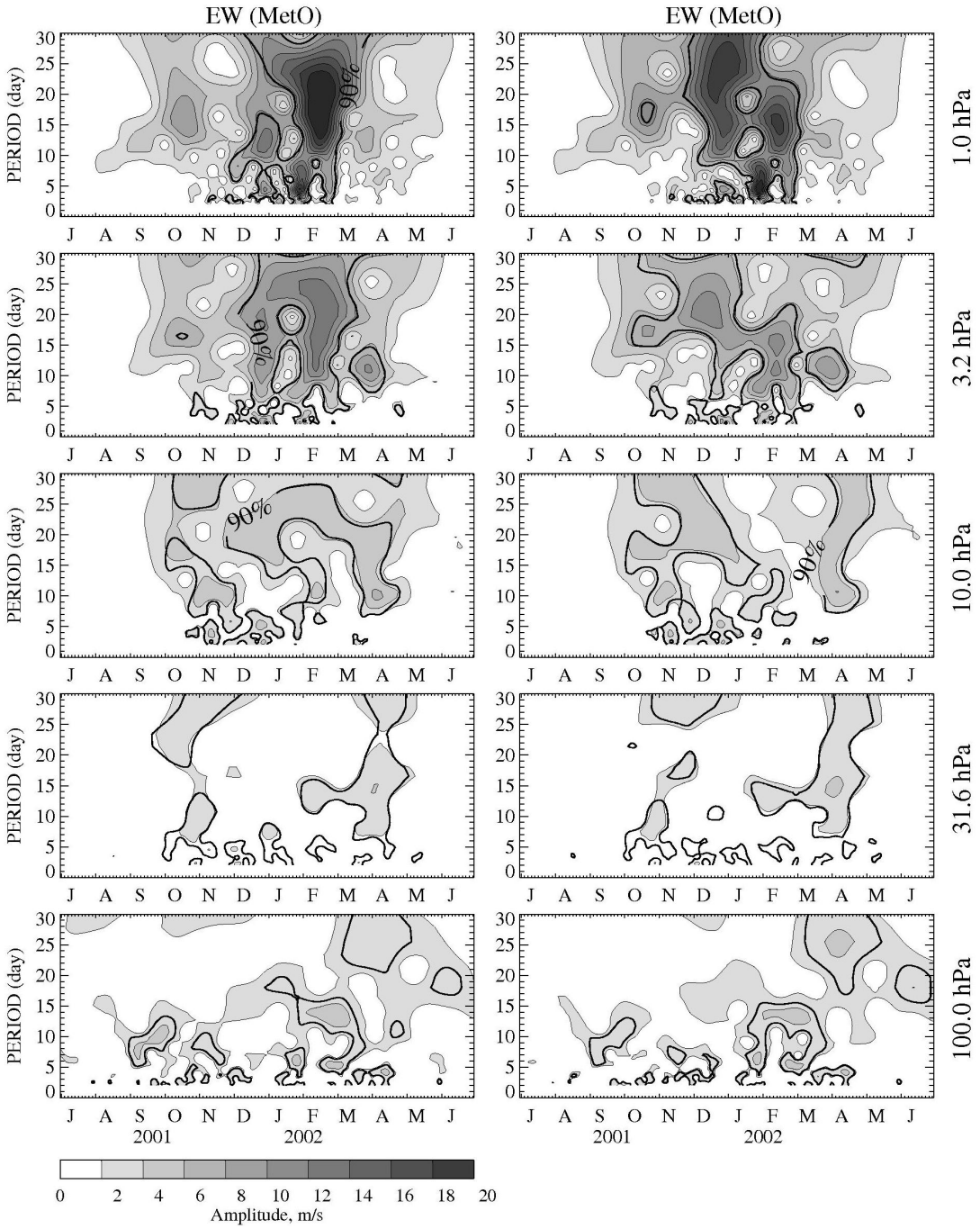

Figure 2.6 The wavelet amplitudes of the EW component of the MetO wind are demonstrated for several heights (from 100 hPa at the bottom up to 1 hPa at the top) for the Saskatoon location from July 2001 until June of 2002. The calculations have been carried out for the data with (right column) and without (left column) subtraction of the zonal mean values.

Chapter 3

VERTICAL PROPAGATION OF PLANETARY WAVES IN THE MIDDLE ATMOSPHERE

3.1 Introduction

Planetary waves (PW) are often generated in the lower atmosphere and may propagate upward carrying energy and momentum, thus providing dynamical coupling between the lower and middle atmosphere. Due to a lack of observations, which would have to cover a large altitude range at many geographical locations, as well as due to the complexity of the atmospheric processes themselves, different atmospheric regions are quite often considered separately. Although there are still not enough observational data at MLT (Mesosphere/Lower Thermosphere) heights, the development and improvement of numerical models and assimilation techniques over the last 10-15 years have helped to provide evidence for coupling between different atmospheric regions.

Over the last decade several papers, which involve both the lower and middle atmosphere, have been published. *Lawrence and Randel* [1996] examined the variability of daily temperatures, geopotential heights, and "balance-wind" (similar to the geostrophic wind) estimates that had been retrieved from the radiance data measured by a pressure modulator radiometer (aboard Nimbus 6). They found strong evidence of coupling between the stratosphere and mesosphere (30-85 km) for daily variations of the zonal-mean flow and for "wave-like events". However, the authors have noted that not all wave-like disturbances seen in the mesosphere are due to propagation from below.

The idea of complex relationships between planetary wave activity in different atmospheric regions has also been supported by *Lawrence and Jarvis* [2003], who studied PW with near 16-, 10- and 5-day periods using ECMWF (The European Centre

for Medium-Range Weather Forecasts) assimilative operational analysis and a High Frequency (HF) radar located at Halley (76^{o}S, 27^{o}W), Antarctica. It was demonstrated that simple vertical propagation of PW could not explain the observed picture of planetary wave activity at different atmospheric levels. The in-situ generations of planetary waves and PW-tide or PW-GW (Gravity wave) interactions have been suggested as possible additional mechanisms.

Manson et al. [2005] continued investigation of the atmospheric variability with PW periods (2-30 days) in total ozone, background MLT winds, and semidiurnal (12h) and diurnal (24h) tides, using satellite (TOMS) and Medium Frequency radar (MFR) data from the CUJO (Canada US Japan Opportunity) network. The results have indicated that the character of variability at PW periods for the tidal amplitudes differs from that for the PW themselves, which could be explained by different sources for their variability. However, there were some events that demonstrated oscillations at PW periods in both the tides (12-, 24-h) and winds of the MLT, and in the total ozone data, at the middle latitude stations. Mechanisms discussed included direct PW propagation into the MLT, non-linear PW-tide coupling, direct and variable forcing of tides by ozone sources, and GW forcing at PW periodicities.

In this chapter the vertical propagation of PW from the lower atmosphere to the mesospheric region is studied using TOMS data, MetO assimilated fields and mesospheric winds provided by five MFR from the CUJO network. The data cover the time interval from December 2000 to December 2002. In Section 3.2 the correlation between total ozone and MetO parameters are investigated. The spectral content of all parameters at all available heights from the lower stratosphere to the mesosphere are compared in Section 3.3. The amplitudes of the eastward and westward propagating waves with different periods have been calculated using the wave number analysis (Section 2.8). The different abilities of eastward and westward waves to propagate upward are demonstrated in Section 3.4. The results obtained are summarized in Section 3.5.

3.2 **Correlation between MetO Parameters and TOMS Data**

Different mechanisms account for variations in ozone concentration at different altitudes. At low stratospheric heights dynamic processes control ozone concentration, while photodissociation becomes more significant in the upper stratosphere [*Salby*, 1996]. Uneven distribution of the ozone with height (most of the ozone is concentrated in the stratosphere) allows the total ozone data to be used as an indicator of planetary wave activity at low stratospheric or tropopause heights (see, for example, *Manson et al.* [2005]). However, it is selective, e.g. the maximum signal in total ozone is thought to be produced by evanescent waves near the tropopause [*Schoeberl and Krueger*, 1983], while the influence of waves with shorter vertical wavelengths will not be as evident. The large altitudinal gap between the ozone and radar heights is another concern. The availability of MetO parameters at 22 pressure levels from the surface to ~55 km makes it possible to test whether the total ozone has a simple correlation with temperature and/or horizontal wind components at any particular level, in order that we can use one of the MetO parameters to represent the total ozone.

Time sequences of MetO temperatures for several heights/pressure levels at the latitude and longitude of Saskatoon during 2001 have been plotted in Figure 3.1. For convenient comparisons the total ozone variations are shown by dashed lines along with temperature sequences (solid lines). The horizontal time-axis lines represent the means for both temperature and the total ozone data, but different scales have been used to plot temperature and ozone data to make their variations comparable. As seen from the figure, the variations of the total ozone (in Dobson units, DU) and temperature can be out of phase (at 464 hPa), in phase (100 and 215 hPa), or exhibit complex relations (above ~10 hPa). Physical processes vary from temperature-dependent reactions to advection of ozone and perturbations associated with PW activity. A similar picture is observed for all three (2000-2002) years and all locations for the CUJO network. To generalize, the cross-correlation coefficients have been calculated between MetO parameters (temperature and horizontal wind components) and the total ozone. For the

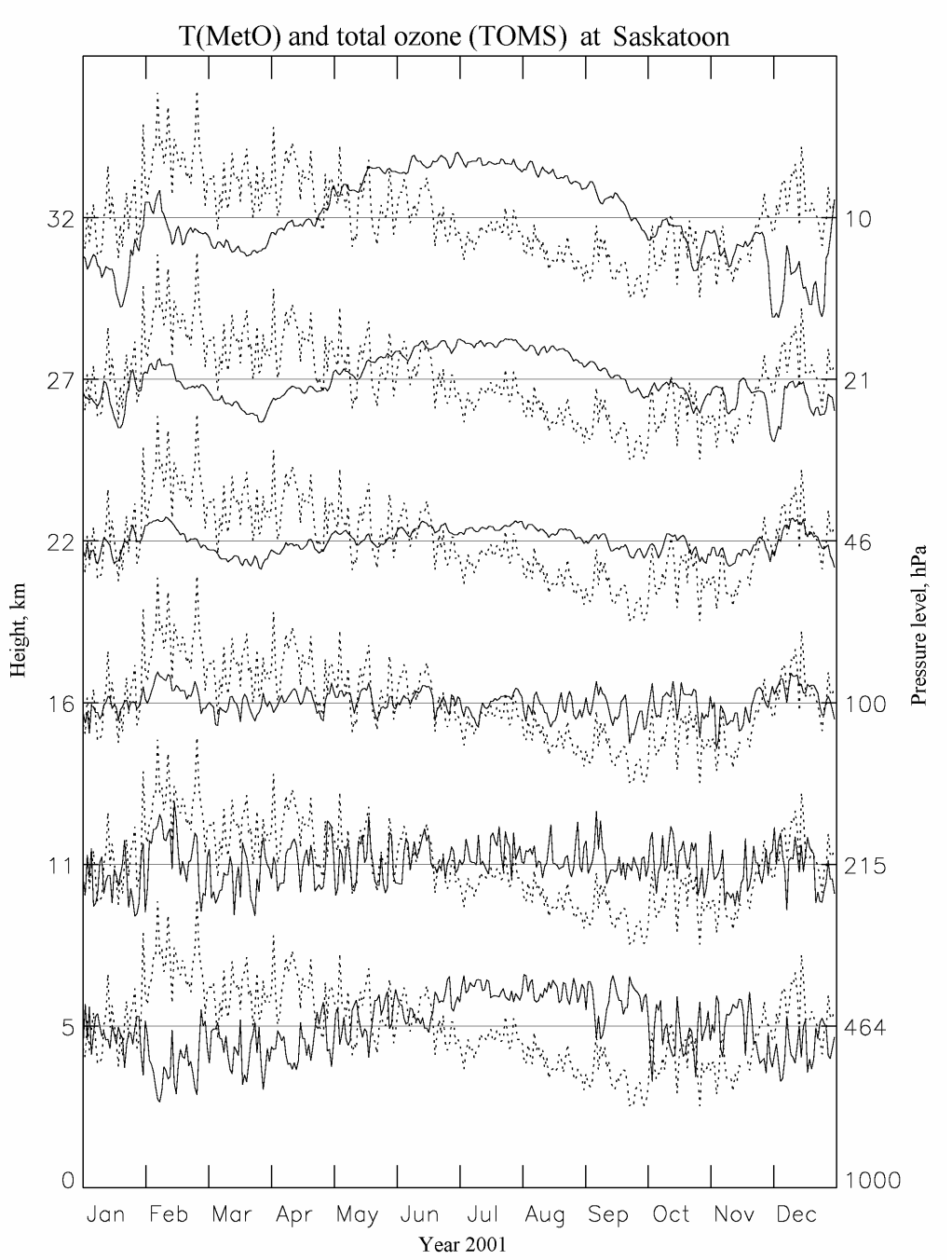

Figure 3.1 The variations of total ozone (dashed line) and MetO temperatures (solid lines) at several heights/pressure levels for Saskatoon, 2001. For convenient comparison the variations of total ozone are shown for each height/pressure level. Different scales have been used to plot ozone (200 DU per division) and temperature (40 K per division) variations to make them comparable.

calculations a window of 30 days and a 10-day sequential step have been employed. Each 30-day time interval has been linearly detrended.

The resultant contour plots of cross-correlation coefficients between temperature and the total ozone versus height and time (year 2001) for three (Saskatoon, Platteville, and Yamagawa) CUJO locations are shown in Figure 3.2a. Positive and negative values are shown by solid and dashed curves, respectively, with 0.2 steps between contours. All stations exhibit this regular pattern in all years: negative correlations at low heights change to positive correlations in the altitude range from ~10 to 25-30 km, while in the upper stratosphere the cross-correlation coefficients are not high and change sign with time. This result is not new and agrees well with strong correlations between atmospheric temperatures and total ozone found for variations with different time-scales in other studies [*Hood et al.,* 1997; *Ziemke et al.,* 1997]; and references therein). Such correlation analysis using the MetO assimilation products is new however. Horizontal winds have smaller cross-correlation coefficients and irregular structures with time and height (Figure 3.2b and c), suggesting a more complex relation with total ozone; the contours of the meridional wind cross-correlation coefficients are consistent with transport from low to high latitudes. Overall the total ozone and the temperature at low stratospheric heights (15-20 km) have similar temporal variations.

3.3 **Spectral Comparison of MetO, MFR and TOMS data**

To investigate the vertical propagation of planetary waves the spectra of the data have been compared at all available heights. All plots shown here (Figures 3.3-3.8) are the normalized wavelet amplitudes (in general well-formed peaks of greater than 0.4 are significant at >90%) versus time and period. The results are demonstrated for five CUJO locations with Saskatoon (52^{o}N) at the top, Yamagawa (31^{o}N) at the bottom, and Platteville, London and Wakkanai (40-45^{o}N) in the middle. As was mentioned in Section 2.1 the pairs of stations Saskatoon-Platteville and Yamagawa-Wakkanai have similar longitudes, which allows studying latitudinal differences. Longitudinal dependence can be estimated by comparing results at London, Platteville and Wakkanai, as locations of these stations are constrained to the narrow latitudinal zone 40-45^{o}N. The first two columns are wavelets of two different parameters, and the third

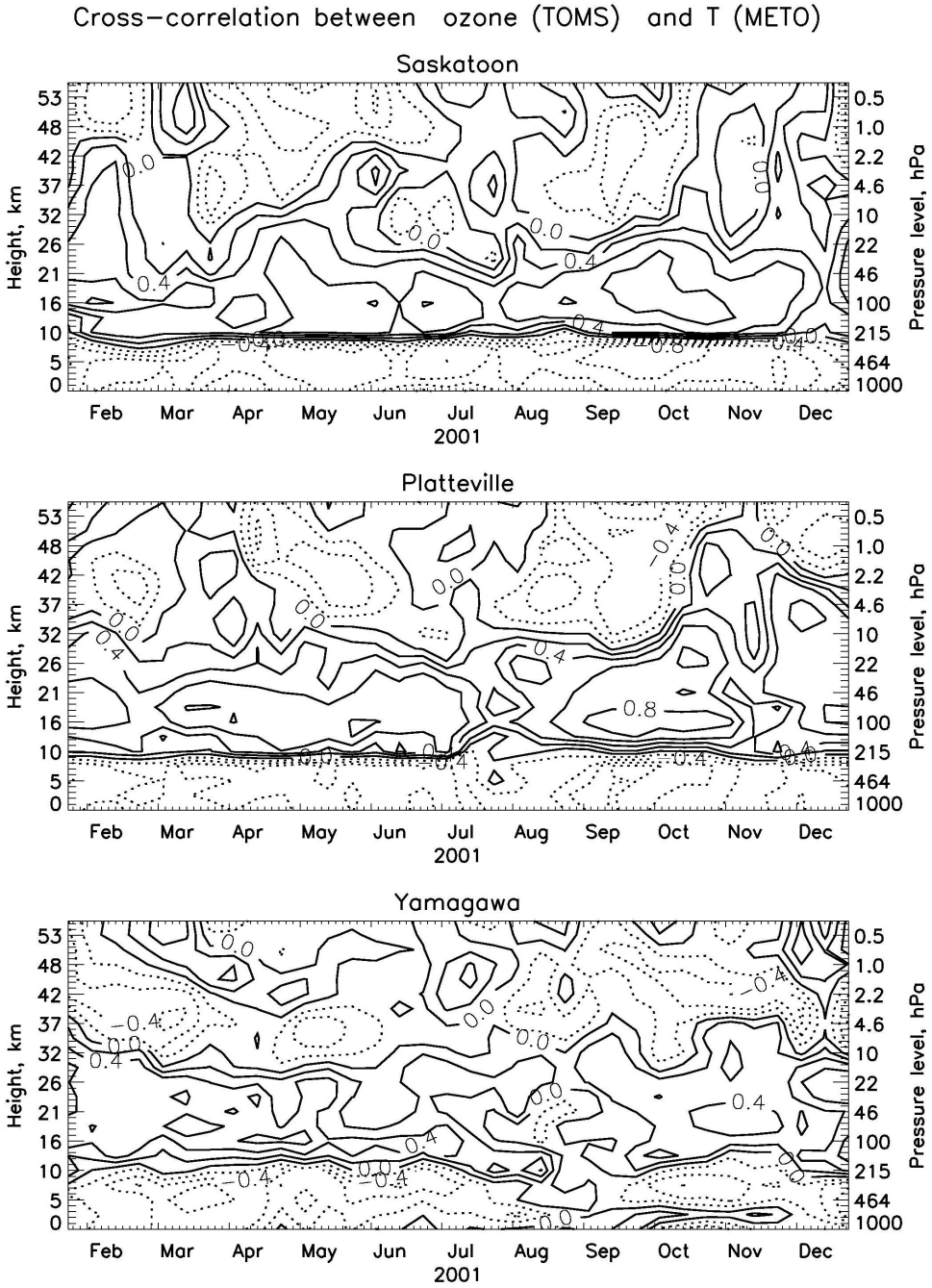

Figure 3.2 (a) The linear cross-correlation coefficients of the total ozone (TOMS) and temperature (T, MetO) versus time and height for three stations: Saskatoon (the top panel), Platteville (the middle panel), and Yamagawa (the bottom panel). The step between contours is 0.2.

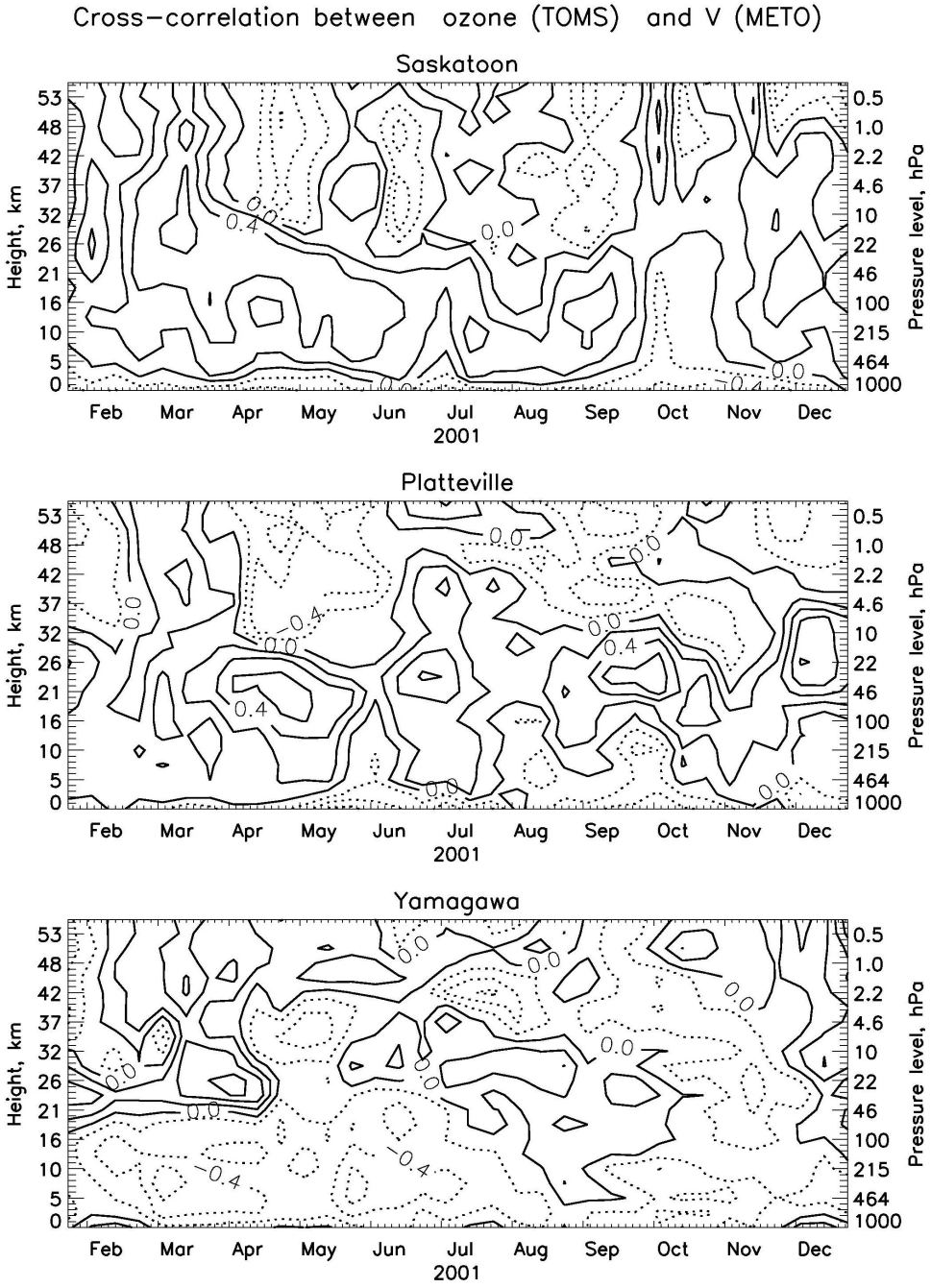

Figure 3.2 (b) The same as Figure 3.2a, but linear cross-correlation coefficients of the total ozone (TOMS) and meridional (V) wind component (MetO).

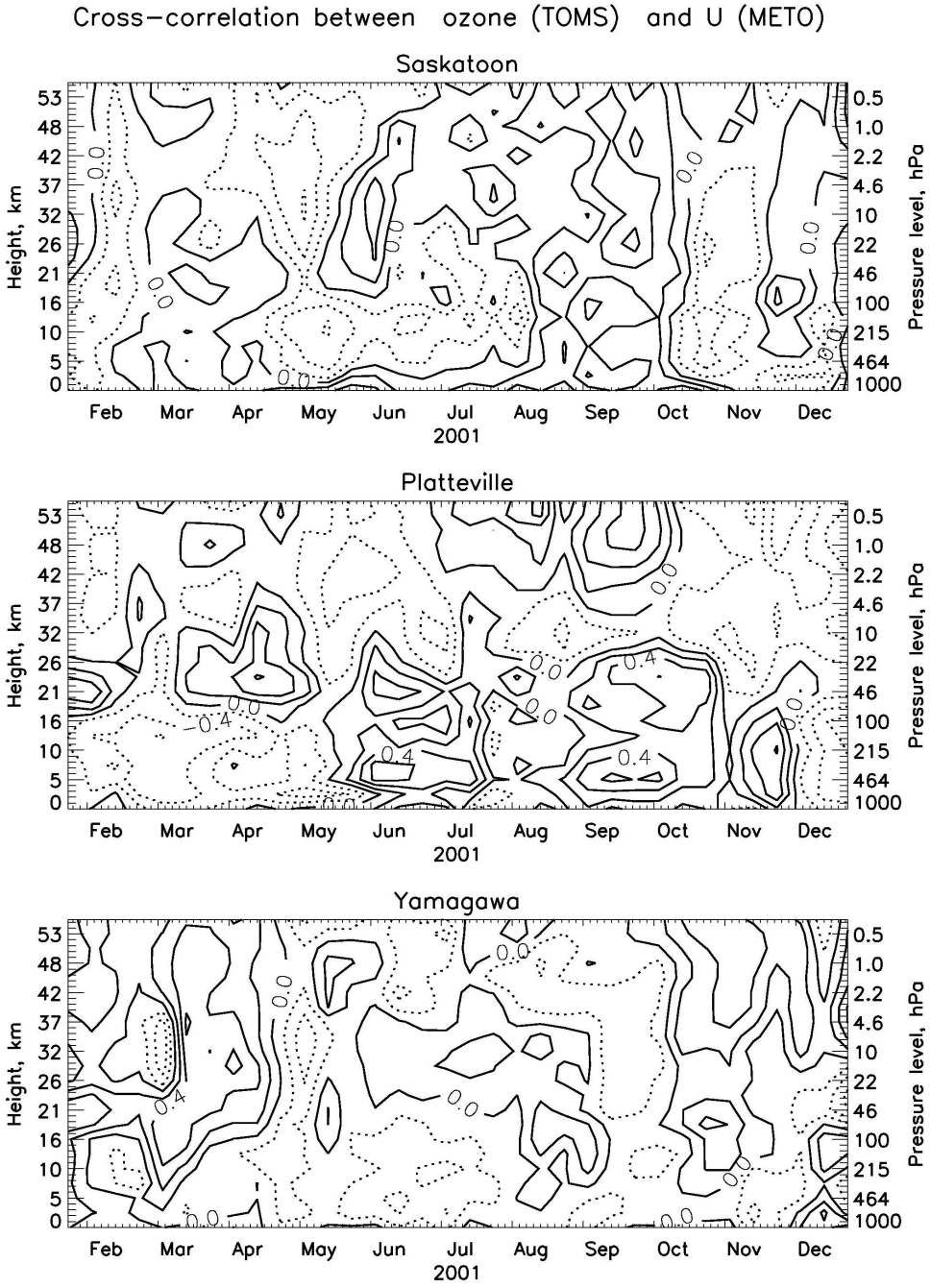

Figure 3.2 (c) The same as Figure 3.2 (a), but linear cross-correlation coefficients of the total ozone (TOMS) and zonal (U) wind component (MetO).

column is their cross-product. Assessment of several years, from our extensive data set at Saskatoon, indicates that year 2001 is quite typical. Therefore it has been chosen for demonstration. To show that the spectral contents of the data exhibit a modest interannual variability and the results of comparisons are consistent from year to year, the comparison of MetO (0.46 hPa) and MFR (82 km) is also presented for year 2002. The model and assimilation method used to produce MetO fields were also the same for 2001 and 2002. Year 2000 was omitted as radar data have poorer coverage (more gaps) at some stations, and a new assimilation system was introduced in MetO in November of 2000.

We first compare wavelets of the total ozone and MetO temperature at 100 hPa (Figure 3.3). According to the result obtained in Section 3.2, the MetO temperatures in the height region from 10 to 26 km (~215 to ~46 hPa) have the highest positive correlation with the total ozone. As can be seen from Figure 3.3, both parameters have similar dominant spectral components, and in most cases amplitude maxima in the cross-products are the results of contributions from spectral maxima in both the temperature and the total ozone. The main difference between these parameters, true for all CUJO locations, is the relatively low spectral amplitudes (hereafter, activity) in the total ozone during late summer. The total ozone not only reaches a minimum during July/August, but it also has smaller variability at that time than during the rest of the year (see Figure 3.1). Figure 3.3 is also interesting in the context of the recent paper by *Manson et al.* [2005] (see Section 3.1) due to these spectral dissimilarities; however very small differences in their results are expected, as the summer PW activity is also small in the MFR wind wavelets. Comparing different locations, the wavelets of the temperature at 100 hPa pressure level and of the total ozone, as well as their cross-products, show few if any similarities between stations. This suggests that the waves connected with these periods are either of small scale, or are localized in latitude (e.g. *Luo et al.* [2002b]). However, cross-wavelets for Platteville and Wakkanai have features near 10-15 day in both winters.

Now consider Figure 3.4, where the spectral variability in temperature is shown for two heights: 100 and 0.46 hPa. The character of the variability at 0.46 hPa pressure level has

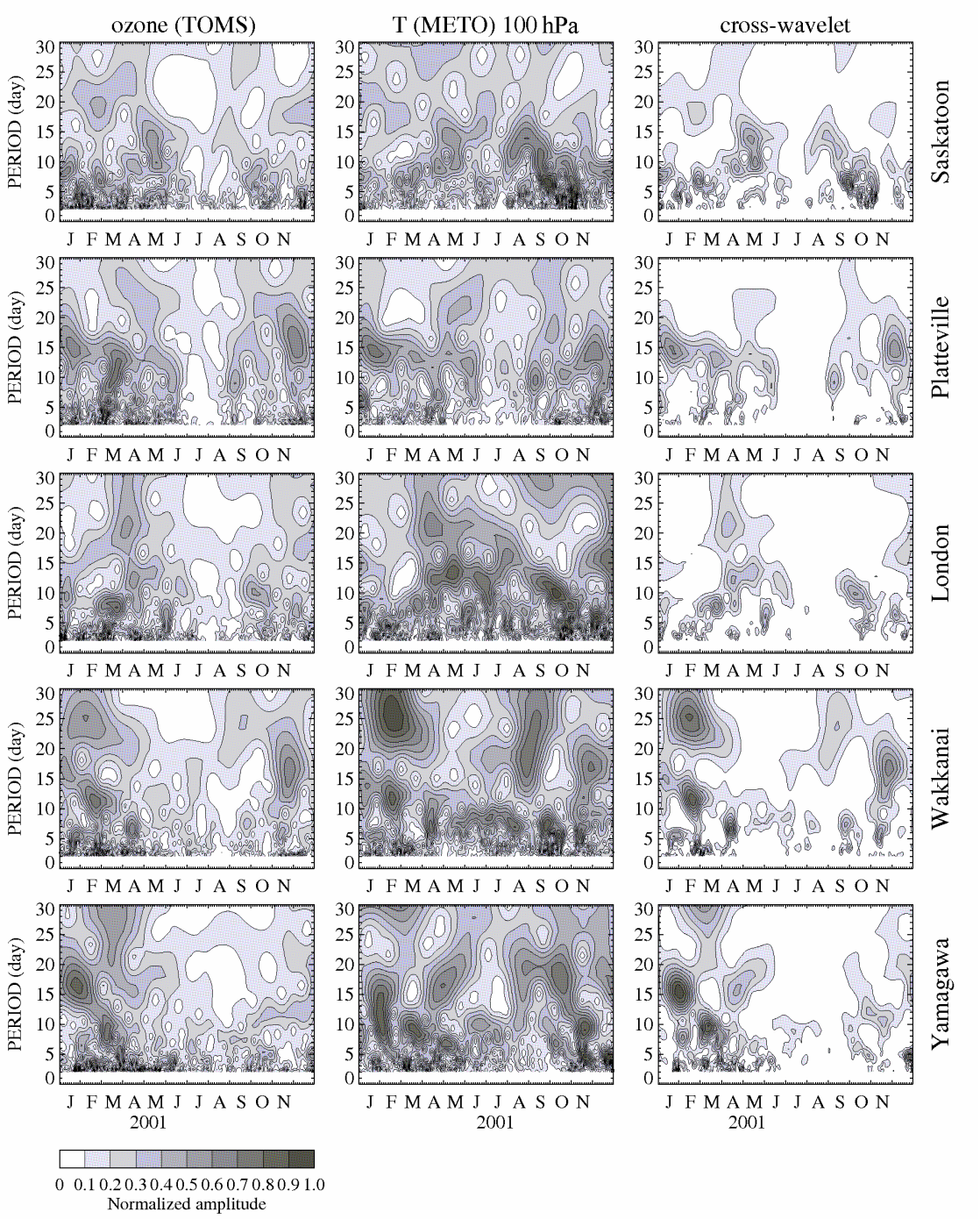

Figure 3.3 The self-normalized wavelet amplitudes versus time (year 2001) and period (2-30 days) calculated for the total ozone (the left column), MetO temperature at 100 hPa (the center column), and their cross-products (the right column) are presented for all five CUJO locations. From the top to the bottom these are for Saskatoon, Platteville, London, Wakkanai, and Yamagawa.

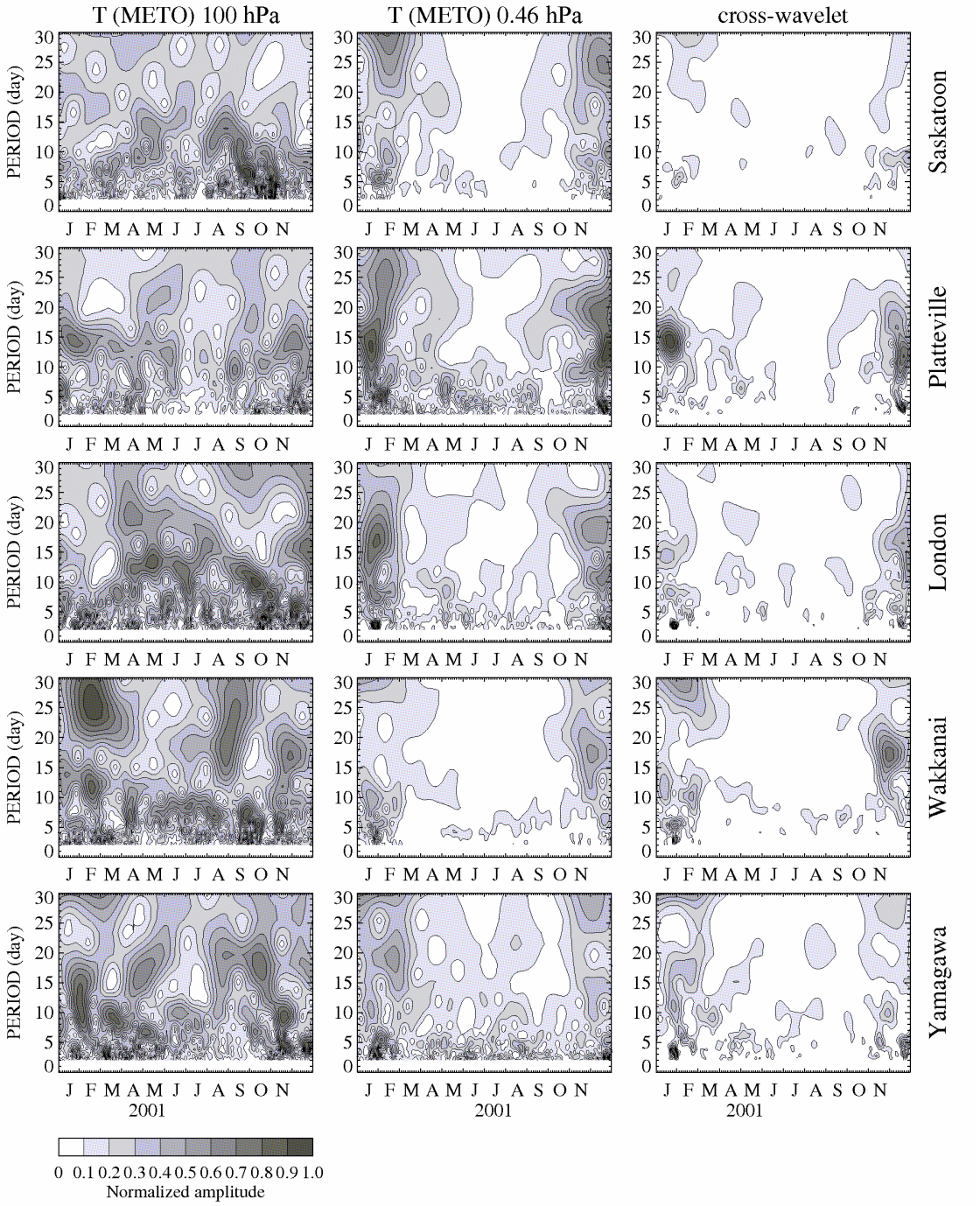

Figure 3.4 The same as Figure 3.3, but for MetO temperature at 100 hPa (~16 km) and 0.46 hPa (~50 km) pressure levels.

changed in comparison with the lower level, as there is now a strong reduction in spectral intensity in the summer months. There are also relatively few features present on the plots for the lower level that also occur on the plots for 0.46 hPa. Actually, the height 20-25 km (22-46 hPa) divides the lower atmosphere into two regions (consistent with Figure 3.2) where the spectral content is different. At Yamagawa this boundary is a little higher than at the other four locations: London, Platteville, Saskatoon and Wakkanai. Zonal winds in this height range have lowest speeds and the reversal from mainly eastward (below 20 km) to westward (above 25 km) in summer occurs there (Figure 2.2). Although such conclusions have been reached by others (e.g. *Shepherd* [2002]), the results are additionally pertinent here as later we will consider the wave numbers of these waves, and the differences in the directions of horizontal propagation at the two heights.

The lower spectral intensity at the higher altitude (0.46 hPa), especially in the long-period range in summer time, could be explained by the dependence of the associated planetary wave propagation on zonal circulation. Only waves with phase speeds that are westward relative to the mean flow, or waves whose phase velocities do not equal the flow at some height can propagate upward (Section 1.4). Note that there is greater similarity between spectral features (≥10 days) in the 0.46 hPa wavelets than at 100 hPa. Some common features, such as a signature of the 5-day period at the end of January (early February), appear at more than one station. Also, in the cross-products for midlatitude stations, especially London and Platteville, there are similar energy distributions in wintertime. The cross-wavelet of the total ozone and temperature at 0.46 hPa is very similar to the cross-product of the temperatures from the two different heights shown here. That is expected based upon comparisons shown in Figure 3.3.

The comparison of the wavelet spectra for the temperature (MetO) and wind (MetO) at the same pressure level show that they have some similarities as well as differences. Not all peaks present in the three parameters individually are present simultaneously in all three. Some of the peaks, such as those with long periods of 20-25 days in January/February at Saskatoon, can be found in 0.46 hPa temperature (the second column of Figure 3.4) and zonal wind plots (the first column of Figure 3.6), while they

are absent from the plots of the meridional wind (the first column of Figure 3.5); others, such as 5-6 day peak in December at Wakkanai is clearly seen in temperature and meridional wind, but not in zonal wind. Some peaks (20-25 days in January/February at London) are present in both components of the wind, but are not evident in the temperature. This is due to the variations with latitude of the Hough modes for the various wave parameters that can be used to characterize each wave [*Forbes,* 1995]: nodes and antinodes for each parameter occur at different locations. Despite this, the spectral distributions for T, U and V are quite similar in general structure at each site, i.e. months of enhanced wave activity and the related approximate periods of the spectral peaks are similar.

Finally we consider the winds from MetO at the 0.46 hPa pressure level (~50 km) and from the MFR at 82 km. Figure 3.5 and Figure 3.6 have been introduced already, but their main purpose is to compare winds at stratospheric and mesospheric heights. The meridional components are used in Figure 3.5 and the zonal in Figure 3.6. It can be seen that the character of wave activity is changed again. More high frequency features appear in the MFR wind wavelets in contrast to those of the MetO winds at the lower (0.46 hPa pressure) level, and there is more mesospheric wave activity in summer months. This former may be due to more inherent smoothing in the MetO model. One common feature for both MetO and MFR zonal winds is a strong peak at 20-25 days in January/February that is present at all stations except Yamagawa. Actually the magnitude of this peak increases with height (i.e. before normalization) and it is not present or is very weak at MetO levels below ~2.15 hPa (40 km). The cross-wavelets highlight these features. In the meridional winds there are some common peaks in the higher frequency range. Among others there are 5-day peaks in wavelets and cross-wavelets in January/February at Saskatoon and (more weakly) at Platteville. This was previously noted in the MetO temperatures (the second column of Figure 3.4) and meridional winds (the first column of Figure 3.5). Another strong 2-4 day peak can be found in the plots for Yamagawa and Wakkanai at the end of January and the beginning of February. It is also seen in the zonal wind component, but it is less prominent. The greater similarity in spectral features between the five locations of CUJO, at these upper

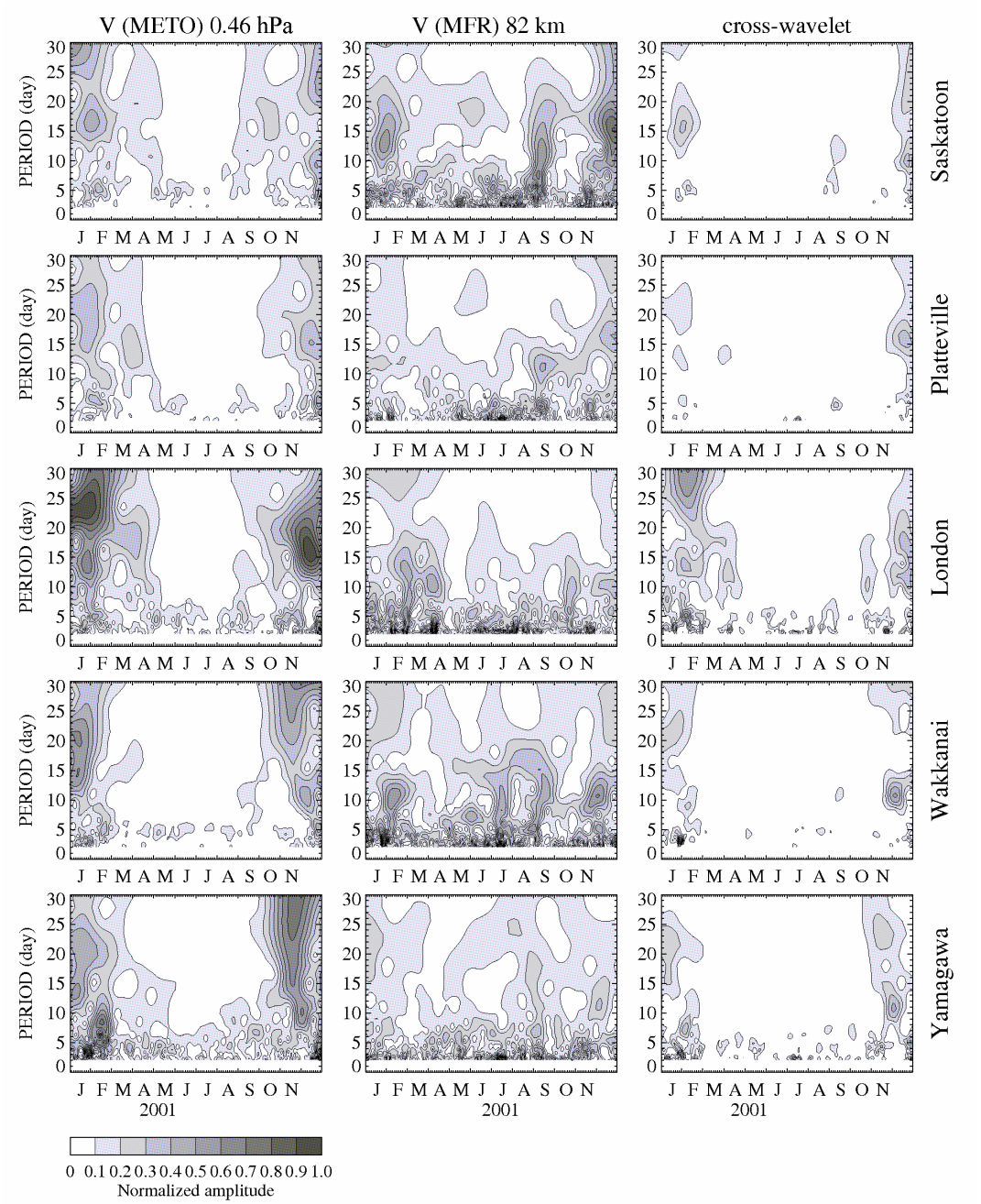

Figure 3.5 The self-normalized wavelet amplitudes versus time (year 2001) and period (2-30 days) calculated for the meridional component (V) of the MetO winds at 0.46 hPa (the left column) and MFR winds at 82 km (the center column), and their cross-products (the right column) are presented for all five CUJO locations. From the top to the bottom these are for Saskatoon, Platteville, London, Wakkanai, and Yamagawa.

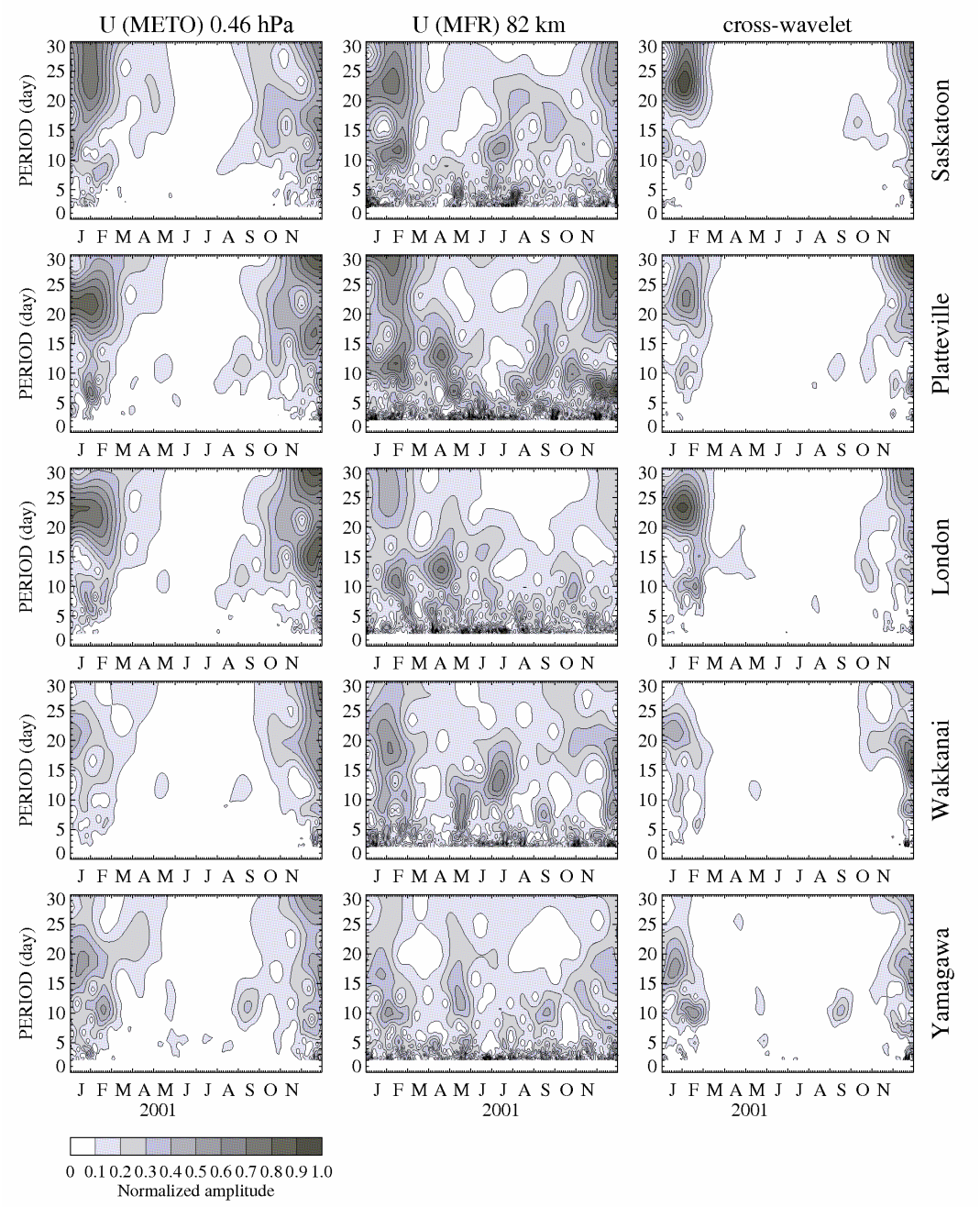

Figure 3.6 The same as Figure 3.5, but for the zonal (U) winds.

heights (stratosphere-mesosphere), suggests larger scale waves and more global coherence. Larger zonal amplitudes are also consistent with characteristics of normal modes [*Luo et al.*, 2002b]. Besides the common features there are differences in wavelets for different CUJO locations. These differences can be explained by latitudinal and longitudinal variations in the response of the atmosphere to the global normal PW modes [*Manson et al.*, 2004a].

The existence of 10-15 day peaks during summer months (June, July, 2001; Figure 3.6) in the zonal MFR winds at Saskatoon and Wakkanai is interesting, but not unusual [*Luo et al.*, 2002a]. It has been assumed that such summer activity could be due to the mesospheric dissipation of upward propagating gravity waves that are modulated at a period of near 16 days at stratospheric heights [*Smith,* 1996]. However, no peaks with similar periods are present in the winds at this time at stratospheric heights (neither at 0.46 hPa, nor at 100 hPa). An alternative source could be in the Southern Hemisphere, and this possibility is assessed later. The absence of the burst at other locations at 82 km can be attributed to the intermittent nature of the 16-day wave and its dependency on the background winds [*Luo et al.*, 2002b].

As was mentioned above, one year differs from another in the details of the dynamic activity. For example, MetO (0.46 hPa) and MFR (82 km) wind wavelets for year 2002 (Figure 3.7 and Figure 3.8) have no strong spectral feature in zonal winds at long periods as was the case for the winter of 2000/01. Instead there is often spectral energy at the mid-latitude locations (82 km) at periods near 15 days in January and ~10 days at the end of March. Consistent with this, there are peaks around 15 and 10 days in the zonal component of the MetO winds at the 0.46 hPa pressure level at some locations. Otherwise however, there is somewhat less consistency (period and time) between peaks at stratospheric and mesospheric levels, or between different locations, than during 2001. In the plots for the meridional winds, only the 5-day peak in January appears at all CUJO locations.

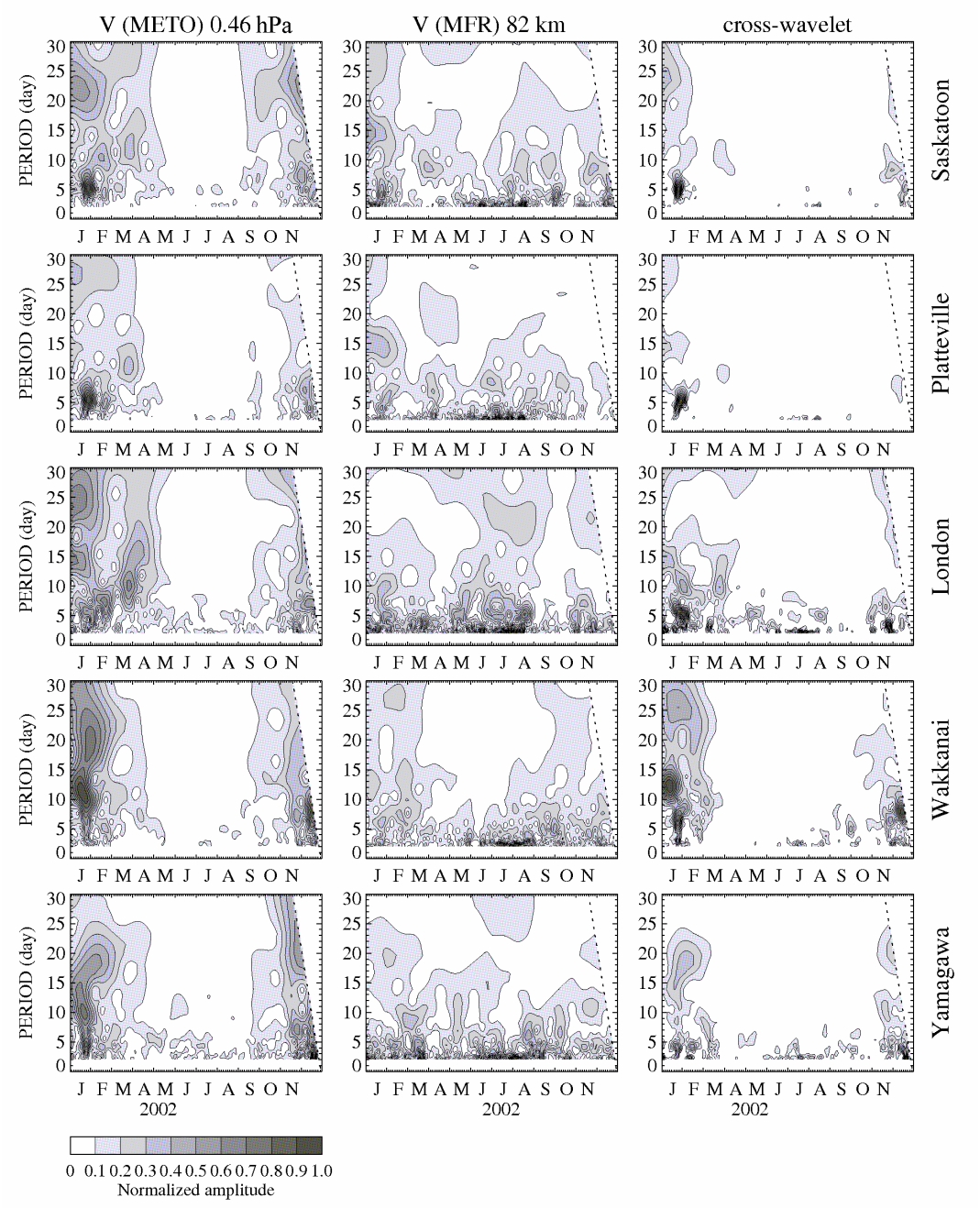

Figure 3.7 The same as Figure 3.5, but for the year 2002.

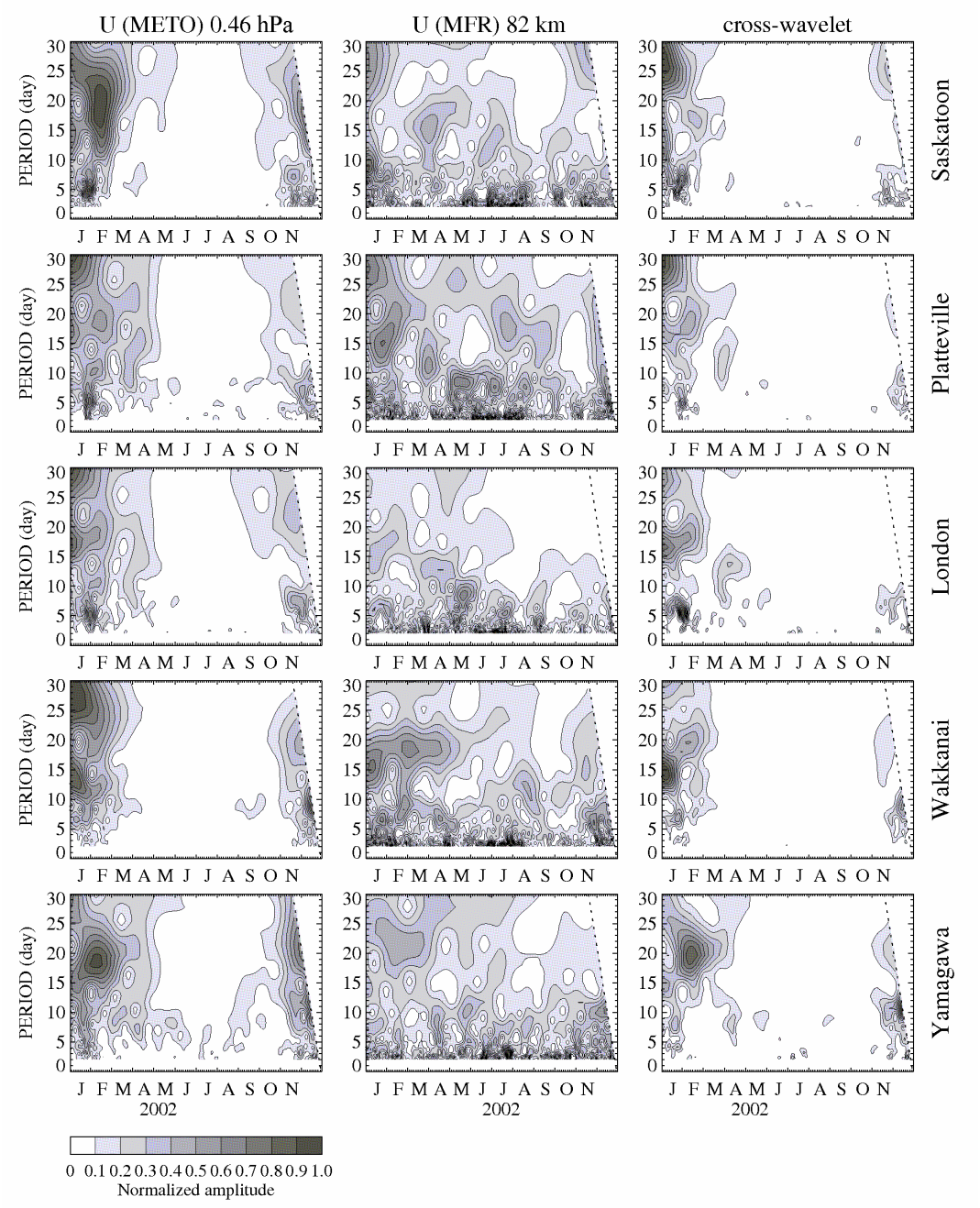

Figure 3.8 The same as Figure 3.6, but for the year 2002.

3.4 **Results of the Wave Number Analysis**

The results of the wave number analysis (see Chapter 2 for description) for a given sub-set of MetO temperature and winds are presented as contour plots of their amplitudes over period (days) and wave number. Figure 3.9 is for the 100 hPa (~16 km) and 0.46 hPa (~ 50 km) pressure levels during winter (December 2000 — February 2001) and summer (June-August, 2001). In each part, the plots (wave number vs. period) for MetO temperatures (left column) and zonal (middle column) and meridional (right column) components of the winds are presented for 42-46^{o}N latitudinal band. The same dB levels are used for each plot of Figure 3.9 for easy inter-comparison. The value in dB is equal to 20*$\log_{10}$ (wave amplitude in m/s and K).

Looking first at the 2000/01 winter (the two upper rows of Figure 3.9), the three parameters have different patterns. At 100 hPa low wave numbers (-2<m<2) dominate in temperatures and zonal wind component, while in the meridional component there is a "valley" around m=0 (between eastward and westward directions) for all frequencies. The width of this "valley" depends on the height, so that the valley is wider at the lower 100 hPa pressure level than at 0.46 hPa. Among all parameters the contours of the EW component of the winds have highest amplitudes, especially in the low frequency range. The results of the wave number analysis for the winter of 2001/02 (the two upper rows of Figure 3.10) have quite similar characteristics. The individual patterns of the parameters do not depend on the latitude; but on the other hand the amplitudes or intensities of the temperature and zonal wind contours at higher latitudes tend to be larger than for low latitudes especially in the upper stratosphere during winter. This is clearly seen in Figure 3.11 that demonstrates the results for 31-35^{o}N and 51-55^{o}N latitudinal bands during winter of 2001/02.

Comparisons of the two pressure levels reveal two main differences. First of all, at 100 hPa the MetO parameters have rich spectral content with dominant eastward motions; while at 0.46 hPa the spectral intensities for the westward motions become comparable to, or larger than, eastward motions. Secondly, the amplitudes are larger (more red color, > 0 dB) at 0.46 hPa than at 100 hPa for all components.

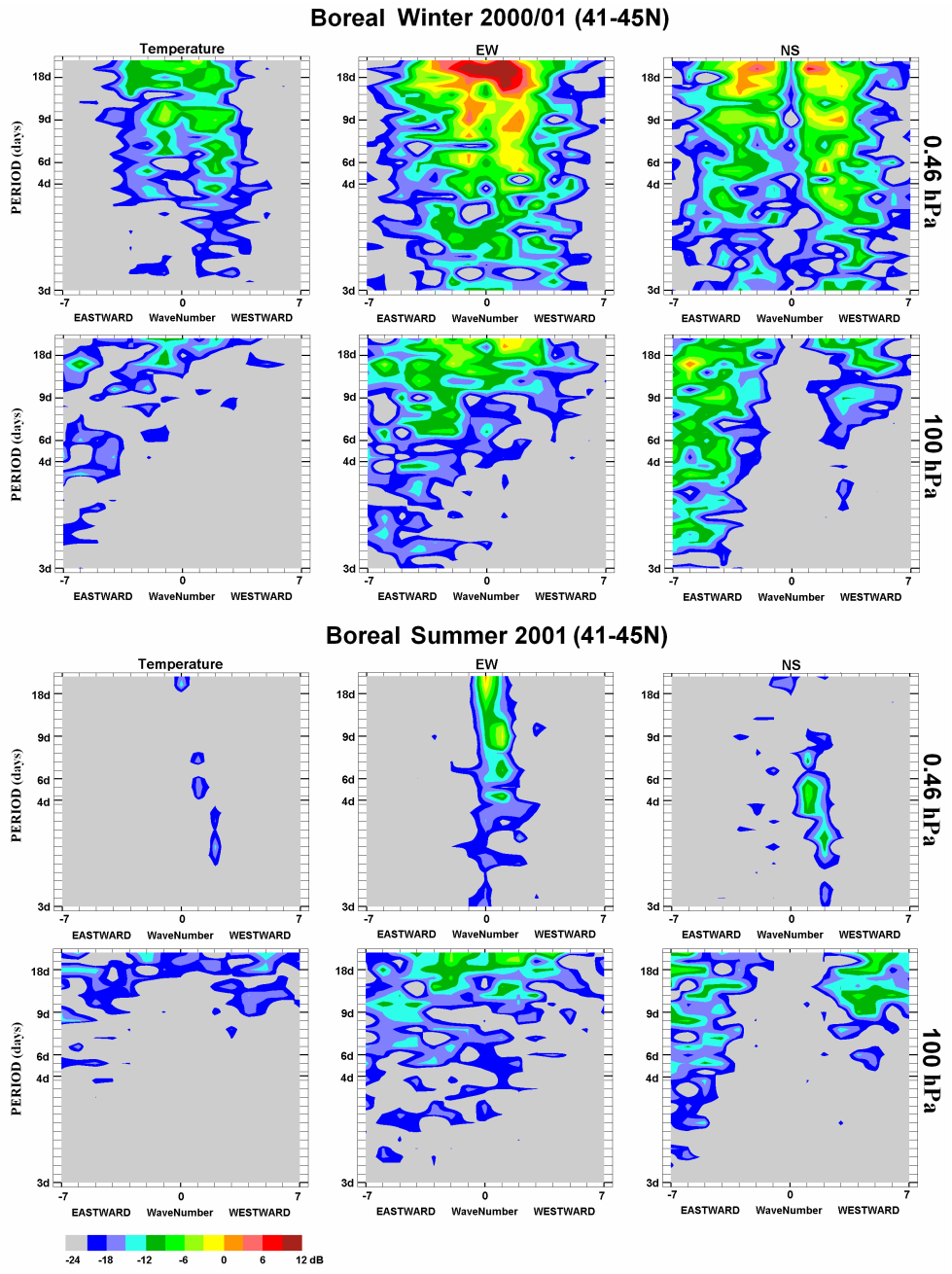

Figure 3.9 Wave numbers versus period calculated for MetO temperatures [left], zonal, EW, [middle] and meridional, NS, [right] wind components at the 0.46 and 100 hPa pressure levels for the 42-46^{o}N latitude band during the 2000/01 winter (December 2000-February 2001) [two upper rows] and the 2001 summer [two bottom rows]. Also, divisions corresponding to frequencies, which are cycles per 90 days, are shown from 3 (top) to 30 (bottom).

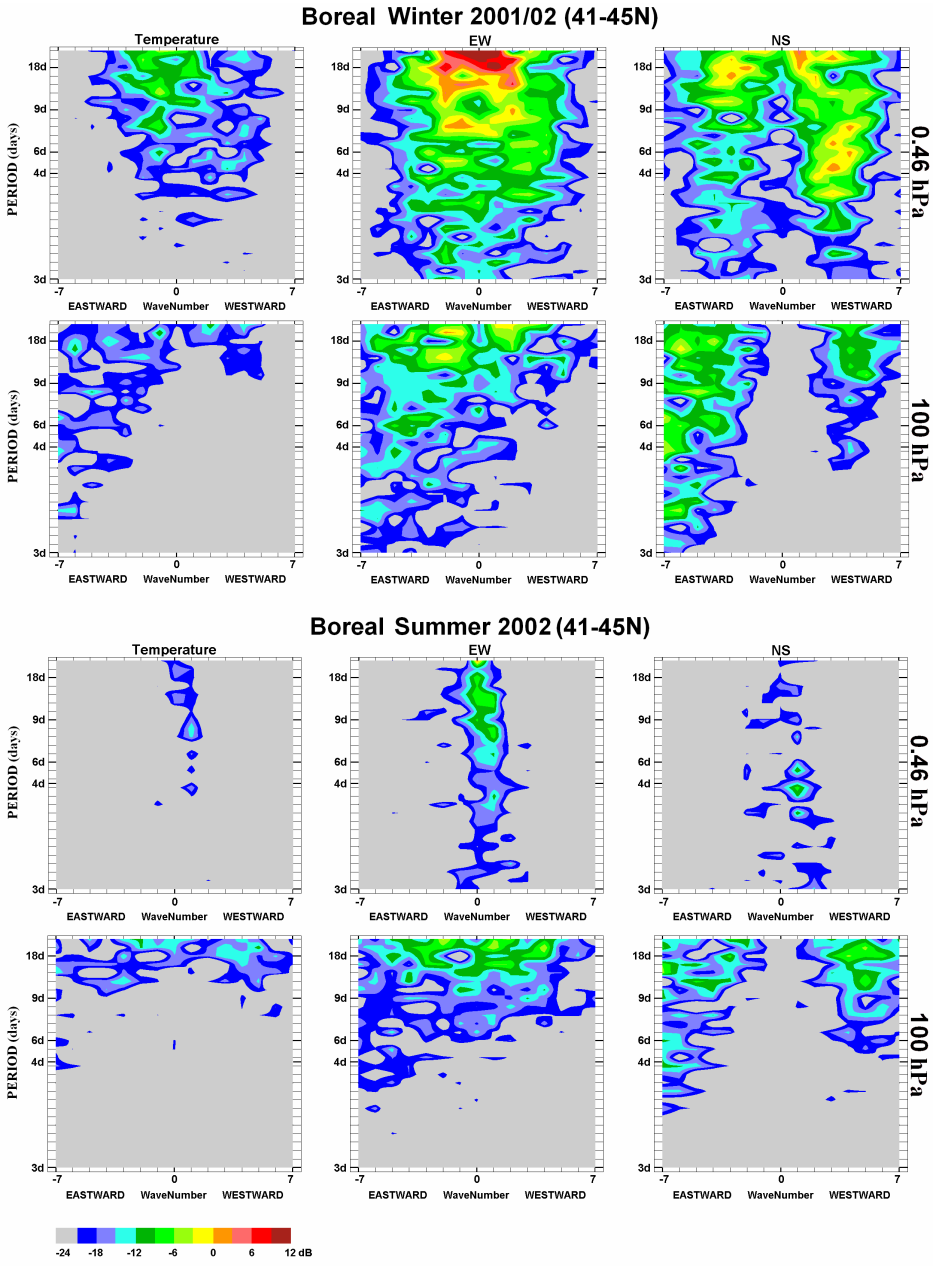

Figure 3.10 The same as Figure 3.9, but for boreal winter of 2001/02 (December 2001-February 2002) [two upper rows] and summer of 2002 (June-August 2002) [two bottom rows].

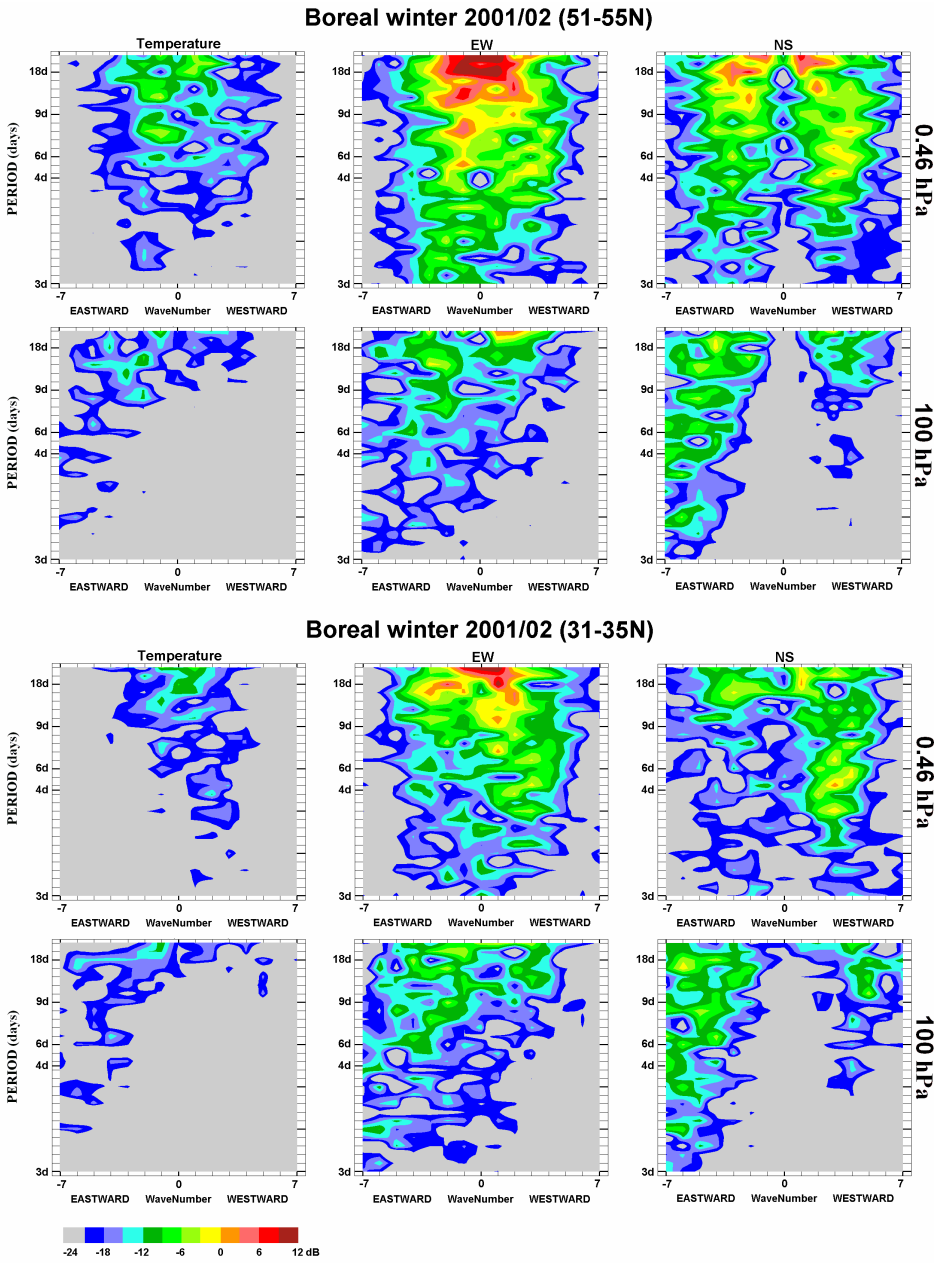

Figure 3.11 Wave numbers versus period calculated for MetO temperatures [left], zonal, EW, [middle] and meridional, NS, [right] wind components at the 0.46 and 100 hPa pressure levels for 31-35^{o}N [two bottom rows] and 51-55^{o}N [two upper rows] latitude bands during the 2001/02 winter (December 2001-February 2002). Also, divisions corresponding to frequencies, which are cycles per 90 days, are shown from 3 (top) to 30 (bottom).

The wave activity varies with the season, which is clear, for example, from the plots of the monthly average Eliassen-Palm flux divergences presented in the atlas of atmospheric general circulation [*Randel,* 1992]. As expected, in Figure 3.9 and Figure 3.10 in summer (the two lower rows of the figures) there is much less wave activity at both levels (and for all locations 27-56^{o}N). At the 100 hPa level the spectral energy is spread more evenly between eastward and westward wave numbers than it was in winter at this level, while at 0.46 hPa pressure level most of the contours are aligned along m=0 and +1. Compared to the winter, relatively more energy can be found at high frequencies at the 0.46 hPa level. As noted before (Figure 3.6), there is no evidence of the mesospheric (82 km) 10-15 day oscillation in these wave number plots.

Now we focus upon a couple of the features, which it is believed could be associated with truly global events. The first feature is a 15 day eastward-propagating oscillation with the zonal wave number m=-6 in boreal winter 2000/01 (Figure 3.9). The "footprint" of this wave also can be found in winter 2001/02 (Figure 3.10), but it has smaller amplitude. The peak is evident in all parameters and all latitudinal bands at the 100 hPa pressure level. It seems that this oscillation does not propagate upward; at least the peak is not present at the 0.46 hPa pressure level. On the plots of wave number versus latitude for the oscillation with period near 15 days (Figure 3.12) this feature is clearly seen as a bright red (in NS winds) or green (in EW winds and temperatures) area, which extends from the low to middle latitudes, at the 100 hPa pressure level (the bottom row). It is not present at the higher altitude (the upper row). Also, the 15-day peak can be easily identified at all CUJO locations except Saskatoon in Figure 3.3 (comparison of the wavelets of the TOMS ozone and MetO temperatures at 100 hPa). In the TOMS wave number plots for January-February, 2001 (Figure 3.13) the 15-day oscillation (4 cycles per 60 days) with m=-6 is also clearly seen for 39-44^{o}N and 49-54^{o}N latitudinal bands with the strongest amplitudes at lower latitudes (*Manson et al.* [2005], their Figure 7).

The second feature during the winter of 2000/01 involves the long period portion of the wavelets and wave number plots. This case is dominated by a peak near 22.5 days with m=+1 (westward). The long period oscillation (with T>20 days, Figure 3.6) has already

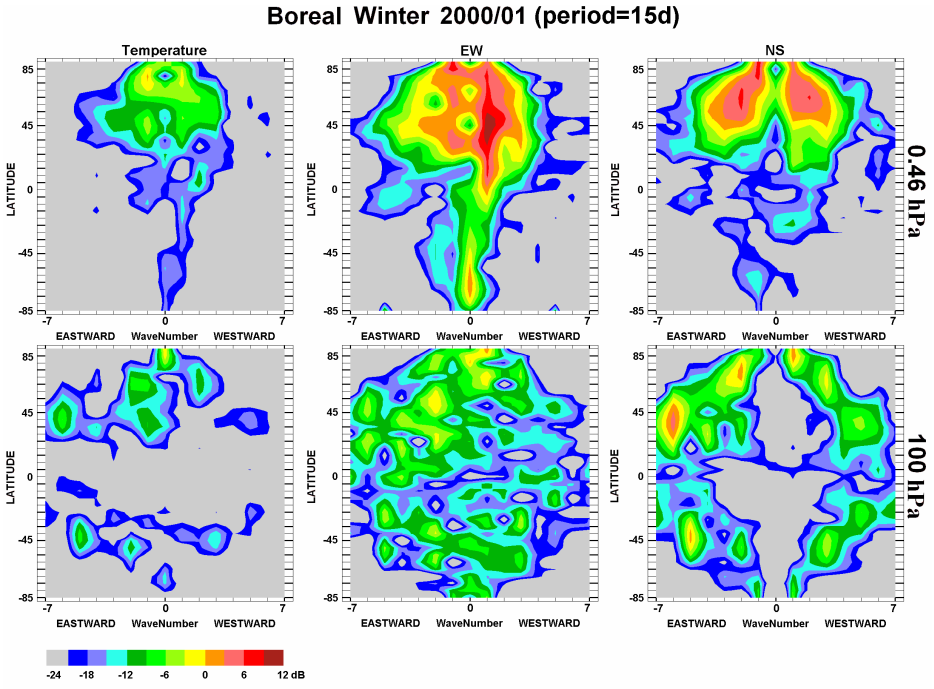

Figure 3.12 Plots of wave number versus latitude for the oscillation with the period of 15 days in temperature (left), zonal, EW, (middle) and meridional, NS, (right) wind components at 100 hPa (at the bottom) and 0.46 hPa (at the top) pressure levels during 2000/01 boreal winter (December 2000-February 2001).

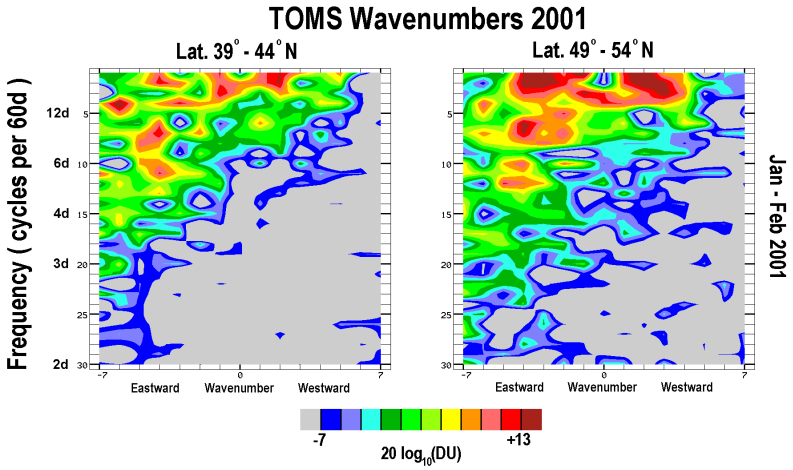

Figure 3.13 Wave numbers versus frequency calculated for 39-44^{o}N [left plot] and 49-54^{o}N [the right plot] latitude bands for 60-day time interval starting on January 1 of 2001. Some periods are shown for convenience, the divisions are cycles per 60 days and range from 2 (top) to 30 (bottom).

been mentioned in Section 3.3 in connection with the 0.46 hPa zonal wind component. According to the wave number plots (Figure 3.9) the peak maximizes at the higher (0.46 hPa) pressure level and is even stronger at higher latitudes (not shown). There is a signature of this oscillation at MFR heights in the zonal winds as well (Figure 3.6) for most CUJO locations, and the cross-wavelets show the feature consistently.

A frequency filter (20-40 days) was applied to the MFR and MetO (0.46 hPa) winds for this winter. The resulting time sequences (not shown) are complex, and consistent phase shifts between locations are difficult to establish except in January/February. However between Platteville/London and Wakkanai a wave number of 1.4 – 1.7 is estimated at the 82 km level. The filtered sequences at London, Platteville and Saskatoon (the three closest locations of CUJO network) are remarkably similar (as are raw data) at both levels, and close to zero phase shifts exist. On the plots of wave number versus latitude for the oscillation with period near 22.5 days (Figure 3.14), the amplitudes are relatively strong along m=1 in the Northern Hemisphere as seen in all parameters and at both 100 hPa (bottom) and 0.46 hPa (top) pressure levels, strengthening and extending along low and middle latitudes at the higher altitude.

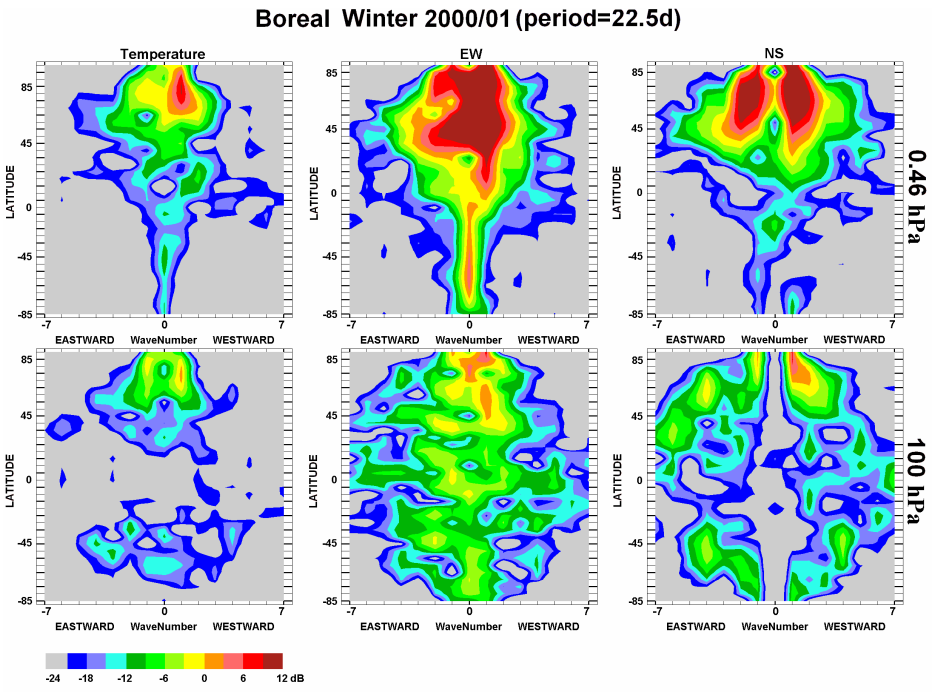

Figure 3.14 The same as Figure 3.12, but for the oscillation with the period near 22 days.

In the winter of 2001/02 (Figure 3.10) there is again no evidence for the 16-day wave with m=1. Although a “near 15-day” oscillation was observed in the MFR winds at mesospheric heights (discussion in previous Section 3.3), it shows little coherency between locations at stratospheric heights. Indeed MetO wavelets for other locations (Europe, Asia, and Pacific) along the 40^{o}N latitudinal circle (not shown) did not consistently show this oscillation. The absence of the signature of the wave in the wave number plots can be explained by the fact that these calculations employ all grid points along the latitudinal circle rather than a few particular locations. Such intermittency and localization of 16-day oscillations is consistent with the planetary wave studies of *Luo et al.* [2002a], and the HRDI analysis of Burrage (see *Luo et al.* [2002b]).

As one of the possible sources of the upper mesosphere 10-15 day disturbance, which is evident in the summer of 2001, ducting from the southern hemisphere has been named in Section 3.3 (Figure 3.6). In Figure 3.15 plots of wave number versus latitude are shown for oscillations with periods near 10 and 15 days. The "patchy" picture at 100 hPa changes to a more elongated structure (extended along the wave numbers between -2 and +2) at 0.46 hPa pressure level. There is substantial spectral energy at m=+1 in the austral winter which could therefore be the stratospheric source of the 10-15 day oscillation observed at mesospheric heights at Saskatoon and Wakkanai (Figure 3.6) during this (northern summer) time. Differences between northern and southern hemispheric winters are also clear from Figure 3.12 and Figure 3.15. In general, the amplitudes are smaller in the southern hemisphere (note that the scales are different for the figures). Also, during the winter in the northern hemisphere eastward as well as westward motions are present at 100 hPa pressure level, while eastward motions largely dominate during the southern hemisphere winter. At the 0.46 hPa pressure level the amplitudes are greater and the westward direction is favored during the boreal winter.

3.5 **Summary**

In this chapter the vertical coupling due to PW in the middle atmosphere (20-90 km) has been studied using TOMS, MetO and MFR winds measured at five mid-latitude

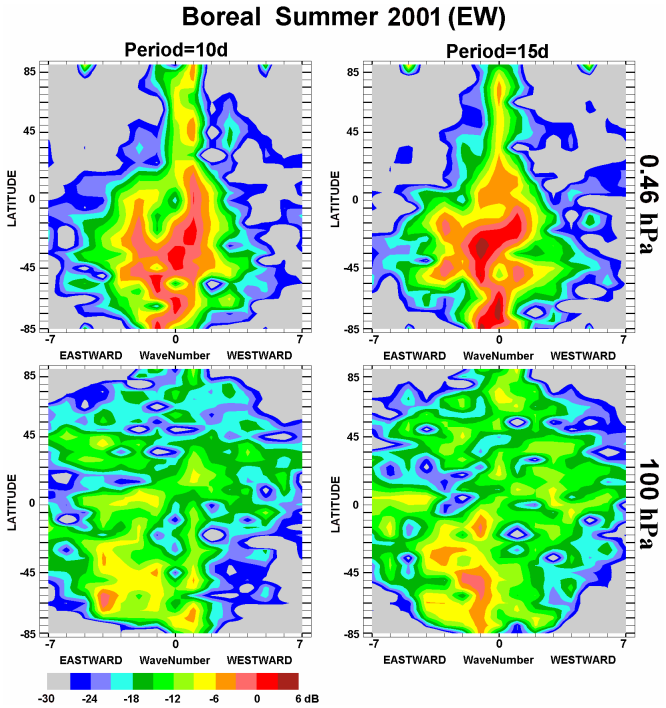

Figure 3.15 Plots of wave number versus latitude for the oscillation with the period near 10 (left) and 15 (right) days in zonal (EW) wind components at 100 hPa (at the bottom) and 0.46 hPa (at the top) pressure levels during 2001 boreal summer (June –August 2001).

locations in the North American-Pacific sector (CUJO network). The data covers the time interval from December 2000 to December 2002. All data have been subjected to wavelet, cross-wavelet and wave number analyses.

Results of comparisons and correlations between several parameters show that of the MetO parameters, temperatures at low stratospheric heights (typically 100 hPa, 15-25 km) show the best correlation with the total ozone. This is consistent with the study by *Schoeberl and Krueger* [1983], which suggested that the variation of (total) ozone is a useful indicator of PW disturbances of medium zonal wave number near the tropopause. It was also demonstrated that the MetO (0.32 hPa, 55 km) and MFR winds (circa 60 km) are in good general agreement, especially for the zonal component at particular mid-latitude locations. There are differences in values that could be attributed to the poorer reliability of the daily data parameter at the highest MetO and lowest MFR

levels. The bias (small by a factor of ~1.5) of the MFR winds was noted. This is the first comparison of its type between MetO and radar data.

The wavelet transform has been applied to the MetO temperature and wind fields at all available pressure levels. It was shown that the annual variations of spectral content at PW periods change significantly between MetO 100 hPa (15-20 km) and 0.46 hPa (50 km) levels, consistent with much reduced PW activity at the upper level during the summer months. This can be attributed to the westward zonal winds of the middle atmosphere (e.g. *Charney and Drazin* [1961], *Luo et al.* [2002b]). This result is not new, in general form, but it is useful to demonstrate it with the MetO data.

Based upon annual wavelet analyses for particular locations at low to middle latitudes, the spectral features of the MetO temperatures (T), zonal (U), and meridional (V) winds differ somewhat at the same level. [T and V are more similar for the periods less than 10 days. T and U have more in common at long periods (more than 12 days)]. Such behavior is expected even for the classical "normal" planetary wave (PW) modes, due to different global harmonic (Hough mode) structures [*Forbes*, 1995]. This is important to keep in mind when comparing different parameters from different heights.

Spectral features common to MetO (0.46 hPa, ~50 km) and MFR (82 km) heights, as indicated by wavelet and cross-wavelet analysis, are restricted to winter months and are typically of 15-25 day periods for the zonal and less than 10 day periods for the meridional components. Such strong events usually also provide evidence for the associated PW over a range of latitudes (10-15^{o}) and, of course, longitudes; there may even be PW signals at 100 hPa.

Wave number analysis shows that the eastward motions dominate at low stratospheric heights, while westward motions become comparable or even stronger in the upper stratosphere/lower mesosphere. Earlier analysis [*Manson et al.*, 2004a] demonstrated westward motions at upper middle atmosphere heights (~85 km). The eastward waves at the lower heights are dominated by small scale synoptic waves, which will be absorbed at greater heights (due to their small "critical speeds" [*Charney and Drazin*, 1961], or eastward motions relative to the background winds). The mean background wind also

apparently plays an important role in determining the spectrum of waves that are able to propagate upward, especially due to the existence of critical levels (where wave phase speed is equal to background wind) in summer months. However, the increasing influence of westward propagating waves with height may be due to in situ generation [*Lieberman et al.*, 2003] or a southern hemisphere source [*Luo et al.*, 2002b]. It was also noted that at mesospheric heights there are more similarities in the characteristics of the wave activity between different locations (1000-7000 km in the CUJO network) compared to low stratospheric heights, where local weather phenomena dominate.

Overall, there are relatively few oscillations in the PW spectrum which can be followed from low stratosphere heights near 100 hPa (MetO) to the upper mesosphere near 82 km (MFR), and which are also hemispherically coherent (with well defined wave numbers). This is consistent with the intermittency in time and space of bursts of PW energy obtained at mesospheric heights. Although the three considered years (2000-2002) differ one from another in the details of the dynamic activity, the general results of comparisons are consistent from year to year. The results obtained are in agreement with findings by *Lawrence and Randel* [1996] and by *Lawrence and Jarvis* [2003], but expand upon them in the range of heights used, numbers of MLT observational sites, and the calculations of wave numbers and propagation directions throughout the middle atmosphere.

The main results presented in this chapter have been published in Annales Geophysicae [*Chshyolkova et al.*, 2005a].

Chapter 4

INTER-HEMISPHERIC COUPLING

4.1 Introduction

Year 2002 stands out for the atmospheric research community. For the first time since the beginning of the regular observations in 1957, a major Sudden Stratospheric Warming (SSW) was detected in the Southern Hemisphere. By definition, during a major SSW the zonal mean temperature significantly (at least 25 K per week) increases poleward from ~60^{o} latitude and the usual winter eastward winds reverse and become westward at 10 hPa (~32 km) or below. Although these events are not unusual in the Northern Hemisphere, they have never been observed before in the Southern Hemisphere and it was believed to be unlikely due to comparatively weak planetary wave (PW) activity there. This unprecedented event has generated huge interest amongst atmospheric scientists and motivated detailed investigations, which have resulted in dozens of publications (see, for example, a special issue of the Journal of the Atmospheric Sciences published in March of 2005).

The paper by *Dowdy et al.* [2004] has provided results of mesospheric radar observations during the austral winter of 2002. The authors reported an increased PW activity in the MLT (Mesosphere/Lower Thermosphere) region. In particular, a 14-day oscillation was detected in the mesospheric winds at several Antarctic stations. It was suggested that this oscillation had originated in the troposphere and propagated upward. This was an opportunity for us to examine the vertical coupling in the Antarctic Middle Atmosphere (MA) and compare it with the results from the Northern Hemisphere.

Another aspect of this study is that the warming occurred at the end of September, which is an interesting time by itself. Twice a year, in spring and autumn, at extra-tropical locations the circulation of the middle atmosphere changes between summer

(westward winds) and winter (eastward winds) patterns. During these intervals, the so-called equinoctial transitions, large temperature and airglow variations are observed at Mesosphere/Lower Thermosphere (MLT) heights in satellite and ground-based measurements [*Stegman et al.,* 1992; *Shepherd et al.,* 1999; *Taylor et al.,* 2001; *Shepherd et al.,* 2002]. Dynamical processes seem to be the most logical cause for such temperature and airglow variabilities. *Manson et al.* [2002a] investigated dynamical processes at mesospheric heights during spring time transitions (STT). The study involved several years of airglow data from Sweden and the United States, along with MFR data. It was found that the rapid changes (STT) in the airglow are usually associated with regional and hemispheric winter-to-summer zonal wind reversals and with changes in gravity wave (GW) activity (10-120 min periods); meanwhile the thermal tides (diurnal, semi-diurnal) and propagating planetary waves (PW; 2-16 days periods) showed little evidence of linkages with STT. It was also suggested that STT can be associated with the final stratospheric warming event of the Northern Hemisphere, observed at the end of March and early April [*Manson et al.,* 2002a; *Shepherd et al.,* 2002]. This implies strong dynamical coupling between the stratosphere and mesosphere.

Liu and Roble [2004] performed numerical simulations for the boreal autumnal transition using the National Center for Atmospheric Research (NCAR) Thermosphere-Ionosphere-Mesosphere-Electrodynamics general circulation model (TIME-GCM, *Roble and Ridley* [1994]). They suggested that large temperature, wind, and airglow variations can be caused by fast changes in both phase and amplitude of the quasi-stationary PW. *Liu and Roble* [2002] also studied the coupling of the lower and upper atmosphere during a stratospheric sudden warming (SSW) using the coupled TIME-GCM/CCM3 (Climate Community Model version 3). They showed that during this event a combination of PW and GW altered the mean wind circulation. Changes in the meridional circulation in the upper mesosphere (from poleward/downward to equatorward/upward) caused a depletion of atomic oxygen. Further model simulations [*Liu and Roble,* 2004] demonstrated that changes in the stratospheric and mesospheric circulations during equinoxes lead to changes in the propagation conditions for GW, which in turn, alter the meridional circulation. And as was mentioned above, the

meridional circulation, in particular its vertical component, has the largest effect in oxygen depletion. In this model study PW seem to be not directly responsible for the equinox transitions. However, the authors noted that rapid PW changes during these time intervals can introduce additional variability into the MLT region, and as a consequence affect the atomic oxygen concentration. *Shepherd et al.* [2004] focused on airglow and its relationship to winds. It was suggested that atomic oxygen variability is caused mostly by vertical motions, which is in agreement with the numerical results obtained by *Liu and Roble* [2004]. Comparisons of the airglow and wind observations with simulation results from the TIME-GCM model showed overall good agreement.

Atmospheric waves (PW, GW) and mean wind circulation are closely interdependent. As in the case of equinoctial transitions, their complex interactions can cause strong variabilities in different atmospheric parameters observed in the middle atmosphere. Therefore, it is important to understand the dynamical processes that occur during the vernal and autumnal equinoxes as these are times of strong coupling processes between different atmospheric regions.

In this chapter global PW variability in the stratosphere and MLT has been investigated. The MetO data are used to characterize the stratospheric state during 2001 and 2002 years (Section 4.2). The results of the wavelet transform of MetO stratospheric winds with reference to MFR in the Southern Hemisphere illustrate an example of the vertical coupling in the Antarctic (Section 4.3). The possibility of inter-hemispheric coupling is discussed in Section 4.4. Section 4.5 presents spectral analysis of the MetO and MFR winds in the Northern Hemisphere. The main results are summarized in Section 4.6.

4.2 Zonal Mean Stratospheric Temperature and Winds during 2001 and 2002

As was mentioned in previous chapters, the propagation of the planetary waves forced in the troposphere depends crucially on the zonal mean flow. To assess the state of the atmosphere at stratospheric heights, the MetO zonal mean temperatures and EW winds are presented in Figure 4.1 for 2001 and 2002 (the left and right panels, respectively). Each parameter is shown for all latitudes (positive and negative in the Northern and

Southern Hemispheres, respectively) at three heights 10, 1, and 0.3 hPa (~30, 47, and 54 km). The white line is a zero line that divides eastward and westward wind fields. The mean zonal values are calculated by averaging over all longitudes at each latitudinal circle. The rapid change in temperatures seen as a thin line at the end of November 2002 at two upper heights is not a natural event, but rather an artificial variation due to changes made to NOAA-16 processing, which affected the data at upper stratospheric heights.

At stratospheric heights the temperatures (the bottom section of Figure 4.1) are lower over the winter hemisphere and higher over the summer one. Large meridional temperature gradients during solstice seasons create strong stratospheric winds according to the thermal wind equation (eq. 1.5). The EW winds (the upper section of Figure 4.1) exhibit typical stratospheric circulation with strong eastward flow in winter and westward flow in summer at middle/high latitudes with relatively weak westward winds at low latitudes. There are two time intervals, March/April and September/ October, when at the upper stratospheric heights relatively weak eastward winds blow throughout all latitudes due to the longer duration of the winter season. The inter-hemispheric differences are apparent from the figure: temperatures over the winter South Pole are lower than over the winter North Pole. This creates stronger temperature gradients leading to stronger eastward winds in the Southern Hemisphere winter.

Another difference between the two hemispheres is high winter variability in the Northern Hemisphere. For example, a couple of positive temperature pulses appear in both 2000/01 and 2001/02 boreal winters through all stratospheric altitudes. Corresponding reversals in eastward winds (at the end of January and December months) are also evident on the plots (upper section of Figure 4.1). The Southern Hemisphere usually exhibits less temperature variability and strong steady eastward winds are present during the whole winter of 2001, which was a typical year. In contrast, 2002 was very unusual in the dynamical sense for the Southern Hemisphere. Temperatures and EW winds were highly variable with a wind reversal at the end of

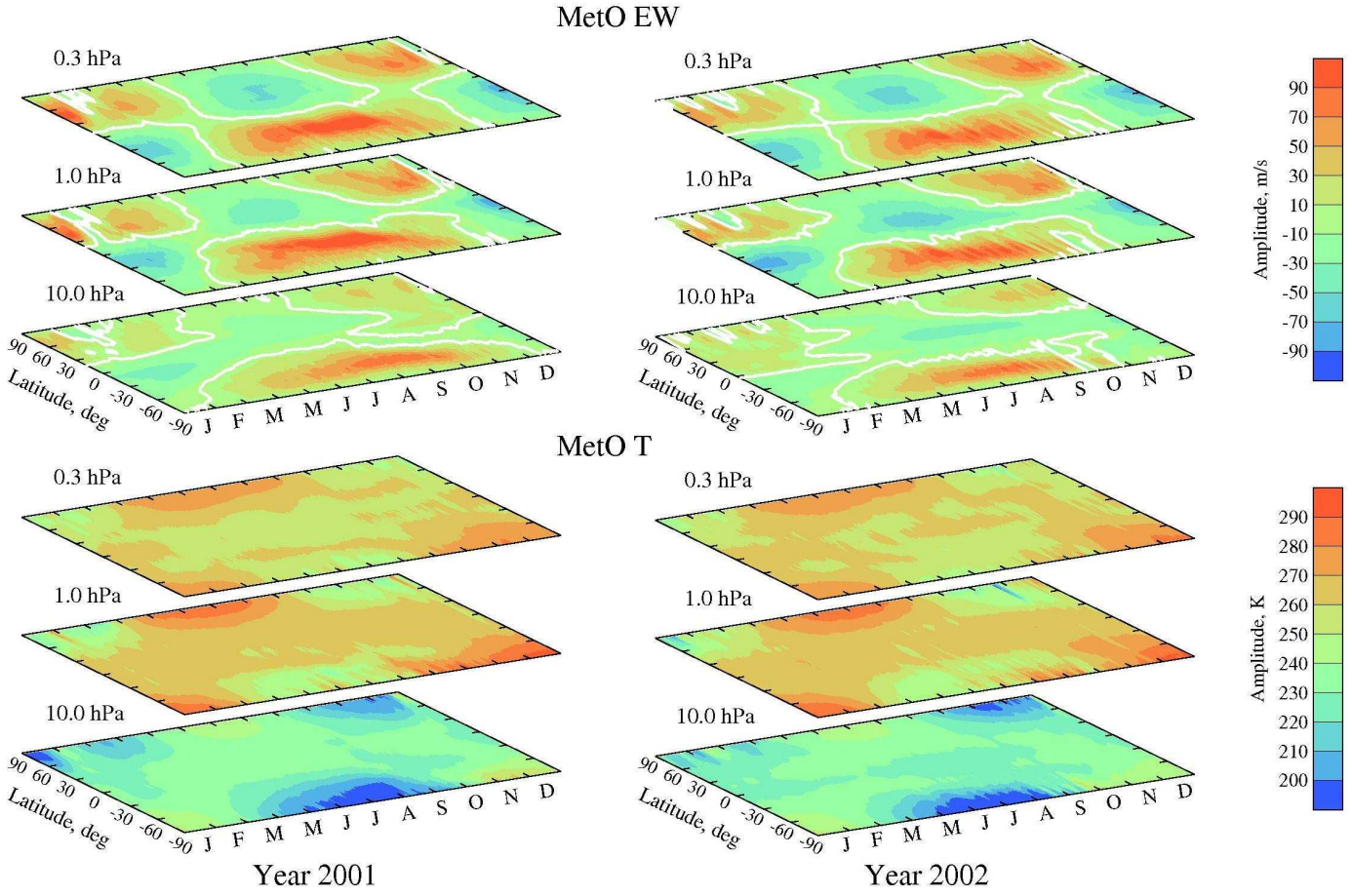

Figure 4.1 The MetO zonal mean EW winds (the upper row) and temperatures (bottom row) versus latitude (positive numbers correspond to the Northern Hemisphere) are presented for 2001 (left column) and 2002 (right column). Each parameter is shown at three heights: 10, 1, and 0.3 hPa. The white line is the “zero-wind” line.

September at all shown heights. At 10 hPa the temperature gradient between low and high southern latitudes was evidently less in 2002 than in 2001 and on the plot a strong positive (yellow) temperature impulse can be found at high southern latitudes in late September. While 2001 was characterized by continuous warming since the end of August, the warming in 2002 started earlier and was interrupted in September at upper stratospheric levels before the final warming and wind reversal in late October.

4.3 Vertical Coupling in the Antarctic Middle Atmosphere during Winter of 2002

According to *Baldwin et al.* [2003] the year 2002 stands out in the last two decades: throughout the austral winter the polar eastward jet exhibited regular oscillations, amplitudes of wave numbers 1 and 2 (quasi-stationary PW) were the largest compared to previous years and several minor warmings (July 8-15, August 2-10 and August 20-28) were observed. It appears that this unusually high variability led to the first recorded Southern Hemispheric major stratospheric warming (mid-winter or spring) with the splitting of both the vortex and the Antarctic ozone hole on September 26. The meridional temperature gradient and wind reversal of Figure 4.1 meet the classic definition of a warming [*Baldwin et al.,* 2003].

Mesospheric winds also demonstrated unusual behaviour and reversals. *Dowdy et al.* [2004] presented the MFR winds measured at Davis (69^{o}S, 78^{o}E), Syowa (69^{o}S, 40^{o}E) and Rothera (68^{o}S, 68^{o}W). They showed that, compared to previous years, year 2002 was characterized by weaker zonal winds and increased PW activity at mesospheric heights. During the major stratospheric warming the reversal of the eastward winds was observed at ~80 km. The westward winds were replaced by the typical winter (eastward) winds again a week before the final transition to the summer (westward) winds. During August-October a westward propagating oscillation with period ~14 days and wave number 1 was detected in winds at 76-84 km height range over all three stations. The amplitudes of the oscillation in the meridional winds were estimated to be 1.5-2 times larger at Davis and Syowa than at Rothera. The authors suggested that this

oscillation propagated from the lower atmosphere, although they did not show any stratospheric analysis.

Here the wavelet amplitudes of the MetO meridional and zonal wind components at 1 hPa (~48 km) altitude are shown for the Davis and Rothera grid-locations (Figure 4.2). The black thick solid lines encircle areas with spectral features exceeding the 90% confidence level. The time interval covers four years from December 1998 to December 2002, which includes two extra years (1999 and 2000) for better assessment of the PW activity in the Southern Hemisphere. Unlike the boreal winter, where PW activity exists from the winter solstice (Figure 4.3), the austral winter exhibits less PW activity. In particular, there is a minimum of PW activity in the middle of the austral winter (1999-2001), which is believed to arise as a consequence of the inability of PW to propagate through the strongest EW winds. It is also As noted in Section 1.4, vertical propagation can not occur if the sum of eastward winds and westward PW phase velocity is too large (larger than critical speed U_c). It is evident from Figure 4.2 that the austral winter of 2002 differs from previous years in that it is more similar to the winters in the Northern Hemisphere. It is interesting that strong peaks of around 10-15-day period in September 2002 are clearly seen in both wind components for both stations, with NS wind amplitudes ~1.5 times larger at Davis than at Rothera. Another pulse with slightly longer period (15-20 days) occurred in August. There is also strong spectral activity at shorter periods (5-10 days) at these times. Such similarities between stratospheric (Figure 4.2) and mesospheric [*Dowdy et al.,* 2004] heights probably indicate that the 14-day oscillation observed in MLT winds was generated at tropospheric heights and propagated upward to the mesosphere. It is also apparent from Figure 4.2 that MetO shows much weaker PW activity in 2001 at both stations at 1 hPa pressure level, which also was the case for the mesospheric winds (at least for Davis) [Andrew Dowdy, private communication 2004]. Alternation of years with weak PW activity (1999, 2001) with those with stronger PW (2000, 2002) might indicate the influence of the quasi-biennial oscillation (QBO), which is the variation of the stratospheric zonal flow over the equator with period near to 2 years. However, analysis of more years of data is required before definite conclusion can be made.

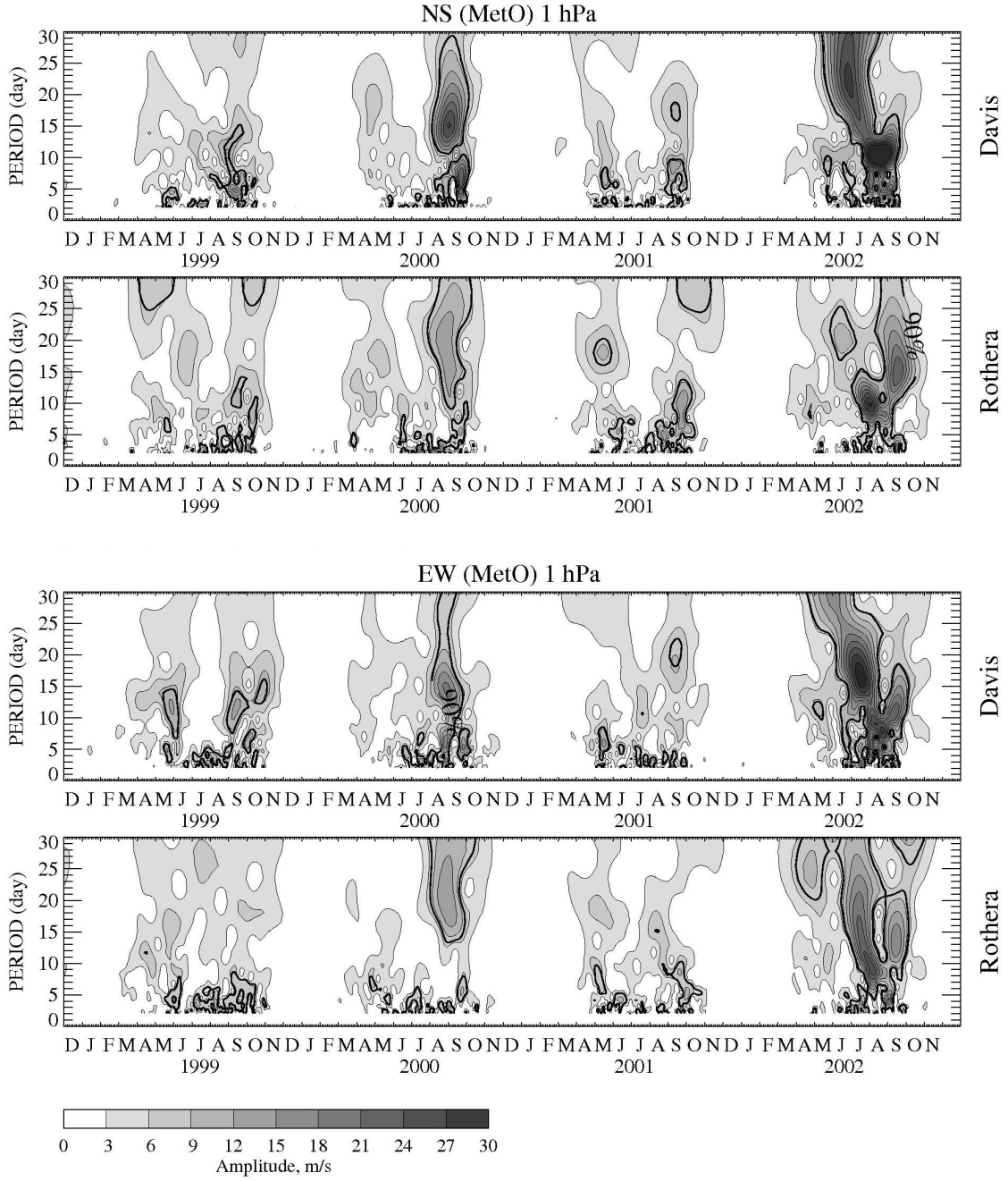

Figure 4.2 Wavelet amplitudes versus time (December 1999-December 2002) and period (2-30 days) calculated for the meridional (top two rows) and zonal (bottom two rows) components of the MetO winds at 1 hPa for the Davis (69^{o}S, 78^{o}E) and Rothera (68^{o}S, 68^{o}W) locations. The black thick solid lines indicate features that exceed the 90% confidence level.

4.4 **Inter-Hemispheric Coupling**

Since the Southern Hemisphere was unusually disturbed during the winter season (June-September) of 2002, it is interesting to compare it with the variability in the Northern Hemisphere. The wavelet amplitudes of the MetO wind components for 1 hPa pressure level were calculated for the period range from 2 to 30 days and the time interval from December 2000 to December 2002. The contours of the amplitudes obtained are shown in Figure 4.3 for five CUJO locations in the same order as in the previous chapter: with the most poleward CUJO station [Saskatoon (52^{o}N)] on the top, the most equatorward CUJO station [Yamagawa (31^{o}N)] in the bottom, and three mid-latitudinal stations [Platteville, London, and Wakkanai (40-45^{o}N)] in the middle. The results for meridional (NS) and zonal (EW) winds are presented on the left and right column, respectively. The black thick solid lines indicate features that exceed the 90% confidence level. Clearly the strongest PW activity is in winter and the weakest is in summer months. During spring and autumn, the transition times, some wave activity with periods around 10-12 days are evident. Although these peaks have smaller amplitudes compared to winter peaks, they occur repeatedly from year to year. The PW activity during the two winters (2000/01 and 2001/02) and the beginning of the winter season 2002/03 are quite different in terms of the occurrence and periods of disturbances. However, in contrast to the Southern Hemisphere (Figure 4.2), wavelet peaks have comparable amplitudes from year to year.

To investigate the possibility of inter-hemispheric PW propagation, cross-wavelets of the MetO (1 hPa) EW winds were calculated between Southern Hemispheric stations (Davis and Rothera grid-locations) and Northern Hemispheric CUJO grid-locations (other locations could have been chosen, but we retained these as there are complementary MLT-MFR data). The results are presented in Figure 4.4. The cross-products between Davis/Rothera and five CUJO locations are shown on the left/right panel. In most cases cross-product maxima on the plots are results of contributions from spectral maxima in both parameters. Contours drawn by black thick solid lines correspond to areas where peaks have exceeded the 50% confidence level in

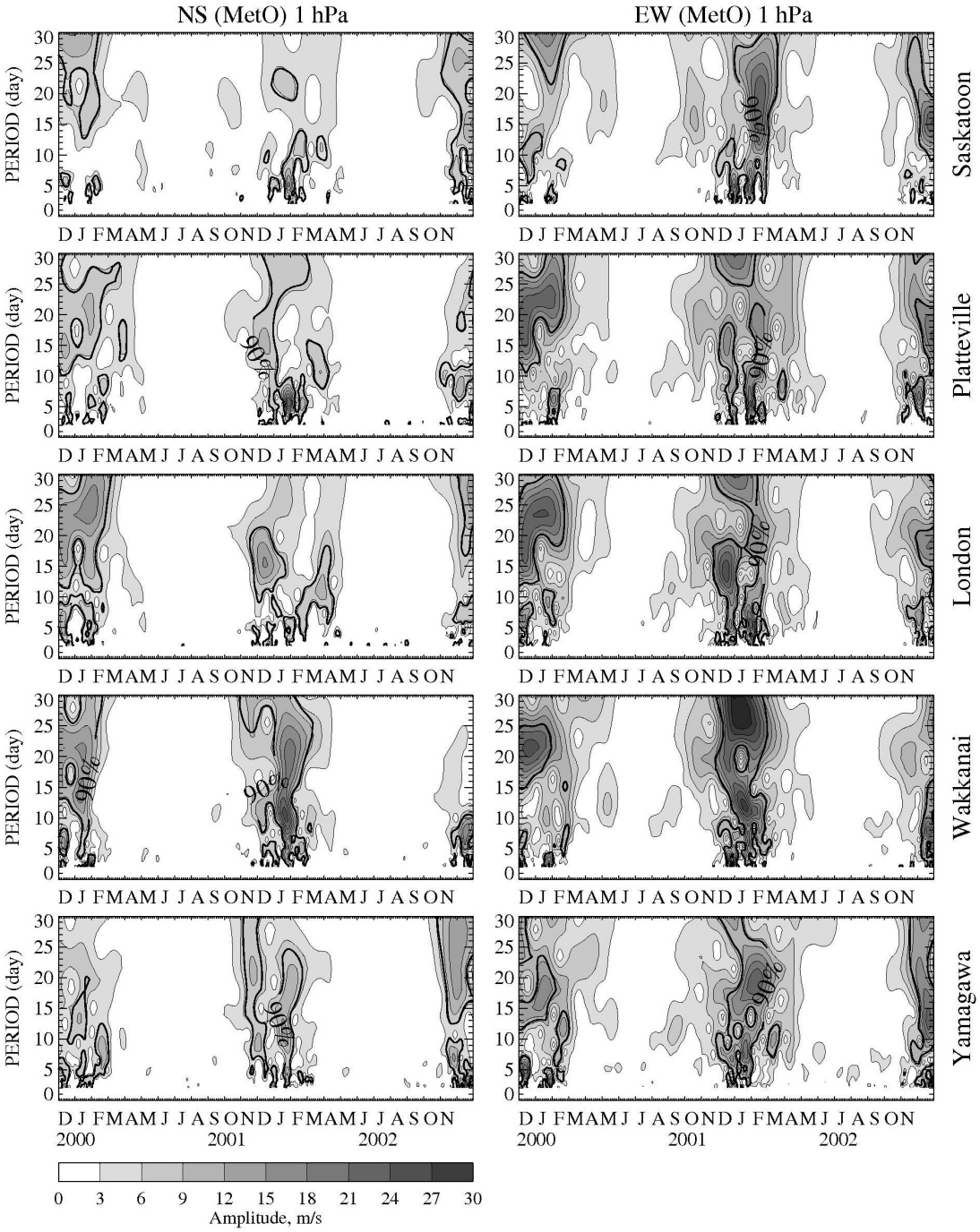

Figure 4.3 Wavelet amplitudes versus time (December 2000-December 2002) and period (2-30 days) calculated for the meridional (left column) and zonal (right column) components of the MetO winds at 1hPa for five CUJO locations. From the top to bottom these are Saskatoon, Platteville, London (Canada), Wakkanai, and Yamagawa. The black thick solid lines indicate features that exceed the 90% confidence level.

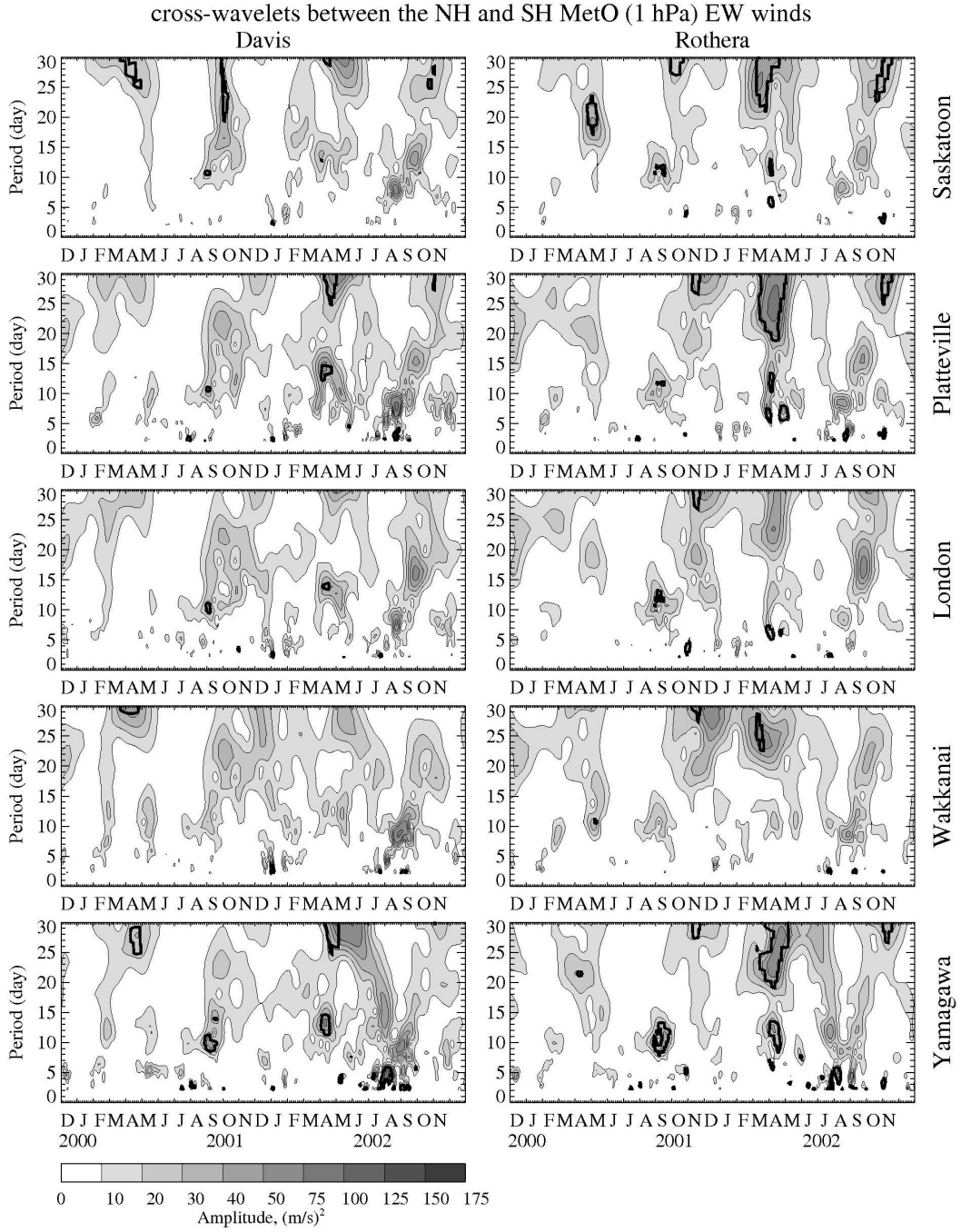

Figure 4.4 Cross-wavelet amplitudes versus time (December 2000-December 2002) and period (2-30 days) calculated for the MetO (1 hPa) EW winds between Southern and Northern Hemispheric stations. Cross-products between Davis/Rothera and five CUJO locations are shown on the left/right column. The black thick solid lines encircle areas where spectral features are larger than 50% confidence level in both original wavelets.

both original wavelet spectra. As can be seen from Figure 4.4, the spectral energies tend to be situated in spring and autumn months, with weak but well-formed peaks. Again, the peaks at 6-8 and 10-15 days in August and September 2002 (Figure 4.2) are clearly seen, and they are stronger than in previous years. In particular the 6-8d peak in the cross-wavelets for Davis/CUJO pairs (Figure 4.4) is evident, but that is likely due to the stronger Southern Hemispheric activity in this particular year. Although there is spectral energy at these periods at CUJO locations, the cross wavelets did not reach the 50% confidence level. During September 2001 there are very clear 10-15d peaks (Figure 4.4) that are present at each of the Antarctic-CUJO pairs (the 50% confidence level is met at all but Wakkanai). Their clarity suggests even stronger cross-hemisphere coupling in this year, given that the Antarctic PW activity (Figure 4.2) was weaker. The fact that, in spite of scattered distribution of the southern and northern hemispheric stations, the common features are still evident suggests the global nature of these oscillations in both years, but with greater confidence in 2001. Figure 4.4 has features consistent with Figure 4.1, which showed continuity of the eastward mean winds from pole to pole (or Southern to Northern Hemisphere) during equinoxes and especially in 2001 when no austral major sudden stratospheric warming occurred: under these conditions a cross-equatorial propagation path exists for these PW in the stratosphere.

Wave number calculations for the dominant PW of 2001 and 2002 were also completed to provide further insight into the hemispheric dynamics and inter-hemispheric coupling. The amplitudes were calculated for several oscillations with different periods (T) and wave numbers (m) using the Least Square fit for two years, 2001 and 2002 (Section 2.8). For waves with periods of 12 and 16 days the fits were performed using a time window of 48 days and 4-day step. The calculations were also made for the 12 day wave with the 36-day window. No significant differences between results obtained with either window length were found. For consistency, amplitude plots calculated for 12-day waves using the same window length as for 16-day wave calculations are presented. Variations of the amplitudes with time and latitude of oscillations with T=12d (upper panels) and T=16d (lower panels) and wave numbers m=+1 (westward propagating)

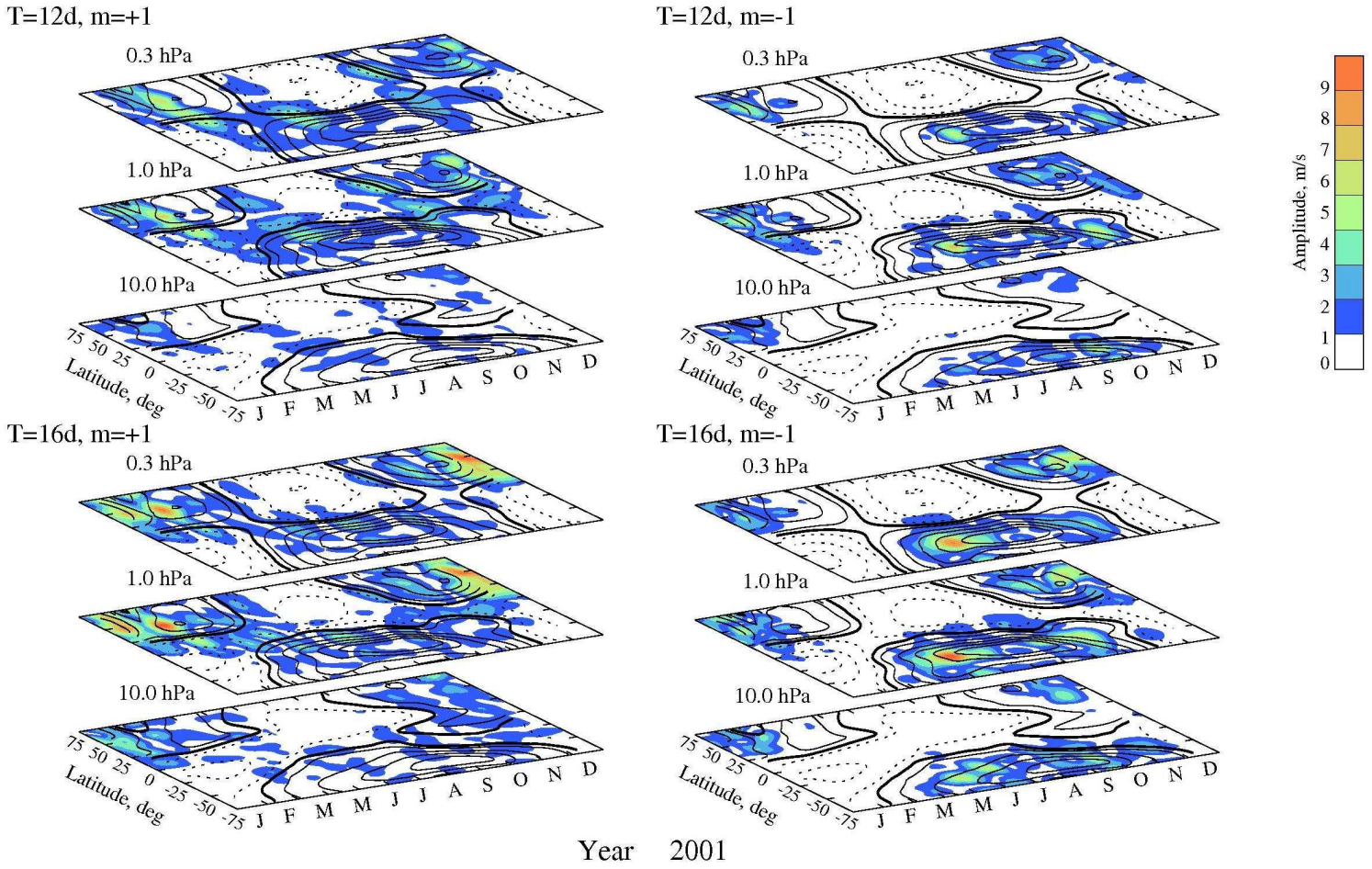

Figure 4.5 The amplitudes of the MetO EW wind oscillations with periods 12 (the upper row) and 16 (the bottom row) days and westward/eastward wave numbers +/-1 versus latitude are shown for year 2001. The mean zonal EW winds smoothed over 30 day intervals with 5 day step are contoured by solid (positive, eastward) and dashed (negative, westward) lines. The thick line is the "zero wind" line. The other contours are …-30, -10, +10, +30 ... m/s.

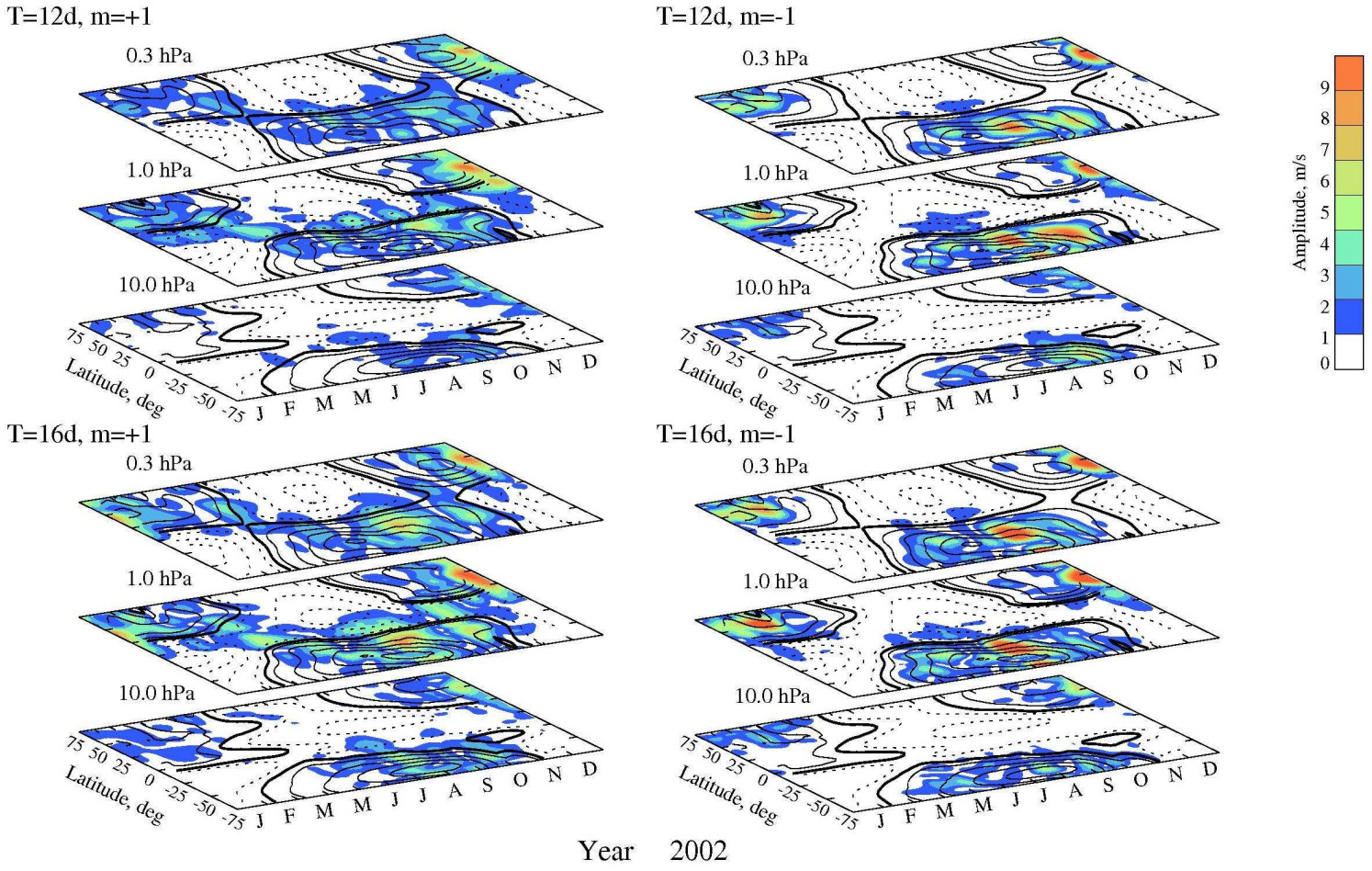

Figure 4.6 The same as Figure 4.5, but for year 2002.

and m=-1 (eastward propagating) for each are demonstrated in Figure 4.5 and Figure 4.6. Two periods are shown, as distinguishable differences are evident, and both periods were apparent in August-September 2002 (Figure 4.2). The zonal mean EW winds smoothed over 30 day intervals with a 5 day step are shown by solid (positive, eastward) and dashed (negative, westward) lines. The thick line is the "zero wind" line. First consider year 2001 (Figure 4.5). Overall, the PW activity is higher (in amplitudes – red/orange) in the Northern Hemisphere with westward propagating waves (especially 16d) being strongest, while eastward propagating oscillations dominate the less PW-active Southern Hemisphere. In January/February and December the 16-day westward propagating oscillations have the biggest amplitudes, which appear near the reversals of the eastward winds in the winter hemisphere. While waves with negative m (eastward) are confined to the winter region (with the eastward flow) in both hemispheres, the waves with positive m (Rossby) penetrate through the equator into the opposite hemisphere during equinox months at the upper stratospheric levels. For the boreal spring of 2001 the 12d PW stretches across the hemisphere from February to March and the 16d from March to April (Figure 4.5). Also in the austral spring there is 12d and 16d PW activity stretching across the hemispheres in August/September. The latter matches the spectral features with regard to vertical coupling in the Northern Hemisphere (Figure 4.7, 1hPa and 82 km) and inter-hemispheric coupling (Figure 4.4, 1hPa). This global wave number analysis adds weight to the notion of inter-hemispheric PW propagation.

During the unusual year 2002 (Figure 4.6), the Southern Hemisphere exhibits more PW variability: eastward as well as westward waves are strong with prominent enhancements in July, August and September for both 12d and 16d periods. Combination of m+/-1 at 12d and 16d periods in both winter hemispheres can lead to standing wave features, and these latter were commented upon by *Baldwin et al.* [2003]. In late September the westward propagating 16-day oscillation is the strongest (the eastward mode has decayed) and it crosses the equator reaching up to ~25^{o}N. The 12-day wave behaves similarly, although it is weaker. Remnants of that spectral energy are seen in the CUJO network, as discussed with regard to Figure 4.4 and Figure 4.7 above.

Again, eastward waves are restricted to central portions of the winter eastward flow, while westward waves (Rossby) extend to reversals and beyond. Phase variations with height indicate that these waves have either very long (80-100 km) vertical wavelengths or evanescent structures, which is consistent with theoretical expectations for Rossby or "long" waves.

In interpreting Figures 4.4-4.6, it should be noted that Rossby normal modes (Section 1.4), globally resonant oscillations, may be excited by geophysical noise, and do not require forcing, which is temporally or spatially unique to the wave's global structure (Hough modes). Thus although forcing from the winter-spring hemisphere, where the PW modes have existed, could have led to PW presence in the opposite hemisphere, this may not be the case. The presence of the PW in both hemispheres in March/April and September/October could simply be due to global amplification and vertical propagation to stratospheric heights. More detailed analysis will be required to distinguish these two possibilities.

4.5 Vertical Coupling in the Northern Hemisphere MA

To demonstrate the coupling between the stratospheric and mesospheric heights in the Northern Hemisphere, cross-wavelets of MetO (1 hPa, Figure 4.3) and MFR (82 km, middle columns of Figure 3.5-3.8) winds were produced and are shown in Figure 4.7 for five CUJO locations. Again thick black lines indicate confidence levels above 50%. Although these results are very similar to the cross-wavelets of MetO (0.46 hPa) and MFR (82 km) winds (the right columns of Figure 3.5-3.8), the new figure is shown for consistency with the results of this chapter and to make intercomparison simpler. As expected the largest activity is observed during winter months and practically nothing is seen during summer. Strong peaks around 10-12 and 20-25 days in February 2001 are examples of strong stratosphere-mesosphere coupling. These peaks can be found at all stations in the EW cross-products as well as in MFR wind wavelets (middle column of Figure 3.6). There are also similar 10-12d weak peaks in Figure 4.4 ("inter-hemispheric coupling"). Since the PW activity in spring and autumn is much weaker than in winter (Figure 4.7), the scale on these figures has been made non-linear to make the

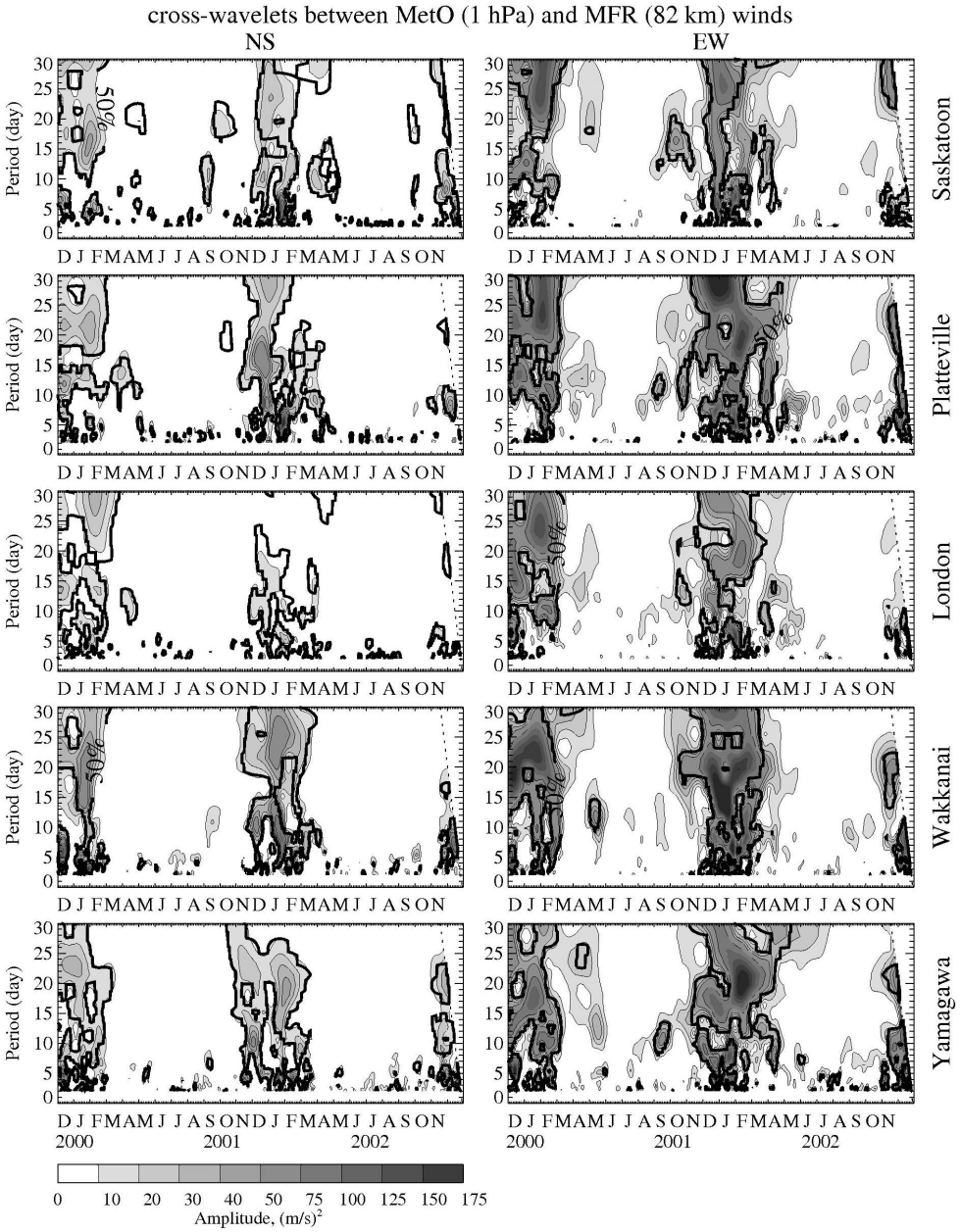

Figure 4.7 Cross-wavelet amplitudes versus time (December 2000-December 2002) and period (2-30 days) calculated between the MetO (1 hPa) and MFR (82 km) winds for five CUJO locations. Meridional and zonal wind components are shown on the left and right column, respectively. From the top to bottom these are Saskatoon, Platteville, London (Canada), Wakkanai, and Yamagawa. The black thick solid lines encircle areas where spectral features are larger than 50% confidence level in both original wavelets.

equinoctial peaks more evident. It is intriguing that there are weak indications of energy near 15 days (EW winds) at the end of September 2002 (at Platteville and Saskatoon), as well as around 6-8 days at the end of August 2002 (at Platteville, Yamagawa, and Wakkanai). These are very similar peaks to those in the Northern Hemispheric MFR winds (middle column of Figure 3.8), in MetO winds for the Rothera and Davis grid-locations (Figure 4.2), and in the inter-hemispheric wavelets (Figure 4.4).

Also in comparison with Figure 4.4, there are indications of 1 hPa - 82 km coupling during September 2001: the PW peaks near 10-15 days, which were very clear at 1 hPa (Figure 4.4), are evident in EW winds at Yamagawa, Platteville, and weakly at London and Wakkanai (middle column of Figure 3.6), as well as in NS winds at Saskatoon and Wakkanai (middle column of Figure 3.5). Variations in PW propagation into the MLT with longitude were previously indicated in 16-d PW studies [*Luo et al.,* 2002b].

The effects of strong PW activity during austral winter 2002 upon the dynamics in the northern summer MLT were also discussed by *Becker et al.* [2004]. They linked several unusual features observed in the polar summer MLT during 2002 to unusually high PW activity in the Southern Hemispheric winter at lower atmospheric heights. These authors argue that changes of PW activity in the winter troposphere affect the global stratospheric circulation, which modulates the saturation of gravity waves in the MLT in both hemispheres. They used the Kühlungsborn Mechanistic General Circulation Model to show that the enhanced PW activity affects the summer stratosphere causing stronger zonal-mean westward winds and a downward shift in gravity wave saturation (lower altitudes for the breaking levels) in the summer MLT. The model results qualitatively agree with the observations (obtained at Andøya, Norway) that showed unusually cold/warm temperatures below/above ~83 km, a stronger lower-mesospheric easterly (westward) jet, a strong westerly anomaly in the upper mesosphere, a reduced/enhanced southward meridional wind above/below 75 km, and turbulent activity down to 72 km compared to the usual 80 km level. It is interesting that the lower boundary of the meridional southward cell observed at the Saskatoon (52^{o}N) radar (not shown) was lower than usual in 2001 (76 km), and the reversal of the westward zonal jet was also lower than usual at 83 km altitude. These are consistent

with observations discussed by *Becker et al.* [2004], and demonstrate another coupling process that involves global inter-hemispheric meridional flow at mesospheric heights.

4.6 **Summary**

The time interval considered includes an unprecedented event – the major stratospheric warming of 2002 with vortex splitting and wind reversals in the Southern Hemisphere. The character of planetary wave activity during this year and a more typical year 2001 is compared. The results indicate that in contrast to the usually weak planetary wave activity dominated by eastward motions, both strong eastward and westward propagating waves existed during austral winter of 2002. During 2002 the westward propagating quasi 16-day oscillation ("~14d") is clearly seen at stratospheric and mesospheric heights of the Southern Hemisphere in September, and some modest spectral energy is also observed at middle northern latitudes. It is concluded that this disturbance has probably originated in the lower atmosphere of the Southern Hemisphere and was able to propagate to the mesospheric heights, where it was detected in MFR winds as an oscillation with T~14+/-1 days and m=+1 [*Dowdy et al.*, 2004]. It also propagated to the Northern Hemisphere, and was identified at 1 hPa and MLT heights.

The longer duration of the stratospheric-mesospheric winter vortex (7 months) compared to that of the summer jet in the Northern Hemisphere provide equinoctial months when eastward winds dominate globally. Results suggest that in March/April and September/October both hemispheres share the same dynamical features, and the planetary waves with periods ~10, 16 and 25 days can penetrate deep into the opposite hemisphere at stratospheric heights. In case of favourable conditions such waves can propagate upward to mesospheric heights. Proper conditions vary with hemispheres, e.g. in 2002 the planetary waves of September-October were only weakly seen in the upper mesosphere of the Northern Hemisphere; in 2001 the planetary waves of the austral spring were weaker in the stratosphere and mesosphere and stronger in the upper mesosphere of the Northern Hemisphere. The "inter-hemispheric coupling" appears to be weaker (smaller cross-wavelet amplitudes) than the vertical coupling. It is interesting that of the two years studied, inter-hemispheric coupling was stronger (more significant)

when there was no austral stratospheric warming: although the Southern Hemispheric planetary wave activity was weaker, the global band of stratospheric eastward winds was stronger and less disturbed. This apparently allowed more hemispheric coupling.

We conclude by briefly repeating the alternate interpretation mentioned in Section 4.4: the presence of Rossby normal modes in both hemispheres during equinoxes may instead be due to their global amplification and propagation to the stratosphere.

Based on this material a paper has been published in the Journal of the Atmospheric and Solar-Terrestrial Physics in 2006 [*Chshyolkova et al.,* 2006].

Chapter 5

QUASI-TWO DAY WAVE

In the Introduction (Section 1.2, Figure 1.2) it was noted that there is considerable variance in the mean (background) wind at mesospheric heights during summer, and that this variance is due to short period PW (predominantly with periods near 2 days). Unfortunately, due to MetO resolution (daily), the studies described in Chapter 3 and Chapter 4, and associated analyses, do not allow complete determination of the role of this variance. We have tried to extract a quasi-2-day wave (hereafter Q2DW) component from the NCEP 6-hourly data (Section 2.6). These data were processed using a finite impulse response (FIR) band-pass filter with 0.025 and 0.018 cycles per hour (40-55 hours). The Q2DW amplitudes obtained were very small, and did not exceed ±2m/s. The NCEP Reanalysis 6-hourly data are available only up to 10 hPa level; that is too low for a clear Q2DW signal. Therefore, we have limited our study of the Q2DW to the mesospheric heights only.

Section 5.1 introduces the Q2DW and gives a review of the literature on this topic. Climatology of the Q2DW over Saskatoon is described in Section 5.2 using wind data measured by the MFR for fourteen years (1990-2003). Longitudinal and latitudinal variabilities of the Q2DW are discussed in Section 5.3. Results are summarized in Section 5.4.

5.1 Review of Q2DW studies (1972-2006)

The Q2DW is a well known phenomenon that has been studied for almost four decades. However it continues to puzzle researchers, who are trying to determine the characteristics of the wave, its sources and its role in the atmosphere. In the first case *Muller* [1972] reported a Q2DW (T~51h) in wind data measured at meteor heights (~97 km) during August 1968 at Sheffield (53^{o}N, 2^{o}W). Later reports include ground-based

and satellite observations of Q2DW at the low, middle and high-latitude regions in both hemispheres [*Kal'chenko and Bulgakov*, 1973; *Clark*, 1975; *Glass et al.*, 1975; *Manson et al.*, 1978; *Aso et al.*, 1980; *Craig et al.*, 1980; *Salby and Roper*, 1980; *Ito et al.*, 1984; *Manson et al.*, 1987; *Poole*, 1988; *Clark*, 1989; *Phillips*, 1989; *Harris and Vincent*, 1993; *Fritts and Isler*, 1994; *Pancheva and Mukhtarov*, 1994; *Thayaparan et al.*, 1997; *Gurubaran et al.*, 2001]. The obtained measurements have indicated that the Q2DW has large horizontal scale size and its characteristics vary with place (latitude, longitude, altitude) and time (days, seasons, from year to year). However, through years of observations some similarities in Q2DW behavior have emerged.

The Q2DW, with its amplitude reaching up to 50 m/s over the tropics, can be comparable to or even dominate the diurnal and semidiurnal tides. Simultaneous measurements at several stations (e.g. *Kal'chenko and Bulgakov* [1973], *Craig et al.* [1980]) suggested that the amplitude of the wave decreases with increasing distance from the equator. The satellite temperature and water vapor measurements revealed the asymmetrical structure of the Q2DW amplitude in the mesosphere with largest amplitude at low latitudes of the summer hemisphere [*Rodgers and Prata*, 1981; *Limpasuvan and Leovy*, 1995].

The amplitude of the wave is different in the meridional and zonal components of the wind: the Q2DW amplitude of the meridional component is generally twice as large as that of the zonal wind. Reports on Northern Hemisphere data indicated that the ratio between Q2DW amplitudes in the zonal and meridional wind components increases over middle-to-high latitude regions, where the Q2DW amplitudes become comparable in both wind components. The latter is consistent with the normal mode structure, for which the ratio is close to 1 at ~70^{o} latitude [*Salby*, 1981].

The Q2DW exhibits strong seasonal dependence: its activity maximizes shortly after solstices in July/August (Northern Hemisphere) and January/February (Southern Hemisphere). Both maxima are clearly seen at low latitude stations. At mid-latitude stations only summer activity is usually reported. However, some studies show that Q2DW can be found at other times of the year as well [*Muller and Nelson*, 1978; *Lima et al.*, 2004]. *Jacobi et al.* [1997a] studied Q2DW activity in wind measurements at 95

km altitude at Collm (52^{o}N) for 1983 – 1995. Their results suggest that the Q2DW can be found throughout the year, but with smaller amplitudes and less regularity compared to summer months. *Namboothiri et al.* [2002] also noted some increased amplitudes (up to 15 m/s) in winter months at Yamagawa (31^{o}N) and Wakkanai (45^{o}N) in 1997-1999 (see their figures 8 and 9). However, these amplitudes are still weaker than summer ones. Results obtained by *Nozawa et al.* [2003a] are, at first sight, inconsistent with previous findings. Using data from high-latitude MFR stations, they found that the Q2DW amplitudes are larger in winter than in summer in the 70-91 km height region. However, simultaneous observations of EISCAT (European Incoherent SCATter) and MFR for a July 1999 event have shown that the Q2DW has maxima at 95 km [*Nozawa et al.,* 2003b]. *Craig et al.* [1983] suggested a cross-equatorial leakage of the Q2DW from the summer to winter hemisphere as this oscillation was simultaneously detected at Sheffield (53^{o}N), Townswille (19.4^{o}S), and Adelaide (35^{o}S) in July and August of 1980. Another case of the simultaneous presence of the Q2DW in both hemispheres (Kyoto (35^{o}N, 136^{o}E) and Adelaide (35^{o}S, 138^{o}E)), during January was reported by *Tsuda et al.* [1988]. The meridional and zonal wind components were observed to be in-phase and out-of-phase between Northern and Southern Hemispheres, respectively. It was not clear as to the extent of this "leakage", i.e. how far poleward the Q2DW can reach. Explanation of the winter activity may require different (from summer) sources of the Q2DW (these are discussed later in this section).

The Q2DW behaves differently during the austral and arctic summers. Generally the Q2DW amplitudes are bigger in the Southern Hemisphere. There are also differences in the average period of the wave (48±5 hrs): it is reported to be close to 48 hrs over the locations in the Southern Hemisphere and to be longer (~51 hrs) in the Northern Hemisphere. Over the equatorial region the Q2DW period is near 50 hrs in July/August and 48hrs in January/February [*Harris and Vincent,* 1993]. The dominant period of the oscillation also changes during the respective events so that the period shortens as amplitude grows and lengthens as amplitude decreases [*Palo and Avery,* 1995; *Jacobi et al.,* 1997a; *Namboothiri et al.,* 2002] and from one year to another.

Several studies that included two or more ground-based stations distributed along a narrow latitudinal belt were conducted to obtain the longitudinal structure of the wave. The most often reported wave numbers are 2, 3, and 4 for different events. Some of the studies [*Glass et al.,* 1975; *Muller and Nelson,* 1978; *Craig et al.*, 1980; *Tsutsumi et al.*, 1996] indicated that the oscillations have a longitudinal wave number 3 (m=3). This was also supported by the earliest satellite observations of the Q2DW in the temperature measurements [*Rodgers and Prata,* 1981]. While *Meek et al.* [1996] using nine radar sites and *Jacobi et al.* [2001] using four European radars found wave number 4 for Q2DW events. Analyzing data from two MFR located at Hawaii (22^oN, 160^oW) and Puerto Rico (18^oN, 67^oW) during summer of 1995, *Zhou et al.* [2000] also found one oscillation with wave number 4, but another had wave number 3. Wave number less than 3 with propagation in a direction South of West was reported by *Poole* [1990] and *Poole and Harris* [1995] for the Southern middle latitudes.

The Q2DW has also been observed in the lower atmosphere. *Muller and Kingsley* [1974] believed that 2-day oscillations in the meteor winds were linked with periodic variations of tropospheric parameters. They suggested that the coupling might involve GW, generated by the passing of tropospheric weather systems and propagating to the upper mesospheric heights, where they dissipate. However, the weather systems have a local character, while the Q2DW is of planetary scale. *Stening et al.* [1978] found Q2DW in August mesospheric wind data at Saskatoon (52^oN, 107^oW) as well as a similar oscillation in the stratospheric temperatures. *Coy* [1979] examined daily meteorological rocket data taken during January and February over Marshall Islands (9^oN, 168^oE), and found a large oscillation (30m/s) in the meridional component of the wind at stratopause level (~50 km). *Reddi et al.* [1988] have analyzed the stratospheric and mesospheric wind data obtained from M-100 rocket launches over Trivandrum (8.5^oN, 77^oE) and found the presence of the Q2D wind oscillation in both meridional and zonal components. The authors showed increase of the wave amplitude with height from ~15 m/s near 40 km to ~30 m/s in the mesosphere (60-80 km). *Craig et al.* [1980] used observations from three Southern Hemispheric MF radars, and also found that the amplitude of the Q2DW increases up to ~85-90 km and decays above. *Palo and Avery* [1996] observed Q2DW with maximum amplitudes between 87 and 92 km in the

meteor winds. However, their analyses of the data from the stratosphere/troposphere radar showed no coherent oscillations with period near 2 days in the low atmosphere at the same time.

The vertical wavelength is estimated to be very long (reports include values from ~50 to 150 km), and varies with latitude: tends to be shorter at lower latitudes [*Wu et al.*, 1993]. The phase progression is downward, which is consistent with upward propagation of wave energy (e.g. *Craig and Elford* [1981]). Along with cases of descending phase, *Lima et al.* [2004] also observed upward phase propagation mainly for events with small Q2DW amplitudes.

The structure of the observed quasi 2-day oscillation suggests that this disturbance can be associated with the wave number 3 Rossby-gravity normal mode of a windless isothermal atmosphere, which propagates westward with period of 2.1 days. *Salby* [1981] calculated the structure of the normal mode in realistic mean fields, and showed that it is magnified near 2.25 days. The amplitude increases with height in regions of weak eastward winds relative to the wave and equatorward temperature gradients, while regions of strong eastward winds and poleward temperature gradients are not favorable for the amplitude's growth. The meridional structure of the normal mode was shown to be antisymmetric for perturbations in temperatures and zonal winds (they are out of phase between the hemispheres), whereas meridional wind perturbations are in phase. Although the characteristics of the Rossby-gravity mode and observed Q2DW were similar in general, there were some differences as well. For example, the former showed increase in both equinox and solstice conditions, while observations indicate minimum Q2DW activity in spring and autumn. *Hagan et al.* [1993] supported the hypothesis that the Q2DW is the westward propagating zonal wave number 3 (m=3) mixed Rossby-gravity mode. Their conclusion was based on the results obtained from a series of numerical experiments for January conditions using a linearized spectral model, which included realistic mean winds and dissipation. The authors showed that the structure of the Q2DW and its period are sensitive to variations in upper stratospheric and mesospheric zonal mean winds. For instance, the resonance period is 48 hrs in summer

and 50-52 hrs in winter. This is in agreement with observations from the equatorial station Christmas Island [*Harris and Vincent*, 1993].

Plumb [1983] has suggested another possible origin of the Q2DW observed in the middle atmosphere. He used a stability analysis of a one-dimensional (variation with height) model of the summer mesospheric flow to show that baroclinic instability of the westward mesospheric jet may be a source of the wave. It was demonstrated that the mesospheric jet is unstable if the eastward shear is larger than 6 m/s per km in the upper mesosphere. The most rapidly growing wave has a zonal wavelength of ~10,000 km and westward phase velocity of ~60m/s, which corresponds to a wave with period of ~2 days and zonal wave number m=3. In fact baroclinic growth may occur for a range of wave numbers with similar wave speeds (some waves with m=2 and 4 were observed). The wave periods are primarily determined by the strength of the jet, so the difference between the summer jet velocities in the Northern and Southern Hemispheres can explain observed inter-hemispheric period differences. *Pfister* [1985] has introduced latitudinal variation of the flow in addition to the altitudinal variability and found that the baroclinic waves are trapped in the middle and high latitudes. The results of this two-dimensional analysis suggested that the growth spectrum peak at zonal wave number 3 with a period close to 2 days matched well for the observed Q2DW. However, it was unable to account fully for this planetary wave phenomenon. For example, the calculated temperature structures have their maximum amplitude at 40-60^o latitude, rather than the observed 20^o. Despite this the author requested caution with this conclusion as the quasi-geostrophic approach he used is “marginal” for waves with periods less than 3 days. Besides, there is a possibility that baroclinic unstable waves may penetrate to the equatorial regions by 'tunneling' and excite free or forced modes there. Also, baroclinic instability can explain some spectral peaks observed in the summer mesosphere (T=1.7 days with m=3 for 60^o jets and m=4 for 40^o jets; T=3-10 days with m=2 for 45^o jets and m=1 for 60^o jets). Despite this *Salby and Callaghan* [2001] argued that instability can explain neither seasonal variabilities in appearance of the Q2DW nor its global structure. This is because instability calculations produce oscillations that are confined to a neighborhood of the unstable region in the summer hemisphere.

Using numerical simulations *Salby and Callaghan* [2001, 2003] explored the connection between the 2.1-day normal atmospheric mode and waves resulted from instability. The results indicated presence of an oscillation with the wave number 4 along with the dominating m=3 component. The authors advocated that the global size and summer solstice-maxima of the Q2DW are explained by the Rossby-gravity normal mode and its intensification through interaction with the stratospheric westward jet. However, authors noted that this mechanism cannot explain the observation of the Q2DW at other times of year. Therefore, it seems that the Q2DW is a combination of the normal mode and a baroclinically unstable wave. Satellite observations of stratospheric and mesospheric temperatures [*Burks and Leovy,* 1986] revealed simultaneous presence of a wave that corresponds to the atmospheric normal mode (T=2.1 days, m=3) and an oscillation with period of 1.8 days and wave number 4, which arose from instability of the jet near the stratopause. This suggests that generation mechanisms of these waves could be coupled. *Randel* [1994] has reached the same conclusion by studying the characteristics of the Q2DW based on five years of National Meteorological Center operational stratospheric analyses. The combination of the normal mode structure and instability signature implied that the Q2DW "is a near-resonant mode forced by dynamical instability". The Q2DW diagnosed using the extended version of the UK Universities Global Atmospheric Modelling Programme also had global structure similar to a Rossby normal mode, but it resulted from instability [*Norton and Thuburn,* 1996]. Satellite (UARS, TIMED, Aura) measurements using HRDI [*Wu et al.,* 1993; *Fritts et al.,* 1999; *Lieberman,* 1999], MLS [*Wu et al.,* 1996; *Limpasuvan and Wu,* 2003; *Limpasuvan et al.,* 2005], and SABER [*Garcia et al.,* 2005] showed several strong events of the Q2DW in mesospheric winds and upper stratospheric temperatures over low-to-middle latitudes. The observed structure of the Q2DW looked like the distorted atmospheric normal mode with period of 2.1 days and m=3. All of these data are consistent with suggestions made on the basis of earlier observations and numerical modeling mentioned above.

The observational intermittency of the Q2DW characteristics can be attributed to several factors. Firstly the instability of the atmospheric jets can generate oscillations with different periods and wave numbers. Secondly the Q2DW itself can be unstable, in

which case secondary waves with longer periods and smaller zonal wave numbers are generated [*Merzlyakov and Jacobi*, 2004; *Merzlyakov et al.*, 2004]. The Q2DW variability can also be explained by its sensitivity to the variations of the summer and winter jets in the middle atmosphere [*Hagan et al.*, 1993]. The variability and significant longitudinal modulation of the Q2DW amplitude may also result from interference of the Rossby-gravity mode with a set of "pseudo-two-day" secondary waves generated by nonlinear interaction of the primary Q2DW with a quasi-stationary PW [*Pogoreltsev et al.*, 2002]. In the case of the Rossby-gravity normal mode with T=2.1 days and wave number 3, it is likely modulated by variations of the mean flow over the equator (QBO). The annual variation of amplitude and period of the Q2DW might be, at least in part, a result of solar influence [*Clark et al.*, 1994]. *Jacobi et al.* [1997a] found a correlation of 0.6 at the 95% significance level between the Q2DW amplitude and relative sunspot number, R.

5.2 Climatology of the Quasi-Two Day Wave over Saskatoon

For an initial look, the Q2DW is extracted from hourly mean MFR winds using a finite impulse response (FIR) band-pass filter between 0.025 and 0.018 cycles per hour (40-55 hours). An example of the meridional (NS, Figure 5.1) and zonal (EW, Figure 5.2) components of the filtered wind measured during year 2002 is shown for five heights from 82 to 94 km. It is clearly seen in the figures that the Q2DW activity manifests itself as a series of sequential enhancements or bursts in both NS and EW components over all range of heights. Possible explanations of such behavior could be the modulation of the Q2DW by other planetary waves with longer periods [*Pancheva et al.*, 2004] and/or the interference between several co-existing spectral components [*Merzlyakov and Jacobi*, 2004; *Merzlyakov et al.*, 2004]. The duration of a burst can vary from 3 to 10 cycles (6-20 days). The amplitude reaches its maximum (20-30 m/s) at approximately 88 km altitude in July (day numbers 182-212) and starts to decay above. The decrease of the Q2DW amplitudes with height in the upper mesospheric–lower thermospheric region is in agreement with other observations [*Nozawa et al.*, 2003b] and model results that indicated damping of the Q2DW by breaking GW [*Jacobi et al.*, 2006] at these heights. During this particular year the Q2DW amplitudes

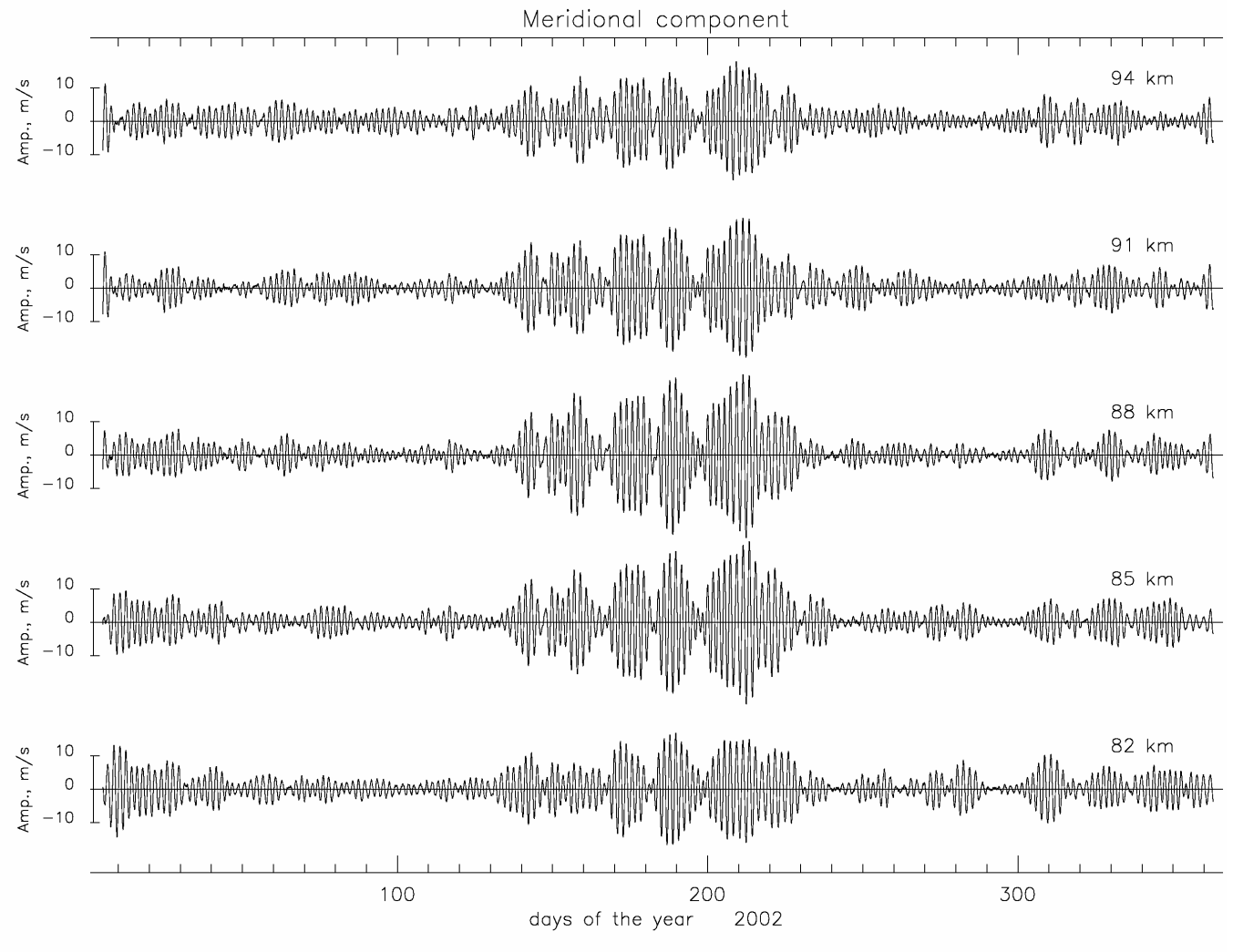

Figure 5.1 Filtered (40-55 hrs) meridional component of the wind measured at Saskatoon in 2002 for 5 heights from 82 to 94 km.

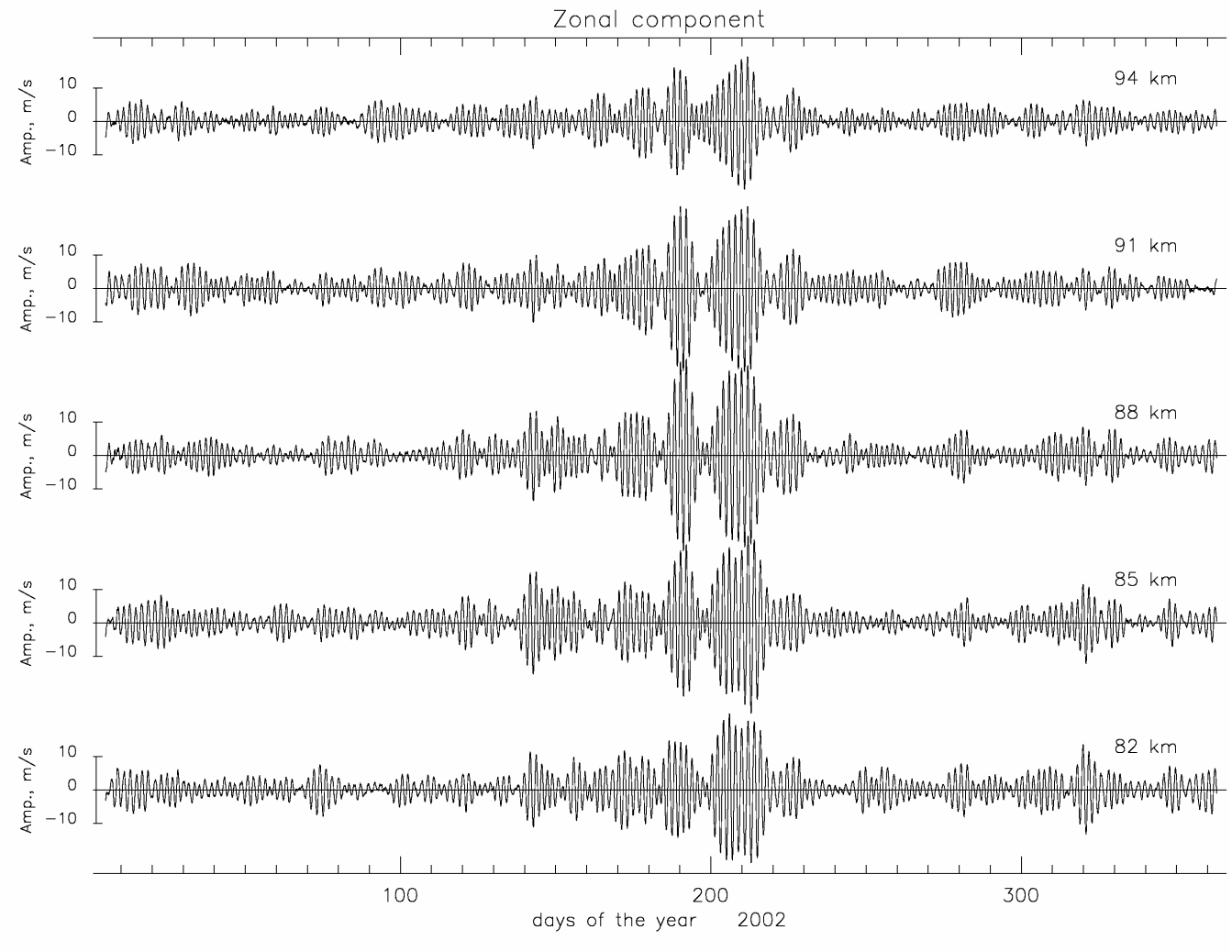

Figure 5.2 Filtered (40-55 hrs) zonal component of the wind measured at Saskatoon in 2002 for 5 heights from 82 to 94 km.

were larger in the zonal wind component. In addition to large summer bursts of the Q2DW there is also weaker activity in winter. The amplitudes are approximately three times smaller than during the summer and the maximum occurs below ~79-82 km. These features of the Q2DW are in general agreement with the observational results discussed in the previous section.

The height profiles of amplitudes and phases are shown in Figure 5.3 for both meridional (upper two panels) and zonal (lower two panels) components for each day of July 2002 (day 182 = July 1) when the Q2DW was strongest. To calculate the amplitudes and phases of the Q2DW, a Fourier Transform (FT) of a 48-hr sequence has been employed. Day 182 and every fifth day after it are shown by thick lines. One division on the amplitude plot corresponds to 10 m/s, while one division on the phase plot is 120 degrees. During the bursts of the Q2DW the clear maximum around 88 km altitude is evident in both components. However the height at which the maximum amplitude occurs is more consistent for the meridional component. The amplitude in zonal winds reaches its maximum at different heights, e.g. it maximizes at ~88, 82 or 91 km around days 187, 198, and 207, respectively. Descent of the height of the maximum is seen most clearly at the end of the month starting on day number 207. Phases for both components generally progress downward indicating upward propagation of wave energy. They also change slowly with height, which is consistent with very long vertical wavelengths (~100 km). According to the published studies (Section 5.1) these results are typical for Q2DW observations at similar middle latitude stations.

It has been already noted that bursts of amplitude occur, and studies involving phase research have also been published [*Clark et al.,* 1994]. The amplitude of the wave varies for durations of a few periods, and phase reversals occur occasionally. This suggests modulation of the amplitude by some effect [*Ito et al.,* 1984]. For example, the modulation of the 12h tide by the 2.1-day wave would cause non-harmonic oscillations with periods ~9-10 and ~16 hours, which have been observed at mesospheric heights [*Manson et al.,* 1982; *Harris and Vincent,* 1993; *Gurubaran et al.,* 2001; *Jacobi et al.,* 2001]. The spectra for a period range from 6 hours to 6 days have been calculated using

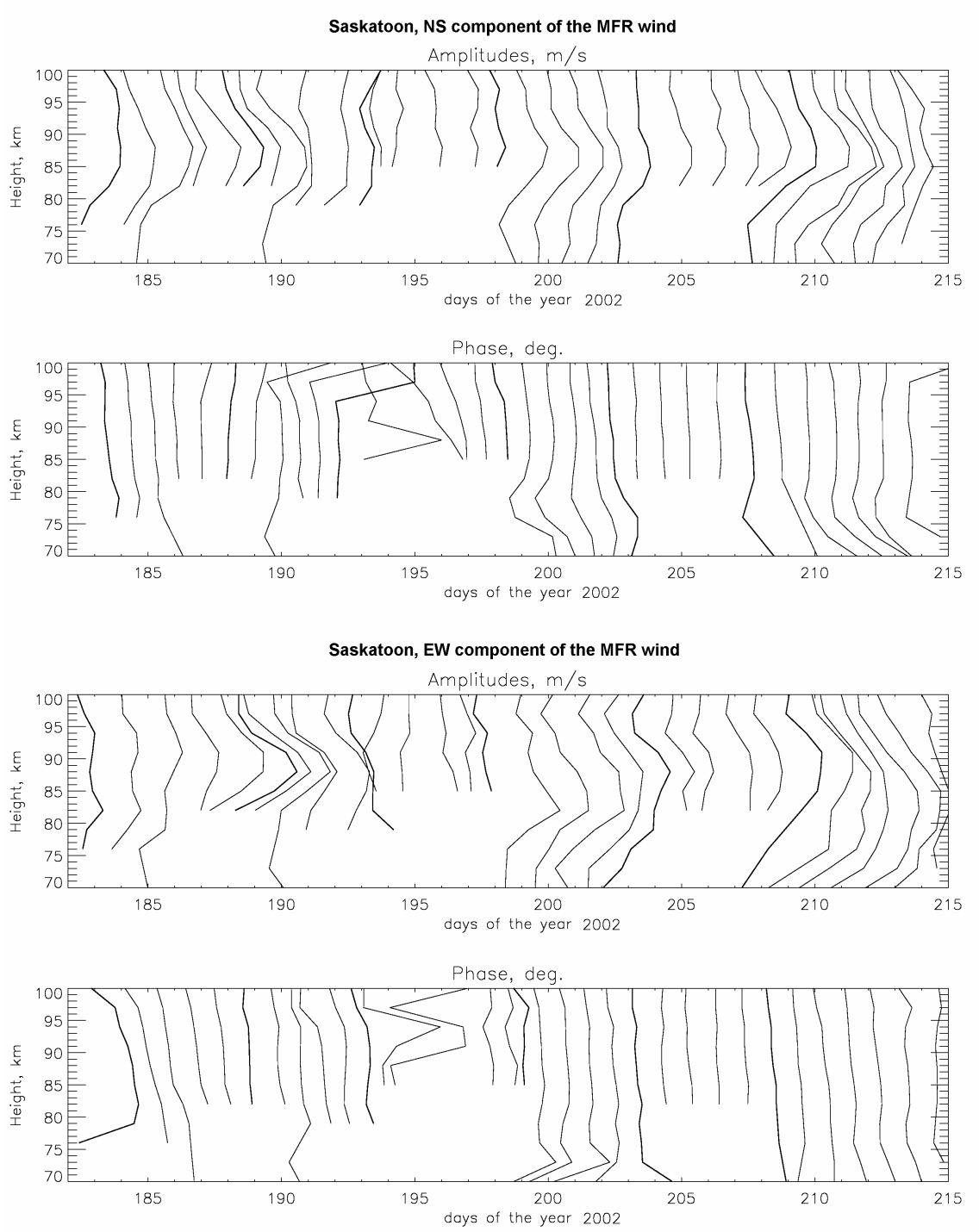

Figure 5.3 The height profiles of amplitudes and phases of the Q2DW for both NS (top panels) and EW (bottom panels) wind components observed at Saskatoon for each day of July 2002 (day 182 = July 1). Day 182 and every fifth day after it are shown by the thick line. One division on the amplitude plots corresponds to 10 m/s, while one division on the phase plots is 120 degrees.

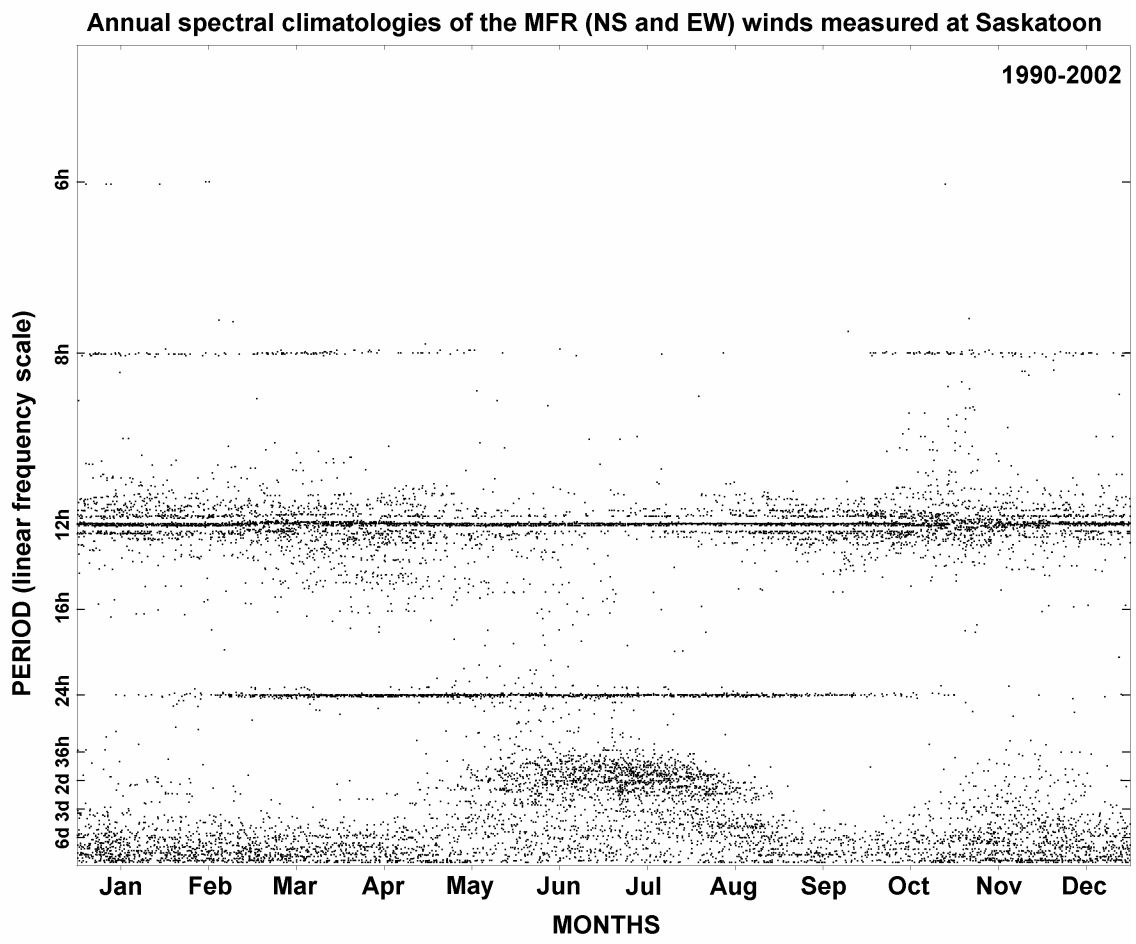

Figure 5.4 Annual climatologies of periods from 6 hours to 6 days in the NS and EW components for 82-94 km height range.

the Lomb-Scargle spectral analysis for winds measured over several years (1990-2002). This is essentially a Least-Square fit that includes a significant level. A 30-day window and 15-day step have been used. Figure 5.4 demonstrates the combined results obtained for NS and EW wind components. The number of dots shown for each period depends upon the occurrence of the oscillation at the 95% level.

The most prominent and continuous oscillations correspond to the tidal (24-, 12- and 8-hr) periods. The narrow gaps near 12hr are artifacts of the box-car filter used in the time sequence. The Q2DW is also seen as a dense area of dots during summer. Some dots near the 2-day period can be found in winter as well. Although there is a weak indication of the 16-hour oscillation, its occurrence does not always coincide with the Q2DW appearances. This may indicate other sources for this oscillation in addition to

the modulation of the semidiurnal tide by the Q2DW. Studying meteor wind data over Cachoeira Paulista (22.7^{o}S, 45^{o}W) Lima et al. (2004) also did not establish any relationships between Q2DW and a 16-hr oscillation. They explained it by very small amplitudes of the latter.

The fairly large spread around the 2-day period in summer can be explained by the variability of the Q2DW period (Section 5.1) as well as by subsidiary components with periods ~40 and 60 hrs, which have often been reported along with the strong Q2DW [*Kingsley et al.,* 1978]. *Jacobi et al.* [1998] investigated the non-linear interactions between the Q2DW and long-term oscillations. Their results indicate that the Q2DW is modulated by 10-day and especially 16-day PW. The interaction between the quasi-2-day and 16-day waves, for example, leads to oscillations with periods of 54.9 hrs and 42.7 hrs. Another study of non-linear interactions between Q2DW and PW was conducted by *Pancheva et al.* [2004] using 15 radars from the Northern Hemisphere. The significant day-to-day variability of the Q2DW was considered to be a result of non-linear interactions between the Rossby normal mode (T=2.1 days, m=3) and PW with periods of 9-10 and 14-17 days.

To investigate year-to year variability, the amplitudes of the Q2DW have been calculated from hourly mean winds using FT analysis (band pass: 0.333-0.666 day^{-1}) for several years (1990-2003). A window of 20-day width, which is slid in 5-day steps, has been chosen for calculations. The length of the window is long enough to exclude small details that would complicate the picture, while it is short enough to distinguish the separate bursts of the Q2DW. Note that the averaging and the effects of a Hanning window tend to reduce the calculated amplitudes, especially when the window used is longer than the duration of a Q2DW burst. The resulting Q2DW amplitudes as a function of height (65-95 km) versus time (January-December) for EW and NS components of the winds for Saskatoon are shown in Figure 5.5 for each year from 1990 to 2003. The background-mean winds (BGW, 20-day window) are also shown by solid (eastward and northward winds) and dashed (westward and southward winds) lines. The two plots in the last row (Figure 5.5c) are contour plots of the amplitudes and BGW averaged over all 14 years.

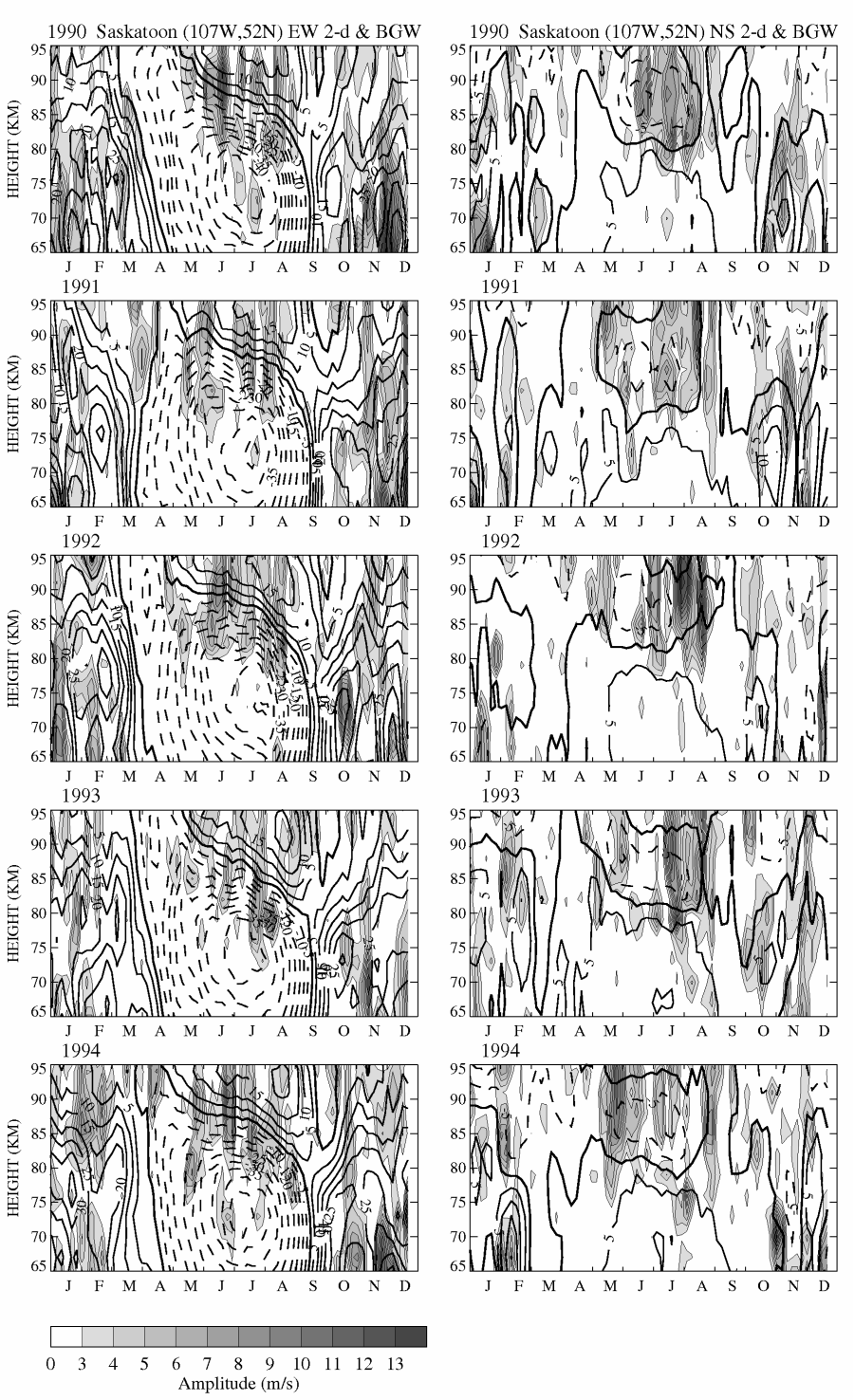

Figure 5.5 (a) Annual contours of Q2DW amplitudes as a function of height versus time for the zonal (left) and meridional (right) components of MFR winds at Saskatoon are shown for 1990-1994. The background mean winds are displayed by continuous (eastward/northward) or dashed (westward/southward) lines.

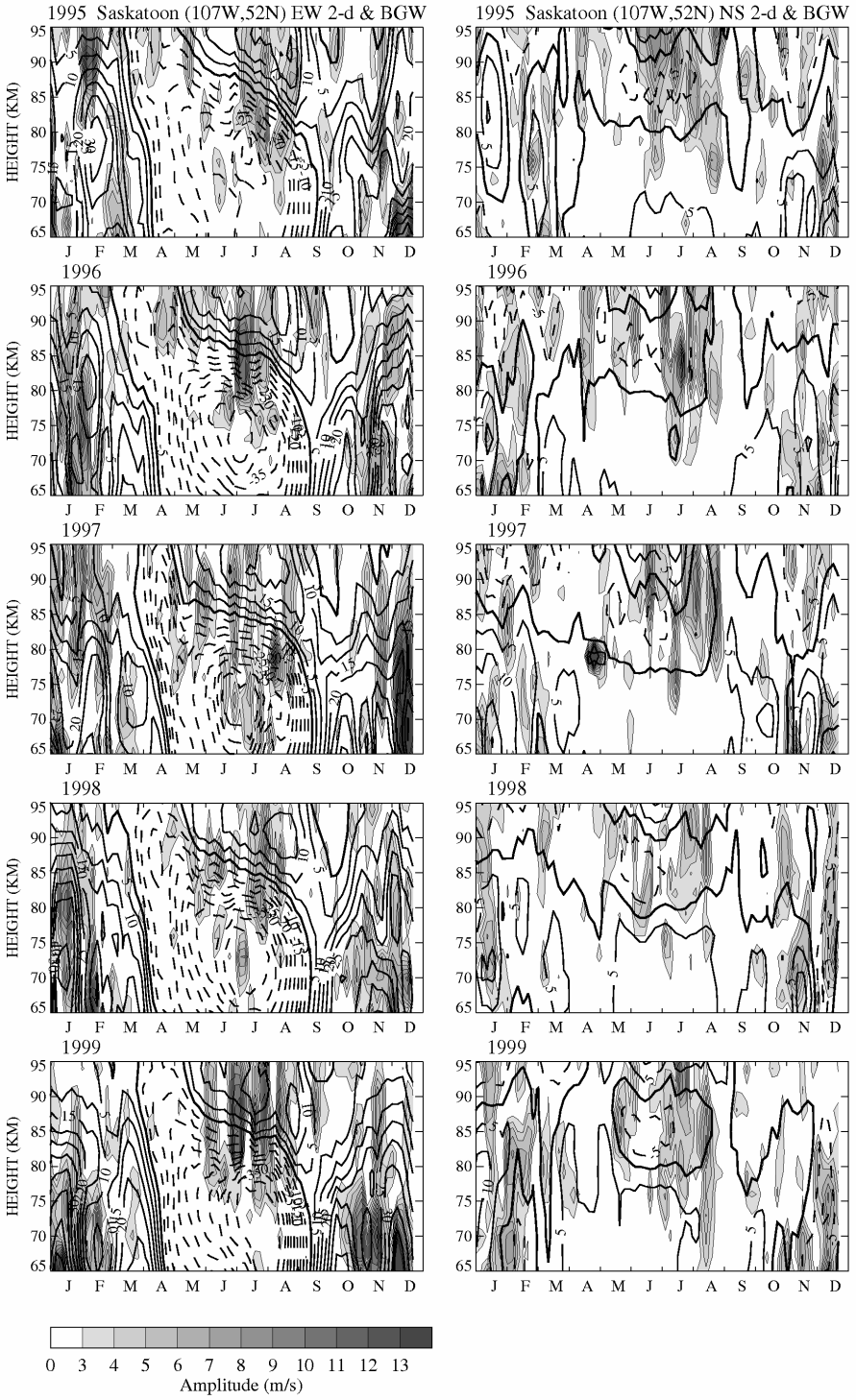

Figure 5.5 (b) The same as Figure 5.5 (a), but for 1995-1999.

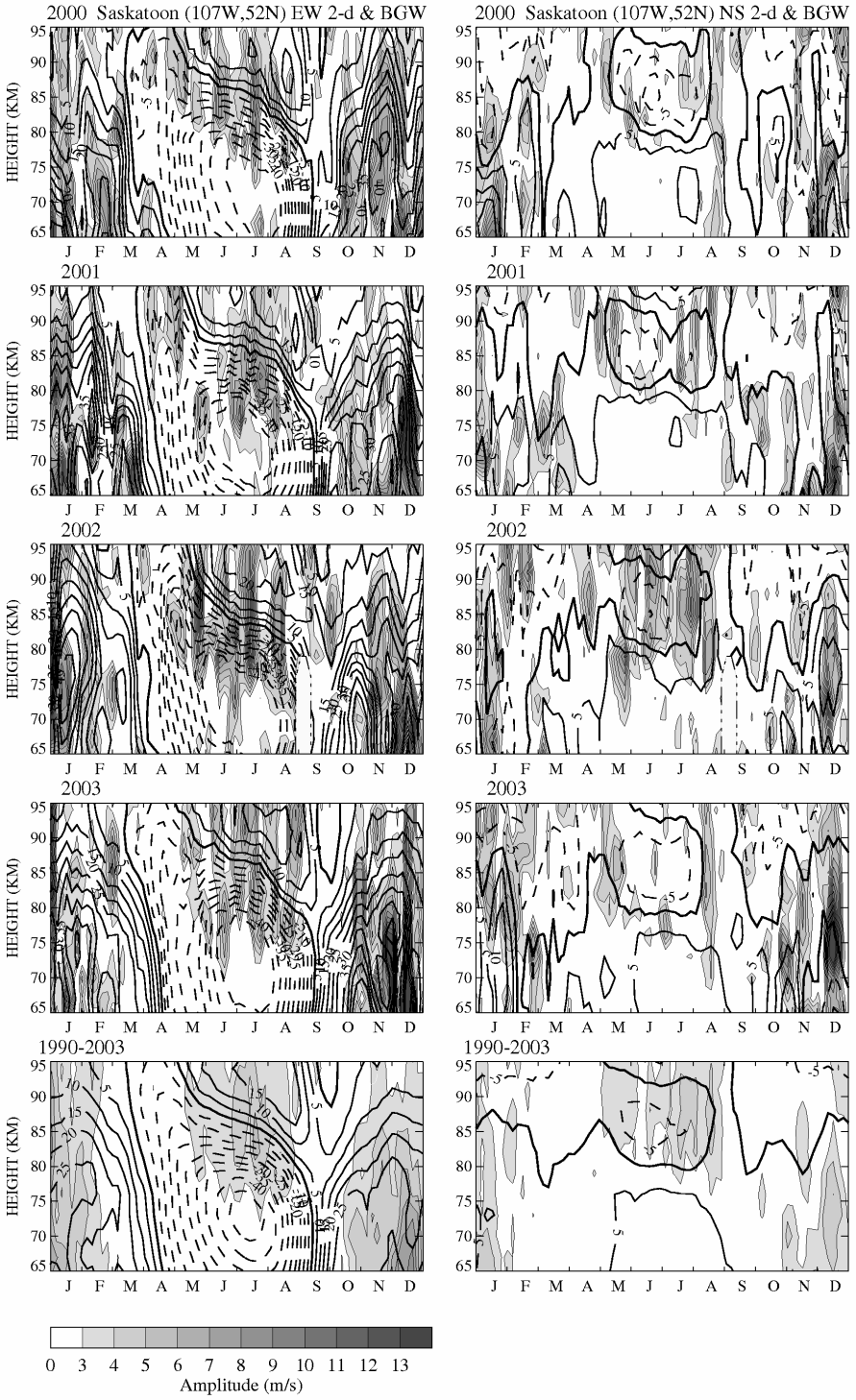

Figure 5.5 (c) The upper four rows are similar to Figure 5.5 (a), but for 2000-2003. The bottom two plots are Q2DW amplitudes and background winds averaged over all 14 years (1990-2003)

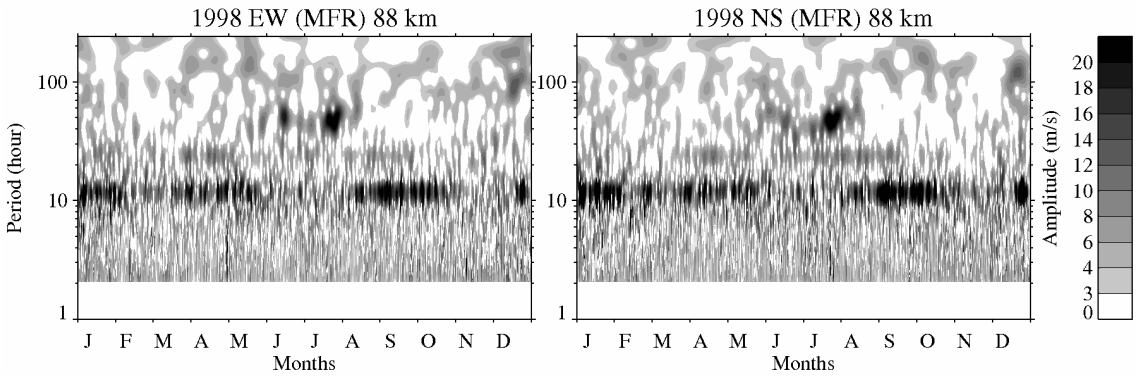

Figure 5.6 Annual contours of wavelet amplitudes as functions of period (2 hours-10 days) and time for the zonal and meridional (EW, NS) components of the winds measured in Saskatoon in 1998 are shown for the 88 km height.

As can be seen from Figure 5.5, the Q2DW exhibits strong interannual variations in amplitude (cf. 2002, 2003 in Figure 5.5c), time of the occurrence, and duration of the bursts. In spite of this, there is a clear seasonal variation with maxima in solstice seasons and minima during equinoxes. This pattern is more obvious from the 14-year average (the last row of Figure 5.5c). During summer, bursts tend to occur in clusters in early (when they are weaker) and later summer (May/June and July/August, respectively). The amplitudes of EW and NS components are comparable and reside near the reversal of the summer westward jet (85-90 km). There is also consistent Q2DW activity in winter throughout the mesospheric region. However, the character of the winter Q2DW activity differs from the summer activity in that the EW component of the winter Q2DW tends to have larger amplitudes than NS, and their maxima lie below 70-75 km. It appears that the preferable time of the winter Q2DW occurrence coincides with weaker eastward flow and zero meridional winds (thick solid line). The presence of significant Q2DW activity in winter months over several mid-latitude stations of the Northern Hemisphere was mentioned previously by *Manson et al.* [2004a] and *Thayaparan et al.* [1997]; but only limited data sets were shown.

The period of the Q2DW also varies from one year to the next, as was mentioned above, as well as during each particular year. In general, in summer time the variation of the period exhibits a “dish”-like shape. In the beginning of the summer the Q2DW has periods of the order of 53 hrs. Then as summer proceeds the period decreases to ~44

hrs, and again increases toward the end of the summer. As an example, annual contours of wavelet amplitudes as functions of period (2 hours-10 days) and time for the EW and NS components of the winds at 88 km are shown in Figure 5.6 for year 1998. The amplitudes have been calculated by applying the Morlet wavelet transform (Section 2.7) to the hourly mean data.

Similar computations of Q2DW period have been performed for MFR wind data measured over thirteen years (1990-2002) and results are demonstrated as histograms of occurrences in Figure 5.7. The ratio of the number of occurrences for a particular period value to the total number of "eligible" periods is along the y-axis, and possible period values are along the x-axis. First only oscillations with amplitudes stronger than 10 m/s are considered (the top row). The data are considered separately for winter, summer and equinoxes (blue, red, and green lines, respectively). Although the black line represents all data without separation into seasons, these annual values are dominated by summer Q2DW events as strong amplitudes are rarely observed during winter and equinoxes. The period of Q2DW varies from ~40 to ~60 hrs with preference to smaller values (44-47 hrs) for meridional components for all seasons. For the zonal component period distributions vary slightly with season, and have maxima around 42-43 hrs in winter and 46-48 hrs in summer.

To investigate the variability of the period with height, all periods obtained (no amplitude limitations) were divided into three groups depending on the altitude (70-79 km, 82-88 km, and 91-97 km) and considered for summer and winter seasons separately. During summer months the Q2DW period is consistent throughout the MLT region; it is ~45 hrs for the NS and ~47-48 hrs for the EW wind components. The distributions are also very similar to those for strong Q2DW events (top row). In winter time the preferable period is 47-48 hrs for both components, although for the EW component the period has a rather flat distribution. Q2DW peaks are not seen as clearly in winter as during summer months (Figure 5.6) because of comparatively small amplitudes at 88 km in winter. Note from Figure 5.5 that the maximum amplitudes in winter months have been obtained at heights below 70-75 km, and the period distribution has the clearest peak for the lowest height range as well (Figure 5.7, bottom

row). It should also be noted that the dominant period is not the same from one year to another.

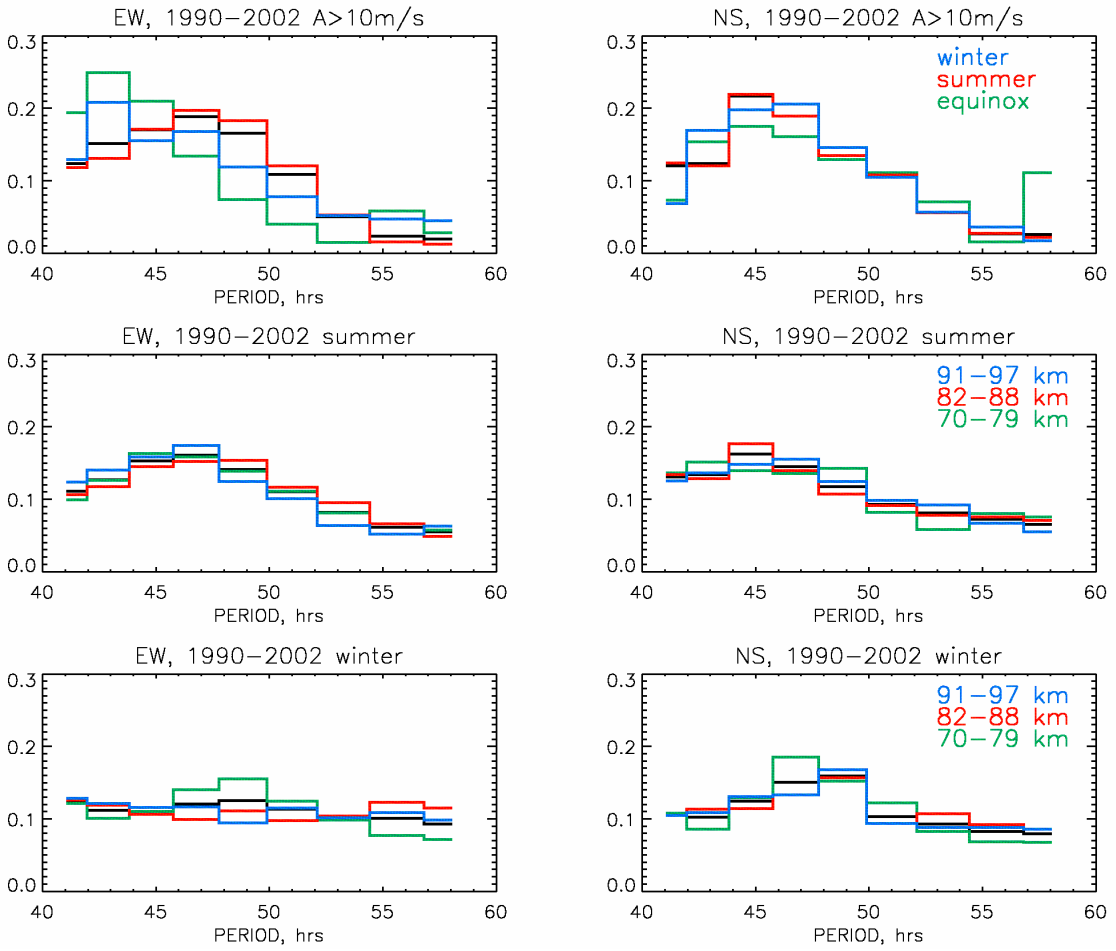

Figure 5.7 Distribution of the Q2DW periods obtained using 13 years (1990-2002) of MFR wind measurements at Saskatoon. The results are shown for zonal (left column) and meridional (right column) wind components. For the top panels, only periods of strong (amplitudes larger than 10 m/s) Q2DW are used. The results obtained for summer and winter seasons are shown in the middle and bottom rows, respectively. The black line represents all data without separation into seasons (top panel) or heights (middle and bottom panels).

5.3 **Multi-radar observations of the Q2DW**

Winds measured by five CUJO radars were filtered and plotted (Figure 5.8 and Figure 5.9) in the same way as Saskatoon data in the previous section (Figure 5.1 and Figure 5.2). The 88 km altitude was chosen as at middle latitudes it is a height of Q2DW summer maximum. Comparison of wind measurements from Yamagawa, Wakkanai, London, Platteville, and Saskatoon reveal longitudinal and latitudinal variations of the Q2DW. At Saskatoon, Platteville and Wakkanai NS and EW components of the wind are comparable, while at Yamagawa the NS component is dominant. Over Yamagawa the Q2DW demonstrates the expected sub-tropical behavior, with maxima in both solstices. This location has the strongest Q2DW activity during winter of all the stations considered, and is consistent with wave propagation from the Southern Hemisphere in northern winter months. At London the amplitudes are quite small. Dr. C. Meek (private communications, 2006) has found a difference in the wind analysis process being used for London data, which will require an increase of those winds by 20%. Even with this, the London Q2DW amplitudes are smaller than nearby sites.

Saskatoon and Platteville are very close to common longitude, while Platteville and Wakkanai are close to common latitude. From their comparison it is seen that the observed structures of the Q2DW are more similar for the first pair of stations than for the second one, i.e. unexpectedly, the variations with longitude exceed those with latitude. A scatter plot of amplitude products versus phase difference of the Q2DW at Saskatoon and Platteville are shown in Figure 5.10. To reveal the seasonal differences, results are plotted for three seasons (winter, equinox, and summer) separately. Also, different height ranges are shown by different symbols. It is clear from the figure that in summer the Q2DW oscillations observed in Saskatoon and Platteville are in phase, i.e. the phase difference is close to 0 degrees for the large amplitude-products. For equinoxes and winter the phase differences exhibit random scattering except for the meridional component (upper panels), for which several points with relatively large products are located between approximately 0 and 50 degrees in the winter plot.

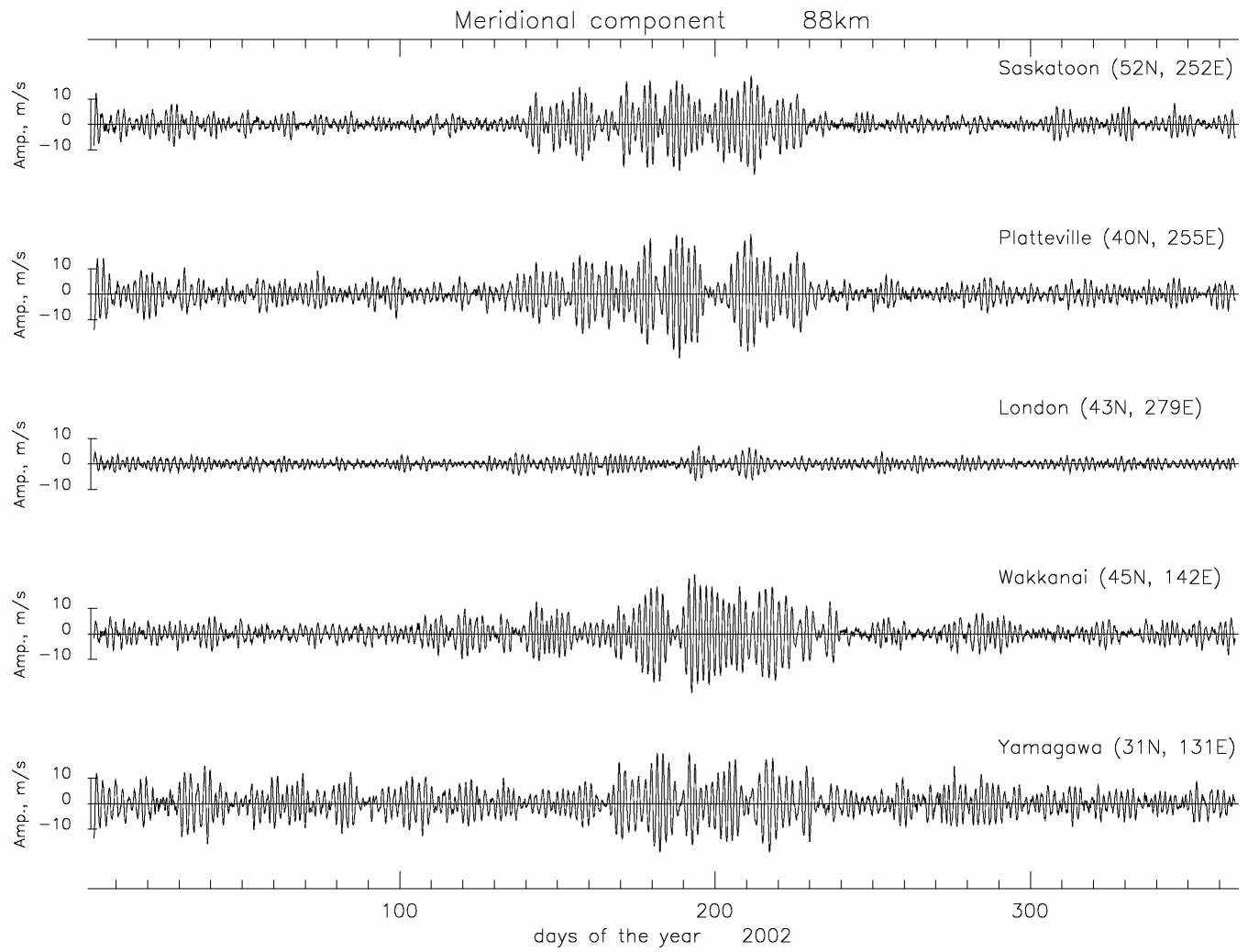

Figure 5.8 Filtered (40-55 hrs) meridional component of the wind measured at five CUJO locations in 2002 at 88 km altitude.

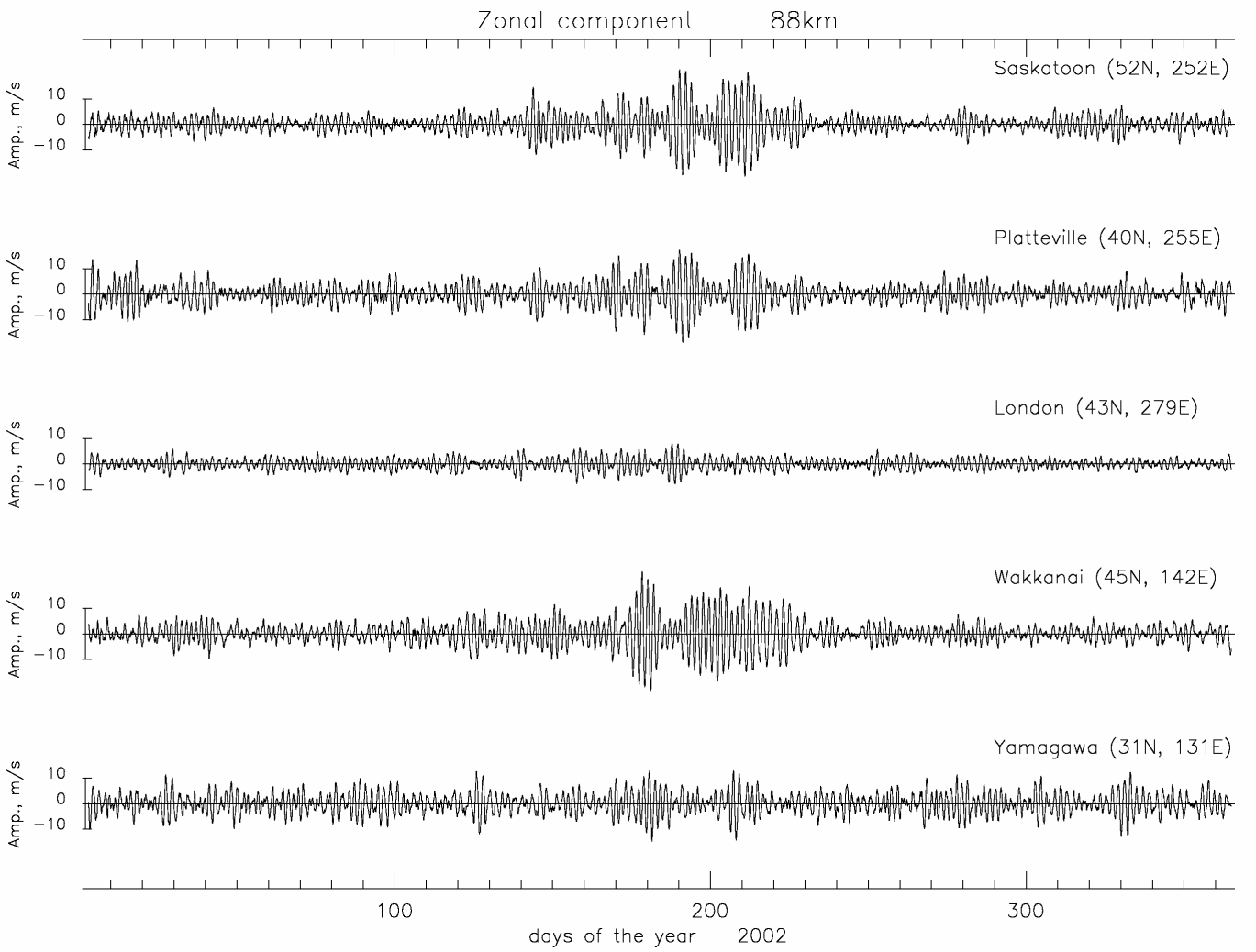

Figure 5.9. The same as Figure 5.8, but for zonal wind component

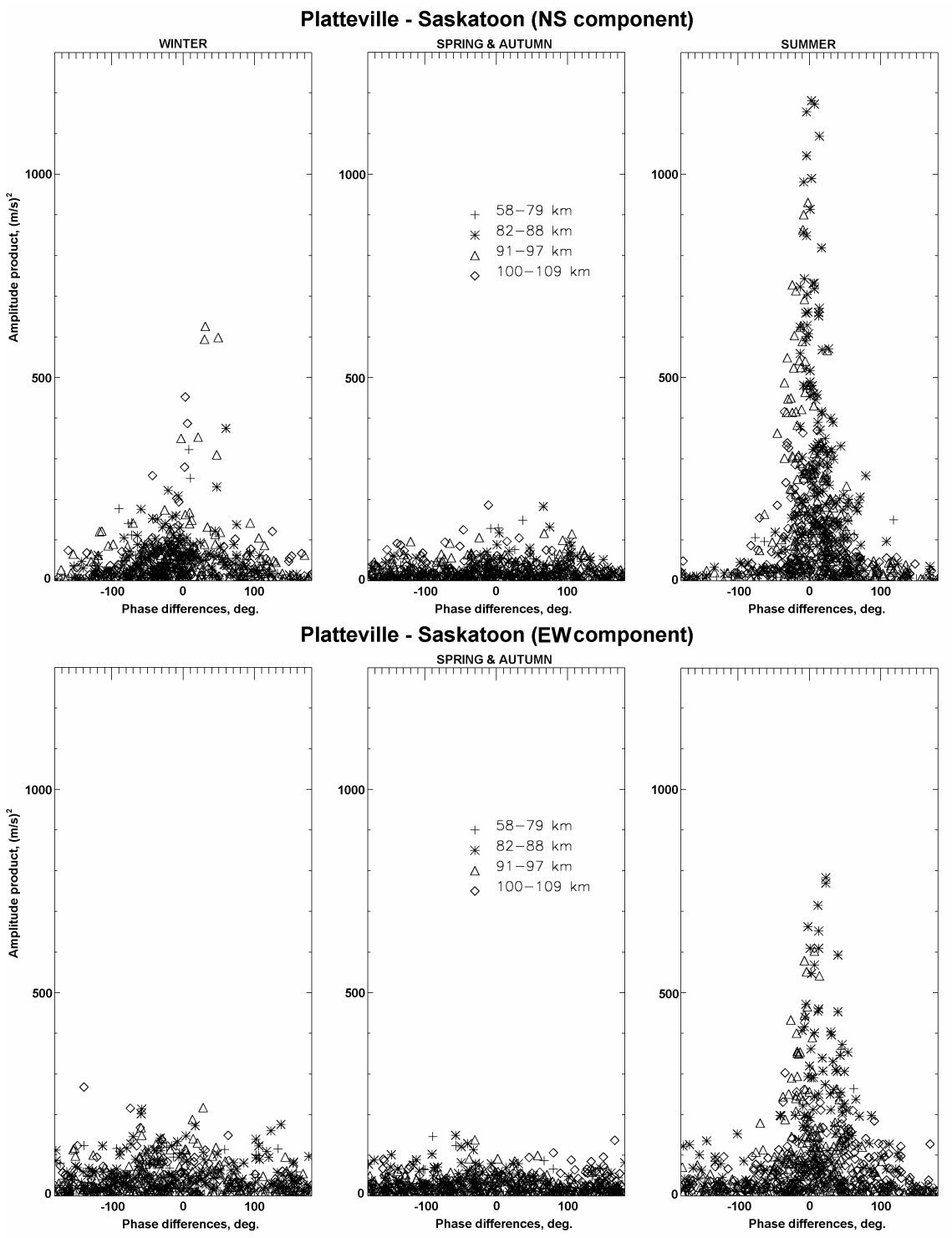

Figure 5.10. Scatter plots of cross-spectral amplitudes (m^2/s^2) versus phase differences (degrees) of the Q2DW between Saskatoon and Platteville.

To establish the wave number of the 2-d wave the planetary wave model developed by Dr. Meek (private communication) has been used. The model restricts the waves to EW propagation, and the positive wave number m is for the westward direction. For each value of m (0, +/-1, +/-2, etc.), and each frequency, the fit between the phase-observations for the sites and the wave model (a function of phase (longitude), wave number, and wave frequency) for least squared error is calculated. For summer 2002, using 3 mid-latitude stations, the favored wave numbers are m=0,+/-3 for the NS component and m=4 for the EW component. This is in agreement with previous results [*Meek et al.,* 1996]. The existence of Q2DW with period shorter than 48 hrs and m=4 can be explained by the summer jet instability (Section 5.1).

The annual contour plots (Aug. 2001-July 2002) of the Q2DW amplitudes versus height (55-95 km) measured by five MFR (CUJO network) are shown in Figure 5.11 for meridional (left column) and zonal (right column) components. The CUJO stations are arranged according to their latitude with the most poleward station (Saskatoon) on the top and the most equatorward station (Yamagawa) on the bottom. The amplitudes are results of a Fourier analysis with 24-day window length and 5-day step. Solid and dashed contour lines represent the eastward and westward background wind, whose values are essentially the mean of each window interval. As is seen from the figure, the amplitudes are large in summer with the strongest peaks in July (up to 15-25 m/s) in both components near 85 km height and extending to the upper heights (95 km). There are also Q2DW peaks in winter maximizing at lower heights (~75 km) and reaching up to 85 km. The summer and winter activity are comparable (magnitude and height of the maximum) at the most equatorward stations (bottom two rows), especially at Yamagawa. Also, the Q2DW amplitudes in the meridional component are stronger than in the zonal winds there. This is in agreement with data from other tropical/equatorial stations. Therefore, the longitudinal variability (Platteville, London, and Wakkanai) is at least as large as latitudinal differences (Saskatoon-Platteville pair).

The comparison of the observed Q2DW activity at CUJO locations with the Canadian Middle Atmosphere Model (CMAM) results demonstrates reasonable agreements

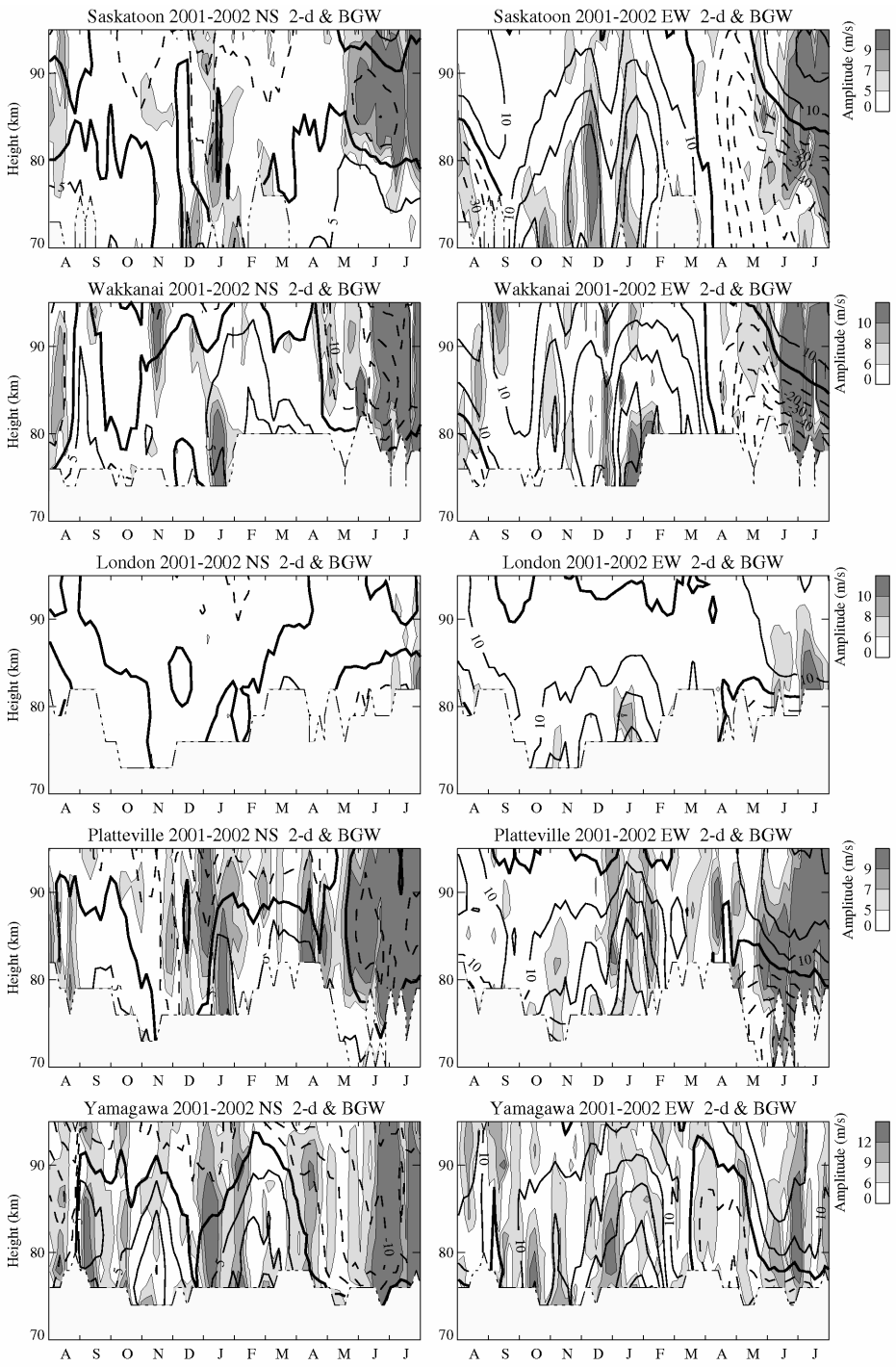

Figure 5.11. Amplitudes of the Q2DW in the meridional (NS, left column) and zonal (EW, right column) wind components of radar data obtained at five CUJO locations from August 2001 till July 2002. Continuous solid and dashed lines represent eastward (positive) and westward (negative) background winds, respectively.

[*Manson et al.*, 2006]. Both CMAM and MFR data show summer and winter Q2DW activity, and also longitudinal differences. However, in the model the Q2DW amplitudes are smaller (rarely as big as 10 m/s) and they are attenuated above 87 km (the CMAM zero transition line) in summer. Weak and intermittent winter activity occurs, as in observations, at lower heights (60-80 km), but in the MFR measurements it is more extended, i.e. it can reach up to 90-95 km. Such comparisons are essential, as PW propagation is dependant on so many factors that 1 or 2-dimensional models are inadequate.

5.4 **Summary**

The complexity of the Q2DW behavior requires more studies to be done. We have provided results of a study of the Q2DW climatology at mesospheric heights over Saskatoon [*Chshyolkova et al.*, 2005b]. In this investigation fourteen years (1990-2003) of MFR data over Saskatoon were subjects of the Lomb-Scargle and wavelet spectral analyses. Q2DW manifests itself as a series of bursts in both meridional (NS) and zonal (EW) wind components. The duration of a burst varies from 3 to 10 cycles. According to results obtained here the Q2DW has strong interannual variation. There are differences in occurrence, duration, and amplitudes of the bursts of the Q2DW. However, the common features of each individual year are obvious. The Q2DW maximizes in summer and winter, with generally weaker winter maximum, especially in the NS component. The activity is minimal during equinoxes, though sporadic bursts can be observed occasionally. The amplitude reaches its maximum at 85-88 km altitude during the summer time. In winter the maximum occurs at lower heights, near 70 km. Both EW and NS components have comparable amplitudes in summer, while larger amplitudes have been observed in the EW component in winter. The period of the Q2DW also varies with time. In general, it decreases during the first part of summer and increases by autumn. Relatively short (~44 hrs) periods at the middle of summer seem to be favored for both components. Winter periods tend to be slightly longer (47-48 hrs).

Slow downward phase progression was found for strong summer events, which indicates long (~100 km) vertical wavelengths and upward energy flux. Elsewhere, a

16-hr oscillation has been found along with the Q2DW, which might indicate interactions between the latter and the semidiurnal tide. However the results over fourteen years were not conclusive as there were times when the 16-hr oscillation was present without Q2DW and vice versa.

Our results show strong interannual variabilities in the Q2DW. More investigations need to be conducted to determine their cause or causes. For example the variabilities could be linked to the solar activity and/or the Quasi Biannual Oscillation over tropics.

The comparisons of the Q2DW activity over five MFR from the CUJO network reveal significant longitudinal as well as latitudinal variabilities. The Q2DW exhibited typical mid-latitudinal behavior over Saskatoon, Wakkanai, London, and Platteville; and the expected sub-tropical behavior over Yamagawa. The pair of stations with similar longitudes (Platteville-Saskatoon) had more Q2DW characteristics in common than the three ~40^{o} stations (Platteville-London-Wakkanai). Again, more detailed analysis and GCM experiments are required to determine the source of this variability.

An attempt was made to estimate the zonal wave number of the observed Q2DW oscillation. As expected, the phase differences between Platteville and Saskatoon (similar longitudes) for the strong Q2DW were close to zero, i.e. the oscillations were in phase, indicating that small differences in latitude should not be a factor when comparing radars at very similar latitudes but different longitudes. Thus, using data from the three ~40^{o} radars the wave number was calculated for summer 2003. The Q2DW had different wave numbers for meridional and zonal components: 3 and 4, respectively. This does not contradict the earlier reported results (see Section 5.1).

Finally, the Q2DW activity observed over CUJO locations have been compared to the outputs from a model (CMAM). It was demonstrated that in general Q2DW obtained from CMAM and MFR data has similar seasonal variations: maxima right after solstices and minima during equinoxes. However, there are differences in details. The observed amplitudes are larger compared to those available from CMAM for both seasons. Also the observed Q2DW activity extends to high altitudes compared to CMAM.

Unfortunately, unavailability of the upper stratospheric data with time resolution better than a day made it impossible to investigate different aspects of coupling due to Q2DW between stratospheric and mesospheric regions. Also, it is desirable to have more data at mesospheric heights for better understanding of the latitudinal and longitudinal variabilities.

Chapter 6

ATMOSPHERIC VARIABILITY DURING THE WINTER SEASON

6.1 Introduction

The stratospheric polar vortex, a system of strong eastward winds, is the main dynamical feature of the winter middle atmosphere (20-100 km) at the middle and high latitudes. Each day after the autumnal equinox less sunlight reaches the polar stratosphere, and as a consequence the primary heating due to ozone decreases. As a result of the radiational cooling at high latitudes a strong negative temperature gradient develops between polar and tropical regions. This leads to the formation of the polar night jet, comprising strong eastward winds encircling the pole. These winds reach speeds of ~80 m/s at ~60 km altitude in the Northern Hemisphere and isolate polar air (the core of the polar vortex) from air in the tropics and middle latitudes [*Schoeberl and Hartmann,* 1991; *Wallace and Hobbs,* 2006]. Therefore the polar vortex not only dominates the dynamics, it also has a profound effect on the distribution of chemical constituents.

At mesospheric heights, due to gravity wave (GW) drag, the eastward wind speeds decrease and eventually become westward at the lower thermospheric levels [*Lindzen,* 1981; *Holton,* 1983]. This GW drag also drives the mean meridional circulation at these heights and the associated downward motion at higher latitudes is responsible for a much warmer mesopause than would be expected from considerations of radiative equilibrium.

The polar vortex in the Arctic is highly variable throughout its life cycle. Intervals of a strong vortex (symmetrical and centered over the pole) with high wind speeds are interrupted by sudden stratospheric warmings (SSW). During SSW temperatures significantly increase (at least 25 K per week) at high latitudes (>50^{o}). The stratospheric

warming is called major (MSW) if the temperature enhancement leads to reversal of the middle latitudes-to-pole zonally averaged temperature gradient and results in reversal of the mean zonal winds from eastward to westward at heights near 30 km. Usually a MSW develops in the middle of winter. If there is no reversal of the mean zonal circulation then the stratospheric warming is called minor. The warming that occurs in late winter/early spring, and marks the transition from winter to summer circulation, is the final warming. There is also one more type of warming, the so-called Canadian warming, which occurs as a result of intensification of the Aleutian anticyclone (westward flow) with the reversal of the temperature gradient poleward of 60^{o}N over Canada.

Labitzke [1972] investigated temperature changes in the middle atmosphere at higher latitudes (circa 65^{o}N) during stratospheric warmings using satellite radiance and rocket measurements. The results indicated that the effects of stratospheric mid-winter warmings extend into the upper mesosphere. It was shown that at first the temperature increases around 60 km height (near the stratopause), and then during several days the middle stratosphere warms up, while the lower stratosphere and upper mesosphere cool. During the breakdown of the vortex, temperatures rise in the lower stratosphere and upper mesosphere and decrease in the layer between 30 and 60 km.

At mesospheric heights, reversals of the dominating eastward winds have been observed in association with stratospheric disturbances [*Gregory and Manson,* 1975; *Greisiger et al.,* 1984; *Jacobi et al.,* 1997b; *Hoffmann et al.,* 2002]. *Hoffmann et al.* [2002] studied the response of the mesospheric winds measured with MFR to stratospheric circulation disturbances at Juliusruh (55^{o}N) during 1989-2000 and at Andenes (69^{o}N) during 1998-2000. Reversals of mesospheric winds were observed on days near those of stratospheric warmings and of enhanced activity of quasi-stationary waves. However, clear coincidences between stratospheric and mesospheric events occurred only for planetary-scale phenomena. It was also noted that wind reversals occurred at different time at two stations, with the later reversal at the more poleward station (Andenes). Some cases, when the mesospheric zonal winds decreased and/or reversed during cold stratospheric conditions, were reported as well [*Greisiger et al.,* 1984].

Another European study [*Jacobi et al.,* 2003] involved mesospheric radar wind measurements over Castle Eaton (52^{o}N), Collm (52^{o}N) and Esrange (68^{o}N) during the February 2001 major stratospheric warming. They also found that the warming resulted in a reversal of both the zonal and meridional wind components. Earlier, *Jacobi et al.* [1997b] had argued that although the beginning of the warming at low stratospheric heights (~20 km) often appears simultaneously with the weakening or reversal of the mesospheric zonal winds (~90 km), this is not the result of large vertical scale or wavelength process, but is rather due to the fact that the warming needs approximately the same time to reach the lower stratosphere and the mesosphere from the stratopause, where it starts. Both *Hoffmann et al.* [2002] and *Jacobi et al.* [2003] observed long period oscillations around 10 and 20 days in their radar data. The 20-day spectral peak was assumed to be merely the response time of the MLT (Mesosphere/Lower Thermosphere) winds to the stratospheric warming, while the 10-day spectral peak could have been the signature of a planetary wave propagating from below. Therefore the variability at the mesospheric heights could be the result of the combined effect of a vertically propagating planetary wave and decreasing zonal winds, i.e. a trend rather than an oscillation. *Manson et al.* [2002a] using both radar winds and airglow intensities during the SSW and final warmings of several winters, found no relationship between these events and phases of the long period oscillations associated with planetary waves.

During the same stratospheric warming event (February 2001) that had been studied by *Jacobi et al.* [2003], hydroxyl (~86 km) and oxygen green line (~97 km) emissions were measured using a ground-based wide angle Michelson Interferometer at Resolute Bay, Canada (75^{o}N, 95^{o}W). Winds obtained by Doppler-shifting technique from both emission layers showed reversals around the times of SSW [*Bhattacharya et al.,* 2004]. Spectral analyses of the data indicated that during the periods of cold or undisturbed stratospheric temperatures the amplitudes of oscillations with periods from 6 hours to 2 days decreased. The authors also noted an increase in short (<12 hours) period oscillations over the course of the warming.

The generally accepted mechanism of SSW [*Matsuno,* 1971] assumes that tropospherically forced planetary waves propagate upward, where they decelerate the

mean zonal flow as they dissipate, and through related enhanced poleward motion initiate a stratospheric warming. Due to the increase of the wave amplitude with altitude, the deceleration of the eastward flow becomes stronger with height until at a certain level (50-75 km) wave-induced acceleration may reverse the wind flow. This creates a critical level at which planetary waves are absorbed and temperature disturbances may be large. Intense warming is expected at and below the critical level in the poleward region with some (~30 K) cooling above the critical level due to adiabatic descent and ascent, respectively. It was also shown that at lower latitudes the temperatures decrease below the critical level and may increase slightly above it. Then, due to breaking and dissipation of planetary waves near the critical level, the winds increase in the westward direction and the critical level shifts downward. The region of warm temperatures at high latitudes starts to descend.

The model [*Matsuno,* 1971] predicts a decrease in temperature above the critical level at high latitudes, which is much smaller than the increase beneath it. *Holton* [1983] argued that cooling due only to adiabatic ascent near the critical level is not enough to explain the observed decrease of mesospheric temperatures during the SSW, especially when the critical level descends to the lower heights. It was suggested that the significant temperature decrease in the mesosphere could be mainly caused by a reduction of the mean poleward meridional circulation due to a decrease of the GW drag. This latter was considered to be a result of the changed propagation conditions for GW in the lower atmosphere during the course of a SSW event.

More recently *Liu and Roble* [2002] carried out a numerical study of the impact of a self-generated stratospheric warming on the MLT region. The Thermosphere, Ionosphere, Mesosphere, and Electrodynamics General Circulation Model/Climate Community Model (TIME-GCM/CCM3), which is a new generation state of the art GCM with GW parameterization, was used. They showed that growth of the planetary wave with the zonal wave number m=1 precedes the SSW, and that this growth could be due to wave resonance. The resonant amplification of the wave causes the deceleration and reversal of the zonal wind and induces poleward and downward (the latter at high latitudes) circulation in the stratosphere and equatorward circulation in the

lower mesosphere. These lead to the adiabatic warming in the polar stratosphere and cooling in the lower mesosphere, which is in agreement with *Matsuno* [1971]. In addition, a thermospheric (100-120 km) warming has been indicated by the model. The authors [*Liu and Roble*, 2002] also demonstrated that changes in the wind field alter the propagation conditions for gravity waves (GW), so that more eastward GW can reach the MLT region during the warming, where they can cause weakening and eventual reversal of the newly formed westward jet. The resulting vertical gradient of the winds is consistent with a cool polar mesosphere. The dissipation of GW at mesospheric heights may also generate planetary waves in situ [*Smith*, 1996].

This chapter presents results of studies of the propagation of PW from below during the winter season. PW propagation depends on the state of the atmosphere and in particular the strength of the polar vortex. In the first part of the chapter the polar vortex has been characterized using the conventional method that employs potential vorticity (Section 6.2.1) and the relatively new Q-diagnostic (Section 6.2.2). Both methods are applied to MetO data and compared in Section 6.2.3, which also includes the results of Q-diagnostic calculations using a different assimilation model (NCEP) and comparisons with temperatures from the Aura satellite. As an example, the evolution of the polar vortex using the Q-diagnostic during the winter of 2004/05 is described in Section 6.3. The stratospheric-mesospheric coupling due to PW during this winter is investigated in Section 6.4. The application of the vortex characterization for chemical studies is illustrated in Section 6.5. Section 6.6 summarizes the results of the chapter.

6.2 Methods of the Polar Vortex Characterization

6.2.1 Potential vorticity

The general definition of potential vorticity or “Ertel’s potential vorticity” (PV or EPV) is as follows [*Andrews et al.*, 1987a]:

$$PV = \rho^{-1}\vec{\omega}_a \cdot \nabla\theta, \tag{6.1}$$

$$PV = \rho^{-1}(\nabla \times \vec{u} + 2\vec{\Omega}) \cdot \nabla\theta, \tag{6.2}$$

where ρ is air density, $\vec{\omega}_a$ is the absolute (total) vorticity, $\vec{\Omega}$ is the Earth's angular velocity, $\vec{u}$ is air velocity relative to the Earth, and θ is the potential temperature, which is the temperature achieved when a parcel of air is moved adiabatically up to, or down to, the reference level (p_0=1000 hPa).

Neglecting the small horizontal component of $\nabla\theta$ (an approximation valid for non-turbulent flows) and estimating the vertical component $\partial\theta/\partial z$ from data using the hydrostatic relation $\partial p/\partial z = -\rho g$ leads to the simplification:

$$\frac{1}{\rho}\frac{\partial\theta}{\partial z} = -g\frac{\partial\theta}{\partial p}, \tag{6.3}$$

where p is the pressure, z is the altitude, and g the acceleration due to gravity.

The EPV on a constant surface (isentropic or isobaric) can then be approximated as

$$PV = -g(\varsigma_z + 2\Omega Sin\varphi)\frac{\partial\theta}{\partial p}, \tag{6.4}$$

where the expression in the brackets is the component of the absolute vorticity ($\vec{\omega}_a$) perpendicular to the constant surface, ζ_z is the vertical component of the relative vorticity, and φ is the latitude [*McIntyre and Palmer,* 1983]. For adiabatic (the material derivative of the potential temperature Dθ/Dt=0) and frictionless flow PV is invariable, i.e. D(PV)/Dt=0: therefore, for time scales up to a week or so, PV and θ can be assumed to be constant following the motion [*McIntyre and Palmer,* 1983]. In autumn when the vortex starts to develop, eastward winds increase and a relatively coherent air mass with high values of PV forms at the pole. An example of the PV calculated using equation 6.4 with MetO data at the isentropic surface of 1000 K for December 25 of 2004 (the strong vortex) is shown on the top of Figure 6.1. The PV generally increases poleward with uneven (peaks and troughs) distribution. It is likely that the PV has even smaller, fine-grain, structure, which is not seen due to the resolution of the MetO data. Although PV is very useful and often used to characterize the polar vortex [*Baldwin and Holton,* 1988; *Nash et al.*, 1996; *Karpetchko et al.*, 2005], it does not allow the identification of anticyclones (areas of low PV), which play an important role in the dynamical evolution of the winter stratosphere.

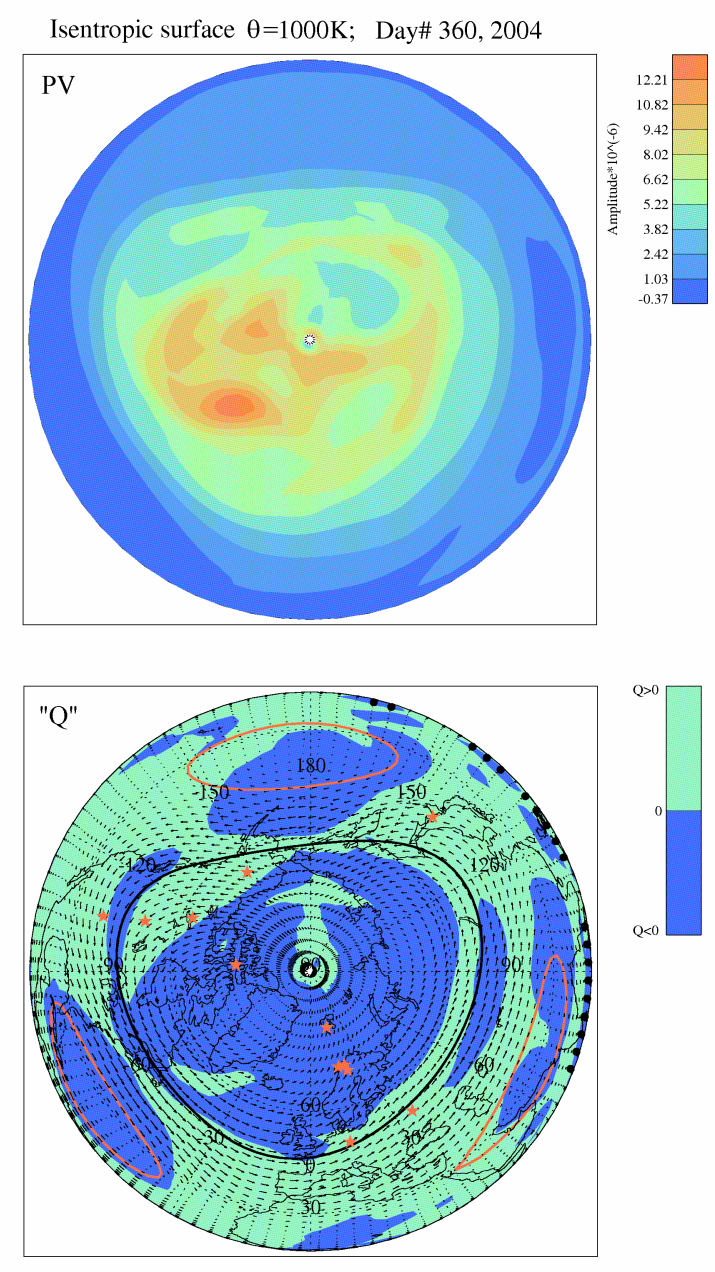

Figure 6.1 PV (top) and Q-values (bottom) calculated from MetO data at isentropic surface of 1000 K for the Northern Hemisphere on day # 360 (December 25, 2004). Also on the Q-plot, the stratospheric winds are shown by black arrows; red stars indicate the locations of mesospheric radars for which data are available; and thick black and red contour lines indicate the edges of the polar vortex (cyclones) and anticyclones, respectively.

6.2.2 **Q-diagnostic**

The Q-diagnostic includes calculation of the scalar quantity Q, which is "a measure of the relative contribution of strain and rotation in the wind field" [*Harvey et al.*, 2002], streamfunction (ψ), relative vorticity (ζ), and integration of Q, ζ and winds along ψ isopleths. The following description of the Q-diagnostic is a summary based on *Fairlie* [1995], *Harvey et al.* [2002], and *Malvern* [1969].

The motion is generally the combination of solid rotation and a "pure strain". In tensor notation Q is defined as

$$2Q=D:D-W:W\ ,$$

where $\mathbf{D}=1/2(\mathbf{L}+\mathbf{L}^{\mathbf{t}})$ is "the rate of deformation" tensor with components $\frac{1}{2}\left(\frac{\partial u_i}{\partial X_j}+\frac{\partial u_j}{\partial X_i}\right)$,

$\mathbf{W}=1/2(\mathbf{L}-\mathbf{L}^{\mathbf{t}})$ is "the solid body spin" tensor, $\frac{1}{2}\left(\frac{\partial u_i}{\partial X_j}-\frac{\partial u_j}{\partial X_i}\right)$,

t denotes a transposed tensor,

$\mathbf{L}=\mathbf{u}\tilde{\nabla}$ is the velocity gradient tensor (its transpose is the matrix of $\vec{\nabla}\,\mathbf{u}$**),** and the operator **':'** represents the general tensor scalar product ($\mathbf{A:B}=\mathbf{A}_{ij}\mathbf{B}_{ij}$).

For two-dimensional flow *Q* is given by

$$Q=\frac{1}{2a^2}\left\{\left(\frac{1}{\cos\varphi}\frac{\partial u}{\partial\lambda}-v\tan\varphi\right)^2+\left(\frac{\partial v}{\partial\varphi}\right)^2+2\frac{\partial u}{\partial\varphi}\left(\frac{1}{\cos\varphi}\frac{\partial v}{\partial\lambda}+u\tan\varphi\right)\right\}, \qquad (6.5)$$

where φ is latitude, λ is longitude, *u* is zonal wind, *v* is meridional wind, and *a* is the radius of the Earth. In areas where *Q* is positive the strain dominates and fluid elements are stretched, and in regions with negative Q rotation dominates the flow. For example, shear-zones beyond the edges of vortices and near jet streams have positive Q while negative Q is associated with stable rotational flow [*Babiano et al.*, 1994] and is generally observed inside vortices. However, as was noted by *Harvey et al.* [2002], in the presence of elongated polar vortices, polar vortex divisions, and elongated anticyclones, shear-zones can also be found inside vortices. Therefore, for identification

of the vortex edges the integrated values of Q along streamfunction lines are used, and those streamlines that have $\oint Q \approx 0$ are chosen to represent the vortex "edges". In general there could be more than one streamfunction isopleth that satisfies this condition. In this case the one with strongest integrated winds is chosen. The integration of relative vorticity along the streamlines helps to distinguish cyclonic and anticyclonic vortices. Q is most effective at identifying vortex-edges when the circulation is strong and shear zones are well defined. This is often the case in the middle and upper stratosphere and when the vortex is cold. In the lower stratosphere and during vortex formation and decay, the Q field is more complex and integration around streamfunction (ψ) isopleths is a poorer indicator of vortices.

The Q-parameter has been used to study coherent vortices in two dimensional turbulence [*McWilliams,* 1984; *Brachet et al.,* 1988; *Elhmaidi et al.,* 1993] and stratospheric dynamics [*Haynes,* 1990; *Fairlie,* 1995; *Paparella et al.,* 1997; *Fairlie et al.,* 1999; *Waugh and Rong,* 2002].

As part of the present program of research, a software package that includes the calculation and plotting of the Q-diagnostic along with PV, streamfunction and wind fields for characterization of the cyclonic and anticyclonic vortices of winter (and other seasons) has been created. This software package, so-called "USask Vortex Characterization Software Package", is a self-consistent and effective system to allow additional studies of dynamics and chemical changes occurring during events such as SSW and seasonal transitions. Its detailed algorithm can be found in the Appendix B. An example of the Q calculation for December 25, 2004 using MetO data is shown on the bottom plot in Figure 6.1. The Northern Hemispheric Q is shaded with blue (negative Q) and green (positive Q) colors. Also, the stratospheric winds are shown by black arrows; red stars indicate the locations of mesospheric radars for which data were available for this study; and thick black and red contour lines indicate the edges of the polar vortex (cyclones) and anticyclones, respectively. Generally, the edge of the polar vortex coincides with the core of the eastward jet, so the magnitude of the zonal wind decreases away from the edge (poleward as well as equatorward).

6.2.3 **Comparisons**

First, look at both plots of Figure 6.1: their comparison shows that there is good agreement between PV and Q contours. The vortex edge estimated from the Q-diagnostic (black line) corresponds well to the region where the meridional gradient of PV increases, while edges of anticyclones (red contours) are located in areas of low PV.

In the bottom panel of Figure 6.2 the Q values calculated from NCEP/NCAR data are shown for the same date (January 20, 2005) and the same isentropic surface (700 K). The comparison of the top panel (calculated from MetO) and bottom panel of Figure 6.2 demonstrates very good agreement between results (vortex location and shape) obtained using two different sources of assimilated temperature and wind fields. The differences can be partly explained by spatial longitude resolution: the Q contours calculated from the more "coarse" ($2.5^o \times 3.175^o$) MetO data look smoother, while Q areas obtained from NCEP data ($2.5^o \times 2.5^o$) show more details.

Now compare the Q-diagnostic results with measurements from a satellite. The Aura temperature field measured over the Northern Hemisphere at ~27 km on January 20, 2005 is shown in the bottom panel in Figure 6.3, below the result of the Q-calculations using MetO data for January 20, 2005 (a repetition of the top panel of Figure 6.2) for the 700 K isentropic surface (~27 km). It can be seen from the figure that the distribution of the cold and warm areas is very similar to the locations of cyclones and anticyclones. In particular, the identified polar vortex (black thick contour) resembles the shape of the cold polar region (blue shadings of the bottom plot) very well.

The positive results of all these comparisons indicate that the program works correctly and increases our confidence in the Q-diagnostic technique.

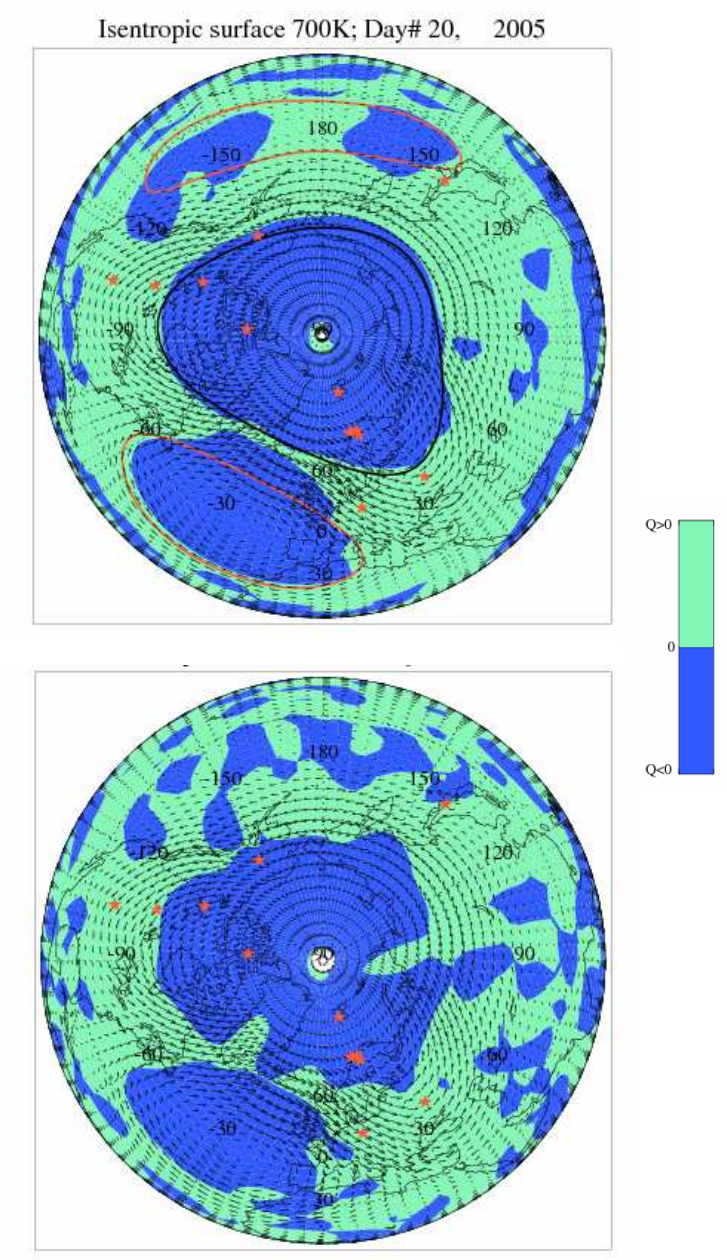

Figure 6.2 The Q-diagnostics calculated using MetO and NCEP datasets for the isentropic surface 700 K (~27 km) on January 20, 2005 are shown on the top and bottom plots, respectively. Also, the stratospheric winds are shown by black arrows; red stars indicate the locations of mesospheric radars for which data are available; and thick black and red contour lines indicate the edges of the polar vortex (cyclones) and anticyclones, respectively.

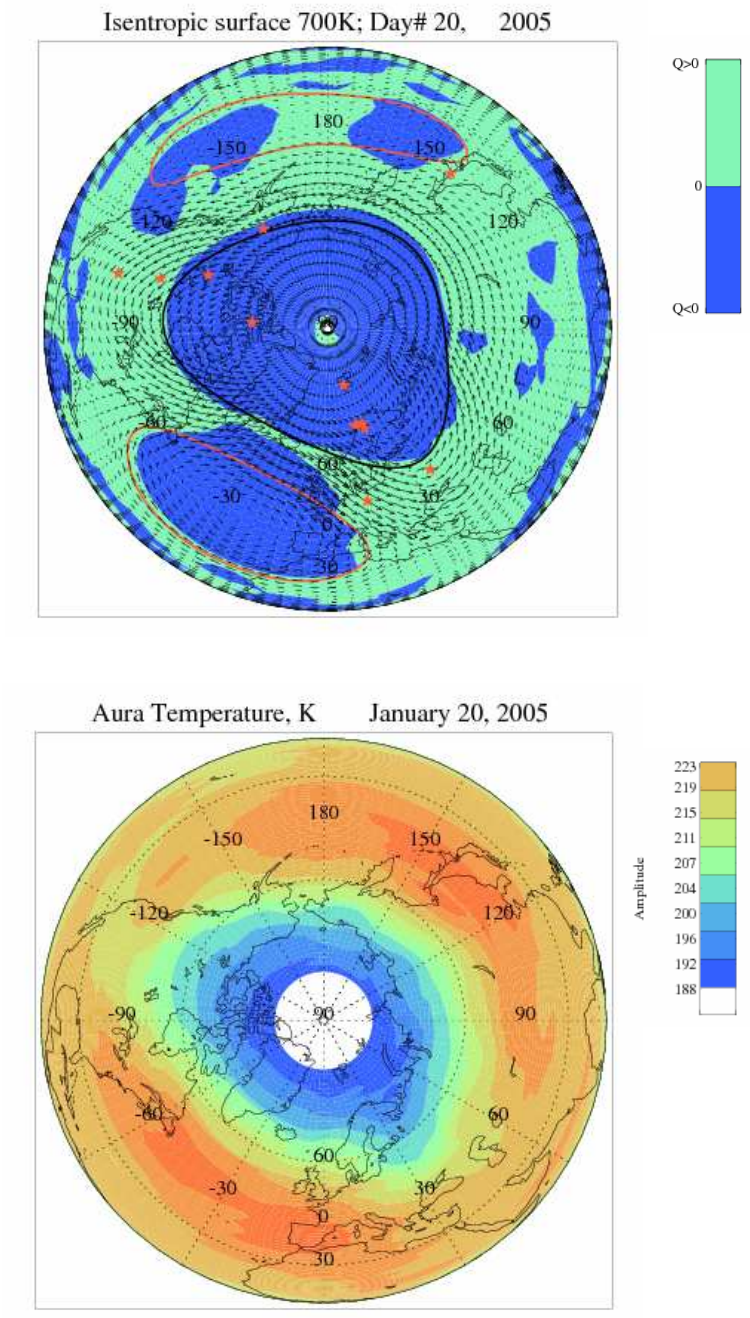

Figure 6.3 The Q-diagnostics calculated using MetO dataset for the isentropic surface (700 K, ~27 km) on January 20, 2005 (at the top), and temperatures measured by Aura satellite at approximately 27 km and during the same day (at the bottom). Also on the Q-plot, the stratospheric winds are shown by black arrows; red stars indicate the locations of mesospheric radars for which data are available; and thick black and red contour lines indicate the edges of the polar vortex (cyclones) and anticyclones, respectively.

6.3 **Evolution of the Stratospheric Polar Vortex during Winter of 2004/05**

The Arctic winter of 2004/05 was relatively cold, especially in the lower stratosphere. More days and larger areas with temperatures below 195 K were observed during this winter [*Manney et al.*, 2006]. Due to decreases in temperature, a reduction of up to ~0.5 ppmv in water vapor was detected over Spitsbergen in the ~12–20 km height region on January 25-27 due to ice formation [*Jiménez et al.*, 2006]. Figure 6.4 shows variations of MetO temperatures (top panel), meridional (NS, middle panel) and zonal (EW, bottom panel) wind components averaged around the 60°N (solid line) and 70°N (dotted line) latitudinal circles at the 10 hPa pressure level (~32 km), for the time interval from October 2004 (starting from day number 275) until the end of March 2005 (day number 456). The MetO temperatures (top) decrease until the end of December (day number 366) down to 202K and 180K at 60°N and 70°N, respectively, and exhibit similar temporal variations at both latitudes, with temperatures averaged over 70°N being lower than those averaged over 60°N. Starting in January the temperatures have positive trends increasing up to ~225K in March. During the second part of the winter, zonal mean temperatures at 70°N

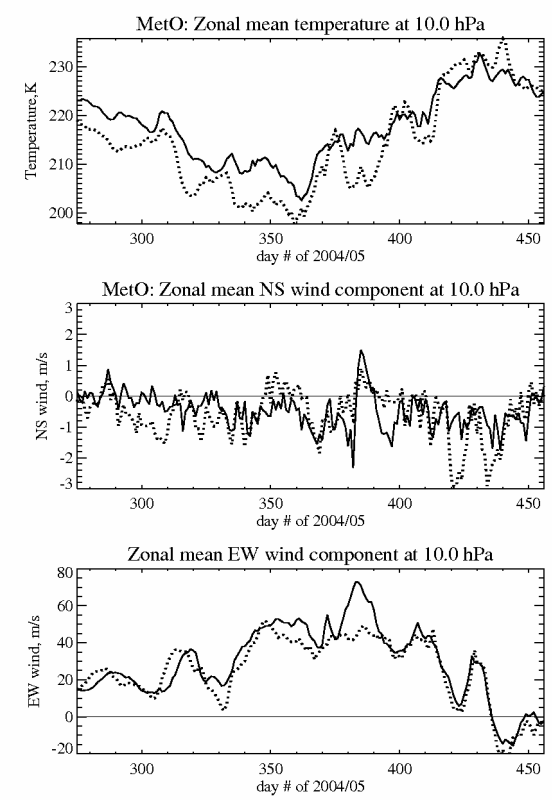

Figure 6.4 Temperature (top), NS (middle) and EW (bottom) wind components from MetO 10 hPa level averaged along the 60°N (solid) and 70°N (dashed) longitudinal circles for the time interval from October 1, 2004 till March 31, 2005 (day numbers 275-456).

demonstrate larger oscillations and occasionally exceed the zonal mean temperatures at 60^{o}N. The meridional component of the wind (middle panel) is weak and directed mostly equatorward. During the first half of the winter, the zonal component of the wind increases (becomes more eastward) reaching up to 70 m/s at 60^{o}N and 55 m/s at 70^{o}N in December and January. After that, zonal winds decrease and become westward in the second part of March; this is the transition toward the summer-like circulation.

The absence of significant temperature increases in Figure 6.4 (more than 25 K over a week) and associated reversals of the zonal winds indicates that the winter of 2004/05 was cold and without midwinter major sudden warmings (MSW). However, there are several time intervals when the MetO temperatures exhibit rapid increases; for example, at the end of December/beginning of January (between day numbers 360 and 375), at the end of January/beginning of February (between day numbers 390 and 400), and at the end of February (between day numbers 410 and 425). During these time-intervals the zonal mean temperatures rise (~20K at 70^{o}N), zonal winds decelerate, and meridional winds become southward. This is likely due to the heat and momentum deposition by the planetary waves as the result of their interaction with the mean flow [*Shepherd,* 2000].

Usually, stratospheric disturbances are associated with the enhanced activity of the quasi-stationary waves as well as transient planetary waves. The amplitudes (left) and phases (the eastward longitude of the wave maximum, right) of the stationary wave with zonal wave number m=1 that are calculated using MetO temperature (top) and geopotential height (bottom) fields at 60^{o}N are shown in Figure 6.5 for January, February, and March of 2005. Although both parameters show peaks in amplitude of the wave during the previously mentioned intervals of interest, the characteristics of the peaks are quite different. The amplitude of the wave m=1 in geopotential heights grows from tropopause upward, maximizing above ~40 km. Its first two peaks are strongest compared to the weak increase at the end of February. In contrast, the amplitudes of the wave m=1 in the temperature field show increases between 32 and 40 km during

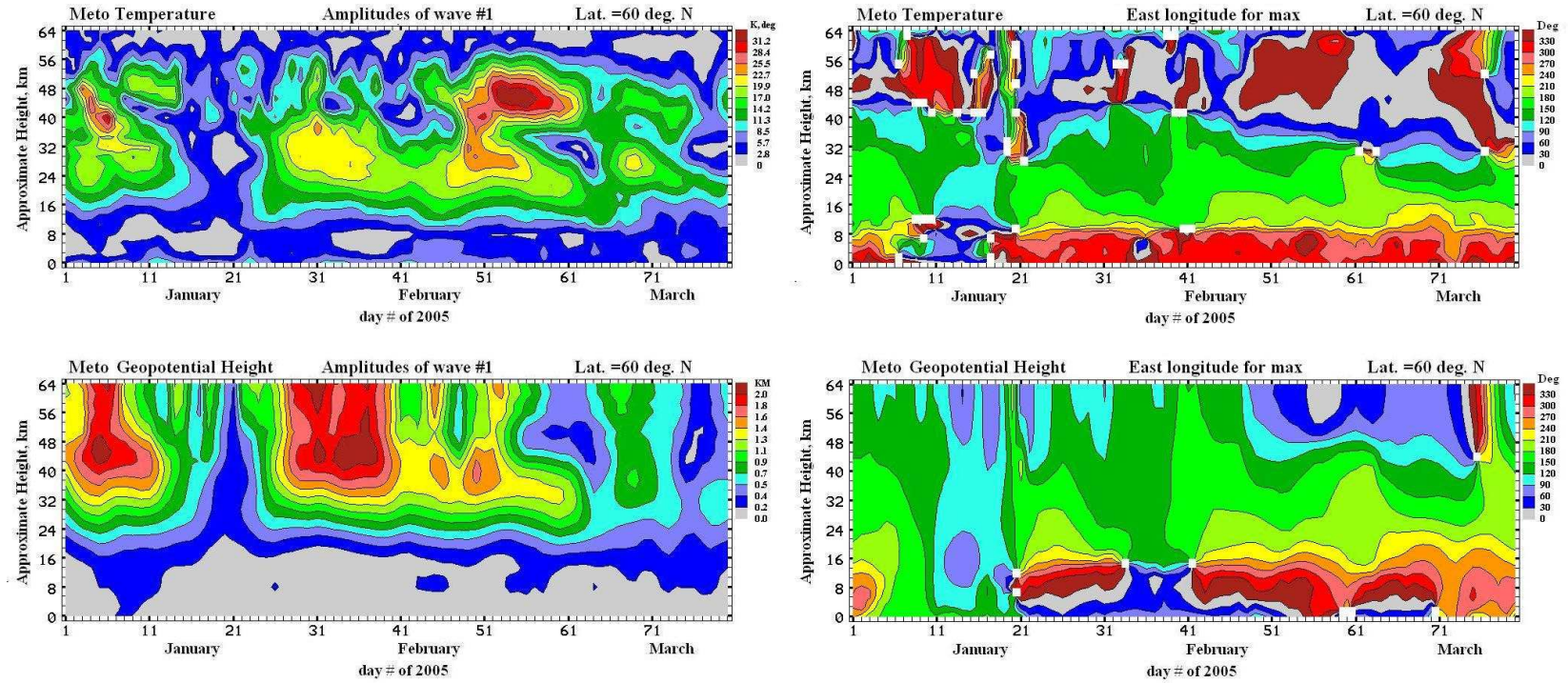

Figure 6.5 Time (January-March) versus height (0-64 km) contours of the amplitudes (left) and phases (right) of the wave number 1 temperature (top) and geopotential height (bottom) perturbations. The phase is defined as longitude (east of Greenwich meridian) of the wave maximum.

the first two intervals and at 48 km at the end of February, with the last peak being the strongest among them. The wave phases change gradually clockwise (westward) with height from ~360^o in the troposphere to 210-150^o in the lower-middle stratosphere, and near zero in the upper stratosphere. Although below ~40 km the phase tendencies are similar for both perturbations, in temperature and geopotential height, in the upper stratosphere the phase of the temperature-wave changes faster. Around the day of maximum warming (day number 61, end of February/beginning of March) the lines of constant phase for the temperature-wave coalesce near 32 km, i.e. there is a very rapid phase change, while below that height the gradient is very small. The phases for the geopotential height wave (Figure 6.5, bottom right) also change slowly with height up to ~40 km during this time. It is worth noting that this vertical phase structure for temperature closely resembles that calculated by *Liu and Roble* [2002] for the wave number one of the geopotential height perturbation (their Fig. 6a). The maximum amplitudes of the wave number m=2 (Figure 6.6) are smaller (half) and are located between the peaks (in the time domain) of the wave m=1 for the first part of the winter. However, the last enhancements of the two waves, in late February, coincide.

The amplitudes for several horizontally propagating oscillations (PW) with different periods (T) and zonal wave numbers (m) were calculated from MetO zonal winds using the least-square fitting process (Section 2.8). Figure 6.7 demonstrates the amplitudes of eastward (m=-1) and westward (m=+1) propagating waves with periods 10 and 15 days for three heights 10, 1 and 0.3 hPa. As discussed in *Chshyolkova et al.* [2006], the eastward waves are baroclinic and westward are normal modes [*Andrews et al.*, 1987b]. The solid and dashed lines indicate eastward and westward zonal mean winds, which are smoothed over 30-day intervals with a 5-day time-step. The thick solid line is the "zero-wind" line, and the step between contours is 10 m/s. Notice that the winter months of the Northern Hemisphere are in the middle of each rectangle. It is seen from the figure that in the Northern Hemisphere the eastward waves are more active in the beginning of the winter when the eastward mean winds are strongest, and are confined to the winter hemisphere (eastward background flow). Activity of the westward waves of the Northern Hemisphere increases by the end of the winter, and they penetrate to the

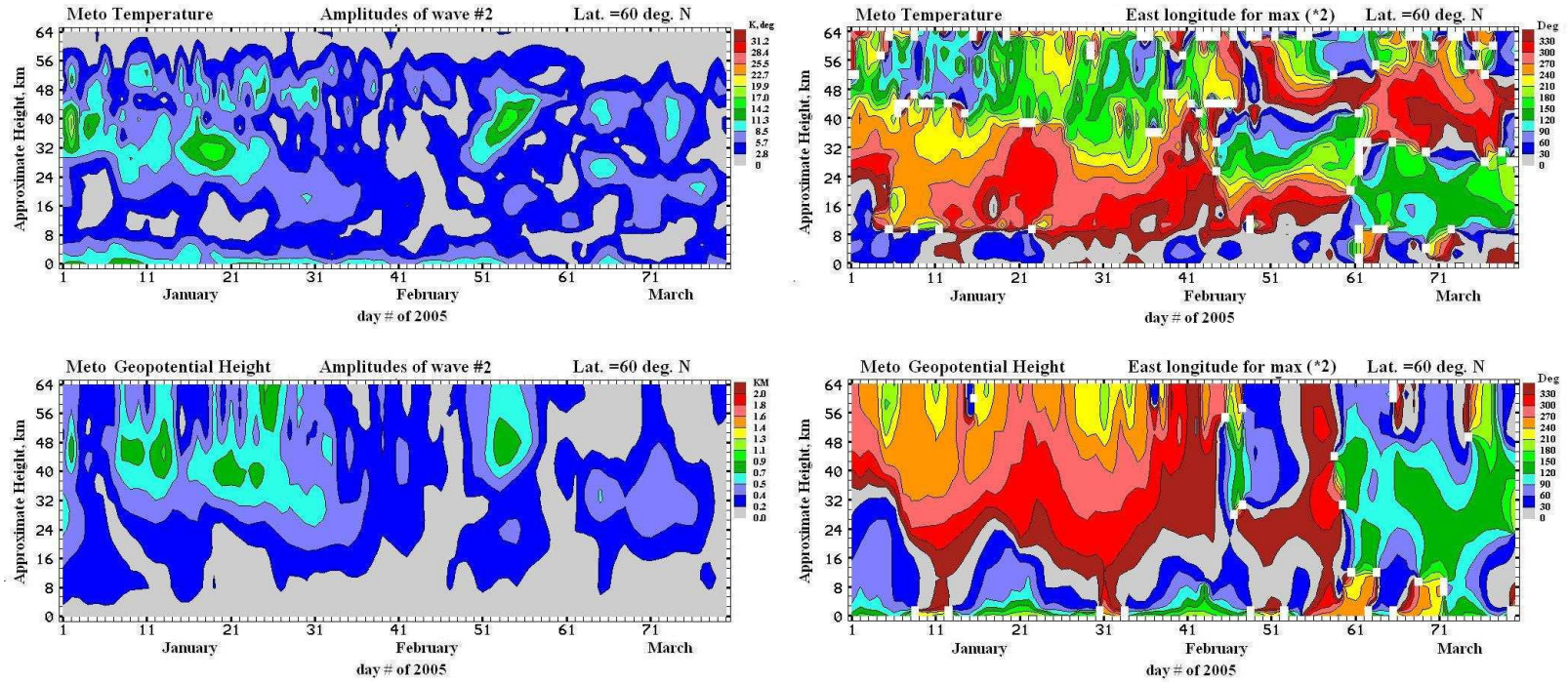

Figure 6.6 The same as Figure 6.5, but for the wave number 2.

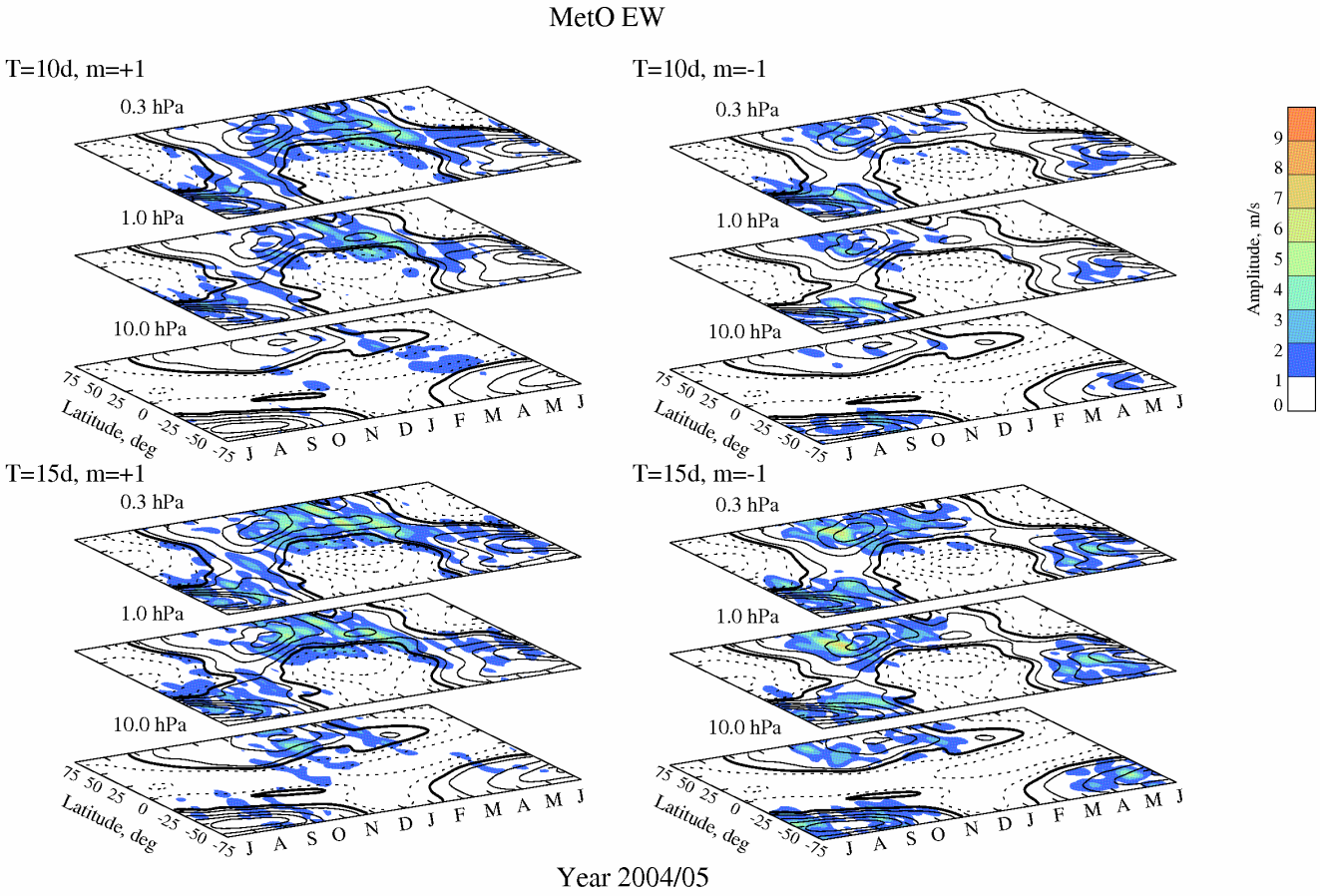

Figure 6.7 The amplitudes of the MetO EW wind oscillations with periods 10 (the upper row) and 15 (the bottom row) days and westward/eastward wave numbers +/-1 versus latitude are shown for the time interval from July, 2004 until June, 2005. The mean zonal EW winds smoothed over 30 day intervals with 5 day step are contoured by solid (positive, eastward) and dashed (negative, westward) lines. The thick line is the "zero wind" line. The other contours are …-30, -10, +10, +30 ... m/s.

Southern Hemisphere in March. In October the cross-hemispheric coupling of the westward waves is somewhat smaller than in the Arctic spring (March). Compared to the winter months of 2001 and 2002 considered in Section 4.4 (Figure 4.5 and Figure 4.6), the amplitudes are ~1.5 times weaker this year [*Chshyolkova et al.,* 2006].

To study the longitudinal variabilities of the polar vortex, the Q values have been calculated from MetO data at 24 isentropic surfaces (from 300 to 2000 K) for each day of the winter of 2004/05 (November 1, 2004 - March 31, 2005) using the equation (6.5) given in Section 6.2.2. The identified edges of vortices (Section 6.2.2 and Appendix B) have been used to color the cyclonic polar vortex with blue and anticyclones with orange; and then they are contoured as overlapping projections for isentropic surfaces from 500 to 2000 K (~20-50 km). The lowest isentropic surfaces were omitted as the existence of the tropospheric jet makes determination of the vortex edges difficult at those heights. The results are shown in Figure 6.8 for four chosen days. The vortex for December 25 (2004) is a typical example of a cold vortex: the blue area has a cone-shape reflecting the increase of the vortex area with height. On this day there were two relatively small anticyclonic areas located over Asia and the Atlantic Ocean. During most of the Arctic winter of 2004/05 the polar vortex exhibited similar characteristics except for three time intervals when it was disturbed (cf. Figure 6.4). Two short-lived and weak disturbances occurred around January 1 and February 1. The vortex became elongated and twisted with height. The anticyclones then occupied larger areas. The strongest disturbance for this winter occurred at the end of February. For example the vortex structure for February 25 is demonstrated in the bottom right corner of Figure 6.8. In the lower stratosphere the polar vortex splits into two parts, while at the upper levels the vortex is just strongly elongated and displaced from the pole. Again, the whole structure is elongated and rotated westward with height.

Zonal asymmetry of the winter circulation is obvious during the disturbed days, but there are also longitudinal peculiarities when the vortex is relatively strong and circular. This is clearly seen from the comparison of the latitude-altitude cross-sections for 253^{o}E (North America) and 16^{o}E (Scandinavia-Europe) that are shown for December 25th

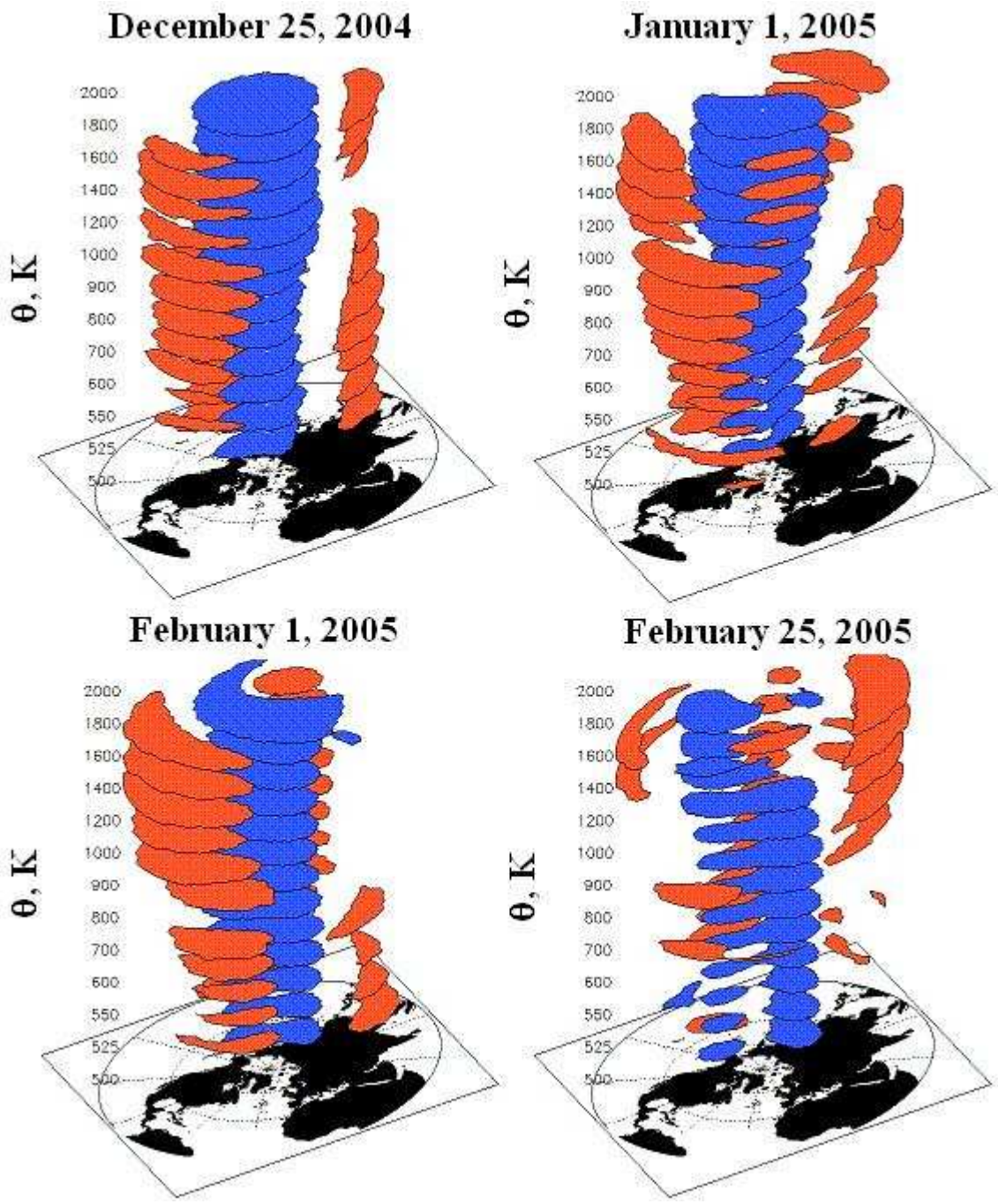

Figure 6.8 Representation of the polar vortex (blue) and anticyclones (orange) from the θ=500 to 2000 K (~20-50 km) isentropic surfaces on December 25th, 2004; January 1st, February 1st, and February 25th, 2005.

(Figure 6.9) and for February 25th (Figure 6.10). These plots demonstrate the Q parameter (dark/light grey shadings), "scaled" PV (dot-dashed lines), and zonal winds (solid and dashed lines) for 20°N-90°N latitudes and from 20 to 50 km heights. The areas dominated by rotation (negative Q values) are shaded with darker grey color. Eastward and westward winds are plotted using solid and dashed lines, respectively, and the thick solid lines denote the "zero-wind" line. The PV was modified by scaling it with a dimensionless factor, $\left(\theta/420\right)^{-4}$, to remove altitudinal dependence due to the potential temperature (θ) changes with height [*Muller and Gunther*, 2003 and 2005].

The Arctic polar vortex is clearly visible as a region bounded by closely spaced dot-dashed lines (large gradients of scaled PV in Figure 6.9 and Figure 6.10); it is centered almost over the pole and occupies a large area (up to ~40-50°N). As can be seen in Figure 6.9, during December the cyclonic rotation is dominant over Europe (the top panel) at latitudes poleward of 55-60° with the maximum latitudinal gradients of PV also occurring near 55°. In contrast, over North America (the bottom panel) there is a zone of positive Q ("shear zone") at ~55 ° between the central (~60-90°N) and mid-latitudinal (40-50°N) parts of the cyclonic vortex. Also notice the strong latitudinal gradients in PV near 40° and 55° latitude. Although the eastward winds demonstrate similarly very strong speeds (~90m/s) near the "edge" of the vortex in both meridional cross-sections, positions of the maxima are different. Maximum winds are reached at ~50°N over Europe and ~40°N over the North American continent.

Figure 6.10 shows that even more differences exist between European and North American locations on February 25th during the strongest disturbance for this winter. At the North American longitude (253°E) a westward wind cell centered near 70° occupies the middle to high latitudes at stratospheric levels, and the eastward wind-jet is shifted equatorward (centered near 30°N) and upward. At the same time, at the European longitude (16°E), the eastward winds are still strong (~60 m/s) and maximize near 50°N. This is due to the deformation and shift of the vortex away from the pole.

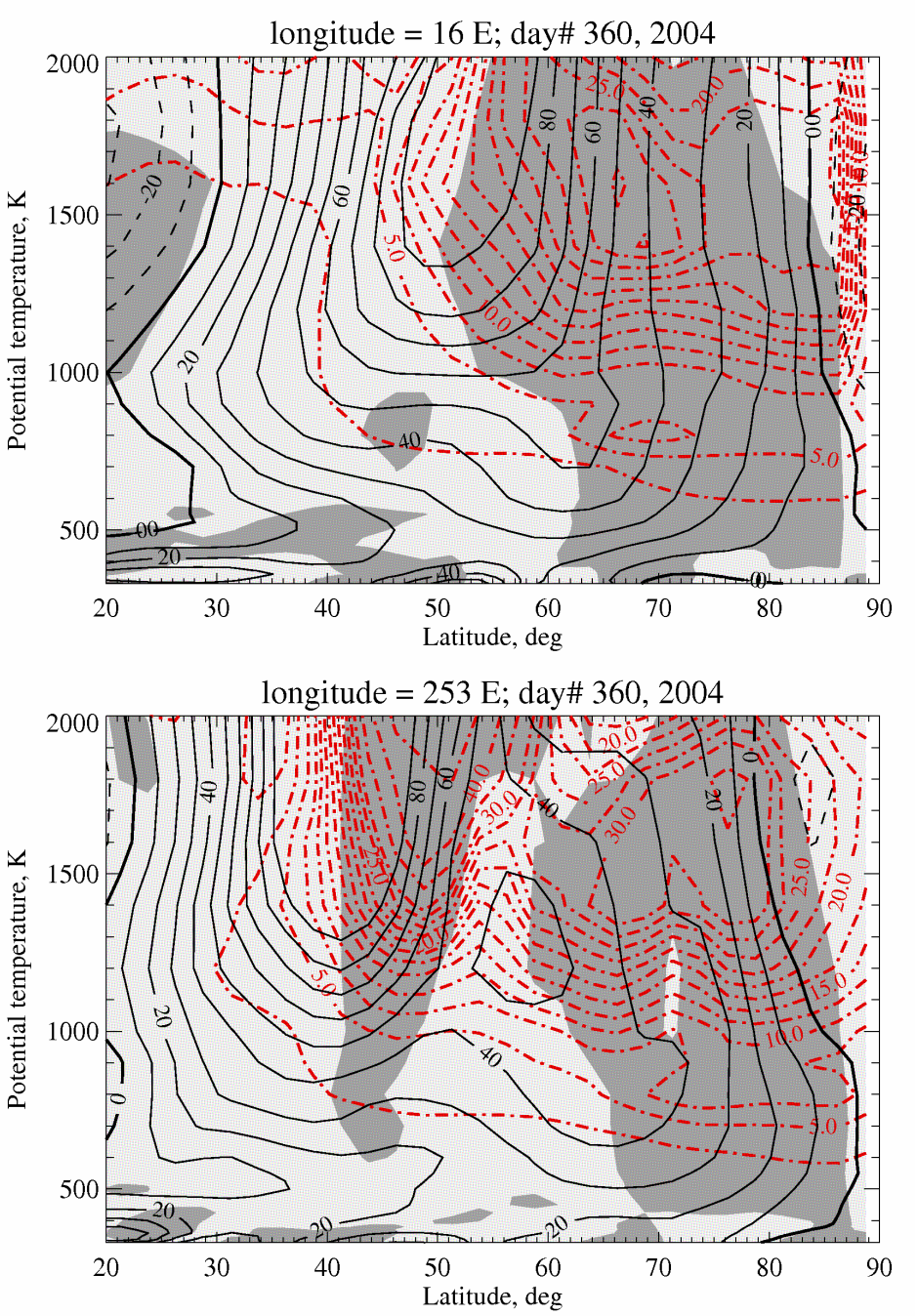

Figure 6.9 Latitude-altitude cross sections of the Q parameter (dark grey is negative, light grey is positive) at 16^{o}E (top) and 253^{o}E (bottom) longitudes on December 25th, 2004 (day number 360). Solid and dashed lines are positive (eastward) and negative (westward) MetO zonal winds (m/s), respectively. Dash-dot lines are contours of modified PV (1PV unit=10^{-6}m^{2}Ks^{-1}kg^{-1}).

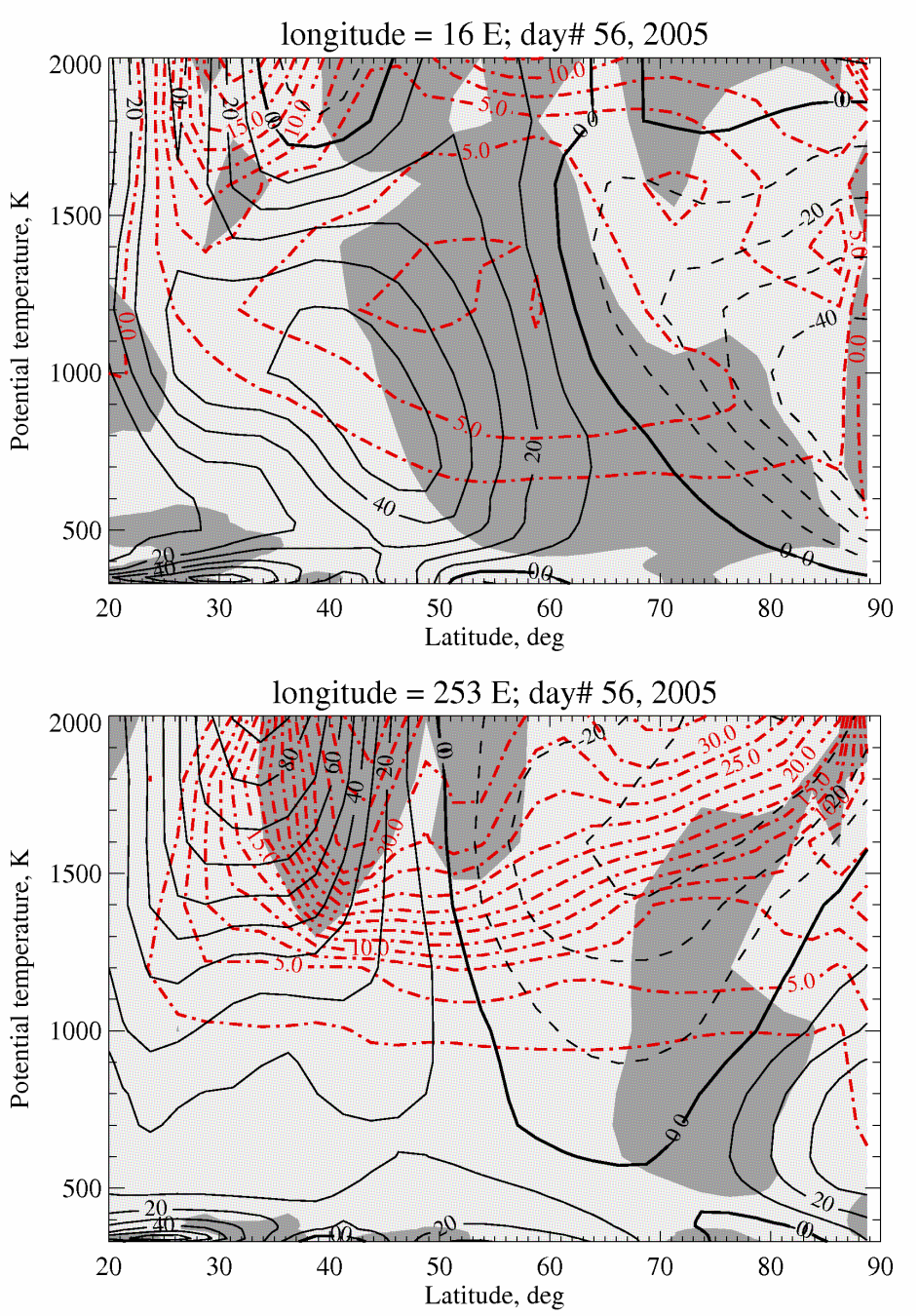

Figure 6.10 The same as Figure 6.9 only for February 25, 2005 (day number 56).

The part of the vortex over North America weakened, while its second part over Europe was still strong.

6.4 Stratospheric-Mesospheric Coupling during Winter of 2004/05

6.4.1 Zonal winds in the 0-97 km height region

In this section analysis of winds in the height region from ~20 to 97 km is discussed for 12 locations; this allows investigation of connections between stratospheric disturbances and mesospheric variability during winter 2004/05. Figure 6.11 shows zonal winds for altitudes between 0 and 97 km and for the time interval from October 2004 till March 2005 for six stations: Svalbard, Tromsø, Collm, Resolute Bay, Yellowknife, and Saskatoon. The stations are divided into two groups: data from three Scandinavian-European and three Canadian radars are shown on the left and right sides of the figure, correspondingly. Each side is arranged so that the data from the most poleward stations are on the top and the most equatorward stations are on the bottom of the figure. Each plot consists of three altitudinal sections: 0-55 km, 55-80 km, and 82-97 km. The MetO daily zonal winds are presented at the lowest heights. Mean winds at the uppermost heights are from zonal winds measured by VHF (meteor) and MFR and obtained by the fitting of the mean, 24hr- and 12hr-tides to the hourly radar measurements. The fitting uses a window of 3 days shifted by 1 day to optimize the quality of the means. For the sake of continuity, the middle altitudinal section shows daily winds calculated using the thermal wind equation (eq. 1.5, Section 1.1) with the MetO winds at the low boundary (0.1 hPa). A simple linear fit was employed to calculate latitudinal temperature gradients from Aura MLS daily measurements within $\pm 10^{o}$ in latitude and $\pm 12^{o}$ in longitude over the stations. The similar plots for the rest of the locations (Poker Flat, Andenes, Obninsk, Esrange, Wakkanai, and Platteville) are shown in Figure 6.12.

The different datasets agree well near both their boundaries: ~55 and 82 km. Good agreement is expected around 55 km as we use MetO winds at its highest levels to calculate the wind field above (55-80 km). Around ~82 km discrepancies could be found between winds calculated using thermal wind equation and radar measurements.

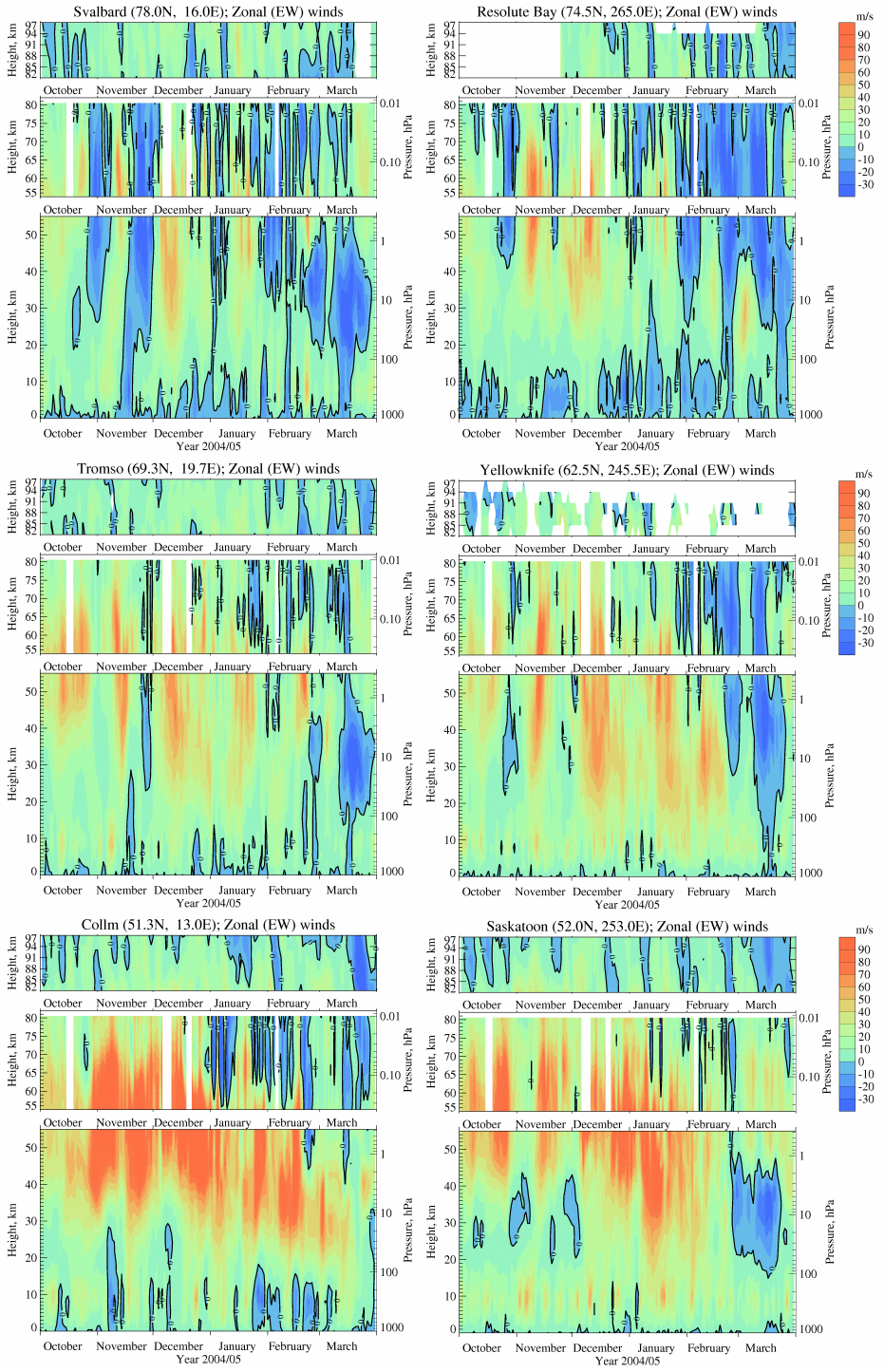

Figure 6.11 Evolution of zonal winds in the height range from the surface up to the upper mesosphere (97 km) in the time interval from October of 2004 until March of 2005 for the Svalbard, Resolute Bay, Tromsø, Yellowknife, Collm, and Saskatoon locations. See text for details.

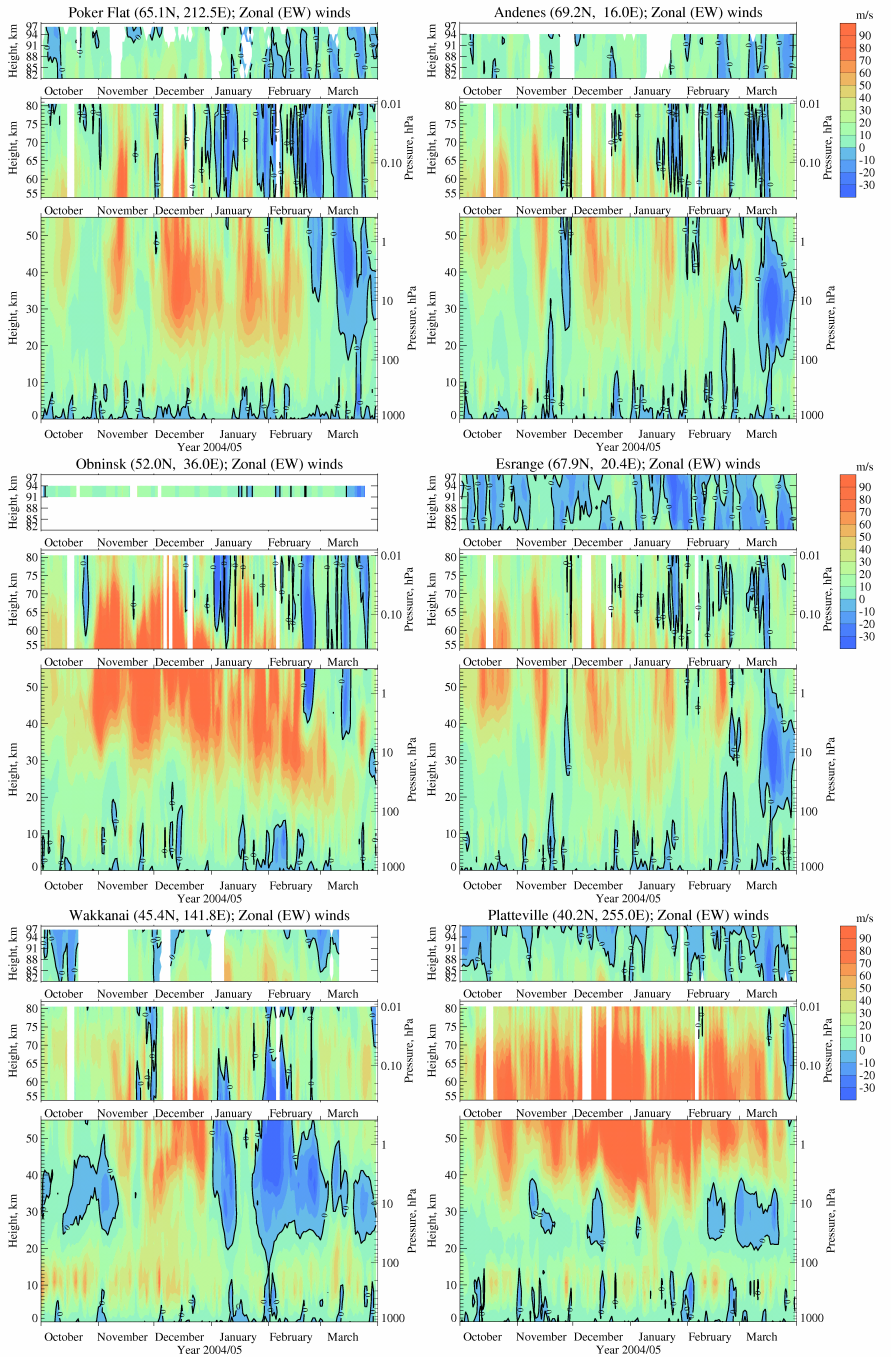

Figure 6.12 The same as Figure 6.11 only for the Poker Flat, Andenes, Obninsk, Esrange, Wakkanai, and Platteville locations.

There are several reasons for these discrepancies:

- As was mentioned in Section 2.5, Aura MLS temperature data are less accurate at the upper levels (0.001 hPa), while the MFR can have speed bias of ~20% (Section 2.1). Note also that there is a 2 km gap between the datasets.
- There are unknown tidal signatures in Aura data. Two adjacent tracks 12 hrs apart have been used in calculations, so the 24-hr tide is minimized, while contamination due to the stronger 12-hr tide at these latitudes could be significant. The radar winds (82-97 km) are "tidally corrected".
- The approach used to calculate temperature gradients may be too simple. For example, in general the zonal temperature gradients are smaller and do not strongly affect the results. However this assumption will not apply if a sharp boundary between cyclonic and anticyclonic vortices exists across a longitude range used for the radar station. Also the largest errors are expected for the stations located poleward of ~72^{o}N as the satellite measurements only cover up to 82^{o}N.
- The thermal wind equation (1.5) assumes geostrophic balance (no drag), which is rarely the case in the atmosphere above 55 km. For example, at mesospheric heights the drag due to GW is strong enough to break this assumption. Without drag the zonal winds would continue to become more eastward throughout the 55-80 km height interval.
- Data have different resolutions: 3 days in the 82-97 km and 1 day in the 55-82 km height regions.

The availability of the MFR data (Tromsø, Saskatoon, and Platteville) at low heights allows comparisons between direct wind measurements and the winds calculated from the thermal wind equation (eq. 1.5, Section 1.1). Figure 6.13 presents the zonal wind time-altitude cross-sections for Tromsø, Saskatoon and Platteville locations. In both columns the lowest parts of the plots (0-55 km) are the same for the corresponding station and present the MetO assimilated daily zonal winds, while at the middle (55-82 km) and upper (82-97 km) heights the mean day-time winds are shown on the left

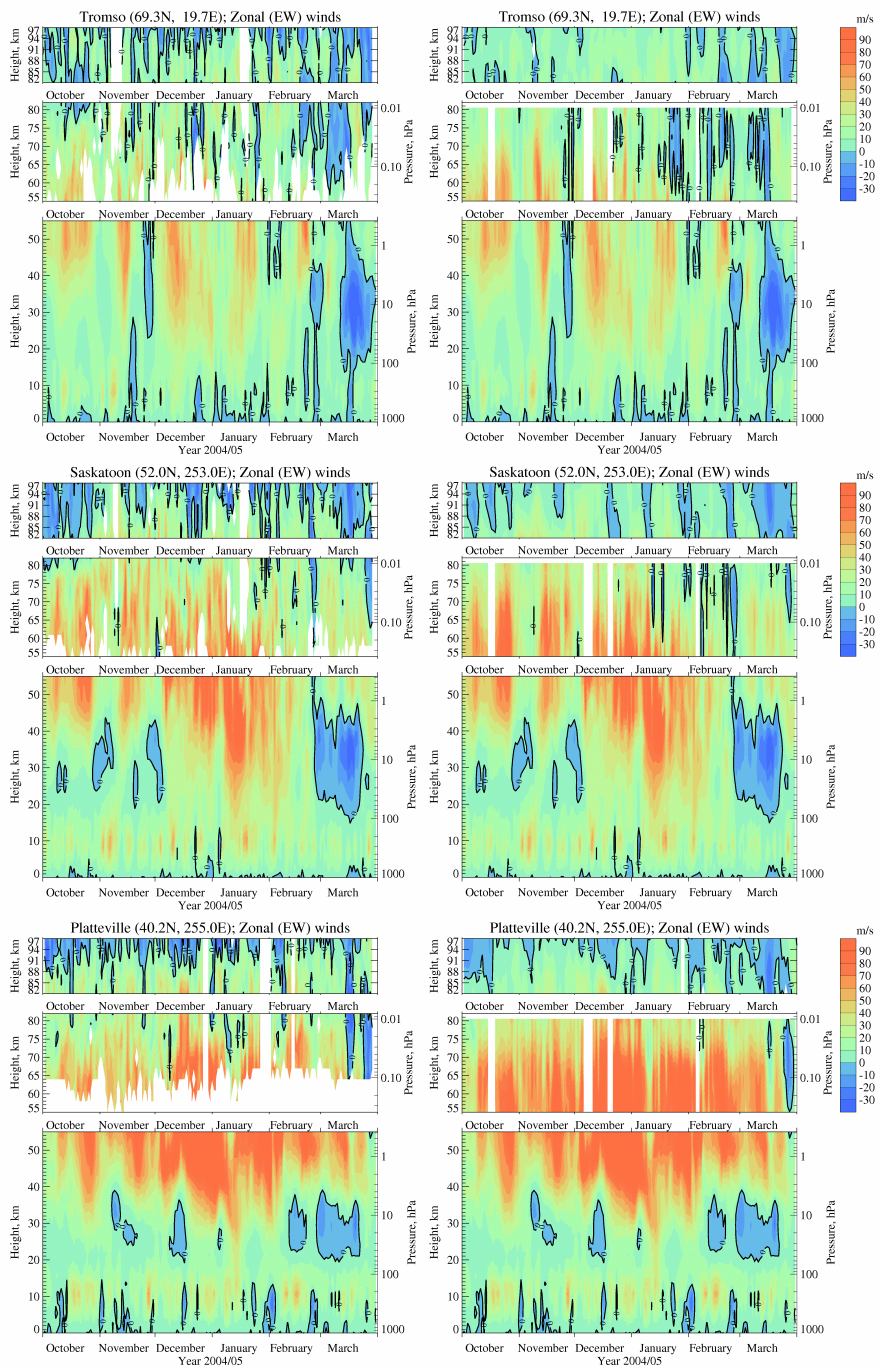

Figure 6.13 Evolution of zonal winds from 0 to 97 km in the time interval from October of 2004 until March of 2005 for Tromsø, Saskatoon and Platteville. The MetO daily winds are shown in the bottom panel of each plot (0-55 km), while for the left column in the middle (55-82 km) and the top (82-97 km) panels day-time mean (≥7hrs of data) centred on noon and obtained from radar measurements are demonstrated. In the right column thermal (55-82 km) and 3-day mean (82-97 km) winds are provided.

column of Figure 6.13. For easier comparison, the plots in the right column of the figure are the same as in Figure 6.11 (Saskatoon and Tromsø) and Figure 6.12 (Platteville). The radar winds in the left column were constructed from hourly data and with at least 7 values per day centered on noon. The averaging over 7 hours minimizes GW influences. Usually, due to the increased noise level and lack of useful radar scatter during the night below ~70 km, the coverage is poorest at low heights, but becomes better near and above 80 km, where the number of hourly mean values approaches 24 [*Luo et al.*, 2002a].

There is very good overall qualitative agreement between calculated and measured winds at all three stations. The largest differences in the middle panel occur near 80 km, where radar data often show westward (blue) winds. This can be attributed to tidal contamination, which is minimal below ~70 km, but increases at upper levels. The comparison of the top panels in Figure 6.13 for the same stations also reveals that the differences are mostly due to tides (the effect of different temporal resolution is insignificant). For example, for Saskatoon (middle plots) in October the fitted mean winds (the right column; no tidal contamination) show westward cells closing at ~82 km, while the mean day-time (middle plot in the left column) westward winds penetrate below ~80 km. Again, remember to keep in mind that the thermal winds are available only up to 0.001 hPa (~80 km), while the radars have no altitudinal gaps in this region. Another factor that would contribute to the discrepancies of Figure 6.13 is the geostrophic assumption. The GW drag is important at the mesospheric heights and, as mentioned above, acts to decrease eastward winds. The geostrophic balance assumes zero drag, so the winds calculated using the thermal wind equation may be more eastward than the actual winds, especially at the upper levels. The smaller radar amplitudes could also be explained by the MFR speed bias of ~20% (Section 2.1). Despite all these differences the calculated thermal winds are a good approximation of the real winds in this height region and can be used for qualitative comparisons and wave analysis purposes.

Returning to consideration of Figure 6.11 and Figure 6.12, the main feature common to all stations is the eastward jet (green-red colors) in the stratosphere-mesosphere height

region (20-90 km), which is often referred to as the polar night jet (PNJ). The maximum of the eastward flow, which is located at ~55-60 km in early winter, decreases in magnitude and progresses downward to ~30-40 km with time. The magnitude of the PNJ varies throughout the winter with occasional reversals (blue) to the westward direction. After each disturbance, winds are restored to their normal winter values until they finally become westward throughout the middle atmosphere, marking the transition to the summer-like wind pattern. Although the general scenario is common for all stations, it differs in detail because the radars have different locations relative to the vortex. The eastward winds are weaker at higher latitudes as was also seen in Figure 6.9 and Figure 6.10. The strong westward events seen at the high latitude Svalbard station below ~85 km are much weaker at Tromsø, and are seen only as relatively small decreases in eastward winds at Collm. Similar latitudinal differences can be seen for Canadian stations. Stations at Andenes, Esrange (Figure 6.12, two top plots at the right), and Tromsø are relatively close (125-270 km), and zonal wind time-variations at these stations are quite similar. In the MLT region winds over Tromsø and Andenes (MFR) are more similar than Esrange MR data (stronger eastward as well as westward amplitudes). The data from these three radars were studied by *Manson et al.* [2004b]. It was shown that there is significant spatial variability across the triangle of these radars and all three indicate differences in wave characteristics from middle latitudes.

Longitudinal variations are apparent between Collm and Saskatoon (bottom plots in Figure 6.11). The eastward winds are weaker at Saskatoon, which can be explained by the different location of the PNJ maximum over Europe and North America: 50^{o}N for 16^{o}E longitude and near 40^{o}N for 253^{o}E (Figure 6.9). Indeed, the wind contours for Platteville (Figure 6.12, bottom right plot) do exhibit much stronger eastward flows than at Saskatoon, which persist above ~40 km throughout all winter until the end of March. Also, at the end of February (the warming event) the transition to the westward winds occurred over Saskatoon between 20 and 97 km, while at Collm the westward wind cell occupies the region between ~40 and 80 km for a few days, with eastward winds at heights near 30 km until the end of March. This reflects the vortex characteristics during this time (Section 6.3, bottom right plot in Figure 6.8), and is consistent with Figure 6.10 which shows weak westward winds at stratospheric levels for latitudes

higher than 50^{o}N (bottom plot) for Saskatoon longitudes, while there are still quite strong (~60 m/s) eastward winds over Europe at 50^{o}N (top plot). Obninsk is located at a similar latitude, but is 20^{o} east of Collm. Zonal winds at Obninsk (Figure 6.12, middle left plot) are similar to those at Collm station, except they were less westward in the 55-82 km height range at the end of January/beginning of February. The meteor radar at Obninsk does not provide height information, and all reflections are assumed to be from the height region centered at approximately 94 km. These winds and Collm winds at 94 km agree well, and have such similarities as wind reversals in the middle of January, the beginning of February, and in the middle of March.

It is also interesting to note that the wind profiles for Poker Flat and Wakkanai (Figure 6.12) are quite different from Scandinavian-European and Canadian stations. For example, the PNJ has stronger magnitudes at Poker Flat (~65^{o}N) than at Canadian/European stations with similar latitudes. Over Wakkanai the first strong westward reversal occurred in the first half of January between 20 and 70 km, and was followed by the second stronger reversal in February. Later the winds became weakly eastward above ~40-50 km, but remained westward in the lower stratosphere until the end of the March. These may be explained by the relatively close proximity of these stations to the Aleutian High.

In the upper mesospheric region (82-97 km) the eastward zonal winds decrease in magnitude at all stations with increasing height, although their particular variations differ. Most of their variability can probably be explained by the local effects of GWs on the mean flow (deceleration of the flow as well as induced variability with periods in the PW range, see for example [*Smith,* 1996]). Some of the reversals of the eastward mesospheric winds can be linked to the wind reversals below. The warming event at the end of February is the best example of such connection between mesosphere and stratosphere. The timing of such reversals appears to be approximately the same throughout the whole height range or sometimes a little earlier at the upper altitudes.

6.4.2 **Comparison of the upper levels MetO (50-60 km) and radar (82 km) winds**

In this section an attempt to compare winds from the upper stratospheric (~50-60 km) heights with those from the mesospheric heights (82 km) is made with the emphasis on the vortex structure rather than consideration of eastward wind profiles at separate locations as has been done in the previous Section. The comparison is difficult mostly due to the lack of mesospheric observations. Although this study involves the largest number of mesospheric stations used in similar investigations published before, it still consists of just 12 locations clustered mainly in two geographical areas. In Figure 6.14 the daily MetO winds at the 2000K (~ 50 km) isentropic surface (left column) along with the 3-day mean wind vectors (82 km) obtained at 12 radar stations (right column) are shown for a sequence of days throughout January and February of 2005. As on previous similar plots, the plots on the left are the stereographic projections (15-90^{o}N) of the Q-diagnostic over the Northern Hemisphere with the blue areas where Q is negative (rotation dominates the flow) and green areas where Q is positive (strain is dominant). Black arrows are winds, red stars are locations of the radar stations, and black/red lines are estimated edges of cyclones/anticyclones. Black filled dots are assigned to the areas with the negative PV, which are usual at low latitudes. Sometimes, however, the black dots can be found more poleward, which indicates an intrusion of the tropical air to the mid-latitudinal region at the upper stratospheric heights [*Harvey et al.*, 2002]. All available 3-day radar vectors were inspected. Days that indicated the usual winter cyclonic flow around the pole and events in February (1st and 25th) were chosen for demonstration. These are probably linked to the disturbances in the stratosphere discussed earlier (Figure 6.4 and Figure 6.8). It is necessary to remind the reader that the radar winds are obtained over a 3-day interval centered on the chosen dates, while daily vortex plots are shown beside the corresponding radar plots.

First of all at the upper stratospheric heights the vortex does not have “solid” or continuous shape as it usually has in the middle stratosphere (see for example Figure 6.3); at these levels patches of blue color are scattered over the hemisphere composing some kind of spiral or comma shapes. The meridional wind component is often strong, and there is, therefore, significant divergence from the cyclonic eastward flow. On the

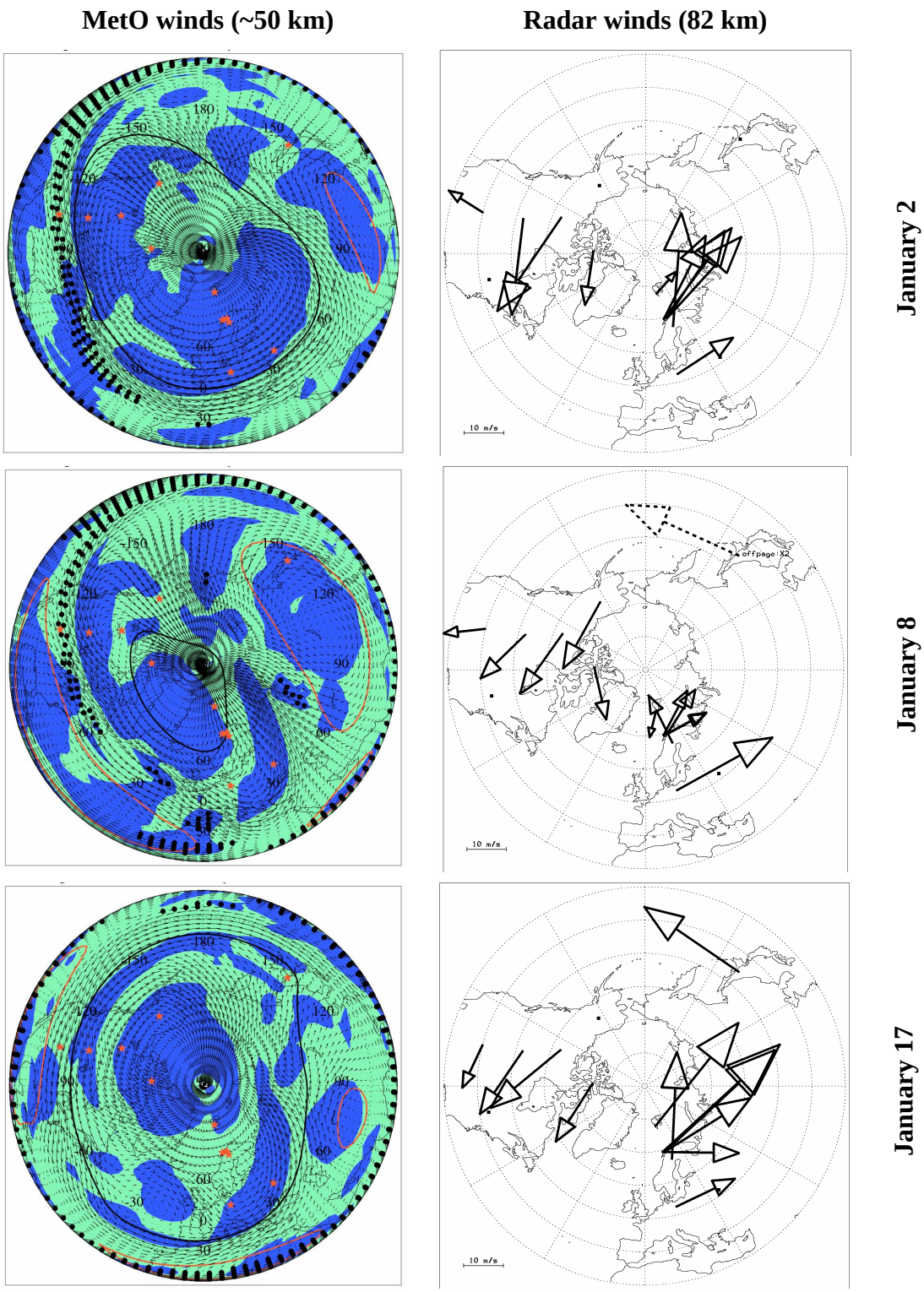

Figure 6.14 Evolution of the daily MetO winds (black arrows) at 2000 K isentropic surface (left column) and 3-day mean winds obtained at 12 radar locations (82 km, right column) through February of 2005.

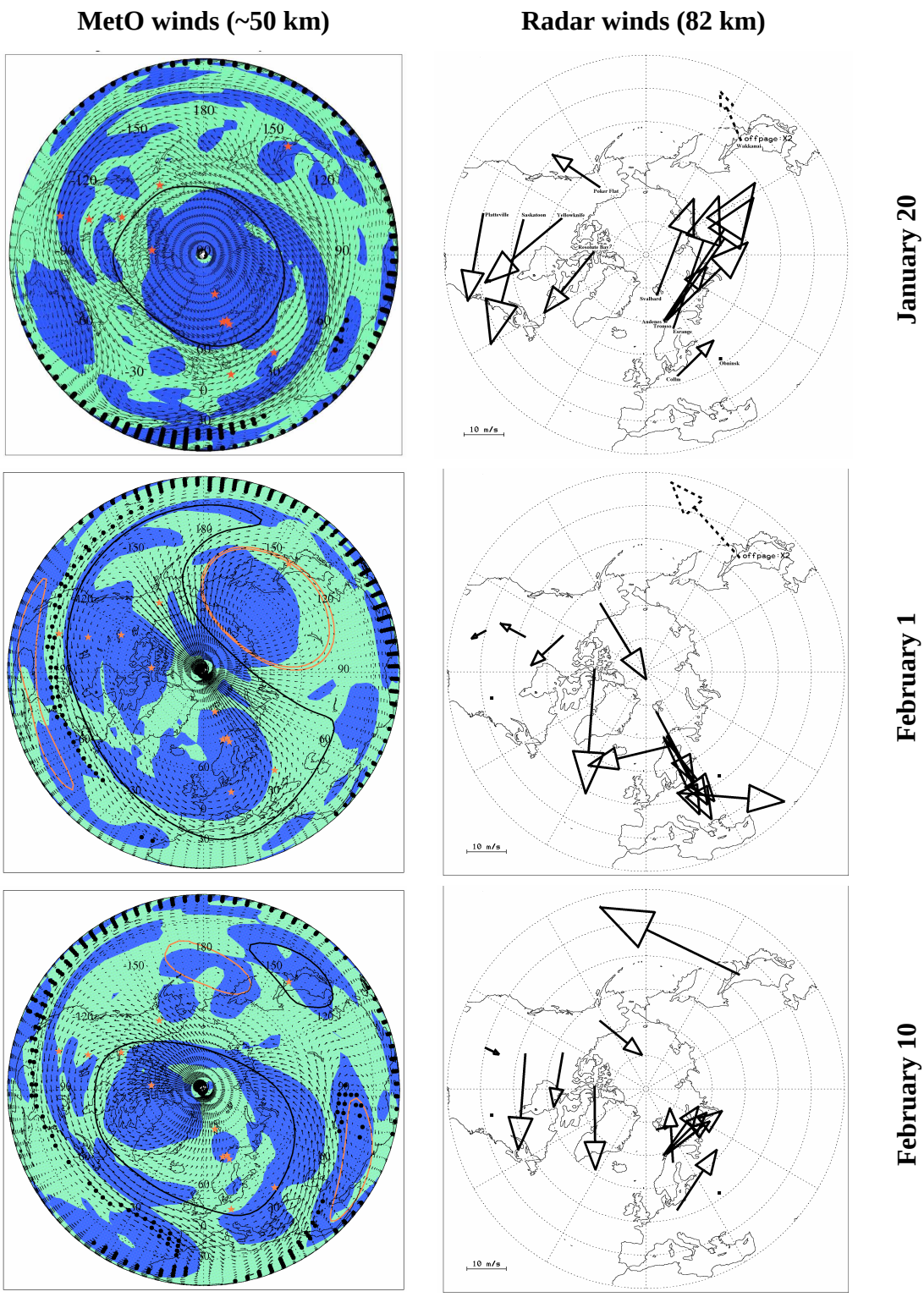

Figure 6.14 (cont.) The dashed arrow indicates the speed is twice as big as that shown.

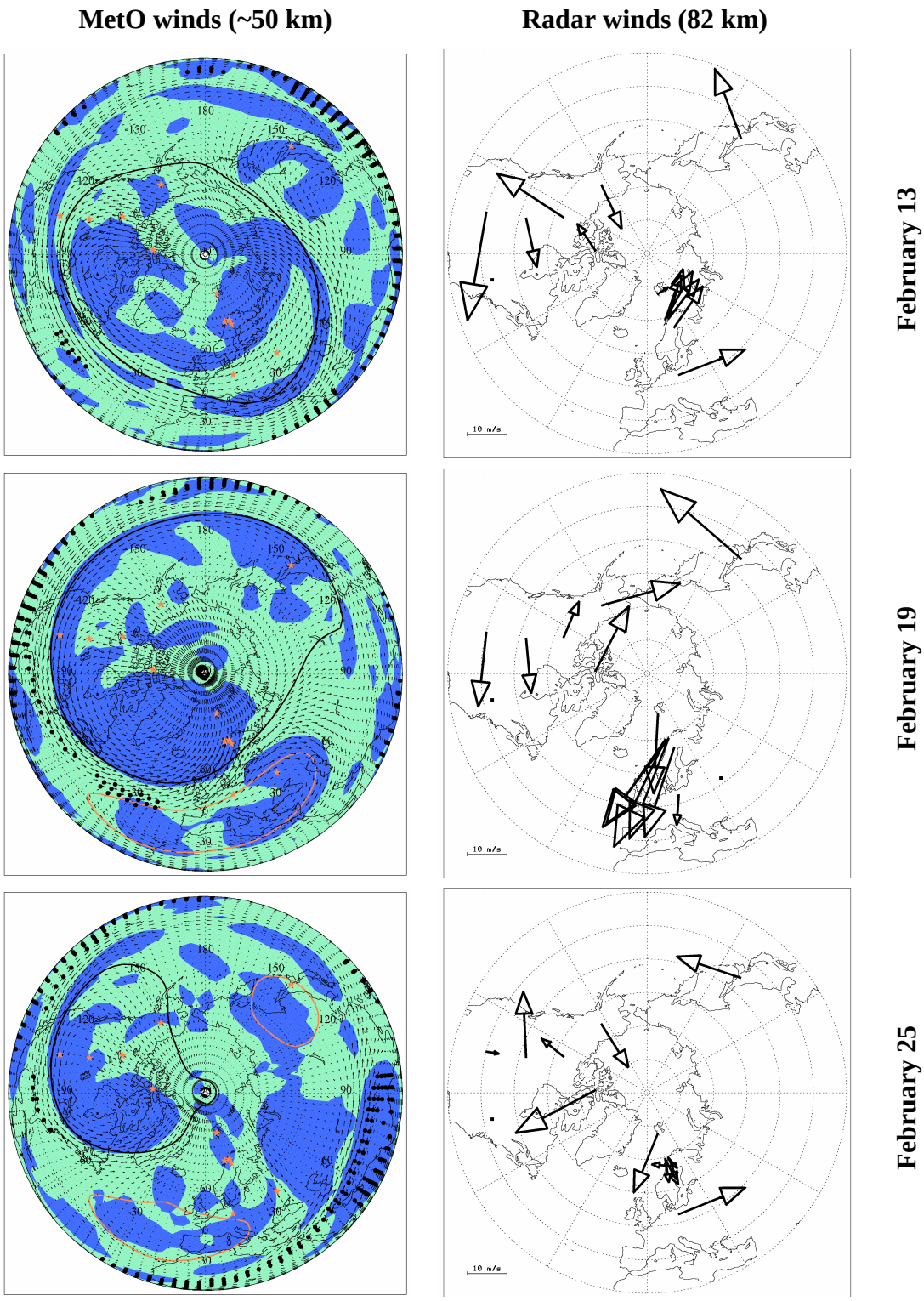

Figure 6.14 (cont.)

right column vectors of the mesospheric mean wind measured at 12 locations (the same locations that are shown by red stars on the left column) are plotted on top of the stereographic map (30-90^{o}N). In January (2, 8, 17, and 20) arrangement of radar wind vectors is consistent with cyclonic motion around the pole, and they match well the MetO winds at corresponding locations. Often, especially when negative areas of Q have consistent large circular shapes with little or no shear (green) zones inside (e.g. January 20), the stratospheric and mesospheric vectors show very close similarity in their directions. Usually best agreement requires a shift of the vortex with height, for example.

On February 1st, the time of the weak stratospheric disturbance, radar and MetO wind vectors over high-latitudinal stations (>60^{o}N) demonstrate opposite directions and have strong meridional components. This suggests an existence of strong thermal gradients of opposite directions at stratospheric and mesospheric heights. The MetO data at ~30 km (not shown) indicate that the polar vortex was squeezed by two anticyclones located at lower latitudes in the 330-360^{o}E and 90-180 ^{o} E longitudinal sectors. The stronger of the two anticyclones (90-180^{o}E) also pushed the polar vortex away from the pole, which is reflected in Figure 6.5 as an amplitude increase in the stationary wave number 1 at 60^{o}N. Therefore the boundary between cold and warm regions lay across the pole, and strong poleward/equatorward flows were established in the 30-60^{o}E and 210-240^{o}E longitudinal segments, respectively (Figure 6.14). At the upper heights (layer 50-80 km) the Aura measurements (not shown) indicate reversed temperature gradients (cold in 120^{o}E sector), so that winds at ~80 km, through thermal wind equation (1.5), now have opposite directions to the stratospheric winds. The winds were weak over Canadian stations (Platteville, Saskatoon, and Yellowknife), which are situated farther from this region of strong temperature gradients.

During the first half of February the stratospheric vortex became stronger. This is reflected in the plots for February 10 and 13: the stratospheric and mesospheric winds are again similar in directions as was the case for most of January. On February 19 the warming has begun and as in February 1 wind vectors have opposite directions at stratospheric and mesospheric heights over the European-Scandinavian sector. But this

time the structure was more complicated and involved strong latitudinal as well as longitudinal temperature gradients. Aura data indicated warm temperatures over the pole, which resulted in South-Westward wind directions at 82 km over Europe. Winds over Platteville, Saskatoon and Wakkanai, stations located in regions of the strong stratopause eastward jet, were not affected and had eastward directions at 82 km, which is consistent with strong vortex conditions. For this day Aura temperature measurements did not show perfect alignment of opposite temperature gradients across the pole at stratospheric and mesospheric heights, which can explain the more diverse relationships between stratospheric and mesospheric winds depending on the locations.

Finally by February 25 the vortex was split in two uneven parts at low stratospheric heights with the stronger part being over Europe. In the upper stratosphere (Figure 6.8) the vortex was deformed and twisted westward with height, so that the stronger cyclonic area was located over North America. At mesospheric heights, as seen from the plot (Figure 6.14), winds were also weak and completely disorganized. Later in March the cyclonic flow was partially restored at 50 and 82 km, before it disappeared during the transition to the summer circulation.

The vector differences between mesospheric winds measured at 82 km and MetO assimilated winds at ~64 km are shown in Figure 6.15 for 3 months: December of 2004, January and February of 2005. The stations located near the center of the PNJ (Obninsk, Collm, Saskatoon and Platteville) consistently demonstrate strong westward (pointed to the left) vector differences, especially in December. The negative (angle of ~180^{o}) differences are consistent with the decrease of the winds with height. This is in agreement, through the thermal wind equation (1.5), with a warm mesopause region, which is normal in winter. However at the end of February, during the strongest, for this winter, stratospheric disturbance the difference-vectors at these stations (except Platteville, a more equatorward station) are smaller or eastward (pointed to the right). This indicates weakening or reverse of the eastward flow in the stratopause.

Significant deviation of the illustrated strong difference-vectors from the horizontal line (EW direction) implies reversed meridional flow between the ~64 km and 82 km

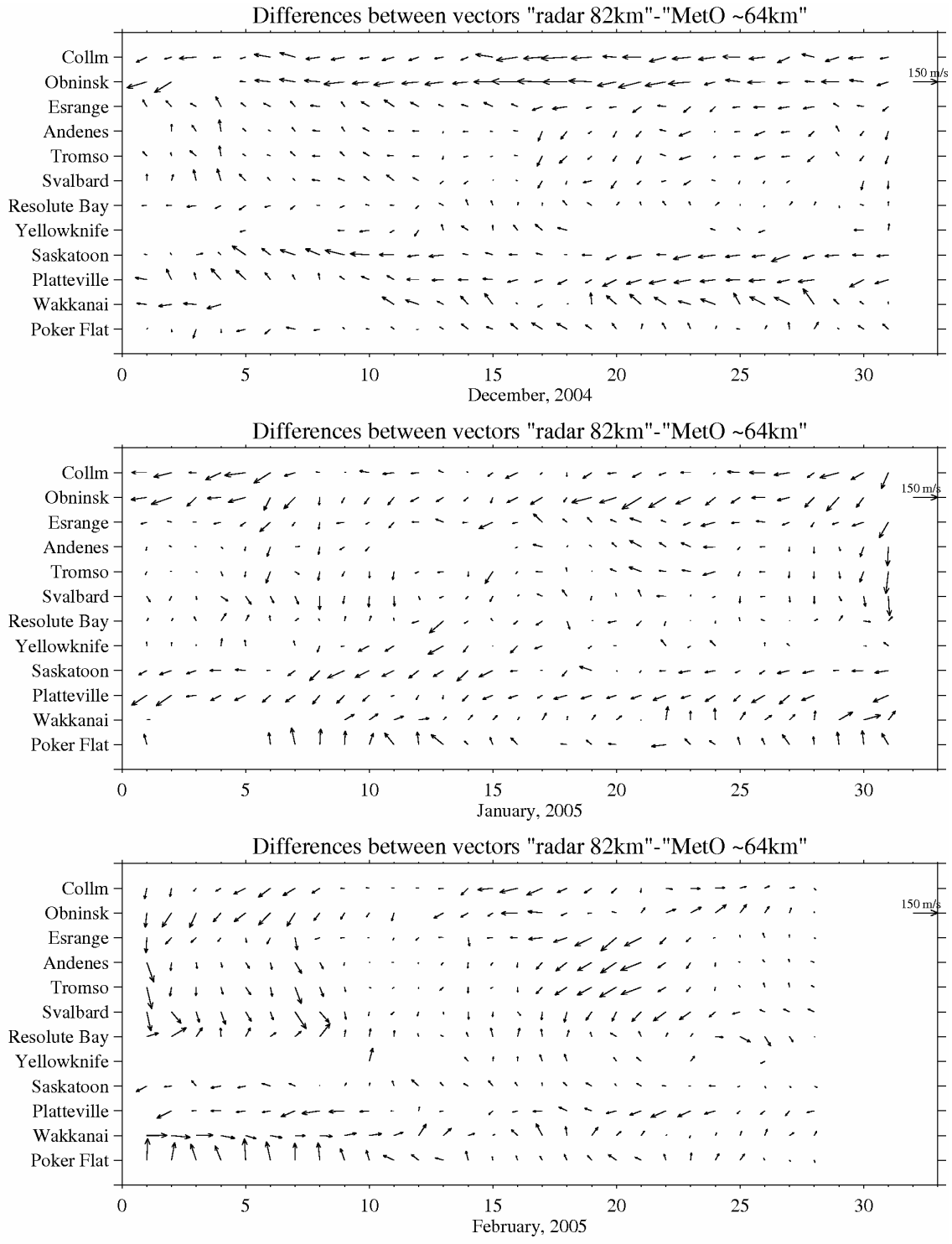

Figure 6.15 Vectors of differences between radar winds measured at 82 km and MetO assimilated winds at ~64 km for 3 months of winter of 2004/05 (December, January, and February) for 12 locations.

heights. The downward (in the figure) or southward directions of the large difference-vectors indicate poleward flow at the stratopause levels and equatorward flow at the mesospheric levels, e.g. near February 1 and 19. Small vector differences normally occur when winds at both heights are in the same direction. The reverse is true for the upward (northward) directions of the large difference-vectors (e.g. early in December). All Scandinavian stations Esrange, Tromsø, Andenes, and Svalbard lie inside the core of the vortex, and the angles of their difference-vectors change with time (generally from 180^o to 270^o, except for one interval in the beginning of December) in a similar way. Although the high-latitude Canadian stations at Yellowknife and Resolute Bay are also close together and located inside the vortex, the angles of their difference-vectors do not always change similarly with time. However, the difference-vectors are predominantly northward, consistent with southward stratopause winds, for both stations. The angles, therefore, differ from those at Scandinavian stations. Again as in the previous Section, the Poker Flat and Wakkanai exhibit their own patterns of angle variations, which have strong northward components, especially at Poker Flat (a more poleward location). The longitudinal variations in the difference-vectors are due to the distortions of the vortex and/or its movement off the pole.

We have also tried to calculate simple cross-correlation coefficients between 12 vectors at mesospheric heights and corresponding 12 vectors at stratospheric heights, as well as between time series of mesospheric and stratospheric winds at each station separately. Unfortunately, the results obtained were not consistent, very variable, and not conclusive. More data, preferably satellite wind measurements at mesospheric heights, are required for better correlation analysis.

6.4.3 **The results of spectral analysis**

To study the wind variability with periods from 2 to 30 days, the Morlet wavelet (Section 2.7) has been employed. Figure 6.16 demonstrates examples of wavelet amplitudes of the MetO (~50 km, left column) and Radar (82 km, right column) zonal winds for Svalbard, Tromsø, Collm, and Saskatoon (from the top to the bottom). The

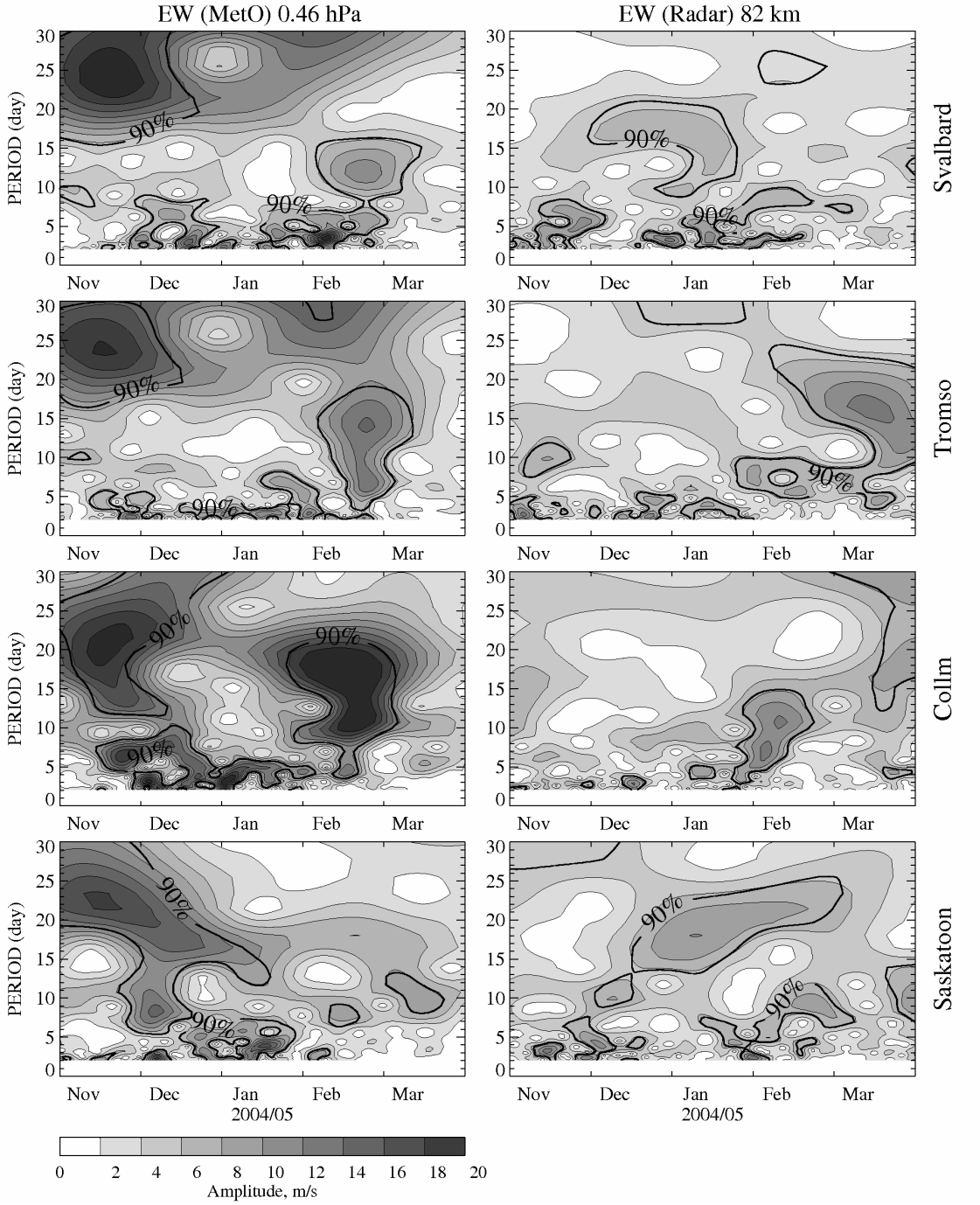

Figure 6.16 Wavelet amplitudes versus time (November 2004-March 2005) and period (2-30 days) calculated for the zonal wind component of the MetO winds at 0.46 hPa (left column) and of radar measurements at 82 km (right column) for the Svalbard, Tromsø, Collm, and Saskatoon locations.

black line indicates areas with 90% significance. The three Scandinavian-European stations have similar spectra: long periods (>20 days) in November, short periods (less than 5 days) throughout the most of the winter, and energy for periods between 4 and 20 days at the end of February. Clearly there are some differences in exact locations of the peaks as well as their amplitudes, which are smaller at more poleward stations. Some of these differences could be due to different propagation conditions for the PW at these three stations. As can be seen in Figure 6.11, at the end of February the westward background winds are stronger below 50 km at Svalbard than at Tromsø, while over Collm the winds have eastward directions. PW propagation is favored by eastward winds of moderate magnitude [*Andrews et al.*, 1987b]. Wavelets of MetO zonal winds at Saskatoon have overall smaller amplitudes. Similar to the other stations there is energy at longer periods in November, but in the middle of February there is only one relatively weak peak around 8 days and 10-day maxima appear in the first half of March. This is consistent with the zero wind line and the cell of westward winds at stratospheric heights over, and northward of, Saskatoon (Figure 6.10, bottom panel), which will favor refraction of PW to lower latitudes. The wavelets at the mesospheric heights (the right column) have much smaller amplitudes and do not have many similarities. This variability of local PW activity (latitudinally and longitudinally) is consistent with the earlier study of 16-day PW activity provided by *Luo et al.* [2002a,b].

The contours of the wavelet amplitudes are presented for the Andenes, Esrange, Poker Flat, and Platteville locations in Figure 6.17, and for the Resolute Bay, Yellowknife, Obninsk, and Wakkanai locations in Figure 6.18. As expected the three radars from the "Scandinavian triangle" Tromsø, Andenes, and Esrange have similar morphologies of wavelet amplitudes at both stratospheric and mesospheric heights. Although wavelets for Platteville and Saskatoon are less similar, they show similar peaks around 10 days at the beginning of December and the end of March with the smaller magnitudes at the more poleward station (Saskatoon).

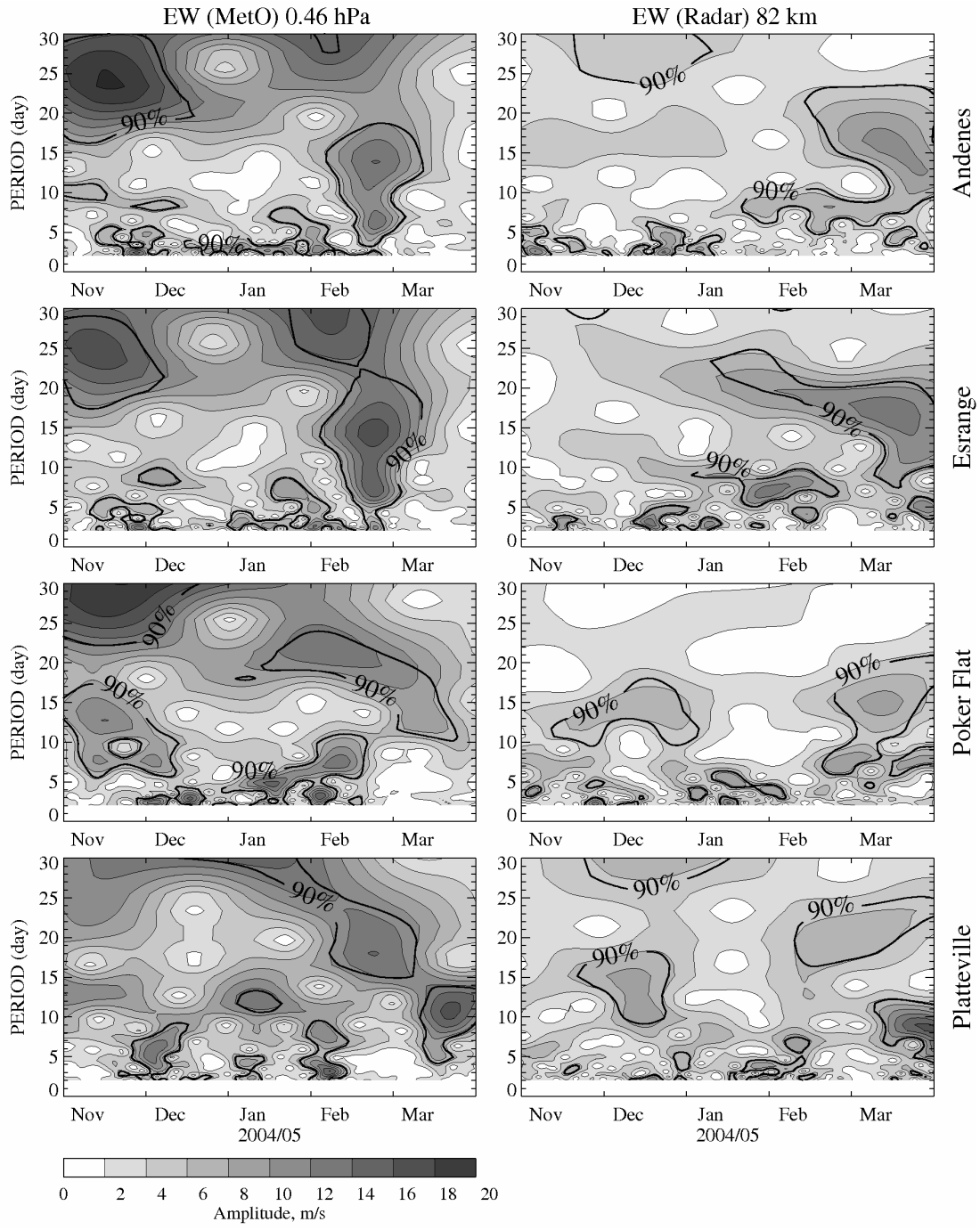

Figure 6.17 The same as Figure 6.16, but for the Andenes, Esrange, Poker Flat, and Platteville locations.

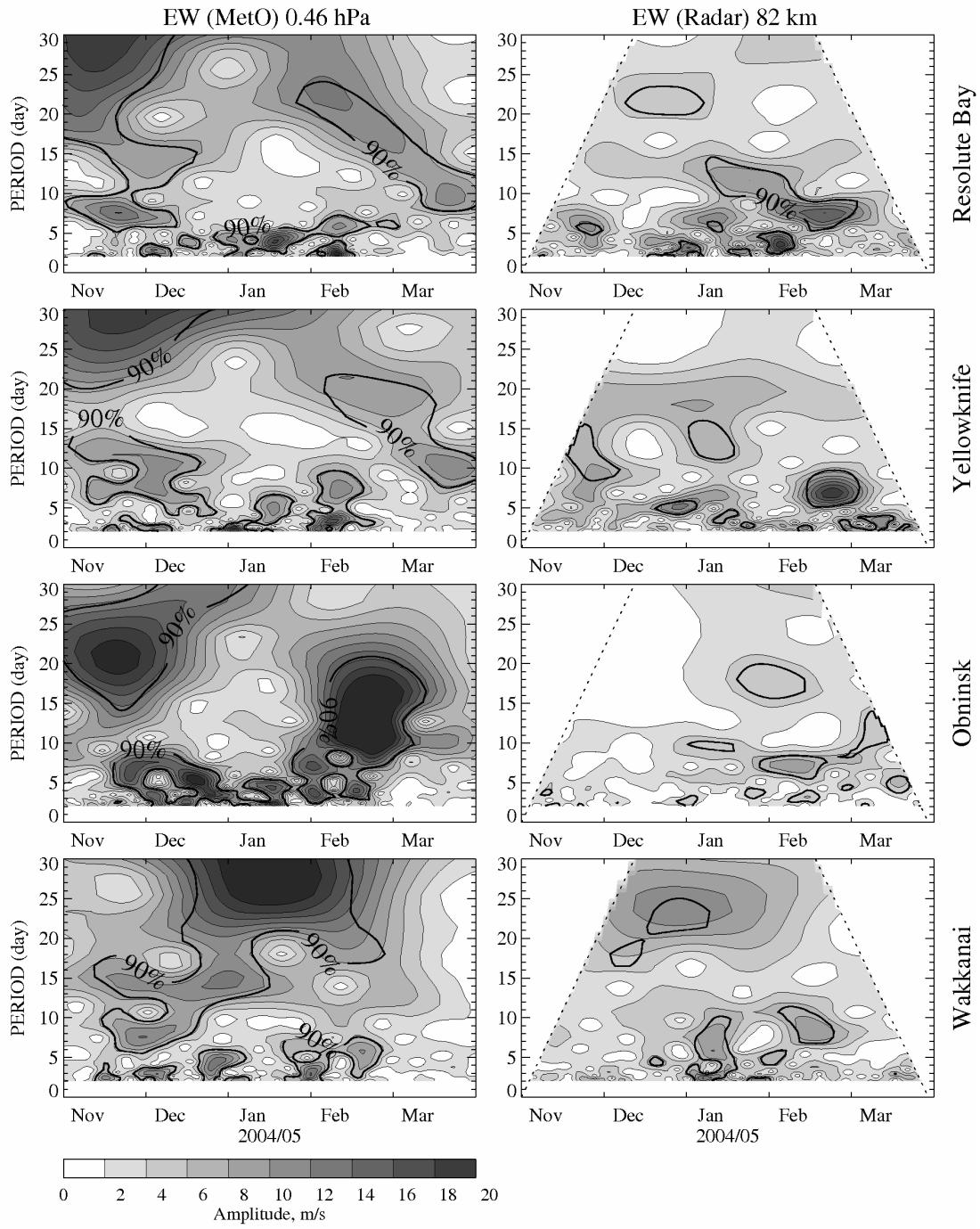

Figure 6.18 The same as Figure 6.16, but for the Resolute Bay, Yellowknife, Obninsk, and Wakkanai locations.

Wavelets at Poker Flat and Wakkanai, which have more westward (Pacific) longitudes, differ from those at other stations. Data in Figure 6.18 for mesospheric heights are not available at longer periods as these time sequences were just provided for a limited time interval. Another pair of relatively closely located stations, Resolute Bay and Yellowknife, has wavelets more similar at stratospheric heights than in the mesosphere. But even at 82 km they share some similar features like a strong peak near 7 days in February. Again the peak is weaker at the more poleward station (Resolute Bay).

In general, compared to previous years, the winter of 2004/05 is characterized by weak planetary wave activity at stratospheric and mesospheric heights. The variability of PW activity is clearly due to the longitudinal variability of the favorable eastward background flow: this is discussed in the paper by *Manson et al.* [2006], which demonstrated this variability in both model and terrestrial atmosphere.

6.5 **Application of the Q-diagnostic for atmospheric chemistry studies**

The vortex characterization is important not only for pure dynamical research, but also for the significant role it plays in atmospheric chemistry studies. Within the stratospheric winter polar vortex the temperatures are low and the air is highly isolated, especially at low and middle stratospheric levels. The ozone is mainly generated over the equatorial region, which is rich in solar radiation all year in contrast to the polar winter nights, and the ozone is carried toward the poles by the meridional circulation. The well-formed strong eastward vortex creates a barrier for PW propagation toward the pole, and, therefore, does not allow the penetration of ozone-rich tropical air to the high latitudes. At the same time the temperatures can be extremely cold ($\leq$185 K) within the vortex, and polar stratospheric clouds can form. Therefore inside the vortex the balance between sources and sinks of ozone may be broken. This leads to perfect conditions for the dramatic springtime depletion of ozone, the so-called “ozone hole”.

This is illustrated in Figure 6.19 and Figure 6.20, where the mixing ratios of ozone are shown as functions of latitude and pressure along 16^{o}E (Europe) and 253^{o}E (North America) longitudes for two days. The mixing ratio of ozone is one of the Aura spacecraft MLS products. The contours filled with black dots correspond to the areas of

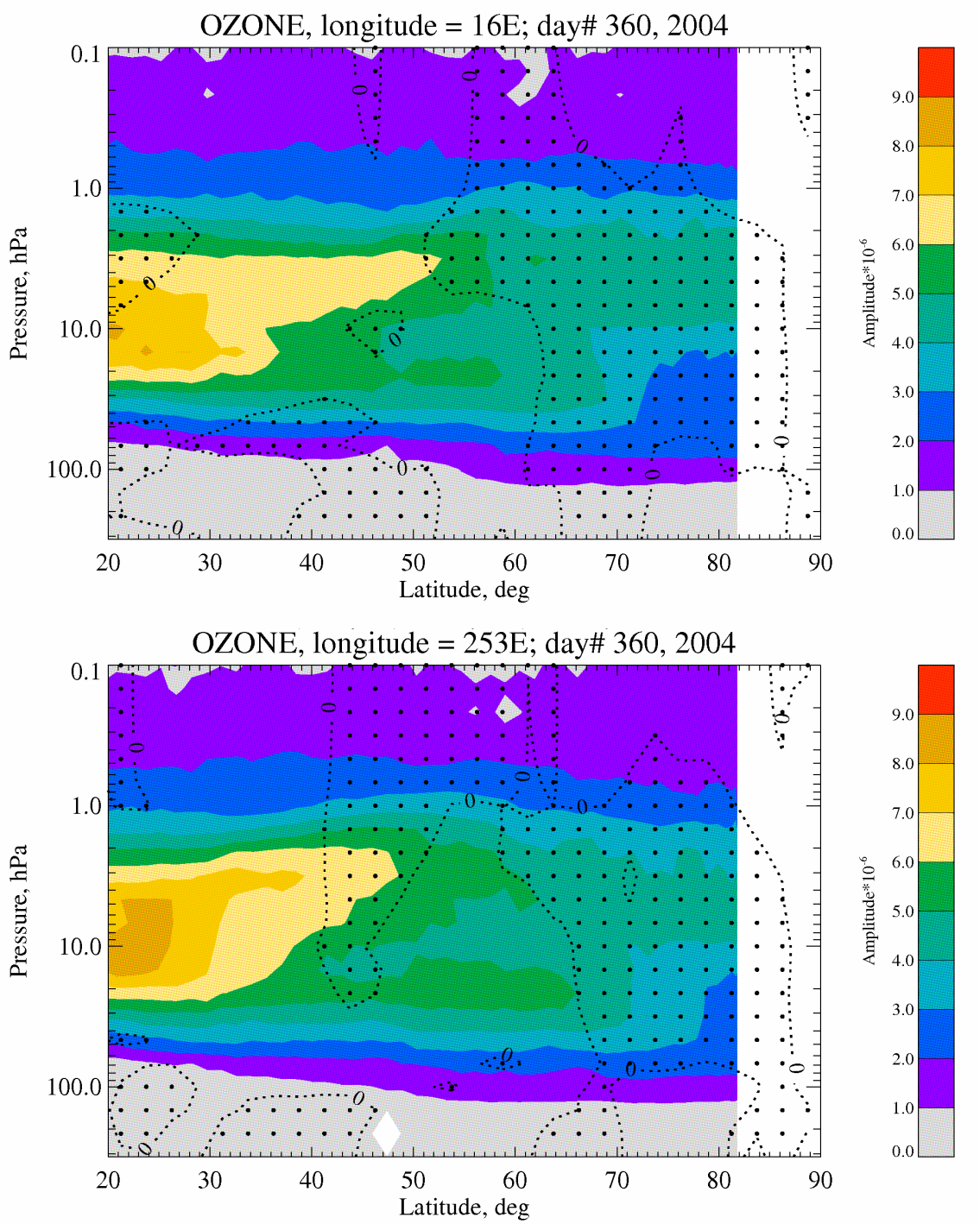

Figure 6.19 The height-latitude cross-section of the ozone mixing ratio cut along 16^{o}E (top) and 253^{o}E (bottom) longitudes for day number 360 (December 25) of 2004. The contours filled with dots indicate areas where Q is negative (rotation is dominate).

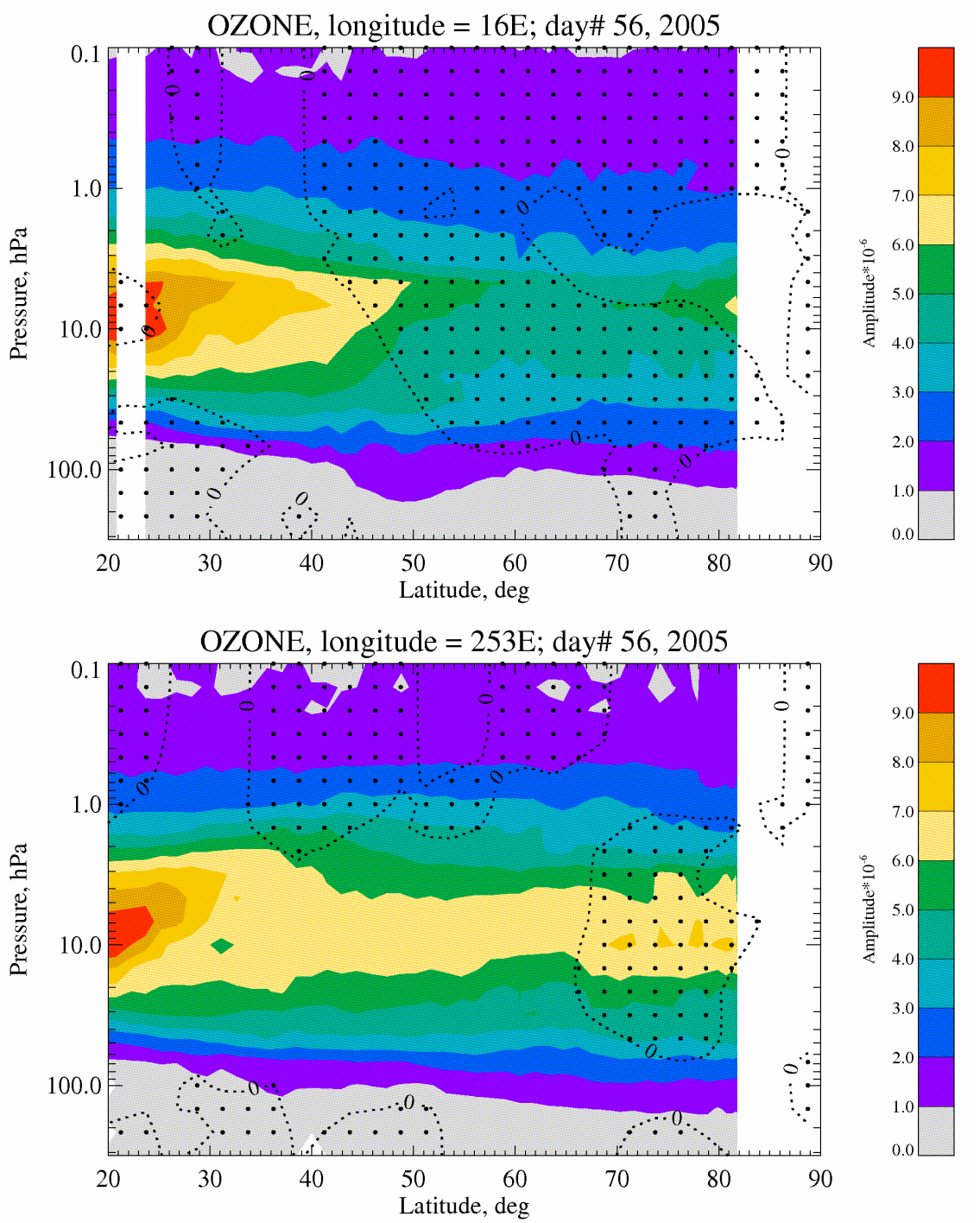

Figure 6.20 the same as Figure 6.19, but for day number 56 (February 25) of 2005

negative Q-diagnostic (the same as the dark grey color in Figure 6.9 and Figure 6.10 for December and February, respectively). On day 360, the 25th of December (2004), the day of an undisturbed stratosphere (Figure 6.19), the distribution of the ozone mixing ratio has a maximum over low latitudes and a minimum northward of 70^{o}N latitude between 100 and 10 hPa pressure levels (~16-32 km) along both longitudes. During February 25 of 2005 (day 56), when the strongest stratospheric disturbance for this winter season occurred, (Figure 6.20) the reduction of the ozone mixing ratio over the pole disappears, and the continuous band of yellow color is seen along all latitudes over North America. The differences in the distribution of the ozone mixing ratio over Europe and North America are consistent with the differences of the polar vortex conditions over these two longitudes: the part of the polar vortex over North America was weaker and practically destroyed, while the stronger part of the polar vortex dominated over Europe

6.6 **Summary**

The evolution of the polar vortex during the Arctic winter of 2004/05 has been studied using MetO assimilated fields and data from MWR and MFR (radars) at 12 mid- and high-latitude locations. The winter of 2004/05 was shown to be relatively cold with no major mid-winter stratospheric warmings. MetO parameters near 32 km averaged over 60^{o}N and 70^{o}N latitudinal circles exhibit neither rapid temperature increases of 25 or more degrees per week, nor corresponding reversals of the zonal winds. However there were 3 time intervals with increasing northern temperatures and corresponding weakening of the zonal winds: the end of December/beginning of January, the end of January/beginning of February, and the end of February. During the first two intervals the disturbances were relatively weak. The event at the end of February was the final and strongest disturbance for this winter, and marked the beginning of the wind transition toward summer-like circulation. These disturbances did not meet the required conditions for classical definition of SSW (p. 114), which may indicate the limitation of the SSW definition based on zonal mean values.

During all three disturbed time intervals the stratospheric stationary wave with zonal wave number 1 in MetO temperatures and geopotential heights had enhanced amplitudes. The amplitudes of the temperature-wave were the strongest during the last event near 50 km and, shortly after the beginning of the warming, the lines of constant phase coalesced near 32 km, i.e. there was a very rapid phase change with height. Oscillations (with periods of 10 and 15 days) associated with eastward and westward propagating PW were also present at upper stratospheric levels. The eastward propagating waves had maxima in the early winter and were confined to the areas with eastward wind flow, consistent with baroclinic waves. The amplitudes of the westward propagating waves (normal modes) increased by the end of winter (February) and were reaching Southern Hemispheric latitudes at upper stratospheric levels in March. Both eastward and westward amplitudes were ~1.5 times smaller than those calculated for the years 2000 and 2001 [*Chshyolkova et al.*, 2006].

To study the longitudinal variations of the polar vortex, the Q-diagnostic was used to characterize the dynamics of the middle and upper stratosphere. The results show that the polar vortex in the Northern Hemisphere formed in mid-autumn, and was fully established by December 1 of 2004. In December the polar vortex reached its strongest state: it was centered on the pole and occupied a relatively large area. During the three disturbed time intervals the vortex was elongated, slightly shifted off the pole, rotated westward with height, and had decreased areas in the lower stratosphere. The deformations were the largest for the last event, when the vortex was divided in two unequal parts below the ~600 K isentropic (~24 km) level.

The comparison of stratospheric data in the Scandinavian-European, North American sectors and Japan revealed significant longitudinal differences during disturbed as well as “quiet” times. In December, for example, the maximum of the eastward wind jet was located 10^{o} more poleward over Europe (at ~50^{o}N) than over North America (at ~40^{o}N). During the late February disturbance the largest differences in the lower and middle stratosphere were between stations located near 50^{o}N latitude: Saskatoon (253^{o}E) and Collm (13^{o}E). The part of the vortex over Europe was stronger and eastward winds continued to be observed at Collm. In contrast, over Canada winds were

westward, as the smaller part of the vortex was practically destroyed and the eastward jet was shifted upward and equatorward. The wavelet amplitudes for the stratospheric oscillations with periods from 2 to 30 days were also remarkably different between European and North American sectors. All stations demonstrated strong activity with periods longer than 20 days in November and an absence of oscillations with periods longer than ~5 days in the middle of winter. In February, though, wavelet analysis indicated lower PW activity at Saskatoon compared to Collm. These variations indicate the strong effect of longitudinal asymmetry in the polar vortex and background winds.

Strong latitudinal differences were also apparent in the zonal wind contour plots and wavelet amplitudes. The eastward winds were systematically weaker and amplitudes of the oscillations associated with PW were smaller at more poleward stations.

Compared to the stratospheric winds, the wavelets of the EW component indicated that the PW had smaller amplitudes and did not show many similarities between stations in the mesosphere. In general, compared to previous years, the winter of 2004/05 could be characterized by weak planetary wave activity at stratospheric and mesospheric heights.

The importance of the polar vortex characterization and a possible application of the Q-diagnostic for atmospheric chemistry studies were demonstrated. As an example the distributions of ozone mixing ratio were shown for “quiet” (December 25, 2004) and disturbed (February 25, 2005) stratospheric conditions. The results indicated that the strong eastward winds of the polar vortex prevent the penetration of ozone-rich tropical air to the high latitudes. Also, the comparison of the ozone distribution over North America and Europe revealed significant longitudinal variabilities consistent with the differences of the polar vortex conditions over these two regions.

Chapter 7

CONCLUSIONS

The Mesosphere/Lower Thermosphere (MLT), an atmospheric layer between 60 and 100 km, is not well understood. This can be attributed to the lack of observational data and to the complexity of the physical processes, which involve global circulations, wave-dynamics and radiative processes. Medium Frequency Radar (MFR) is one of a few techniques that provide data from the MLT on a daily basis. At Saskatoon continuous mesospheric wind measurements using MFR have been carried out since 1978, and a unique data set that allows the investigation of variabilities of differing time scales (from hours to decades) has been formed. The results of these investigations have been published by members of the Atmospheric Dynamics Group (Institute of Space and Atmospheric Studies, University of Saskatchewan) and recognized by the international atmospheric community.

In this research program we continue to study the mesospheric wind variabilities by focusing on the wave-like perturbations with periods from 2 to 30 days. These long-period oscillations, which are observed at mesospheric heights, are often associated with the westward propagating Rossby-gravity normal modes of a windless isothermal atmosphere (T~2, 5-7, 8-12, 12-20 days). These are generated in the troposphere and, under certain atmospheric conditions, may propagate to the mesospheric heights (Charney and Drazin, 1961; Salby, 1981; Forbes et al., 1995). The investigation of vertical coupling using MetO stratospheric assimilated fields, TOMS total ozone, and radar data has shown that only a few events involving such oscillations can be followed from the low stratospheric (~20 km) to the upper mesospheric (82 km) heights, in any one year [*Chshyolkova et al.,* 2005a; *Manson et al.,* 2005] (Chapter 3). The results of wave number analysis for all months have demonstrated that in the lower stratosphere eastward motions (baroclinic waves) dominate, while westward propagating waves

become comparable or even stronger in the upper stratosphere. During summer, PW activity is reduced considerably throughout the middle atmosphere.

The mean background wind plays an important role by filtering out waves that have upward components of propagation (see eq. 1.9). The waves will not propagate if their westward phase speeds are less than or equal to the westward mean wind speed. For example, during summer the middle atmospheric heights (30-90 km) are dominated by westward flow. The 16-day wave is a "slow" mode (westward speed of ~20 m/s) and, therefore, it is expected to be trapped in the strong (up to 60 m/s) summer westward jet. Indeed it was shown [*Luo et al.*, 2002a] that its propagation is prohibited in the 30-80 km region, but permitted above 80 km. In winter, however, eastward flow is generated due to negative poleward temperature gradients, and 16-day waves are able to propagate upward, into the MLT. The present research program included data sets obtained at several MFR and MWR locations, well spaced in latitude and longitude. These data have been used to investigate characteristics of the larger spectrum of PW (~5-30 days) and for heights from 20 to 100 km (Chapter 3).

The quasi 2-day wave (Q2DW) is a relatively fast mode (~50-60 m/s westward) and should be able to reach mesospheric heights in summer; while in winter its "critical speed" will usually be exceeded (eq. 1.9). First results of a Q2DW study based on a very large dataset (14 years of Saskatoon MFR data [*Chshyolkova et al.*, 2005b]) have confirmed that this oscillation occurs regularly and is actually a dominant feature of the summer mesosphere (Chapter 5). This is in agreement with previous findings for similar latitudinal locations, which mainly involved limited data sets (from a few months to a couple of years). It was also shown that relatively weak winter eastward flow (so that the expression in equation (1.9) does not provide values that exceed the critical speed) allows propagation of the Q2DW, which maximizes at low mesospheric heights. Access to upper stratospheric data with better (than a day) time resolution (which is not available to most researchers) is required to examine how and from where the Q2DW propagates.

As was mentioned above, not all mesospheric variability can be explained by direct PW propagation from below. Some perturbations can be attributed to inter-hemispheric

coupling that has been observed in addition to the stronger vertical coupling [*Chshyolkova et al.*, 2006]. The longer duration of winter conditions in either hemisphere provides equinoctial months when weak middle-atmospheric eastward winds dominate globally. The results obtained from spectral analyses have indicated that with favorable conditions PW with periods longer than 10 days can penetrate from the winter to the summer hemisphere (Chapter 4). This is the first time that such results have been shown. Occasional occurrence of the 16-day wave in the summer mesosphere can also be explained by the "ducting" mechanism (Luo et al., 2002b), i.e. the wave propagates to the mesosphere from below in regions where it is allowed (winter hemisphere) and then propagates above 80 km (to the summer hemisphere). There is also indication of the "leakage" of the Q2DW to the winter hemisphere (Section 5.1).

Collaborative studies that employ data from several stations allow for more organized assessments of regional and global variations in the dynamical characteristics of the MLT region. I was a co-author of two studies involving this approach. *Manson et al.* [2004a] presented annual climatologies of oscillations with periods from 8 hrs to 30 days across CUJO (Canada U.S. Japan Opportunity), an operational network of middle-latitude MFR, and showed that longitudinal variations in PW are significant and often larger than the variations with latitude. Despite some discrepancies, results from numerical models (GSWM and CMAM in [*Luo et al.*, 2002a] and [*Manson et al.*, 2006], respectively) also show seasonal and spatial intermittency of the PW. However, if the oscillations observed in the MLT are manifestations of the normal modes described in classical theory then the characteristics of these global waves should be coherent between different locations (substantial variations of PW with longitude were not expected). It has been suggested that local effects on the atmospheric response to PW are considerable, and that, therefore, asymmetry of the background winds (varying speeds and directions around latitude circles) of the middle atmosphere must be considered.

The longitudinal and latitudinal variabilities of the PW have been investigated using MetO and mesospheric wind data obtained from 12 MFR and MWR during the Arctic winter of 2004/05 (Chapter 6). The Q-diagnostic has been employed to characterize the

dynamics of the middle and upper mesosphere. The results obtained indicate that analyses of wind fields in the middle atmosphere should not assume that PW oscillations exhibit similar amplitude variabilities at all longitudes, i.e. that zonal wave number analysis of global data (model or satellite) may be problematic. This variation of PW would be expected when the polar vortex is not centered on the pole and/or is elongated (not circular in shape). Thus this study expands and validates earlier studies [*Luo et al.,* 2002b; *Manson et al.,* 2004a; *Manson et al.,* 2006] on winter time PW characteristics. The existence of hemispheric asymmetry, which results from both of these characteristics, has led to the extreme variability in longitudinal dynamical characteristics shown in this study for 2004/05.

For characterization of winter polar vortices a software package that includes the calculation and plotting of the Q-diagnostic along with potential vorticity (PV), streamfunction and wind fields for characterization of the cyclonic and anticyclonic vortices of winter (and other seasons) has been created. The development of this software package was a major task within the program of research, and required approximately 6 months to complete. There are relatively few groups that have developed packages of such a comprehensive and self-consistent nature, but it was determined that the effort and investment of time was appropriate for the program of studies and also for my future career.

The results presented in this thesis have been reported at several international conferences, and six papers, three of which feature myself as the leading author, have been published in different refereed journals. Another paper based on the findings of Chapter 6 is in the process of submission (February 5, 2007). The studies conducted for this research program have produced the following new contributions to the knowledge of the physics of the middle atmosphere:

- Extensive use of the MetO stratospheric data along with the mesospheric wind measurements at multiple locations has allowed investigation of the coupling processes throughout the middle atmosphere (20-90 km) and assessments of local as well as global dynamical characteristics of this region. Earlier studies

generally included fewer locations and used different parameters from separated heights for intercomparison (Chapter 3, 4 and 6).

- For the first time MetO assimilated wind fields and MFR wind measurements (60 km and above) have been compared at several locations (Sections 2.3 and 6.4). Generally good agreements have been found.

- Thermal winds (50-80 km) based upon Aura temperatures have been shown, for the first time, to be in good agreement with direct radar measurements. Although these actual winds are not geostrophic, the differences are small enough to encourage the use of thermal winds when radar (direct) winds are unavailable.

- The temporal and spectral comparisons between total ozone (TOMS) and MetO parameters has demonstrated that the total ozone and MetO temperatures at low stratospheric heights have high (positive) values of correlation and similar spectral content. Although this result is not new (it existed in the "ozone" community), the correlation analysis using the MetO assimilated products has not been published before.

- Unique climatology of the Q2DW using 14 years of MFR measurements at Saskatoon has been constructed. The temporal and altitudinal (winter and summer) morphologies provide a valuable product for Q2DW studies (Dr Salby, Private Communication 2005)

- The Q-diagnostic has been employed for the first time to compare polar vortex variations (longitude, latitude, time) as characterized up to ~64 km using MetO with winds from radars (~80 km). The vortex has been shown to exist coherently up to 80 km during undisturbed intervals of the 2004/05 winter (December, January, and February). During stratospheric warmings, strong thermal wind gradients (vertical and horizontal) lead to significant changes of direction (~180^{o}) for zonal and meridional winds. More MLT wind data (50 km and above), from additional radars or satellite missions, will lead to a better understanding of this region (60-100 km).

As a post doctoral fellow I will be involved in investigations of the polar vortex and related studies of vertical coupling over Eureka. Characteristics of the stratospheric and mesospheric variabilities over a broad range of periods (hours-days) near the North Pole will be involved. The knowledge of the shape, position and evolution of the polar vortex is essential for the interpretation of the chemical and dynamical measurements conducted there. Thus, the so-called "USask Vortex Characterization Software Package" will be used for chemical and dynamical research at CANDAC-PEARL for the winters of 2005/06, 2006/07 and beyond. This includes the International Polar Year (IPY, March 2007-2009). Comparisons between new data assimilated products (using Canadian CMAM-FDAM model) and vortex characteristics obtained from the MetO assimilated fields will also be very important. Collaborations with other researchers using high-latitude systems (Svalbard, Yellowknife, Resolute Bay, and Antarctica) will allow enriched hemispheric and global studies to be initiated. Investigation of the relationships between the well characterized polar vortex and tropospheric circulation (Canadian Arctic and hemisphere) will provide further insights into the possible downward influence of stratospheric disturbances upon the troposphere, and, hence, long-term weather prediction.

LIST OF REFERENCES

Altadill, D. and E. M. Apostolov (2003), Time and scale size of planetary wave signatures in the ionospheric F region: Role of the geomagnetic activity and mesosphere/lower thermosphere winds, *J. Geophys. Res.*, *108*(A11), SIA 4-1-DOI 10.1029/2003JA010015.

Andrews, D. G., F. W. Taylor and M. E. McIntyre (1987a), The Influence of Atmospheric Waves on the General-Circulation of the Middle Atmosphere, *Philosophical Transactions of the Royal Society of London Series A-Mathematical Physical and Engineering Sciences*, *323*(1575), 693-705.

Andrews D. G., D. G. Holton and C. B. Leovy (1987b), Middle Atmosphere Dynamics, 489 pp., Academic Press.

Aso, T., T. Tsuda, Y. Takashima, R. Ito and S. Kato (1980), Observations of lower ionospheric wind by the Kyoto meteor radar, *J. Geophys. Res.*, *85*, 177-184.

Babiano, A., G. Boffetta, A. Provenzale and A. Vulpiani (1994), Chaotic advection in point vortex models and two-dimensional turbulence, *Phys. Fluids*, *6*(7), 2465-2474.

Baldwin, M. P. and J. R. Holton (1988), Climatology of the Stratospheric Polar Vortex and Planetary Wave Breaking, *J. Atmos. Sci.*, *45*(7), 1123-1142.

Baldwin, M., T. Hirooka, A. O'Neill and S. Yoden (2003), Major stratospheric warming in the Southern Hemisphere in 2002: Dynamical aspects of the ozone hole split, *SPARC Newsletter*, *20*, 24–26.

Becker, E., A. Müllemann, F. J. Lübken, H. Körnich, P. Hoffmann and M. Rapp (2004), High Rossby-wave activity in austral winter 2002: Modulation of the general

circulation of the MLT during the MaCWAVE/MIDAS northern summer program, *Geophys. Res. Lett., 31*(24), L24S03.

Bhattacharya, Y., G. G. Shepherd and S. Brown (2004), Variability of atmospheric winds and waves in the Arctic polar mesosphere during a stratospheric sudden warming, *Geophys. Res. Lett., 31*, L23101-doi:10.1029/2004GL020389.

Brachet, M. E., M. Meneguzzi, H. Politano and P. L. Sulem (1988), The dynamics of freely decaying two-dimensional turbulence, *J. Fluid Mech., 194*, 333-349.

Briggs, B. H. (1984), The analysis of spaced sensor records by correlation techniques, *In International Council of Scientific Unions Middle Atmosphere Program, 13*, 166-186.

Burks, D. and C. Leovy (1986), Planetary waves near the mesospheric easterly jet, *Geophys. Res. Lett., 13*, 193-196.

Carter, D. A. and B. B. Balsley (1982), The Summer Wind Field Between 80 and 93 km Observed by the MST Radar at Poker Flat, Alaska (65°N), *J. Atmos. Sci., 39*(12), 2905-2915.

Cervera, M. A. and I. M. Reid (1995), Comparison of simultaneous wind measurements using colocated VHF meteor radar and MF spaced antenna radar systems, *Radio Sci., 30*(4), 1245-1262.

Charney, J. G. and P. G. Drazin (1961), Propagation of planetary-scale disturbances from the lower into the upper atmosphere, *J. Geophys. Res., 66*, 83-109.

Cho, Y. M., G. G. Shepherd, Y. I. Won, S. Sargoytchev, S. Brown and B. Solheim (2004), MLT cooling during stratospheric warming events, *Geophys. Res. Lett., 31*(10), L10104-doi:10.1029/2004GL019552.

Chshyolkova, T., A. H. Manson, C. E. Meek, S. K. Avery, D. Thorsen, J. W. MacDougall, W. Hocking, Y. Murayama and K. Igarashi (2005a), Planetary wave coupling in the middle atmosphere (20-90 km) : A CUJO study involving TOMS, MetO and MF radar data, *Ann. Geophysicae, 23*(4), 1103-1121.

Chshyolkova, T., A. H. Manson and C. E. Meek (2005b), Climatology of the quasi two-day wave over Saskatoon (52°N, 107°W): 14 Years of MF radar observations, *Adv. Space Res., 35*(11), 2011-2016.

Chshyolkova, T., A. H. Manson, C. E. Meek, S. K. Avery, D. Thorsen, J. W. MacDougall, W. Hocking, Y. Murayama and K. Igarashi (2006), Planetary wave coupling processes in the middle atmosphere (30-90 km): A study involving MetO and MFR data, *J. Atmos. Solar Terr. Phys., 68*(3-5), 353-368.

Clark, R. R. (1975), Meteor Wind Measurements at Durham, New Hampshire (43°N, 71°W), *J. Atmos. Sci., 32*(9), 1689-1693.

Clark, R. R. (1989), The quasi 2-day wave at Durham (43°N): Solar and magnetic effects. *J. Atmos. Terr. Phys., 51*(7), 617-622.

Clark, R. R., A. C. Current, A. H. Manson, C. E. Meek, S. K. Avery, S. E. Palo and T. Aso (1994), Global properties of the 2-day wave from mesosphere-lower thermosphere radar observations, *J. Atmos. Terr. Phys., 43*, 1279-1288.

Coy, L. (1979), A Possible 2-Day Oscillation near the Tropical Stratopause1, *J. Atmos. Sci., 36*(8), 1615-1618.

Craig, R. L., R. A. Vincent, G. J. Fraser and M. J. Smith (1980), The quasi 2-day wave in the Southern Hemisphere mesosphere, *Nature, 287*(5780), 319-320.

Craig, R. L. and W. G. Elford (1981), Observations of the quasi 2-day wave near 90 km altitude at Adelaide (35°S), *J. Atmos. Terr. Phys., 43*, 1051-1056.

Craig, R. L., R. A. Vincent, S. P. Kingsley and H. G. Muller (1983), Simultaneous observations of the quasi 2-day wave in the northern and southern hemispheres, *J. Atmos. Terr. Phys., 45*, 539-541.

Dickinson, R. E. (1968), Planetary Rossby Waves Propagating Vertically Through Weak Westerly Wind Wave Guides, *J. Atmos. Sci., 25*(6), 984-1002.

Dikii, L. A. (1965), The terrestrial atmosphere as an oscillating system, *Izv. Acad. Sci. USSR Atmos. Ocean Phys., Engl. Transl., 1*(5), 275-286.

Dowdy, A. J., R. A. Vincent, D. J. Murphy, M. Tsutsumi, D. M. Riggin and M. J. Jarvis (2004), The large-scale dynamics of the mesosphere-lower thermosphere during the Southern Hemisphere stratospheric warming of 2002, *Geophys. Res. Lett., 31*(14), L14102-doi:10.1029/2004GL020282.

Elhmaidi, D., A. Provenzale and A. Babiano (1993), Elementary topology of two-dimensional turbulence, *J. Fluid Mech., 257*, 533-558.

Fairlie, T. D. A. (1995), Three-dimensional transport simulations of the dispersal of volcanic aerosol from Mount Pinatubo, *Q. J. R. Meteor. Soc., 121*(528), 1943-1980.

Fairlie, T. D., R. B. Pierce, J. A. Al-Saadi, W. L. Grose, J. M. Russell III, M. H. Proffitt and C. R. Webster (1999), The contribution of mixing in Lagrangian photochemical predictions of polar ozone loss over the Arctic in summer 1997, *J. Geophys. Res., 104*(D21), 26597-26610.

Fedulina, I. N., A. I. Pogoreltsev and G. Vaughan (2004), Seasonal, interannual and short-term variability of planetary waves in Met Office stratospheric assimilated fields, *Q. J. R. Meteorol. Soc., 130*(602), 2445-2458.

Forbes, J. M. (1995), Tidal and planetary waves, *The Upper Mesosphere and Lower Thermosphere: A Review of Experiment and Theory, Geophysical Monograph 87*, 67-87.

Fraser, G. J. (1965), The Measurement of Atmospheric Winds at Altitudes of 64–120 km Using Ground-Based Radio Equipment, *J. Atmos. Sci., 22*(2), 217-218.

Fritts, D. C. and J. R. Isler (1994), Mean Motions and Tidal and Two-Day Structure and Variability in the Mesosphere and Lower Thermosphere over Hawaii, *J. Atmos. Sci., 51*(14), 2145-2164.

Fritts, D. C., J. R. Isler, R. S. Lieberman, M. D. Burrage, D. R. Marsh, T. Nakamura, T. Tsuda, R. A. Vincent and I. M. Reid (1999), Two-day wave structure and mean

flow interactions observed by radar and High Resolution Doppler Imager, *J. Geophys. Res., 104*(D4), 3953-3970.

Froidevaux, L., N. J. Livesey, W. G. Read, Y. B. Jiang, C. C. Jimenez, M. J. Filipiak, M. J. Schwartz, M. L. Santee, H. C. Pumphrey and J. H. Jiang (2006), Early validation analyses of atmospheric profiles from EOS MLS on the Aura satellite, *IEEE Trans. Geosci. Remote Sens., 44*(5), 1106-1121.

Garcia, R. R., R. Lieberman, J. M. Russell III and M. G. Mlynczak (2005), Large-Scale Waves in the Mesosphere and Lower Thermosphere Observed by SABER. *J. Atmos. Sci., 62*(12), 4384-4399.

Glass, M., J. L. Fellous, M. Massebeuf, A. Spizzichino, I. A. Lysenko and I. I. Portniagin (1975), Comparison and interpretation of the results of simultaneous wind measurements in the lower thermosphere at Garchy /France/ and Obninsk /USSR/ by meteor radar technique, *J. Atmos. Terr. Phys., 37*, 1077-1087.

Gregory, J. B. and A. H. Manson (1975), Winds and wave motions to 110 km at mid-latitudes. III Response of mesospheric and thermospheric winds to major stratospheric warmings, *J. Atmos. Sci., 32*(9), 1676-1681.

Greisiger, K. M., Y. I. Portnyagin and I. A. Lyssenko (1984), Large-scale winter-time disturbances in meteor winds over Central and Eastern Europe and their connection with processes in the stratosphere, *J. Atm. Terr. Phys., 46*(4), 389-394.

Gurubaran, S., S. Sridharan, T. K. Ramkumar and R. Rajaram (2001), The mesospheric quasi-2-day wave over Tirunelveli (8.7^{o}N), *J. Atmos. Solar Terr. Phys., 63*(10), 975-985.

Hagan, M. E., J. M. Forbes and F. Vial (1993), Numerical investigation of the propagation of the quasi-two-day wave into the lower thermosphere, *J. Geophys. Res., 98*(D12), 23,193-23,205.

Hall, C. (2001), The Ramfjordmoen MF radar (69^{o}N, 19^{o}E): application development 1990-2000, *J. Atm. Sol-Terr. Phys., 63*(2-3), 171-179.

Hall, C. M., T. Aso, A. H. Manson, C. E. Meek, S. Nozawa and M. Tsutsumi (2003), High-latitude mesospheric mean winds: A comparison between Tromsø (69^{o}N) and Svalbard (78 N), *J. Geophys. Res., 108*(D19), 4598-doi:10.1029/2003JD003509.

Hall, C. M., T. Aso, M. Tsutsumi, S. Nozawa, A. Manson and C. E. Meek (2005), A comparison of mesosphere and lower thermosphere neutral winds as determined by meteor and medium-frequency radar at 70°N, *Radio Sci., 40*(4), RS4001-doi:10.1029/2004RS003102.

Harris, T. J. and R. A. Vincent (1993), The quasi-two-day wave observed in the equatorial middle atmosphere, *J. Geophys. Res., 98*(D6), 10,481-10,490.

Harvey, V. L., R. B. Pierce, T. D. Fairlie and M. H. Hitchman (2002), A climatology of stratospheric polar vortices and anticyclones, *J. Geophys. Res., 107*(D20), 4442-doi:10.1029/2001JD001471.

Haynes P. H. (1990), High-resolution three-dimansional modelling of stratospheric flows: Quasi-two dimensional turbulence dominated by a single vortex, in *Topological Fluid Mechanics: Proceedings of the IUTAM Symposium, Cambridge, UK, 13-18 August, 1989,* edited by H. K. Moffatt et al., pp. 345-354, Cambridge University Press.

Hocking, W. K., B. Fuller and B. Vandepeer (2001), Real-time determination of meteor-related parameters utilizing modern digital technology, *Journal of Atmospheric and Solar-Terrestrial Physics, 63*(2-3), 155-169.

Hocking, W. K. (2004), Experimental Radar Studies of Anisotropic Diffusion of High Altitude Meteor Trails, *Earth, Moon, and Planets, 95*(1), 671-679.

Hoffmann, P., W. Singer and D. Keuer (2002), Variability of the mesospheric wind field at middle and Arctic latitudes in winter and its relation to stratospheric circulation disturbances, *J. Atm. Sol-Terr. Phys., 64*(8-11), 1229-1240.

Holton J. (1972), An introduction to dynamic meteorology, 320 pp., Academic Press.

Holton, J. R. (1983), The Influence of Gravity-Wave Breaking on the General-Circulation of the Middle Atmosphere, *J. Atmos. Sci.*, *40*(10), 2497-2507.

Hood, L. L., J. P. McCormack and K. Labitzke (1997), An investigation of dynamical contributions to midlatitude ozone trends in winter, *J. Geophys. Res.*, *102*(D11), 13079-13094.

Ito, R., T. Tsuda, T. Aso and S. Kato (1984), Long period oscillations in the meteor winds observed over Kyoto during 1978±1983, *J. Geomagn. Geoelectr.*, *36*, 173-188.

Jacobi, C., R. Schminder and D. Kurschner (1997a), The quasi 2-day wave as seen from D1 LF wind measurements over Central Europe (52^{o}N, 15^{o}E) at Collm, *J. Atmos. Solar Terr. Phys.*, *59*(11), 1277-1286.

Jacobi, C., R. Schminder and D. Kürschner (1997b), The winter mesopause wind field over Central Europe and its response to stratospheric warmings as measured by LF D1 wind measurements at Collm, Germany, *Adv. Space Res.*, *20*(6), 1223-1226.

Jacobi, C., R. Schminder and D. Kurschner (1998), Non-linear interaction of the quasi 2-day wave and long-term oscillations in the summer midlatitude mesopause region as seen from LF D1 wind measurements over Central Europe (Collm, 52^{o}N, 15^{o}E), *J. Atmos. Solar Terr. Phys.*, *60*(12), 1175-1175.

Jacobi, C., Y. I. Portnyagin, E. G. Merzlyakov, B. L. Kashcheyev, A. N. Oleynikov, D. Kurschner, N. J. Mitchell, H. R. Middleton, H. G. Muller and V. E. Comley (2001), Mesosphere/lower thermosphere wind measurements over Europe in summer 1998, *J. Atmos. Solar Terr. Phys.*, *63*(10), 1017-1031.

Jacobi, C., D. Kurschner, H. G. Muller, D. Pancheva, N. J. Mitchell and B. Naujokat (2003), Response of the mesopause region dynamics to the February 2001 stratospheric warming, *J.Atmos.Solar Terr.Phys.*, *65*(7), 843-855.

Jacobi, C., D. Kürschner, K. Fröhlich, K. Arnold and G. Tetzlaff (2005), Meteor radar wind and temperature measurements over Collm (51.3^{o}N, 13^{o}E) and comparison

with co-located LF drift measurements during autumn 2004, *Rep. Inst. Meteorol. Univ. Leipzig, 36*, 98-112.

Jacobi, C., K. Fröhlich and A. Pogoreltsev (2006), Quasi two-day-wave modulation of gravity wave flux and consequences for the planetary wave propagation in a simple circulation model, *J. Atmos. Solar Terr. Phys., 68*(3-5), 283-292.

Jiménez, C., H. C. Pumphrey, I. A. MacKenzie, G. L. Manney, M. L. Santee, M. J. Schwartz, R. S. Harwood and J. W. Waters (2006), EOS MLS observations of dehydration in the 2004-2005 polar winters, *Geophys. Res. Lett., 33*(16), L16806-doi:10.1029/2006GL025926.

Kal'chenko, B. V. and S. V. Bulgakov (1973), Study of periodic components of wind velocity in the lower thermosphere above the equator, *Geomag. Aeronomy, 13*, 1125-1126.

Karpetchko, A., E. Kyro and B. M. Knudsen (2005), Arctic and Antarctic polar vortices 1957-2002 as seen from the ERA-40 reanalyses, *J. Geophys. Res., 110*(D21), D21109-doi:10.1029/2005JD006113.

Kingsley, S. P., H. G. Muller, L. Nelson and A. Scholefield (1978), Meteor winds over Sheffield (53N, 2W), *J. Atmos. Terr. Phys., 40*, 917-922.

Kumar, P. and E. Foufoula-Georgiou (1997), Wavelet analysis for geophysical applications, *Rev. Geophys., 35*(4), 385-412.

Labitzke, K. (1972), Temperature changes in the mesosphere and stratosphere connected with circulation changes in winter, *J. Atmos. Sci., 29*(4), 756-766.

Lastovicka, J. (1997), Observations of tides and planetary waves in the atmosphere-ionosphere system, *Adv. Space Res., 20*(6), 1209-1222.

Lawrence, B. N. and W. J. Randel (1996), Variability in the mesosphere observed by the Nimbus 6 pressure modulator radiometer, *J. Geophys. Res., 101*(D18), 23475-23490.

Lawrence, A. R. and M. J. Jarvis (2003), Simultaneous observations of planetary waves from 30 to 220 km, *J. Atmos. Solar Terr. Phys.*, *65*(6), 765-777.

Lieberman, R. S. (1999), Eliassen–Palm Fluxes of the 2-Day Wave, *J. Atmos. Sci.*, *56*(16), 2846-2861.

Lieberman, R. S., D. M. Riggin, S. J. Franke, A. H. Manson, C. Meek, T. Nakamura, T. Tsuda, R. A. Vincent and I. Reid (2003), The 6.5-day wave in the mesosphere and lower thermosphere: Evidence for baroclinic/barotropic instability, *J. Geophys. Res.*, *108*(D20), 4640.

Lima, L. M., P. P. Batista, H. Takahashi and B. R. Clemesha (2004), Quasi-two-day wave observed by meteor radar at 22.7^{o}S, *J. Atmos. Solar Terr. Phys.*, *66*(6-9), 529-537.

Limpasuvan, V. and C. B. Leovy (1995), Observation of the two-day wave near the southern summer stratopause, *Geophys. Res. Lett.*, *22*, 2385-2388.

Limpasuvan, V. and D. L. Wu (2003), Two-day wave observations of UARS Microwave Limb Sounder mesospheric water vapor and temperature, *J. Geophys. Res.*, *108*(D10), 4307-doi:10.1029/2002JD002903.

Limpasuvan, V., D. L. Wu, M. J. Schwartz, J. W. Waters, Q. Wu and T. L. Killeen (2005), The two-day wave in EOS MLS temperature and wind measurements during 2004-2005 winter, *Geophys. Res. Lett.*, *32*, L17809-doi:10.1029/2005GL023396.

Lindzen, R. S. (1981), Turbulence and stress owing to gravity wave and tidal breakdown, *J. Geophys. Res.*, *86*, 9707-9714.

Liu, H. L. and R. G. Roble (2002), A study of a self-generated stratospheric sudden warming and its mesospheric-lower thermospheric impacts using the coupled TIME-GCM/CCM3, *J. Geophys. Res.*, *107*(D23), 4695.

Liu, H. L. and R. G. Roble (2004), Dynamical processes related to the atomic oxygen equinox transition, *J. Atmos. Solar Terr. Phys.*, *66*(6-9), 769-779.

Liu, P. C. (1994), Wavelet Spectrum Analysis and Ocean Wind Waves, *Wavelets in Geophysics. Ed. E. Foufoula-Georgiou and P. Kumar. Academic Press, New York*, 151-166.

Longuet-Higgins, M. S. (1968), The Eigenfunctions of Laplace's Tidal Equations over a Sphere, *Phil. Trans. Roy. Soc. London, A262*(1132), 511-607.

Lorenc, A. C., R. S. Bell and B. MacPherson (1991), The Meteorological Office analysis correction data assimilation scheme, *Q. J. R. Meteorol. Soc., 117*(497), 59-89.

Lorenc, A. C., S.P. Ballard, R.S. Bell, N.B. Ingleby, P.L.F. Andrews, D.M. Barker, J.R. Bray, A.M. Clayton, T. Dalby, D. Li, T.J. Payne and F.W. Saunders (2000), The Met. Office global three-dimensional variational data assimilation scheme, *Q. J. R. Meteorol. Soc., 126*(570), 2991-3012.

Luo, Y., A. H. Manson, C. E. Meek, T. Thayaparan, J. MacDougall and W. K. Hocking (2002a), The 16-day wave in the mesosphere and lower thermosphere: simultaneous observations at Saskatoon (52^{o}N, 107^{o}W) and London (43^{o}N, 81^{o}W), Canada, *J. Atmos. Solar Terr. Phys., 64*(8-11), 1287-1307.

Luo, Y., A. H. Manson, C. E. Meek, C. K. Meyer, M. D. Burrage, D. C. Fritts, C. M. Hall, W. K. Hocking, J. MacDougall, D. M. Riggin and R. A. Vincent (2002b), The 16-day planetary waves: multi-MF radar observations from the arctic to equator and comparisons with the HRDI measurements and the GSWM modelling results, *Ann. Geophysicae, 20*(5), 691-709.

Lysenko, I. A., Y. I. Portnyagin, A. N. Fakhrutdinova, R. A. Ishmuratov, A. H. Manson and C. E. Meek (1994), Wind regime at 80-110 km at mid-latitudes of the northern hemisphere, *J. Atmos. Terr. Phys., 56*(1), 31-42.

Malvern L. E. (1969), Introduction to the mechanics of a continuous medium, 713 pp., Prentice-Hall, Englewood Cliffs, NJ.

Manney, G. L., R. W. Zurek, A. O'Neill, R. Swinbank , J. B. Kumer, J. L. MEergenthaler and A. E. Roche (1994), Stratospheric Warmings during February and March 1993, *Geophys. Res. Lett., 21*(9), 813-816.

Manney, G. L., M. L. Santee, L. Froidevaux, K. Hoppel, N. J. Livesey and J. W. Waters (2006), EOS MLS observations of ozone loss in the 2004–2005 Arctic winter, *Geophys. Res. Lett, 33*(4), L04802-10.1029/2005GL024494.

Manson, A. H., J. B. Gregory and D. G. Stephenson (1973), Winds and wave motions/70-100 km/ as measured by a partial reflection radiowave system, *J. Atmos. Terr. Phys., 35*, 2055-2067.

Manson, A. H., J. B. Gregory, C. E. Meek and D. G. Stephenson (1978), Winds and Wave Motions to 110 km at Mid-Latitudes. V. An Analysis of Data from September 1974–April 1975, *J. Atmos. Sci., 35*(4), 592-599.

Manson, A. H., C. E. Meek, J. B. Gregory and D. K. Chakrabarty (1982), Fluctuations in tidal (24-, 12-h) characteristics and oscillations (8-h-5-d) in the mesosphere and lower thermosphere (70-110 km): Saskatoon (52^{o}N, 107^{o}W), 1979-1981, *Planet. Space Sci., 30*(12), 1283-1294.

Manson, A. H., C. E. Meek, J. L. Fellous and M. Massebeuf (1987), Winds oscillations(~ 6 h-6 days) in the upper middle atmosphere at Monpazier (France, 45°N, 1°E) and Saskatoon (Canada, 52°N, 107°W) in 1979-1980, *J. Atmos. Terr. Phys., 49*(11-12), 1059-1069.

Manson, A. H., C. E. Meek, E. Fleming, S. Chandra, R. A. Vincent, A. Phillips, S. K. Avery, G. J. Fraser, M. J. Smith and J. L. Fellous (1991), Comparisons between Satellite-derived Gradient Winds and Radar-derived Winds from the CIRA-86, *J. Atmos. Sci., 48*(3), 411-428.

Manson, A. H., C. E. Meek, A. Brekke and J. Moen (1992), Mesosphere and lower thermosphere (80-120 km) winds and tides from near Tromso (70^{o}N, 19^{o}E)-Comparisons between radars (MF, Eiscat, VHF) and rockets, *J. Atmos. Terr. Phys., 54*(7-8), 927-950.

Manson, A., F. Yi, G. Hall and C. Meek (1996), Comparisons between instantaneous wind measurements made at Saskatoon (52N, 107W) using the colocated medium frequency radars and Fabry-Perot interferometer instruments: Climatologies (1988-1992) and case studies, *J. Geophys. Res., 101*(D23), 29553-29564.

Manson, A. H., C. E. Meek, J. Stegman, P. J. Espy, R. G. Roble, C. M. Hall, P. Hoffmann and C. Jacobi (2002a), Springtime transitions in mesopause airglow and dynamics: photometer and MF radar observations in the Scandinavian and Canadian sectors, *J. Atmos. Solar-Terr. Phys., 64*(8-11), 1131-1146.

Manson, A. H., C. Meek, M. Hagan, J. Koshyk, S. Franke, D. Fritts, C. Hall, W. Hocking, K. Igarashi and J. MacDougall (2002b), Seasonal variations of the semi-diurnal and diurnal tides in the MLT: multi-year MF radar observations from 2^{o}-70^{o}N, modelled tides (GSWM, CMAM), *Ann. Geophysicae, 20*(5), 661-677.

Manson, A. H., C. E. Meek, S. K. Avery and D. Thorsen (2003), Ionospheric and dynamical characteristics of the mesosphere-lower thermosphere region over Platteville (40^{o}N, 105^{o}W) and comparisons with the region over Saskatoon (52^{o}N, 107^{o}W), *J. Geophys. Res., 108*(D13), 4398.

Manson, A. H., C. E. Meek, T. Chshyolkova, S. K. Avery, D. Thorsen, J. W. MacDougall, W. Hocking, Y. Murayama, K. Igarashi, S. P. Namboothiri and P. Kishore (2004a), Longitudinal and latitudinal variations in dynamic characteristics of the MLT (70-95 km): a study involving the CUJO network, *Ann. Geophysicae, 22*(2), 347-365.

Manson, A. H., C. E. Meek, C. M. Hall, S. Nozawa, N. J. Mitchell, D. Pancheva, W. Singer and P. Hoffmann (2004b), Mesopause dynamics from the scandinavian triangle of radars within the PSMOS-DATAR Project, *Ann. Geophysicae, 22*(2), 367-386.

Manson, A. H., C. E. Meek, T. Chshyolkova, S. K. Avery, D. Thorsen, J. W. MacDougall, W. Hocking, Y. Murayama and K. Igarashi (2005), Wave activity (planetary, tidal) throughout the middle atmosphere (20-100km) over the CUJO

network: Satellite (TOMS) and Medium Frequency (MF) radar observations, *Ann. Geophysicae*, *23*(2), 305-323.

Manson, A. H., C. E. Meek, T. Chshyolkova, C. McLandress, S. K. Avery, D. C. Fritts, C. M. Hall, W. K. Hocking, K. Igarashi, J. W. MacDougall, Y. Murayama, D. C. Riggin, D. Thorsen and R. A. Vincent (2006), Winter warmings, tides and planetary waves: comparisons between CMAM (with interactive chemistry) and MFR-MetO observations and data, *Ann. Geophysicae, 24*(10), 2493-2518.

Matsuno, T. (1971), A Dynamical Model of the Stratospheric Sudden Warming. *J. Atmos. Sci., 28*(8), 1479-1494.

McIntyre, M. E. and T. N. Palmer (1983), Breaking planetary waves in the stratosphere, *Nature, 305*, 593-600.

McWilliams, J. C. (1984), The emergence of isolated coherent vortices in turbulent flow, *J. Fluid Mech., 146*, 21-34.

Meek, C. E. (1980), An efficient method for analysing ionospheric drifts data, *J. Atmos. Terr. Phys., 42*, 835-839.

Meek, C. E. and A. H. Manson (1985), Combination of Primrose lake(54°N, 110°W) ROCOB winds(20-60 km) and Saskatoon(52°C, 107°W) MF radar winds(60-110 km): 1978-1983, *J. Atmos. Terr. Phys., 47*(5), 477-487.

Meek, C. E., A. H. Manson, S. J. Franke, W. Singer, P. Hoffmann, R. R. Clark, T. Tsuda, T. Nakamura, M. Tsutsumi and M. Hagan (1996), Global study of northern hemisphere quasi-2-day wave events in recent summers near 90 km altitude, *J. Atmos. Terr. Phys., 58*(13), 1401-1411.

Meek, C. E., A. H. Manson, M. D. Burrage, G. Garbe and L. L. Cogger (1997), Comparisons between Canadian prairie MF radars, FPI (green and OH lines) and UARS HRDI systems, *Ann. Geophysicae*, *15*(9), 1099-1110.

Merzlyakov, E. G. and C. Jacobi (2004), Quasi-two-day wave in an unstable summer atmosphere-some numerical results on excitation and propagation, *Ann. Geophysicae*, *22*(6), 1917-1929.

Merzlyakov, E., D. Pancheva, N. Mitchell, J. M. Forbes, Y. I. Portnyagin, S. Palo, N. Makarov and H. G. Muller (2004), High- and mid-latitude quasi-2-day waves observed simultaneously by four meteor radars during summer 2000, *Ann. Geophysicae*, *22*(3), 773-788.

Meyer, C. K. (1999), Gravity wave interactions with mesospheric planetary waves: A mechanism for penetration into the thermosphere-ionosphere system, *J. Geophys. Res., 104*(A 12), 28181-28196.

Meyer, C. K. and J. M. Forbes (1997), Natural oscillations of the ionosphere-thermosphere-mesosphere (ITM) system, *J. Atmos. Solar Terr. Phys., 59*(17), 2185-2202.

Mitchell, N. J., D. Pancheva, H. R. Middleton and M. E. Hagan (2002), Mean winds and tides in the Arctic mesosphere and lower thermosphere, *J. Geophys. Res., 107*(A1), 1004-doi:10.1029/2001JA900127.

Muller, H. G. (1972), Long-Period Meteor Wind Oscillations, *Phil. Trans. Roy. Soc. London, 271*(1217), 585-599.

Muller, H. G. and S. P. Kingsley (1974), Long period meteor wind oscillations, *J. Atm. Terr. Phys., 36*(11), 1933-1943.

Muller, H. G. and L. Nelson (1978), A travelling quasi 2-day wave in the meteor region, *J. Atmos. Terr. Phys., 40*, 761-766.

Muller, R. and G. Gunther (2003), A generalized form of Lait's modified potential vorticity, *J.Atmos.Sci., 60*(17), 2229-2237.

Muller, R. and G. Gunther (2005), Polytropic atmospheres and the scaling of potential vorticity, *Meteorology and Atmospheric Physics, 90*(3-4), 153-157.

Murayama, Y., K. Igarashi, D. D. Rice, B. J. Watkins, R. L. Collins, K. Mizutani, Y. Saito and S. Kainuma (2000), Medium frequency radars in Japan and Alaska for upper atmosphere observations, *IEICE Trans.Commun., E83-B*(9), 1996-2003.

Namboothiri, S. P., P. Kishore and K. Igarashi (2002), Observations of the quasi-2-day wave in the mesosphere and lower thermosphere over Yamagawa and Wakkanai, *J. Geophys. Res., 107*(D16), 4748-10.1029/2002JD003221.

Nash, E. R., P. A. Newman, J. E. Rosenfield and M. R. Schoeberl (1996), An objective determination of the polar vortex using Ertel's potential vorticity, *J. Geophys. Res., 101*(D5), 9471-9478.

Norton, W. A. and J. Thuburn (1996), The two-day wave in a middle atmosphere GCM, *Geophys. Res. Lett., 23*(16), 2113-2116.

Nozawa, S., A. Brekke, A. Manson, C. M. Hall, C. Meek, K. Morise, S. Oyama, K. Dobashi and R. Fujii (2002), A comparison study of the auroral lower thermospheric neutral winds derived by the EISCAT UHF radar and the Tromsø medium frequency radar, *J. Geophys. Res., 107*(A8), doi:10.1029/2000JA007581.

Nozawa, S., H. Iwahashi, A. Brekke, C. M. Hall, C. Meek, A. Manson, S. Oyama, Y. Murayama and R. Fujii (2003a), The quasi 2-day wave observed in the polar mesosphere: Comparison of the characteristics observed at Tromso and Poker Flat, *J. Geophys. Res., 108*(D24), 4748.

Nozawa, S., S. Imaida, A. Brekke, C. M. Hall, A. Manson, C. Meek, S. Oyama, K. Dobashi and R. Fujii (2003b), The quasi 2-day wave observed in the polar mesosphere, *J. Geophys. Res., 108*(D2), 4039.

Orsolini, Y. J., V. Limpasuvan and C. B. Leovy (1997), The tropical stratopause in the UKMO stratospheric analyses: Evidence for a 2-day wave and inertial circulations, *Q. J. R. Meteorol. Soc., 123*(542), 1707-1724.

Palo, S. E. and S. K. Avery (1996), Observations of the quasi-two-day wave in the middle and lower atmosphere over Christmas Island, *J. Geophys. Res., 101*(D8), 12833-12846.

Palo, S. E. and S. K. Avery (1995), Observations of the meridional quasi two-day wave in the mesosphere and lower thermosphere at Christmas Island. *The Upper Mesosphere and Lower Thermosphere: A Review of Experiment and Theory, Geophys. Monogr. Ser. 87, 87*, 101-110.

Pancheva, D. and P. Mukhtarov (1994), Variability of mesospheric dynamics observed at Yambol (42.5^{o}N, 26.6^{o}E) by meteor radar, *J. Atmos. Terr. Phys., 56*(10), 1271-1278.

Pancheva, D., N. Mitchell, H. Middleton and H. Muller (2003), Variability of the semidiurnal tide due to fluctuations in solar activity and total ozone, *J. Atmos. Solar Terr. Phys., 65*(1), 1-19.

Pancheva, D., N. J. Mitchell, A. H. Manson, C. E. Meek, C. Jacobi, Y. Portnyagin, E. Merzlyakov, W. K. Hocking, J. MacDougall, W. Singer, K. Igarashi, R. R. Clark, D. M. Riggin, S. J. Franke, D. Kurschner, A. N. Fahrutdinova, A. M. Stepanov, B. L. Kashcheyev, A. N. Oleynikov and H. G. Muller (2004), Variability of the quasi-2-day wave observed in the MLT region during the PSMOS campaign of June-August 1999, *J. Atmos. Solar Terr. Phys., 66*(6-9), 539-565.

Paparella, F., A. Babiano, C. Basdevant, A. Provenzale and P. Tanga (1997), A Lagrangian study of the Antarctic polar vortex, *J. Geophys. Res., 102*(D6), 6765-6774.

Parish, H. F., J. M. Forbes and F. Kamalabadi (1994), Planetary wave and solar emission signatures in the equatorial electrojet, *J. Geophys. Res., 99*(A1), 355-368.

Pfister, L. (1985), Baroclinic Instability of Easterly Jets with Applications to the Summer Mesosphere, *J. Atmos. Sci., 42*(4), 313-330.

Phillips, A. (1989), Simultaneous observations of the quasi 2-day wave at Mawson, Antarctica, and Adelaide, South Australia, *J. Atmos. Terr. Phys.*, *51*, 119-124.

Plumb, R. A. (1983), Baroclinic Instability of the Summer Mesosphere - a Mechanism for the Quasi-2-Day Wave, *J. Atmos. Sci.*, *40*(1), 262-270.

Pogoreltsev, A. I., D. Pancheva and N. J. Mitchell (2002), Secondary planetary waves in the middle atmosphere: numerical simulation and analysis of the neutral wind data, *J. Atmos. Solar Terr. Phys.*, *64*(8-11), 1251-1261.

Poole, L. M. (1988), The Grahamstown all-sky meteor radar, *J. Atmos. Terr. Phys.*, *50*, 585-590.

Poole, L. M. G. (1990), The characteristics of the mesospheric two-day wave as observed at Grahamstown(33. 3 deg S, 26. 5 deg E), *J. Atmos. Terr. Phys.*, *52*, 259-268.

Poole, L. M. G. and T. J. Harris (1995), The propagation of the mesospheric two-day wave in the southern hemisphere, *J. Atmos. Terr. Phys.*, *57*(13), 1661-1666.

Portnyagin, Y. I., E. G. Merzlyakov, T. V. Solovjova, C. Jacobi, D. Kurschner, A. Manson and C. Meek (2006), Long-term trends and year-to-year variability of mid-latitude mesosphere/lower thermosphere winds, *J. Atm. Sol-Terr. Phys.*, *68*(17), 1890-1901.

Randel W. J. (1992), Global Circulation Statistics, 1000-1 mb, NCAR/TN-366+STR, NCAR Technical note, National Center For Atmospheric Research, Boulder, Colorado.

Randel, W. J. (1994), Observations of the 2-Day Wave in NMC Stratospheric Analyses, *J. Atmos. Sci.*, *51*(2), 306-313.

Randel, W., P. Udelhofen, E. Fleming, M. Geller, M. Gelman, K. Hamilton, D. Karoly, D. Ortland, S. Pawson, R. Swinbank, F. Wu, M. Baldwin, M. L. Chanin, P. Keckhut, K. Labitzke, E. Remsberg, A. Simmons and D. Wu (2004), The SPARC intercomparison of middle-atmosphere climatologies, *J. Clim.*, *17*(5), 986-1003.

Reddi, R. C., A. Geetha and K. R. Lekshmi (1988), Quasi 2-day wave in the middle atmosphere over Trivandrum, *Ann. Geophysicae, 6*(3), 231-237.

Roble, R. G. and E. C. Ridley (1994), A thermosphere-ionosphere-mesosphere-electrodynamics general circulation model (time-GCM): Equinox solar cycle minimum simulations (30-500 km), *Geophys. Res. Lett., 21*(6), 417-420.

Rodgers, C. D. and A. J. Prata (1981), Evidence for a traveling two-day wave in the middle atmosphere, *J. Geophys. Res., 86*, 9661-9664.

Salby, M. L. (1981), The 2-day wave in the middle atmosphere-Observations and theory, *J. Geophys. Res., 86*, 9654-9660.

Salby M. L. (1996), Fundamentals of atmospheric physics, 622 pp., Academic Press, San Diego, .

Salby, M. L. and R. G. Roper (1980), Long-Period Oscillations in the Meteor Region, *J. Atmos. Sci., 37*(1), 237-244.

Salby, M. L. and P. F. Callaghan (2001), Seasonal Amplification of the 2-Day Wave: Relationship between Normal Mode and Instability, *J. Atmos. Sci., 58*(14), 1858-1869.

Salby, M. L. and P. F. Callaghan (2003), Dynamics of the 2-day wave in a nonlinear model of the middle and upper atmosphere, *J. Geophys. Res., 108*(D23), 4713-doi:10.1029/2003JD003648.

Scaife, A. A., N. Butchart, C. D. Warner, D. Stainforth, W. Norton and J. Austin (2000), Realistic quasi-biennial oscillations in a simulation of the global climate, *Geophys. Res. Lett., 27*(21), 3481-3484.

Schoeberl, M. R. and A. J. Krueger (1983), Medium Scale Disturbances In Total Ozone During Southern Hemisphere Summer, *Bull. Am. Meteorol. Soc., 64*(12), 1358-1365.

Schoeberl, M. R. and D. L. Hartmann (1991), The Dynamics of the Stratospheric Polar Vortex and its Relation to Springtime Ozone Depletions, *Science, 251*(4989), 46-52.

Shepherd, G. G., J. Stegman, P. Espy, C. McLandress, G. Thuillier and R. H. Wiens (1999), Springtime transition in lower thermospheric atomic oxygen, *J. Geophys. Res., 104*(A1), 213-224.

Shepherd, G. G., J. Stegman, W. Singer and R. G. Roble (2004), Equinox transition in wind and airglow observations, *J. Atmos. Solar Terr. Phys., 66*(6-9), 481-491.

Shepherd, M. G., P. J. Espy, C. Y. She, W. Hocking, P. Keckhut, G. Gavrilyeva, G. G. Shepherd and B. Naujokat (2002), Springtime transition in upper mesospheric temperature in the northern hemisphere, *J. Atmos. Solar Terr. Phys., 64*(8-11), 1183-1199.

Shepherd, T. G. (2000), The middle atmosphere, *J. Atm. Sol-Terr. Phys., 62*(17-18), 1587-1601.

Shepherd, T. G. (2002), Issues in stratosphere-troposphere coupling, *J. Meteor. Soc. Japan, 80*(4B), 769-792.

Singer, W., D. Keuer and W. Eriksen (1997), The ALOMAR MF Radar: Technical Design and First Results, *European Rocket and Balloon Programmes and Related Research. Proceedings of the 13th ESA Symposium Held 26-29 may, 1997 in Öland, Sweden*, 101.

Smith, A. K. (1996), Longitudinal variations in mesospheric winds- Evidence for gravity wave filtering by planetary waves, *J. Atmos. Sci., 53*(8), 1156-1173.

Smith, A. K. (2003), The origin of stationary planetary waves in the upper mesosphere, *J. Atmos. Sci., 60*(24), 3033-3041.

Stegman, J., D. Murtagh and G. Witt (1992), Extremes of oxygen airglow intensity, *Abstract in EOS Trans, 73*(14), AGU, Spring Meeting Suppl-S222.

Stening, R. J., C. E. Meek, A. H. Manson and D. G. Stephenson (1978), Winds and Wave Motions to 110 km at Midlatitudes. VI. Tidal, Gravity and Planetary Waves, 1976, *J. Atmos. Sci., 35*(11), 2194-2204.

Swinbank, R. and A. O'Neill (1994), A Stratosphere Troposphere Data Assimilation System, *Mon.Weather Rev., 122*(4), 686-702.

Swinbank, R., W. A. Lahoz, A. O'Neill, C. S. Douglas, A. Heaps and D. Podd (1998), Middle atmosphere variability in the UK Meteorological Office Unified Model, *Q.J.R.Meteorol.Soc., 124*(549), 1485-1525.

Swinbank, R., N. B. Ingleby, P. M. Boorman and R. J. Renshaw (2002), A 3D variational data assimilation system for the stratosphere and troposphere. *Forecasting Research Scientific Paper, No 71*.

Taylor, M. J., H. L. Liu, C. Y. She, L. C. Gardner, R. G. Roble and V. Vasoli (2001), Large amplitude perturbations in mesospheric OH Meinel and 87-km Na lidar temperatures around the autumnal equinox, *Geophys. Res. Lett., 28*(9), 1899-1902.

Thayaparan, T., W. K. Hocking and J. MacDougall (1995), Middle atmospheric winds and tides over London, Canada(43^{o}N, 81^{o}W) during 1992-1993, *Radio Sci., 30*(4), 1293-1309.

Thayaparan, T., W. K. Hocking, J. MacDougall, A. H. Manson and C. E. Meek (1997), Simultaneous observations of the 2-day wave at London (43^{o}N, 81^{o}W) and Saskatoon (52^{o}N, 107^{o}W) near 91 km altitude during the two years of 1993 and 1994, *Ann. Geophysicae, 15*(10), 1324-1339.

Thayaparan, T. and W. K. Hocking (2002), A long-term comparison of winds and tides measured at London, Canada (43^{o}N,81^{o}W) by co-located MF and meteor radars during 1994-1999, *J. Atm. Sol-Terr. Phys., 64*(8-11), 931-946.

Tohmatsu T. (c1990.), Compendium of aeronomy, Terra Scientific Pub. Co., Tokyo.

Torrence, C. and G. P. Compo (1998), A practical guide to wavelet analysis, *Bull. Am. Meteorol. Soc., 79*(1), 61-78.

Tsuda, T., S. Kato and R. A. Vincent (1988), Long period wind oscillations observed by the Kyoto meteor radar and comparison of the quasi-2-day wave with Adelaide HF radar observations, *J. Atmos. Terr. Phys., 50*, 225-230.

Tsutsumi, M., T. Tsuda, T. Nakamura and S. Fukao (1996), Wind velocity and temperature fluctuations due to a 2-day wave observed with radio meteor echoes, *J. Geophys. Res., 101*(D5), 9425-9432.

Wallace J. M. and P. V. Hobbs (2006), Atmospheric science: an introductory survey, 483 pp., Elsevier Inc.

Warner, C. D. and M. E. McIntyre (1999), Toward an ultra-simple spectral gravity wave parameterization for general circulation models, *Earth Planets Space, 51*, 475-484.

Waters, J. W., L. Froidevaux, R. S. Harwood, R. F. Jarnot, H. M. Pickett, W. G. Read, P. H. Siegel, R. E. Cofield, M. J. Filipiak and D. A. Flower (2006), The Earth Observing System Microwave Limb Sounder (EOS MLS) on the Aura satellite, *IEEE Trans. Geosci. Remote Sens., 44*(5), 1075-1092.

Waugh, D. W. and P. P. Rong (2002), Interannual variability in the decay of lower stratospheric Arctic vortices, *J. Meteor. Soc. Japan, 80*(4B), 997-1012.

Wu, D. L., P. B. Hays, W. R. Skinner, A. R. Marshall, M. D. Burrage, R. S. Lieberman and D. A. Ortland (1993), Observations of the quasi 2-day wave from the High Resolution Doppler Imager on UARS, *Geophys. Res. Lett., 20*(24), 2853-2856.

Wu, D. L., E. F. Fishbein, W. G. Read and J. W. Waters (1996), Excitation and Evolution of the Quasi-2-Day Wave Observed in UARS/MLS Temperature Measurements, *J. Atmos. Sci., 53*(5), 728-738.

Zhou, Q. H., H. Monroy, D. C. Fritts, H. M. Ierkic, B. Isham, J. R. Isler and S. E. Palo (2000), Radar observations of longitudinal variability of tidal/planetary waves and mean motions in the tropical mesosphere, *J. Geophys. Res., 105*(D2), 2151-2162.

Ziemke, J. R., S. Chandra, R. D. McPeters and P. A. Newman (1997), Dynamical proxies of column ozone with applications to global trend models, *J. Geophys. Res.*, *102*(D5), 6117-6130.

APPENDIX A

CONVERSION BETWEEN GEOMETRICAL HEIGHT (km) AND PRESSURE LEVELS (hPa)

For an atmosphere with linear temperature variation with height the following approximate relation between the pressure level (p, hPa) and geometrical height (H, km) that has been derived empirically from CIRA-86 data can be used for reference purposes:

$$H_{km} \approx 16.1\left(3 - \log_{10}\, p_{hPa}\right)$$

	p, hPa	**H, km**
1	1000.0	0.0
2	681.3	2.68
3	464.1	5.37
4	316.2	8.05
5	215.4	10.73
6	146.8	13.42
7	100.0	16.10
8	68.13	18.78
9	46.46	21.47
10	31.62	24.15
11	21.54	26.83
12	14.68	29.52
13	10.00	32.20
14	6.81	34.88
15	4.64	37.57
16	3.16	40.25
17	2.15	42.93
18	1.47	45.62
19	1.00	48.30
20	0.68	50.98
21	0.46	53.67
22	0.32	56.35

APPENDIX B

ALGORITHM FOR THE Q-DIAGNOSTIC CALCULATION

Input data are MetO temperature (T), zonal (U) and meridional (V) wind components defined at k=0,1,2,…,21 pressure levels: p(k)=1000*$10^{-k/6}$. The wind fields are given for -88.75+2.5*i latitude degrees and 1.875+3.75*j longitude degrees, while the mass grid is -90+2.5*i latitudes and 3.75*j longitudes; i=0,1,2,…,71 and j=0,1,2,…,96.

1. MetO data have a staggered grid (known as "Arakawa B grid") distribution with the wind grid shifted relative to the mass (temperature, geopotential heights) grid. For each pressure level p temperature data are interpolated to the "wind-grid" points using the bi-linear patch method: V=ax+by+cxy+d. First, the constants a, b, c, and d are calculated using the known values of the wind or temperature data (F_1, F_2, F_3, F_4) and the distance between grid points (x and y, latitudinal and longitudinal steps in radians in our case). According to the sketch on the left:

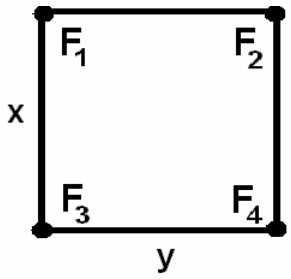

F_1=d
F_2=by+d => b=(F_2- F_1)/y
F_3=ax+d => a=(F_3- F_1)/x
F_4=ax+by+cxy+d => c=(F_4+F_1-F_2-F_3)/(xy)

Then calculate the value of the parameter at the new coordinates. The comparison between the original data (black lines) and interpolated data (blue color) are shown in Figure B.1 for approximately 16 km and 36 km. At the bottom of each plot the mean and variance are given for both fields.

2. The potential temperatures, θ, are calculated using a well-known equation [*Salby*, 1996] on the "wind-grid" points (φ, λ) and all pressure levels p:

$$\theta(\varphi,\lambda,p) = T(\varphi,\lambda,p) * \left(\frac{1000}{p}\right)^{\frac{2}{7}}, \qquad \text{(A1)}$$

where T is temperature; k=R/c_p~2/7, where c_p is the specific heat at constant pressure and R is the specific gas constant. Potential temperature is conserved for adiabatic flow.

3. The next step is to interpolate fields to the constant potential temperature (isentropic) surfaces. For this purpose a linear interpolation IDL routine (INTERPOL) has been employed. The same constant isentropic surfaces as used by *Harvey et al.* [2002] were chosen: 330-400K in 10K steps, 400-550 K in 25K steps, 600 to 1000 in 100 K steps and 1000 to 2000 K in 200K steps. From 330 to 550 K (9-22 km, 310-40 hPa)

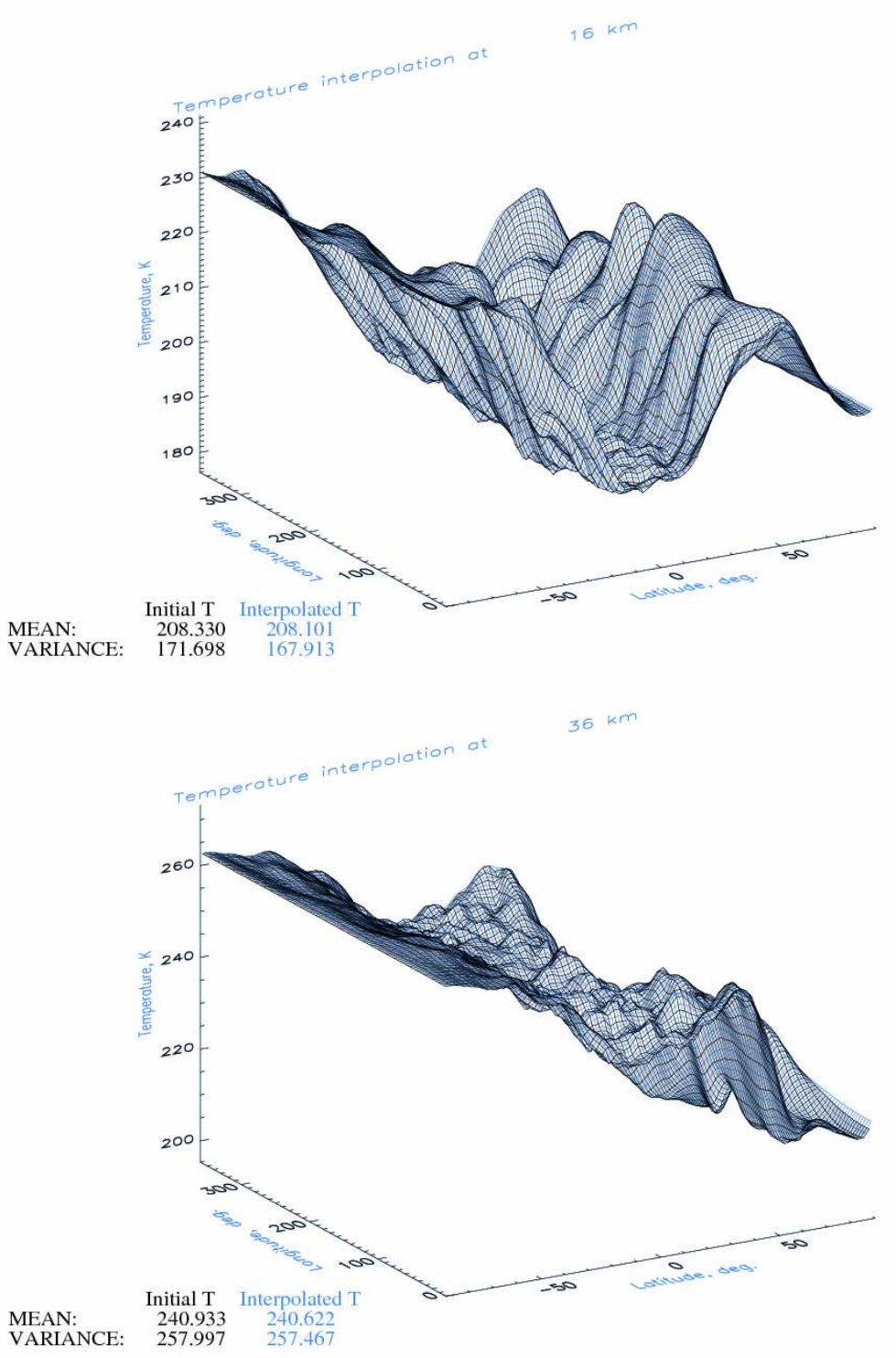

Figure B.1 The comparison between original MetO temperature fields (black) and interpolated on the "wind-grid" data (blue). Data are for day 360, year 2004.

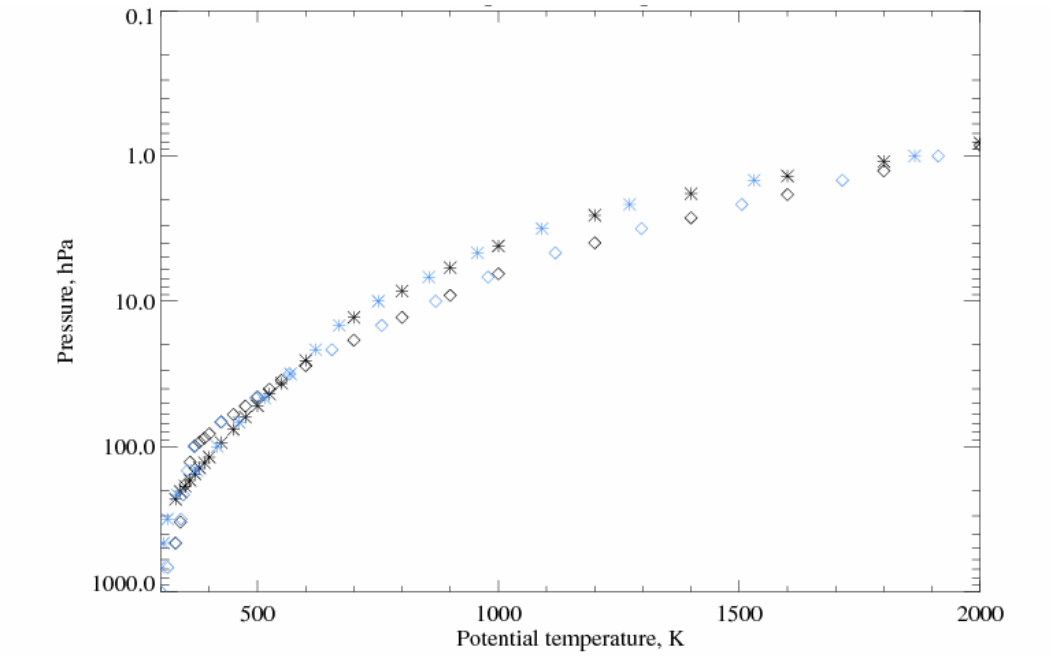

Figure B.2 Results of determination of pressure at constant potential temperature (black) surfaces by interpolation between known constant pressure (blue) values. Values for two latitudes ~0°N (diamonds) and ~60°N (stars) are shown.

the vertical resolution or steps are ~1 km. From 550 to 2000 K (22-50 km, 40-0.75 hPa) there is 2-3 km between θ-surfaces. To ensure that the pressure sequences change monotonically, the SORT routine is used before the interpolation. Examples of the interpolation for two locations (0°N, 1.875°E) and (60°N, 1.875°E) are shown by diamonds and stars, respectively, in Figure B.2.

4. For relative vorticity (ζ) computations the derivatives are calculated using a slightly modified IDL routine DERIV5. To produce greater accuracy (especially in case of generally smaller meridional winds), the DERIV5 calculates derivatives based on five points instead of three as in the standard DERIV routine. The five-point approximation of the derivative of the function f at x_0 is

$$f'(x_0) = \frac{1}{12h}\left[f(x_0 - 2h) - 8f(x_0 - h) + 8f(x_0 + h) - f(x_0 + 2h)\right] \qquad \text{(A2)}$$

Here h is the latitudinal or longitudinal step in radians

5. Scalar streamfunction (ψ) fields are calculated following [*Salby,* 1996]. Isopleths are parallel to the rotational component of the wind and the distance separating the isolines of ψ is proportional to the magnitude of the non-divergent velocity. The streamfunction was calculated numerically from the Poisson equation in spherical coordinates:

$$-\hat{e}_r \nabla^2 \psi = \nabla \times \vec{V}$$

$$-\frac{\hat{e}_r}{r^2\cos\varphi}\left(\frac{1}{\cos\varphi}\frac{\partial^2\psi}{\partial\lambda^2}+\cos\varphi\frac{\partial^2\psi}{\partial\varphi^2}-\sin\varphi\frac{\partial\psi}{\partial\varphi}\right)=\frac{\hat{e}_r}{r\cos\varphi}\left(\frac{\partial v}{\partial\lambda}-\frac{\partial u}{\partial\varphi}\cos\varphi+u\sin\varphi\right)$$

where φ is latitude, λ is longitude, *u* and *v* are zonal and meridional wind components, *r* is the radius of the Earth, and $\hat{e}_r$ is a unit vector along the *r*.

It is not trivial to find the streamfunction when the wind field contains both the irrotational and solenoidal (rotational) components. We have asked for advice from the authors of the analysis (Q-diagnostic), Drs. Lynn Harvey and Duncan Fairlie. They kindly have sent us the FORTRAN code that they used to calculate the streamfunction and velocity potential by computing vorticity and divergence in grid-space, multiplying their Fourier spectral transform by –n(n+1), and transforming the results back (Duncan Fairlie, personal communications, June 2005). At the same time Dr. Benkevitch (personal communications 2005) adapted the computer code for solving the spherical Poisson equation from a standard MATLAB application to the IDL language. It was less time-consuming to modify this application for MetO data and incorporate it into the main program code as a subroutine than rewrite the FORTRAN code. To test the adopted algorithm, a Dirichlet's problem was used: $\nabla^2 U = -6\sin^2(\theta)\cdot\sin(2\varphi)$, where $\theta=\theta_0, \varphi=0,...,2\pi$ is the border line, and the boundary condition is $U(border)=r^2\sin^2(\theta_0)\cdot\sin(2\varphi)$. This problem has the exact solution: $U(\theta,\varphi)=r^2\sin^2(\theta)\cdot\sin(2\varphi)$, which is shown on the middle plot of Figure B.3. The output from the program is plotted above it (on the top panel of Figure B.3). The bottom panel demonstrates the differences of the two results. The relative error per one element: $\frac{\sqrt{\sum(U-Uex)^2}}{\sqrt{\sum Uex^2}}*100\%$ is less than 1%. An example of the streamfunction calculated from the MetO data at 1000K isentropic surface for the December 25 of 2004 is shown in Figure B.4.

6. The Potential Vorticity (PV) is calculated using equation 6.4 (Section 6.2.1), with $\partial\theta/\partial p$ being estimated as the local slope of the curve defined by the appropriate cubic spline (it is assumed that θ varies as a cubic function of p). Figure 6.1 is an example of a PV field calculated from MetO data at isentropic surface of 1000 K for December 25, 2004.

7. Next the Q diagnostic is calculated using equation 6.5 (Section 6.2.2). In Figure B.5 areas with negative and positive Q are shaded with blue and green colors, respectively.

8. A contour program written in FORTRAN by Dr. C. Meek was adapted for IDL and employed to identify the locations for each contour of constant streamfunction value (stream line). In the algorithm, grid-line-contour crossing points are first found for each contour level, and then these points are re-arranged in open or closed contours.

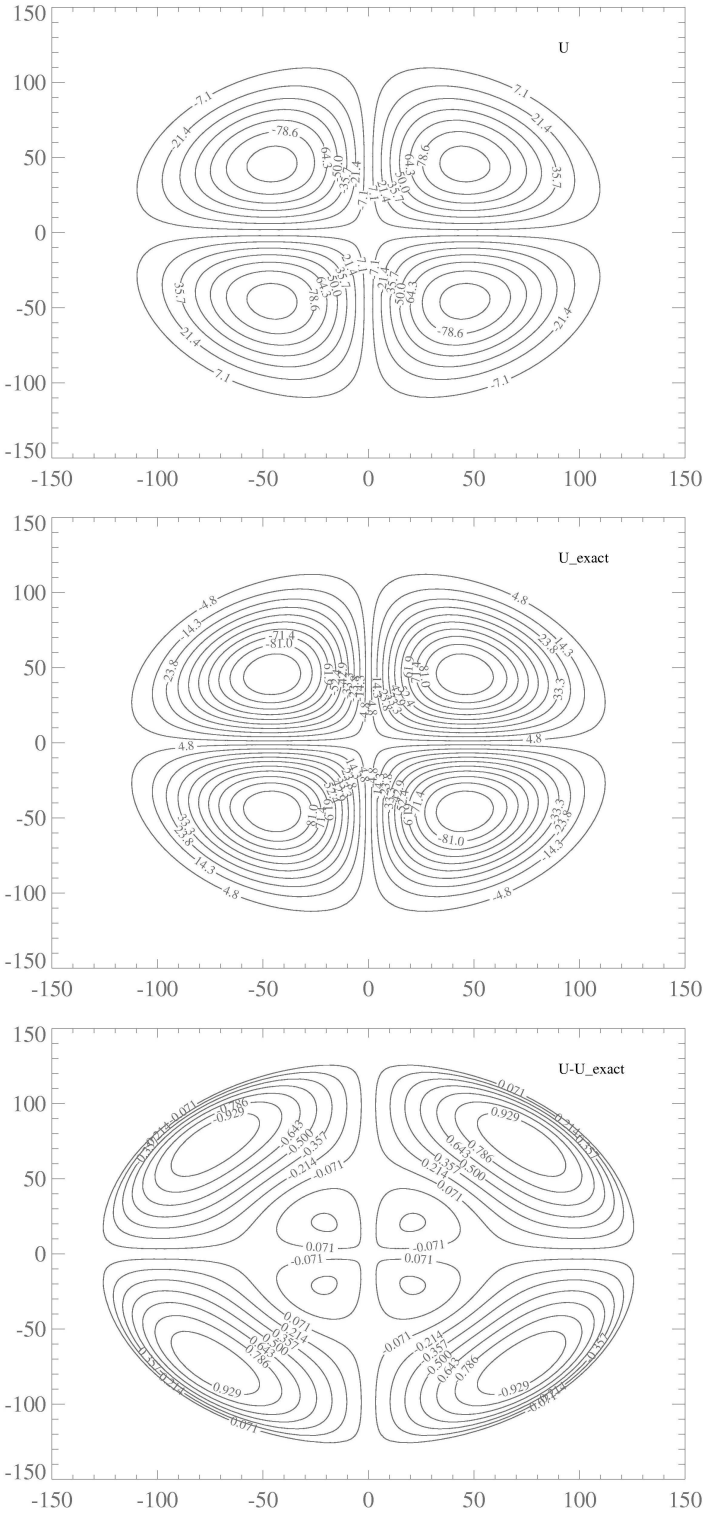

Figure B.3 The results of the Poisson equation calculation of the Dirichlet's problem, U, using the adopted algorithm is shown at the top plot; its exact solution is on the middle plot; and their differences are on the bottom.

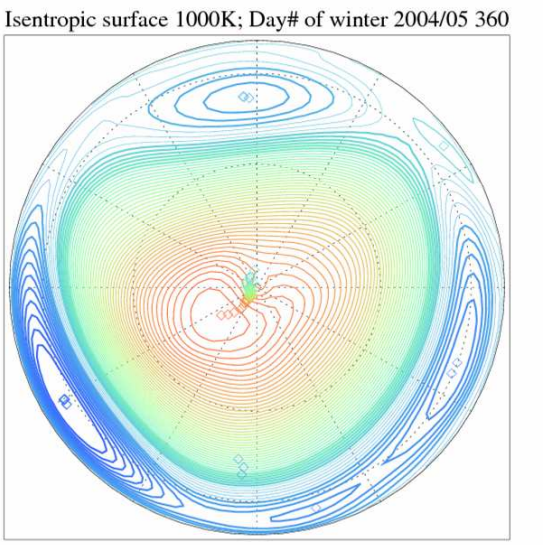

Figure B.4 Contours of constant streamfunction values for the Northern Hemisphere. Values change as colors vary from red (minimum of $-140*10^6$ m^2s^{-1}) to blue (maximum of $160*10^6$ m^2s^{-1}). Steps between contours are equal to $5*10^6$ m^2s^{-1}. Integrated values of relative vorticity are negative along thick contours and positive along thin contours. [Notice that all red and yellow lines are thin.] Diamonds indicate the approximate centers of the contours.

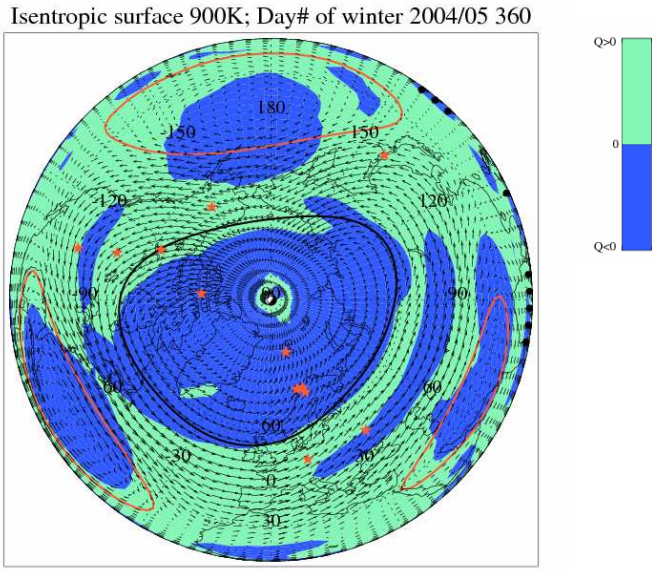

Figure B.5 Q diagnostic (blue is negative, green is positive), winds (arrows), and negative PV (black dots) at 1000 K potential temperature surface for day 345, 2004 over the Northern Hemisphere. Red stars indicate locations of the 13 MF and VHF (meteor) radars. Thick black and red lines are the calculated edges of the cyclones and anticyclones, respectively.

9. Values of Q, relative vorticity and wind speed are integrated along each of the contour lines (scalar streamfunction, ψ, isopleths). Wind integration is a desirable additional criterion as shear zones of Q (green areas) can be found inside of vortices (see, for example Figure B.5).

10. To identify edges of vortices, all data are divided into two groups, cyclones and anticyclones, according to the value of the integrated relative vorticity. Then for each of these groups all contours were considered according to their locations: pole-centered or mid-latitude vortices. The location of each contour is defined by the coordinates of its center. $\oint Q \approx 0$ delineates vortex edges [*Harvey et al.,* 2002], so that ψ contours where $\oint Q$ changes sign are vortex edge candidates. Of these candidate-isopleths, that one having the largest integrated wind speed is considered the vortex edge. An equatorward boundary at ~15^o is imposed and ψ isopleths that intersect this boundary are not considered. Below 450 K (17 km or 100 hPa) the presence of the subtropical jet contaminates edge identification. Unlike polar vortices, several anticyclones can be present on a given day and altitude. Therefore, $\oint Q$ needs to be evaluated one anticyclone at a time. To accomplish this, the longitudinal distribution of anticyclones is identified. For each identified anticyclone integrated Q and wind speeds are compared. The isopleth is excluded if the anticyclone's width exceeds 135^o in longitude. ψ isopleths are also excluded if their size is less than 15^o longitude or 10^o latitude. Space is allocated for 4 (1 pole-centered and 3 mid-latitudinal) cyclones and 4 anticyclones. Coordinates of all identified edges at all 24 isentropic surfaces are saved in an IDL file for future use. Thick black and red lines in Figure B.5 indicate the estimated edges of the polar vortex and anticyclones, respectively.

11. To create plots such as in Figure 6.5 (Section 6.3), each grid point is given a value of -1, 0 or +1 depending on its location (separate IDL program code). If a grid point is located inside a polar cyclone or anticyclone then, respectively, a -1 or +1 value is assigned to it. Grid points outside vortices are set to 0. Areas inside the polar vortex are shaded using a blue color, while areas inside anticyclones are filled with orange color. The resulting contours for isentropic surfaces from 500 K up to 2000 K (~20-50 km) are then stacked on top of each other.